DEVELOPMENT AND EVALUATION OF A BIOMASS-FIRED MICRO-SCALE CHP WITH ORGANIC RANKINE CYCLE

By Yingjuan Shao

Thesis submitted to the University of Nottingham

for the degree of Doctor of Philosophy

July 2011

ACKNOWLEDGEMENT

During the course of my PhD study at Nottingham, many people have helped me. Without their guidance, patience, help and support, I would have never been able to accomplish my thesis. I would like to take this opportunity to acknowledge some of them.

Firstly, I would like to gratefully acknowledge Dr. Hao Liu for his enthusiastic supervision, support, advice and patience which he has granted to me during the course of my PhD study. Special thanks are also to my other supervisor Prof. Saffa Riffat for giving me many valuable comments and great encouragement over the past years.

Dr. Guquan Qiu is gratefully acknowledged for providing generous help and support, particularly for advice and support with the laboratory experiments during the project period. Mr. Jinxin Li and technicians of the Department of Architecture and Built Environment are thanked for their help and support with the laboratory experiments.

I would like to express my special gratitude to Prof. Baoshen Jin and Mrs. Jun Liu of Southeast University, P.R. China, for their constant support, advice and encouragement to my study abroad.

Finally, I owe my deepest gratitude to my parents. This thesis would not have been possible without their love, encouragement and unconditional support.

ABSTRACT

Combined Heat and Power Generation (CHP) or cogeneration has been considered worldwide as the major alternative to traditional energy systems in terms of significant energy saving and environmental conservation. A renewable energy resource-fuelled CHP would deliver even more environmental benefits than a fossil fuel-driven CHP. Biomass is one of the renewable energy resources that plays an important role to the world primary energy supplies and can be used to fuel CHP systems. Many medium- and large-scale biomass-fired CHP plants have been demonstrated and commercialized in the world. However, biomass-fuelled micro-scale CHP (1-10kW$_e$) which is suitable for building applications has yet to be commercialised or demonstrated.

The development and evaluation of a micro-CHP system operating on biomass energy has been the focus of this PhD research. It is an integral part of an externally funded research project which aims to develop and evaluate a novel, first-of-its-kind, micro-scale (1 – 2 kW$_e$) biomass-fired CHP system suitable for public and large domestic buildings' applications. The specific tasks of the present PhD research are:

- To thermodynamically model the micro-scale biomass-fired CHP system with organic Rankine cycle (ORC): different environment-friendly working fluids are to be modelled with the ORC processes.

- To experimentally evaluate the micro-scale biomass-fired CHP system in terms of power generation and combined heat and power performance.

- To experimentally investigate the combustion performance and NOx emissions of the biomass pellet boiler which is a key component of the micro-scale biomass-fired CHP system.

The micro-scale biomass-fired CHP system with ORC developed by the research team of University of Nottingham including the author of this PhD thesis mainly consists of a biomass boiler, an ORC fluid evaporator, an ORC turbine, an alternator, a heat recouperator and a condenser. The boiler produces hot water which transfers heat to the organic working fluid via the evaporator. The generated organic fluid vapour drives a turbine to rotate an alternator, producing power. The expanded

organic fluid vapour leaving the turbine transfers some of its heat to the recouperator and then is condensed by cooling water which can be heated to around 40 – 50 ^{0}C for domestic washing and under-floor heating purposes.

The main methodologies of the present PhD research are the thermodynamic modelling of the proposed micro-scale biomass-fired CHP system with ORC and the laboratory testing of the assembled micro-scale biomass-fired CHP system and its main components (biomass boiler, ORC turbine, alternator, heat exchangers etc.).

Literature review has demonstrated that the biomass-fired micro-CHP systems for buildings present many advantages compared to conventional separate heating and power supply systems (e.g. a dedicated boiler for heating and grid for power supply) as they can present higher primary energy savings and lower CO_2 emissions. ORC is a suitable thermodynamic cycle that could be used for micro-CHP systems while operating with waste heat and renewable energy resources which are available at relative low temperatures.

Thermodynamical modelling of the proposed micro-scale biomass-fired CHP system with ORC has been carried out and the results have been presented and discussed in the thesis. Three different environment-friendly working fluids, namely HFE7000, HFE7100 and n-pentane, have been modelled with various ORC process configurations.

The laboratory testing of the assembled micro-scale biomass-fired CHP system and its main components (biomass boiler, ORC turbine, alternator, heat exchangers etc.) has been carried out initially with a 25kW biomass boiler and then with a 50kW biomass boiler. The main purpose of the laboratory testing has been to evaluate the main energy efficiencies (the electrical efficiency and the total CHP efficiency) of the assembled micro-CHP systems. The combustion performance and NOx emissions of each biomass boiler have also been investigated as the biomass boiler is a key component of the micro-scale biomass-fired CHP system. The experimental findings of these laboratory tests are presented and analysed in the thesis.

Finally, the conclusions of the present PhD research have been given. The modelling results have shown that the electrical efficiency of the micro-CHP system depends on not only the modelling conditions but also the ORC fluid. A comparison of the three fluids generally follows the following order: n-pentane > HFE7000 > HFE7100. For the laboratory test, the 25kW biomass boiler-driven micro-CHP system, having an ORC efficiency in the range of 2.20% – 2.85%, can generate electricity of 344.6W and heat of 20.3kW, corresponding to electricity generation efficiency 1.17% and CHP efficiency 86.22%. And the $50kW_{th}$ biomass boiler-driven micro-CHP system, having an ORC efficiency of 3.48% - 3.89%, can generate electricity of 748.6W and heat of 43.7kW, corresponding to electricity generation efficiency 1.43% and CHP efficiency 81.06%.

CONTENTS

LIST OF FIGURES

LIST OF TABLES

NOMENCLATURE

C_P	Heat capacity at constant pressure	J/(kg.K)
C_V	Heat capacity at constant volume	J/(kg.K)
D_h	Hydraulic diameter	m
e	Thermal internal energy per unit mass	J/kg
h	Enthalpy	J/kg
h_L	Latent heat of vaporization	J/kg
h_1	Pump inlet organic working fluid enthalpy	J/kg
h_2	Pump outlet organic working fluid enthalpy	J/kg
h_{2a}	Evaporator inlet organic working fluid enthalpy(with IHE)	J/kg
h_{2s}	Isentropic Pump inlet organic working fluid enthalpy	J/kg
h_3	Turbine inlet organic working fluid enthalpy	J/kg
h_4	Turbine outlet organic working fluid enthalpy	J/kg
h_{4a}	Condenser inlet organic working fluid enthalpy(with IHE)	J/kg
h_{4s}	Isentropic turbine outlet organic working fluid enthalpy	J/kg
m	Mass	kg
$\dot{m}$	Mass flow rate	kg/s
M	Molar mass	kg/kmol
P	Pressure	KPa
ΔP	Pressure losses	kPa
Q	Heat energy	J
q_{in}	Heat transfer in of the system per unit of mass flowing	J/kg

q_{out}	Heat transfer out of the system per unit of mass flowing	J/kg
RPM	Revolutions per minute	r/min
s	Entropy per unit mass	J/(kg.K)
T	Temperature	K
ΔT_{PP}	Minimum temperature difference between the two sides of the heat exchanger	K
T_C	Condenser temperature	K
T_E	Evaporator temperature	K
T_{cw}	Cooling water temperature	K
T_H	Maximum temperature	K
T_L	Lowest temperature	K
v	Volume per unit mass	m^3/kg
V	Volume flow rate	m^3
$\dot{V}$	Volume flow rate	m^3/s
W	Work	J
W_{net}	Net work per unit of mass flowing	J/kg
W_{pump}	Work per unit of mass flowing of the pump	J/kg
W_{turb}	Work per unit of mass flowing of the turbine	J/kg

Greek Letters

η	Efficiency	%
η_{alt}	Alternator efficiency	%
η_{boiler}	Biomass boiler thermal efficiency	%
η_{Carnot}	Carnot cycle efficiency	%
η_{CHP}	Combine heating and power efficiency	%
η_{cond}	Condenser heat loss factor	%
η_{evap}	Evaporator thermal efficiency	%
η_{IHE}	Internal Heat Exchanger thermal efficiency	%
η_{pump}	Pump efficiency	%
$\eta_{pump\ ,IS}$	Isentropic pump efficiency	%
η_{Rank}	Rankine cycle efficiency	%
η_{turb}	Turbine efficiency	%
$\eta_{turb\ ,IS}$	Isentropic turbine efficiency	%
μ	Dynamic viscosity	Pa.s
ρ	Mass density	kg/m^3
γ	Heat capacity ratio	

Abbreviation

CHP	Combined heat and power
DC	Direct current
DHC	District heating and cooling
eq	Equivalent
GHG	Greenhouse gas

Gt	Giga tonne
GCV	Gross calorific values
GWP	Greenhouse Warming Potential
HHV	High heating values
IC	Internal combustion
IV	Independent variables
IHE	Internal Heat Exchanger
ODP	Ozone Depleting Potential
PJ	Petajoule, 10^{15} joules
Max	Maximum
Min	Minimum
Mt	Million tonne
Mtoe	Million metric tons equivalent of oil
ORC	Organic Rankine cycle
ppm	Parts-per-million, 10^{-6}
ppmv	Parts-per-million by volume
WHR	Waste heat recovery

Chapter 1. Introduction

1.1. World Primary Energy Demand

The development of economy and technology has brought a significant increase in energy demand around the world. According to the data from IEA, in 2007, the total primary energy supply of the world was 12029 Mtoe (million metric tons equivalent of oil), or 492 EJ (1 EJ=1018 J). Comparing with the total primary energy supply of 6115 Mtoe in 1973, there has been a dramatic increase over the past decades (International Energy Agency "World Energy Outlook 2008" 2008). This is illustrated in Figure 1.1.

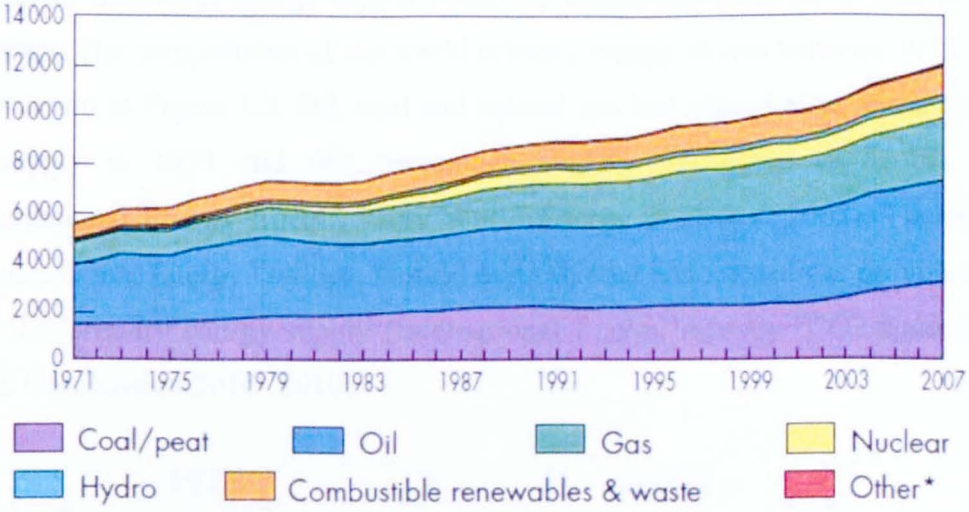

Figure 1.1 World total primary energy supply by fuel (Mtoe) (IEA 2008)

Economic growth is deemed to be the most important determinant of the overall demand for energy services by far. Over the past 30 years, the global economy keeps growing at 3.3% per year. Simultaneously, the electrical energy demand increased at 3.6% per year in this period. The Energy Outlook of IEA (International Energy Agency "World Energy Outlook 2008" 2008) predicted that the world economic growth would recover to around 4.5% per year by the turn of the coming decade (from 2011 to 2020), but would slow progressively through to 2030. This means the world GDP was expected to grow by the same average of 3.3% per year as of the past

30 years over the period 2006-2030. Similar projections have been published with the latest IEA's International Energy Outlook (International Energy Agency "World Energy Outlook 2009" 2009) .

The energy resources can be split into three categories: fossil fuels, renewable resources and nuclear resources(A Demirbas 2000). Fossil fuels have long been recognized as the uppermost conventional energy resources and account for most of the world energy supply. During the past decades, the energy needed for the worldwide economic stability and development which approximately doubled between 1971 and 2007 as shown by Figure 1.1, has been mainly derived from fossil fuels. According to the data of IEA (Figure 1.1), oil was the main source of energy, which followed by coal and natural gas. Although some of the non-fossil energy (such as nuclear and hydropower) have increased visibly, fossil fuels have still maintained their shares of the world energy supply relatively unchanged over the course of the past 35 years. The comparisons of the world primary energy shares between 1973 and 2007 are shown in Figure 1.2. Oil, coal and natural gas had shared 86% of the world energy supply in 1973 and this percentage slightly fell down to 81.4% in 2007(International Energy Agency "Key World Energy Statistics" 2008). The latest IEA's International Energy Outlook showed that oil, coal and natural gas provided 81% of the world primary energy supply (International Energy Agency "CO2 Emissions from Fuel Combustion 2010" 2010).

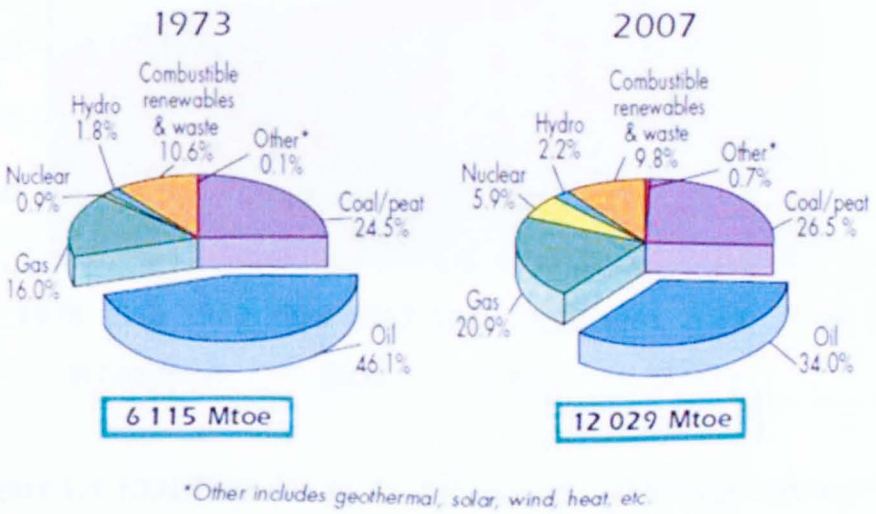

Figure 1.2 World primary energy shares in 1973 and in 2007 (IEA 2008)

1.2. Greenhouse Gas Emissions and Climate Change

As the Intergovernmental Panel on Climate Change (IPCC) concluded in its fourth assessment report: "most of the observed increase in global average temperatures since the mid-20th century is very likely due to the observed increase in anthropogenic greenhouse gas concentrations"(Intergovernmental Panel on Climate Change 2007). This leaves little doubt that human activity is the main cause of the global warming observed over the last 100 years, especially during the last 50 years. Most scientists have now broadly accepted the link between greenhouse gas emissions and global climate change. The increased concentrations of key greenhouse gases (GHG) are a direct consequence of human activities, particularly the continuously increasing consumption of energy which is largely derived from the combustion of fossil fuels. Combustion of fossil fuels always leads to the emissions of greenhouse gases, particularly carbon dioxides (CO_2) which are the main anthropogenic greenhouse gases in the atmosphere.

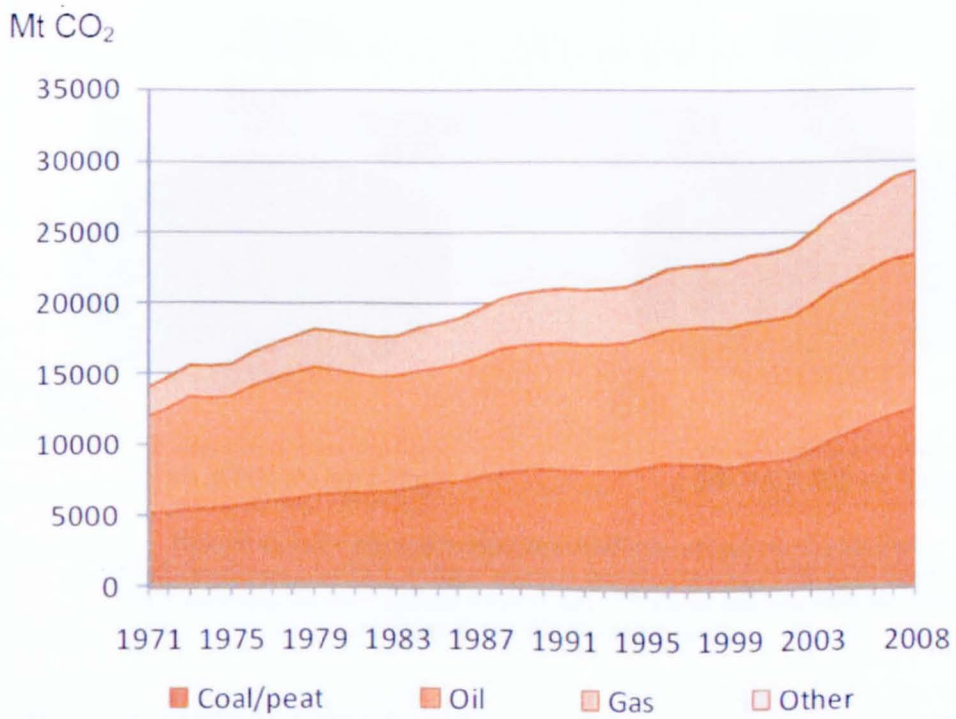

Figure 1.3 CO2 Emission by Fuel (International Energy Agency "CO2 Emissions from Fuel Combustion 2010" 2010)

The total annual emissions of anthropogenic GHGs have been continuously rising for many decades. According to IEA (International Energy Agency "CO2 Emissions from Fuel Combustion 2010" 2010), the energy production and use contributes about 65% of global anthropogenic greenhouse gas emissions. Furthermore, CO_2 emissions from the consumption of fossil fuel are the main source of anthropogenic CO_2 emissions. Figure 1.3 clearly demonstrates that over CO_2 emissions due to energy use have been on the increase for the past decades. Detailed comparisons of CO_2 emissions in 1973 and in 2007 are shown in Figure 1.4. The world man-made CO_2 emissions increased from 15640 Mt of CO_2 in 1973 to 28962 Mt of CO_2 in 2007. In 2007, 42.2% of the world man-made CO_2 emissions was due to coal consumption, whereas 37.6% and 9.8% were due to oil and natural gas consumptions, respectively. For many developing countries such as China and India, coal is to be filling much of the growing energy demands for coming decades. Reducing emissions must necessarily start with actions geared to reduce emissions form fuel combustion. (International Energy Agency "CO2 Emissions from Fuel Combustion 2010" 2010).

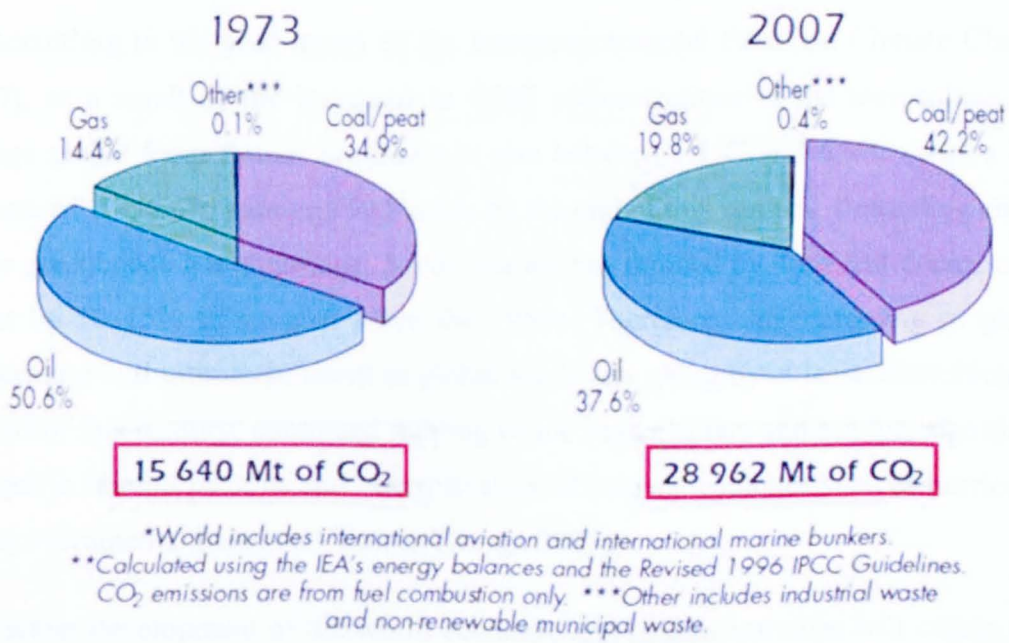

Figure 1.4 1973 and 2007 fuel shares of CO2 emissions(International Energy Agency "Key World Energy Statistics" 2008)

A number of scientific studies have revealed that the overall CO_2 levels in the atmosphere have been on the increase for past 200 years. Over the last three decades, the CO2 emissions have increased by an average of 1.6% per year (as shown by Figure 1.3). With the fastest growth in the last ten years (1.9ppmv per year from 1995 to 2005), the 2005 concentration of CO_2 in the atmosphere had reached 379 ppmv, which was about 35% higher than that of 150 years ago. 20 Giga tonne of CO2 added to environment over the past 150 years. During the pre-industrial era, the CO_2 concentration in the atmosphere had kept at a rather steady level of about 280 ppmv. Meanwhile, over the past 150 years emissions of methane (CH_4) and nitrous oxide (N_2O) have also increased at comparable levels to that of CO_2 emissions. The total CO_2 equivalent (CO_2-eq) concentration of all long-lived GHGs in the atmosphere is currently estimated to be about 455 ppm CO_2-eq (International Energy Agency "CO2 Emissions from Fuel Combustion 2010" 2010). The trends of continually increasing GHGs are expected to continue if additional low-carbon energy policy actions are not taken worldwide.

According to the year report of the Intergovernmental Panel on Climate Change (2007), as a result of the increases in GHG concentrations in the atmosphere, the average global temperatures are likely to rise between 1.1°C and 6.4°C (with a best estimate of 1.8 to 4°C) above 1990 levels by the end of this century, depending on our future greenhouse gas emissions. Arctic sea ice has thinned by 40% and decreased in extent by 10–15% in summer since the 1950s. Therefore, the increasing of global temperature will ultimately result in global sea levels rising by at least 26 to 59cm by the end of this century, continued melting of ice caps glaciers and sea ice, significant changes in rainfall patterns and intensification of tropical cyclones such as hurricanes (Intergovernmental Panel on Climate Change 2007).

Further development of the world economy and human activities will continue to demand more primary world energy supplies. It can be projected that the world GHG emissions would continue to grow if the world sticks with the current energy policy which heavily relies on fossil fuels to meet the global energy demand and ultimately lead to a significant adverse impact on the environment, resulting in increased health risks and the threat of global climate change. The continued increase use of fossil fuels also diminishes the limited world fossil fuel reserves and hence leads to the

problem of energy security for the growing world population. According to (Shafiee *et al.* 2009), the expected fossil fuel reserve depletion times for oil, coal and gas of approximately 35, 107 and 37 years, respectively. This means that coal reserves (Table 1.1) are available up to 2112 and will be the only fossil fuel remaining after 2042.

Table 1.1 Location of the world's main fossil fuel reserves in 2006(Shafiee et al. 2009)

Region	Fossil fuel reserve (Giga tonnes of oil equivalent)			
	Oil	Coal	Gas	Sum
North America	8	170	7	185
South America	15	13	6	34
Europe	2	40	5	47
Africa	16	34	13	63
Russia	18	152	52	222
Middle East	101	0	66	167
India	1	62	1	64
China	2	76	2	80
Australia and East Asia	2	60	10	72
Total	165	607	162	934

It is now clear that any effort to maintain atmospheric levels of greenhouse gas cannot be based fundamentally on a fossil fuel global economy. A transition to renewable-based energy systems should be taken place immediately.

There are a number of renewable energy resources such as biomass, wind, solar, hydropower, and geothermal that can substitute or reduce the use of fossil fuels. The potential of renewable energy resources is enormous as they can in principle meet many times of the world's energy demand.

1.3. Renewable Energy Resources

As pointed out above, currently most of the world primary energy is supplied by the diminishing fossil fuels. To tackle the future problems of the continuously rising CO_2 emissions, the global climate change and the energy crisis, it is imperative for the world and all of the nations to take immediate actions, finding the ways of reducing their CO_2 emissions such as replacing fossil fuels with renewable energy to meet their ever increasing energy demands.

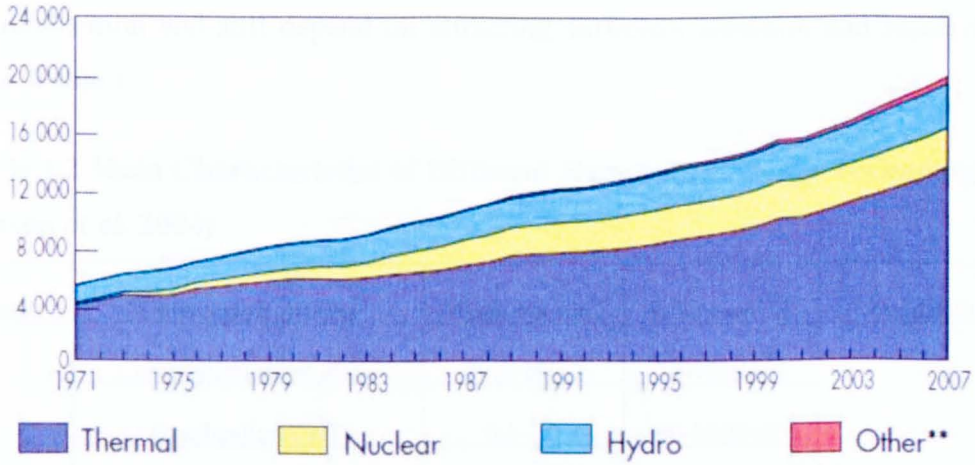

Figure 1.5 Evolution from 1971 to 2007 of world electricity generation by the power plant type (TWh) (International Energy Agency "Key World Energy Statistics" 2008)

Renewable energy is energy which comes from natural resources such as sunlight, wind, rain, tides, and geothermal heat, which are naturally replenished. In 2008, about 19% of global final energy consumption came from renewable resources, with 13% of this supply was dominated by traditional biomass, mostly fuel wood used for cooking and heating in developing countries, and 3.2% from large hydropower stations, which provided over 15% of the global electricity supply (Figure 1.5)(International Energy Agency "Key World Energy Statistics" 2008).Other renewable energy resources (solar energy, wind energy, modern bio-energy, geothermal energy, and small hydropower) are currently contributing for another 2.7% to the world primary energy supply and are growing very rapidly(Sawin *et al.* 2010).The share of renewable energy in electricity generation is around 18%, with 15% of global electricity coming from hydroelectricity and 3% from new renewable resources. Renewable energy

resources are sustainable based on current and future economic and social societal needs, producing minimum environmental impacts, and secondary wastes.

Renewable energy technologies are still under development. Although some of these technologies are widely accepted and have potential comparable to traditional energy technologies. For instances, solar water heater and solar cook are widely used all over the world, and wind energy for electricity production today is a mature, competitive, and virtually pollution-free technology widely used in many areas. There are still many more renewable energy technologies that have limited commercialization and still depend on attracting sufficient attention and research as shown in Table 1.2.

Table 1.2 Main Characteristics of Different Renewable Energy Technologies (Jacobsson et al. 2004)

Category	Conversion System	Scale Range,	Efficiency,%	Availability
Biomass	Combustion/stand alone	20.0-100.0	20-40(elect)	Seasonal, climate dependent
	Combustion/CHP	0.1-1.0	60-60(H+P)	
	Combustion/CHP	1.1-10.0	80-100(H+P)	
	Gasification/Diesel Turbine	0.1-1.0	15-25(elect)	
	Gasification/Gas Turbine	1.0-10.0	25-30(elect)	
	Gasification/BIG/CC	30.0-100.0	40-55(elect)	
	Digestion/Wet Biomass	Up to several	10-15(elect)	
Wind	Modern wind turbines	~50		Highly variable
Geothermal	Dry Steam Plants	35.00-120.0	10-25(elect)	Constant (capacity factor over 90%)
	Flashed Steam Plants	10.00-55.0		
	Binary Cycle Plants	0.25-130.0		
	Combined Cycle Plants	10.00-130.0		
IHRR	ORC	0.25-20.0	10-20(elect)	Constant,
Hydro	Run-of-River	0.1-14,000	80-93(elect)	Hydrology
Hydro	Reservoir storage	1.0-18,000	80-93(elect)	Utilisation factor
Solar	Photovoltaic (PV)	0.05-1.0kW	10-15(elect)	Daily weather dependent
	Thermal	5.0-100.0	10-24(elect)	

Renewable energy resources have the potential to play a more important role in the world's future energy supply than of today. In contrasting to fossil fuels, renewable energy resources such as solar and wind represent clean and inexhaustible energy resources and are the key to the low-carbon energy future(Bilgen *et al.* 2004). Dramatic increases in the use of renewable energy resources for the generation of electricity and heat, and transport should be targeted as soon as possible. At the present time, renewable energy is often founded on small-scale and decentralized applications. For instance in electricity generation, renewable systems based on PV arrays, windmills, biomass or small hydropower, are often used to supplement the main stream large-scale centralized power plants, although over 15% of the world electricity is currently generated from hydropower stations as already illustrated by Figure 1.5. Renewable energy systems can be the mass-produced "energy appliances" capable of being manufactured at low cost and tailored to meet specific energy loads and service conditions. These systems can have dramatically reduced as well as widely dispersed environmental impacts, rather than larger, more centralized impacts that in some cases such as with large-scale fossil fuel power plants are serious contributors to ambient air pollution, acid rain, and global climate change.

A number of studies have investigated the potential contribution of renewable energy resources to the global energy supplies and concluded that in the second half of the 21st century their contribution might range from the present figure of less than 20% to more than 50% with the right policies in place. For example, studies carried out by the European Renewable Energy Council (EREC), together with its member associations, concluded that a share of renewable energy up to 47.7% worldwide is possible by 2040 as shown in Table 1.3. The studies were based on the assumptions, which were derived from their experiences and cumulative knowledge, on expected annual installations growth rates of current different technologies (European renewable energy council 2004).

Table 1.3 clearly shows that renewable energy resources, especially the biomass, are pivotal to our future growth of energy resources. The development and use of renewable energy resources can not only enhance diversity in energy supply markets, but also contribute to securing long term sustainable energy supplies, help reduce local and global atmospheric emissions. Comparing with other renewable energy

resources such as solar and wind, biomass has the advantage for non-intermittent supply and operation. It can also be converted into various useful forms of energy such as heat, electricity and liquid fuels. The generation of electricity and heat was by far the largest producer of CO_2 emissions and was responsible for 41% of the world CO_2 emissions in 2008 (European renewable energy council 2004). Power generation relies heavily on coal, the most carbon-intensive of fossil fuels, amplifying its share in worldwide global emissions. Countries such as Australia, China, India, Poland and South Africa produce between 69% and 94% of their electricity and heat through the combustion of coal. China and India are the currently largest and the fourth largest CO_2 emitters among all nations as shown in Figure 1.6(International Energy Agency "World Energy Outlook 2008" 2008). Biomass can not only provide commercially attractive options to meet specific electricity service needs of developing countries such as China and India and rural areas but also reduce their CO_2 emissions.

Table 1.3 Global renewable energy scenario by 2040(European renewable energy council 2004)

	2001	2010	2020	2030	2040
World Primary Energy Consumption (IIASA)	10038.3	10549	11425	12352	13310
Biomass	1080	1313	1791	2483	3271
Large Hydro	222.7	266	309	341	358
Small Hydro	9.5	19	49	106	189
Wind	4.7	44	266	542	688
PV	0.2	2	24	221	784
Solar Thermal	4.1	15	66	244	480
Solar Thermal Electricity	0.1	0.4	3	16	68
Geothermal	43.2	86	186	333	493
Marine (tidal/wave/ocean)	0.05	0.1	0.4	3	20
TOTAL RES	1364.5	1745.5	2694.4	4289	6351
Total RES Contribution (%)	13.6	16.6	23.6	34.7	47.7

*Projections in million tons of oil equivalent (Mtoe)

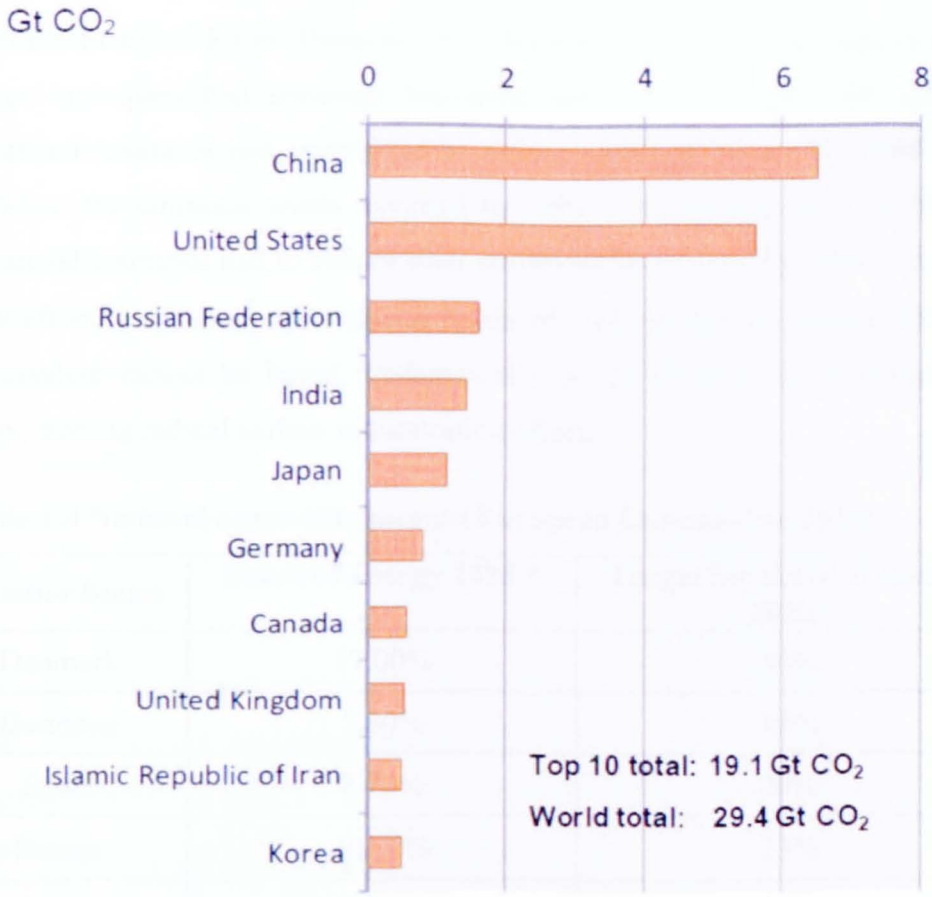

Figure 1.6 Top 10 emitting countries in 2008 (International Energy Agency "World Energy Outlook 2008" 2008)

1.4. Energy Policies of the European Union and United Kingdom

The growth of the world's economy and the development of human activities require an increase in the world energy supply. Conventional energy resources based on oil, coal, and natural gas have proven to be the highly effective drivers of economic progress, but at the same time causing damage to the environment and human health. Therefore, these traditional fossil fuel-based energy resources are facing increasing pressures from a host of environmental organisations worldwide. To reduce the greenhouse gas emissions of different countries, the Climate Convention was signed in Rio in 1992 to forecast, prevent, and limit the causes of climate change and reduces any negative effects to the environment(Second World Climate Conference 1992). This convention had been extended in 1997 in Kyoto,

Japan(United Nations Framework Convention on Climate Change 1997). The international treaty of Kyoto Protocol on GHG reduction targets set legally binding objectives and quantified emission limitation and reduction. The UN and many industrialized countries had committed to reduce GHG emissions by 2008 – 2012 compared to the emission levels recorded in 1990. Furthermore, by year 2050, the industrialized countries had to reduce their emissions by four to five times. It is clear that any effort to maintain atmospheric levels of GHG emissions around 550 ppmv CO_2-equivalent cannot be based fundamentally on an oil and coal-powered global economy, barring radical carbon sequestration efforts.

Table 1.4 National renewable targets(European Commission 2010)

Member States	Share of energy 2005 *	Target for share of energy 2020*
Denmark	17.00%	30%
Germany	5.80%	18%
Spain	8.70%	20%
France	10.30%	23%
Italy	5.20%	17%
Poland	7.20%	15%
Austria	23.30%	34%
Finland	28.50%	38%
Sweden	39.80%	49%
United Kingdom	1.30%	15%

*from renewable sources in final consumption of energy

The European Union has committed to reduce its greenhouse gas emissions by 8% to 12% by 2008-2012, referred to the level of 1990, and 20% GHG reduction among EU countries by 2020. Appropriate energy policies are vital to attain these objectives and bring about the transition to a low-carbon economy within the EU. According to Europe 2020(European Commission 2010), the EU's growth strategy for the coming decade, the Europe Union should reduce greenhouse gas emissions by at least 20% compared to 1990 levels, or by 30% if the conditions are right, and increase the share of renewable energy in final energy consumption to 20%, and achieve a 20% increase

in energy efficiency(European Commission 2010). The strategy specifically set national renewable energy targets for each Member State as shown in Table 1.4. European Commission also passed a directive on the promotion of electricity produced from renewable energy resources setting a target of 21% of renewable energy share in electricity production by 2010. The vision of the EU-25 (European Union 2004) which follows the EU's initial target of 12% renewable energy by 2010 sets the new targets for the share of the renewable energy of 35% by 2030 and 65% in 2050 (European Parliament 2001).

UK signed the Kyoto Protocol in December 1997 which became legally binding in February 2005. Accordingly, GHG emissions of the UK were required to be reduced by 12.5% between 2008 and 2012 and to seek to reduce emissions to 20% below 1990 levels by 2010 (DWFRA UK 2007). However, many parts of the UK's energy policies are governed or affected by the legislations or policy initiatives agreed with other EU countries. For example, renewable energy targets (electricity, bio-fuels and heat) will play a part in achieving the EU's overall 20% target for renewable energy in the energy mix, and the UK's national target of 15%.

In 2005, the UK produced only 1.3% of final energy from renewable resources and the only Member States that produced less percentage of their energy from renewable energies in the Europe Union were Malta and Luxembourg. Therefore, a radical increase in the use of renewable energy in the UK is urgently needed and should be an integral part of the UK energy strategy to decarbonise energy production in the future. This is also a significant economic opportunity for the UK to move into a low-carbon economy as it can not only ensure the security and safety of future energy supplies but also spread the energy costs fairly. Renewable energy has a key role to play in enabling the UK to meet its future energy challenges. Alongside with energy saving, nuclear power, carbon capture and storage and other low-carbon technologies, renewable energy technologies should be well developed to meet the UK's national goals over the coming decades. The UK Renewable Energy Strategy (Secretary of State for Energy and Climate Change 2009) stated that the overall fossil fuel demand of UK should be reduced by around 10% and gas imports decreased by 20–30% against what they would have been in 2020. Another outstanding opportunity for the UK economy with the potential of renewable energy is to create up to half a million

more jobs in renewable energy sectors resulting from around £100 billion of new investment. By the year of 2020, more than 30% of the electricity, 12% of heat , and 10% of transport energy can be generated from renewables as illustrated by Figure 1.7 (Secretary of State for Energy and Climate Change 2009). The UK's renewable fuels, materials and products can be derived from a wide range of crops and other biomass including forestry, agricultural residues and other organic waste. They can substitute for fossil or mineral resources for the production of various products and therefore help mitigate climate.

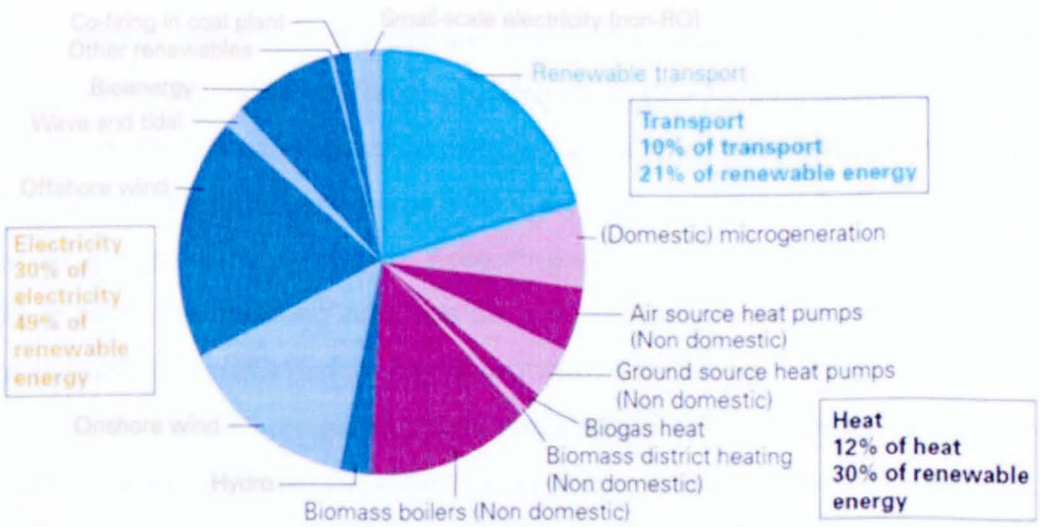

Source: DECC analysis based on Redpoint/Trilemma (2009), Element/Pöyry (2009) and Nera (2009) and DfT internal analysis

Figure 1.7 Illustrative mix of technologies in lead scenario, 2020 (TWh)

In addition to environmental benefits, using more renewable energy resources in the UK energy mix may also have other economic benefits in the future. Demands for fossil fuels are continuously increasing, particularly due to the huge rises in population and wealth of emerging economies such as China and India. Meanwhile, extracting fossil fuels from remote countries and regions always contains unpredictable risks and costs. As the UK's own oil and gas resources decline, UK will be more relying on foreign imports of gas and oil and become more passive to the high oil and gas prices of world energy market. The 2050 Pathways of DECC (Department of Energy & Climate Change "2050 Pathways Analysis" 2010) pointed out that there are various possible combinations of three different low carbon technologies which should work in the UK power sector: renewable energy, nuclear,

and carbon capture and storage. Recently, the UK Government has extended the Carbon Emissions Reduction Target (CERT) of 12.5% to the end of 2012 (Office of Gas and Electricity Markets 2011). According to the Energy Strategy of EU, UK should also move from the current 20% target to a 30% target for GHG emission reductions by 2020 (Department of Energy & Climate Change "Annual Energy Statement 2010" 2010). To achieve these targets, the UK will have to accelerate the applications of renewable energy and energy efficiency measures such as implementing insulation measures to the existing buildings. Renewable energy resources such as biomass, wind, solar, hydropower, and geothermal can provide sustainable energy services to the UK and therefore a transition to renewable-based energy systems in the UK is very much possible and is now looking increasingly more likely. Besides, the costs of renewable energy such as solar and wind power systems have dropped substantially over the past 30 years, and continue to decline, while the price of oil and gas continue to rise. According to the European Renewable Energy Council in 2006, in developed countries there is a growing trend toward employing modern technologies and efficient bio-energy conversion using a range of biomass, which are becoming cost competitive with traditional fossil fuels (Kralova Iva *et al.* 2010). In fact, fossil fuel and renewable energy prices, social and environmental costs are heading in opposite directions. It is becoming clear that the future growth in the energy sector of the UK is primarily in the new regime of renewables, and to some extent natural gas-based systems, and not in conventional oil and coal sources. Financial markets are awakening to the future growth potential of renewable and other new energy technologies, and this is a sign of the economic reality of truly competitive renewable energy systems (A.V. Herzog *et al.* 2002).

1.5. Energy Use in the UK Residential Sector and Its CO_2 Emissions

The UK residential sector accounted for about 30% of the nation's total energy end-use and more than one-quarter of its total GHG emissions. This includes both direct and indirect (such as electricity) energy use as shown in Figure 1.8. The power sector is particularly important in this context because the residential sector accounts for about 35% of the UK's total electricity consumption (R. Kannan. *et al.* 2009). Residential energy end-use also accounts for more than 40% of the EU's final energy demand (European parliament and of the council 2006).

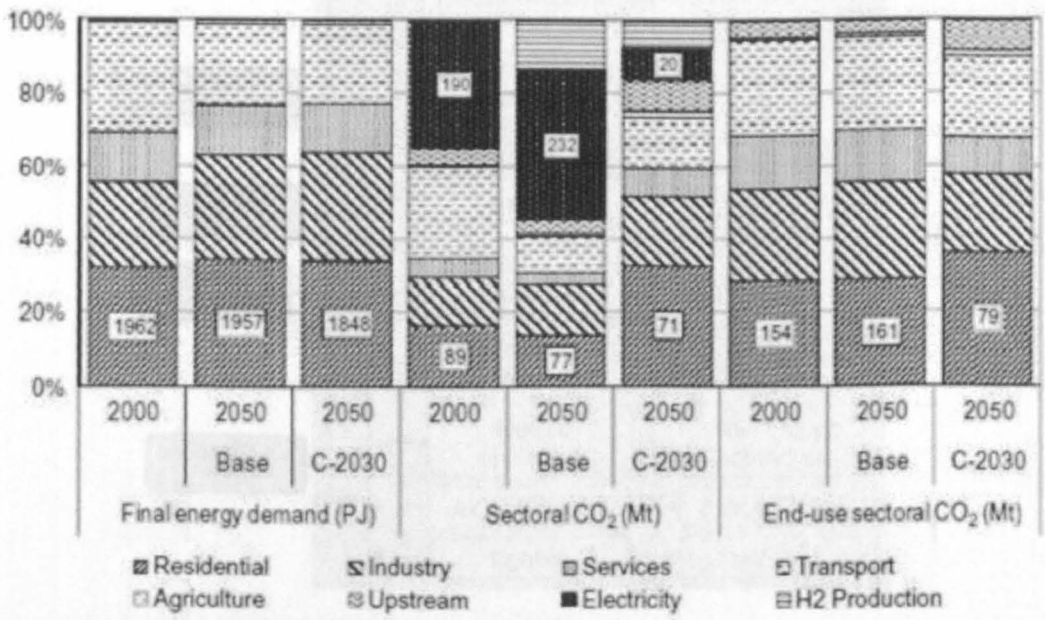

Figure 1.8 Share of sectoral final energy demand and CO2 emissions for the BASE and C-2030 scenarios in 2050(R. Kannan. et al. 2009)

The UK government has set a groundbreaking target of 60% reduction of long-term national carbon dioxide (GHG) emissions by 2050, from the level of 2000(Committee on Climate Change UK 2008). This stringent target needs all sectors including the residential to contribute substantially to emissions reductions. A much broader range of current and anticipated policies are needed to address the emissions reductions options across all sectors of the UK economy(Department for Environment *et al.* 2006). EU had introduced the Directive on the End-Use Efficiency and Energy Services of Building Sector to reduce energy consumption(European parliament and of the council 2006).

Figure 1.9 shows the common energy structure in the UK residential sector(R. Kannan. *et al.* 2009). As listed on the left hand side of the figure, CO_2 emissions from the energy use in the residential sector comprise of the direct emissions associated with the use of fuel (gas, oil, etc) and the indirect emissions associated with the use of electricity, district heating and cooling. A wide application of micro-generation technologies in the residential sector will lead to the reduction of CO_2 emissions from the sector as the micro-generations can lead to higher efficiency, lower demand for grid electricity and/or fuels.

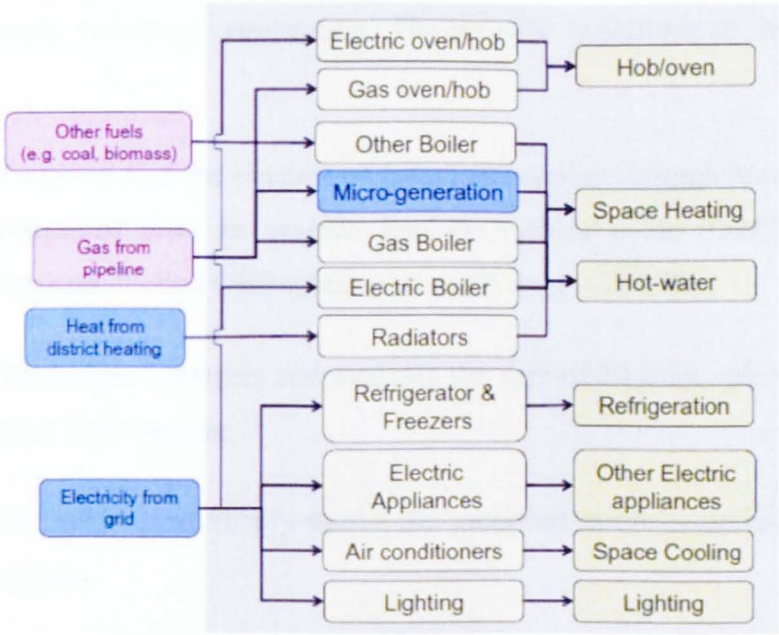

Figure 1.9 Energy structure of residential sector in the UK(R. Kannan. et al. 2009)

In general, there are mainly two types of micro-generation technologies that can be used in the residential sector: one is to generate electricity only such as solar PV and micro wind turbines, and the other is to generate both electricity and heat such as natural gas-based micro-scale combined heat and power (CHP). The use of micro-scale combined heat and power systems in the residential sector could have substantial benefits in terms of energy efficiency and reducing environmental impacts. The environmental benefit of using micro-scale CHP in buildings could be even bigger if the micro-scale CHP is fuelled by a renewable resource such as biomass. The

development of a micro-scale biomass-fuelled CHP has been the main topic of the present research over the past several years.

1.6. Project Objectives, Methodology and Thesis Outline

The present PhD research is an integral part of a bigger externally funded research project which aims to develop and evaluate a novel, first-of-its-kind, micro-scale (1 – 2 kWe) biomass-fired combined heat and power (CHP) system suitable for public and large domestic buildings' application. The specific objectives of the overall project are:

- To prove that the concept of power generation through biomass combustion combined with an organic Rankine turbine cycle (ORC) is suitable for biomass-fuelled CHP systems as small as (1 – 2) kWe;
- To design, construct and evaluate the first-of-its-kind, micro-scale biomass-fired CHP system;
- To thermodynamically model the proposed micro-scale biomass-fired CHP system.

The specific tasks of the present PhD research are:

- To thermodynamically model the micro-scale biomass-fired CHP system with ORC: different environment-friendly working fluids will be modelled with the ORC process.
- To experimentally evaluate the micro-scale biomass-fired CHP system in terms of power generation and combined heat and power performance.
- To experimentally investigate the combustion performance and NOx emissions of the biomass pellet boiler which is a key component of the micro-scale biomass-fired CHP system.

The main methodologies of the present PhD research are the thermodynamic modelling of the proposed micro-scale biomass-fired CHP system with ORC and the

laboratory testing of the assembled micro-scale biomass-fired CHP system and its main components (biomass boiler, ORC turbine, alternator, heat exchangers etc.).

Following the introduction of relevant background of the research in this Chapter (Chapter 1), Chapter 2 of the thesis will review literature related to biomass, CHP and biomass-fuelled CHP. Chapter 3 will present the details of thermodynamic modelling of the proposed micro-scale biomass-fired CHP system with ORC. Chapter 4 will describe the details of the laboratory testing system of the assembled micro-scale biomass-fired CHP system and its main components. Experimental results and their discussion will be presented in Chapter 5, and finally conclusions and future research recommendations will be given in Chapter 6.

Chapter 2. Literature Review

2.1 Biomass as a Renewable Energy Resource

As explained in the last chapter, using fossil fuels to meet the increasing world energy needs have led to environmental pollution globally. However, nowadays many renewable energy sources were defined to be reliable and plentiful alternatives to the depleting fossil fuels and offer improved security of our future energy supply. Biomass, a traditional renewable energy source, currently is the fourth largest world primary energy supply, providing approximately 14% of the world's primary energy. In developing countries, biomass accounts for approximately 35% or higher of the primary energy supply. Biomass is a versatile source of energy in that it can be readily transformed into convenient fuels, electricity and heat by means of a variety of biomass conversion technologies, such as thermochemical (combustion, gasification, pyrolysis) and biochemical (fermentation, anaerobic digestion) approaches. Biomass combustion is the simplest and the most mature technology that has been widely used in both the ancient and modern times. In addition to heat, biomass combustion also releases carbon dioxides, similar to fossil fuel combustion.

2.1.1. Biomass as a solar energy store

Biomass is a very broad term which is used to describe material of recent biological origin that can be used either as a source of energy or for its chemical components(IEA Bioenergy). Biomass includes trees, crops and other plants, as well as agricultural and forest residues. It also includes many materials that are considered as wastes by our society including food and drink manufacturing effluents, sludges, manures, industrial organic by-products and the organic fraction of household waste. In many ways biomass can be considered as a form of stored solar energy. The energy of the sun is 'captured' through the process of photosynthesis in growing plants as shown in Figure 2.1 (Larkin S. *et al.* 2004).

Although bio-energy or biomass energy is usually used to denote the energy that is derived from biomass, biomass and bio-energy have been used interchangeably by many people.

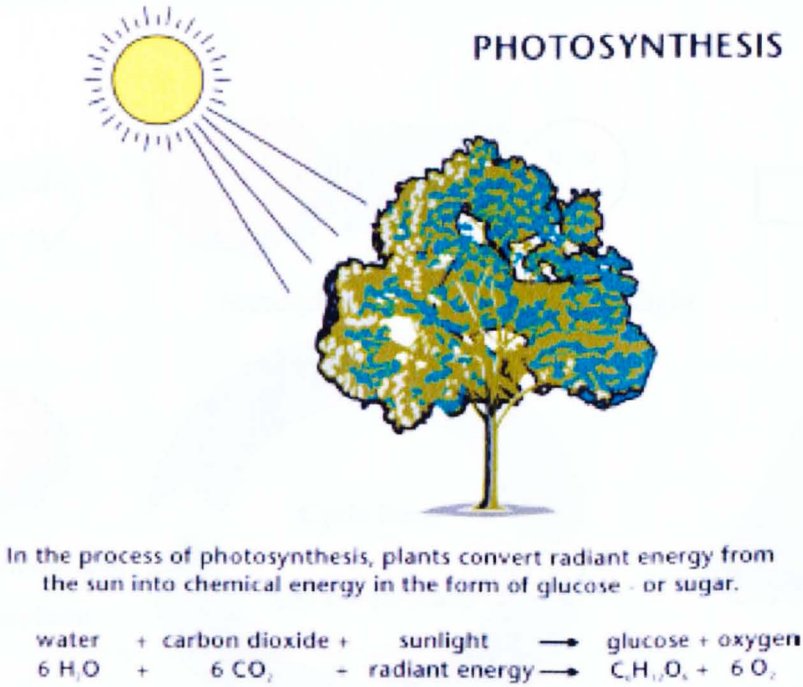

Figure 2.1 Biomass as a solar energy store(Photosynthesis)

2.1.2. Biomass as a renewable energy resource

Biomass can be considered as a renewable energy resource although burning biomass releases carbon dioxides (CO_2) to the atmosphere similar to burning fossil fuels(Liu H. 2011). There is a vital difference in CO_2 releases between burning a fossil fuel and burning biomass. Burning a fossil fuel releases CO_2 that has been locked up for millions of years in the ground, affecting the natural CO_2 cycle and resulting in an increase in the CO_2 concentration in the atmosphere. Burning biomass simply returns to the atmosphere the same amount of CO_2 which was absorbed from the air via the photosynthesis process while the biomass plant was growing over a relatively short period of time (a few years to ca. decade), and there is no net release of CO_2 to the atmosphere, i.e., CO_2-neutral, if the cycle of growth and harvest is sustained.

Therefore, biomass can consider as a renewable energy resource as shown in Figure 2.2 (Liu H. 2011). If the production and transportation of the biomass fuel involves the use of fossil fuels, there would be some net releases of CO_2 with biomass combustion (Liu H. 2011)

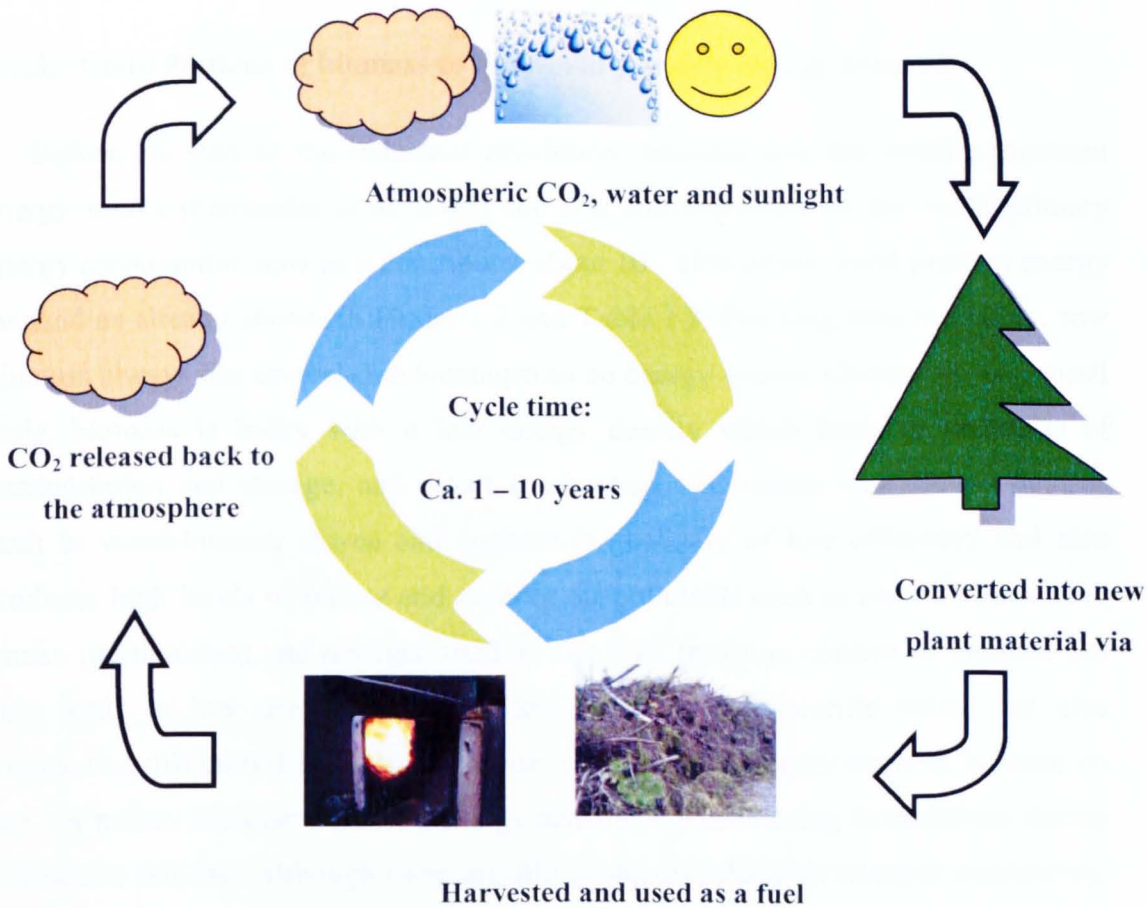

Figure 2.2 Biomass is a renewable energy resource(Liu H. 2011)

In fact, real biomass energy production systems are differing from the ideal carbon cycle shown in Figure 2.2 in two important ways. Firstly, the production of biomass energy always consumes fossil energy for the farming, transportation and production stages of the process (Hill *et al.* 2006). Secondly, land-use change into large-scale biomass plantations may also lead to the climate change locally. The carbon balance of a biomass energy production site is largely depending on the pre-existing vegetation and soil etc. For instance, deforestation typically releases larger amount of the tree and soil carbon dioxides to the atmosphere more than the amount of CO_2 that can absorbed by replanting (Harmon *et al.* 1990). However, in some cases, managing degraded farmland as perennial agriculture bio-fuel production can increase soil

carbon as a consequence of consistent increase of plant root and waste (Schaeffer *et al.* 2006). Although biomass production and use cannot be absolutely carbon-neutral, biomass resources still have many advantages compared with traditional fossil fuels and are potentially the largest renewable global energy source (Herzog *et al.*).

2.1.3. Contributions of biomass to the world primary energy demand

Before the start of the industrial revolution, biomass was the world's dominant energy source (Fernandes *et al.* 2007) and it is still important for the world primary energy consumption now as it contributes about 10 - 15% of the world primary energy demand as already shown in Figure 1.2 and Table 1.3. For long time in history, raw biomass always has several disadvantages as an energy source. Compared with fossil fuels, biomass is bulky with a low energy density which leads to problems of transportation and storage, and direct combustion of biomass with simple devices such as wood-burning stoves and cookers is generally of low efficiency and also produces high levels of indoor and outdoor air pollutants such as carbon monoxides, smoke (particulates) and nitrogen oxides. The high moisture content of biomass not only leads to low useful energy content, i.e. low net calorific value, but also combustion difficulty(Liu H. 2011). Modernized biomass energy research is based on two key points: increase the fuel's energy density, and decreasing its emissions during production and use. Although there are still problems related to resource availability, technologies of utilisation and economic feasibility, etc, biomass is considered as one of the most promising renewable energy resources capable of making greater contribution to the future world energy supply(European Renewable Energy Conference 2004). Table 2.1 shows the current levels of bioenergy production and use in the UK. It is apparent that the contribution of biomass energy to the UK overall energy demand is considerably less than that of the world average. This mean there is a considerable scope of further development of biomass/bio-energy industry within the United Kingdom.

Table 2.1 Current levels of bio-energy production and use in the UK (Defra UK et al. 2007)

	Quantity	Year	Million tonnes of oil equivalent (Mtoe)	Percentage of UK total
Bioenergy use				
Bioethanol	85 million litres	2005	0.04	0.2%
	(169 million litres)	(2006)	(0.05)	(0.2%) of total transport fuel sales
Biodiesel	33 million litres	2005	0.03	0.1%
	(169 million litres)	(2006)	(0.14)	(0.3%) of total transport fuel sales
Bioenergy generation				
Electricity	3.1 Mtoe	2005	3.1	3.5% of UK electricity production
Heat	0.45 Mtoe	2005	0.45	0.6% of heat generation

2.1.4. Categories and characteristics of biomass materials

There are various kinds of categories of biomass resources which can include a wide range of materials. For the economic reason, some high value materials such as good quality large timber may not be used for energy applications. However, there are still large quantity of low value plants, co-products and agricultural waste which could potentially become available as relatively low cost biomass resources such as those listed by the Biomass Energy Centre of the UK (Biomass Energy Centre):

- **Virgin wood**, from forestry, arboriculture activities or from wood processing
- **Energy crops**: high yield crops grown specifically for energy applications
- **Agricultural residues**: residues from agriculture harvesting or processing
- **Food waste**, from food and drink manufacture, preparation and processing, and post-consumer waste
- **Industrial waste and co-products** from manufacturing and industrial processes.

Various forms of bio-energy and bio-fuels can be derived from raw biomass materials using the current available biomass energy conversion technologies which are to be described in the following section. Figure 2.3 shows the flow chart of bioenergy production from raw biomass materials.

Proximate analysis, ultimate analysis and calorific value are commonly used to characterize a biomass material as a fuel. The proximate analysis serves as a simple means for determining the behaviour of a solid biomass fuel when it is heated. It determines the contents of moisture, volatile matter, ash and fixed carbon of the fuel. On the other hand, the main purpose of an ultimate analysis is to determine the elemental composition of the solid fuel substance. The calorific value of a fuel is a direct measure of the chemical energy stored in the fuel. Table 2.2 shows the proximate, ultimate and calorific values of selected biomass materials in comparison with selected lignites and bituminous coal.

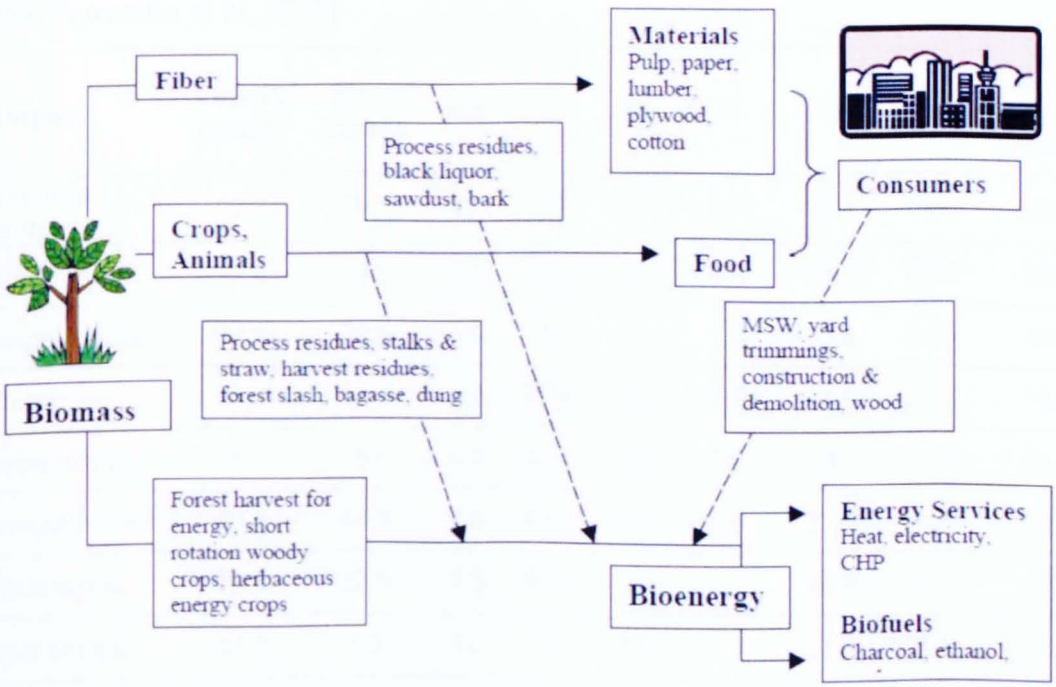

Figure 2.3 Flow chart of biomass to bio-energy(IEA Bioenergy)

As already discussed above, raw biomass materials usually contain high level of moisture. Table 2.2 shows that biomass samples display higher amounts of volatiles than coal samples which could be considered as beneficial to combustion or gasification processes. The ash content of mostly biomass samples is lower than that

of coal, indicating biomass can be a good quality fuel. Gross calorific values (GCV) (or the high heating values (HHV)) of biomass materials vary greatly and can be comparable to the low rank coals such as lignite (Vamvuka *et al.* 2010).

Comparing the chemical characteristics of biomass materials and several traditional fossil fuels, the ultimate analysis shows that the percentage of hydrogen is comparable for all samples, while biomass materials contain lower carbon. Also, the elemental oxygen content of biomass materials is much higher than that of coals. The sulphur content of biomass samples is also usually lower than coals, implying that SO_x emissions from biomass combustion can be of less concern. On the other hand, nitrogen values of some biomass materials can be above 1% (especially for waste wood) and this could present a problem for combustion processes - producing high level of NO_x emissions.

Table 2.2 Proximate, ultimate analyses and calorific values of the fuels (Wt% , dry)(Vamvuka et al. 2010)

Sample	Volatile matter	Fixed carbon	Ash	C	H	N	O	S	GCV* (MJ/kg)
Ptolemais lignite	47.7	39.3	13	55	5.3	1.9	24.1	0.65	20.8
Olive kernel	72.6	24.8	2.6	51.2	6	0.8	39.3	0.09	20.4
Cotton residue	72.8	20.6	6.6	47	6	1.8	38.4	0.19	18.3
Vine shoots	74.5	21.7	3.8	47.6	5.6	1.8	41.1	0.08	16.8
Forest residue	79.8	20	0.2	53.2	6.2	0.3	40	0.09	21.7
German lignite	50.7	44.7	4.6	61.2	5.1	0.9	27.9	0.3	23.9
Waste wood	73.8	22.9	3.3	45.7	6	4.5	40.3	0.13	17.6
Paper sludge	47.7	1.3	51	23	2.8	1.7	21.3	0.1	7.1

* Gross calorific Value

2.2. Biomass Energy Conversion Technologies

Biomass materials can be converted to various useful forms of energy such as heat, electricity and liquid fuels. The technologies used to convert biomass into energy ranged widely from the simple combustion of biomass used for cooking and heating in developing countries to a variety of technologies to generate modern energy carriers – electricity, gas, and liquid bio-fuels. Table 2.1 has already showed that the UK are using various materials including waste and residuals to generate electricity, heat and ,bio-liquid fuels (bio-ethanol and biodiesel) (Defra UK *et al.* 2007). Morden biomass energy can be used at the household (~10 kW), community (~100 kW), or industrial (~ MW) scale. The different technologies used to convert biomass materials into various forms of bio-energy tend to be classed in terms of either the conversion process they use or the end product produced. Liu has discussed three categories of biomass conversion processes(Liu H. 2011).

- Thermo-chemical processes which include direction combustion, gasification and pyrolysis;
- Biological processes which include fermentation and anaerobic digestion;
- Chemical/Mechanical processes which are involved in the production biodiesel.

The main purpose of modern biomass pyrolysis, so-called 'fast pyrolysis', is to produce bio-oil which can be used for a range of purposes including as liquid fuels and chemical ingredients, whereas biomass fermentation is to produce bio-ethanol which can be used for a transportation fuel similar to biodiesel.(Liu H. 2011) Anaerobic digestion of wet biomass such as organic waste can generate biogas which is rich in methane and can be used for various purposes such as cooking and power generation(Liu H. 2011). As the principal categories of biomass conversion technologies that are currently used for combined heat and power generation are direct combustion and gasification, these two biomass energy conversion technologies will be further discussed below.

2.2.1. Direct combustion of biomass

Direct combustion is the most common way of converting biomass to energy - both heat and electricity - and worldwide it already provides over 90% of the energy generated from biomass. Direct combustion of solid biomass fuels is well understood, relatively straightforward, commercially available, and can be regarded as a proven technology. Biomass combustion systems can be easily integrated with existing infrastructure. Direct combustion of biomass for heat generation is widely used in cold climate regions where there are significant annual demands for space heating and hot water. Domestic biomass-fired heating appliances in the developed counties such as the EU and UK have been improved with automation and standardized fuel supplies (e.g. wood pellets). Compared with traditionally open fireplaces, these advanced domestic biomass appliances not only achieve efficiencies of over 70% but also with greatly reduced atmospheric emissions(Liu H. 2011)

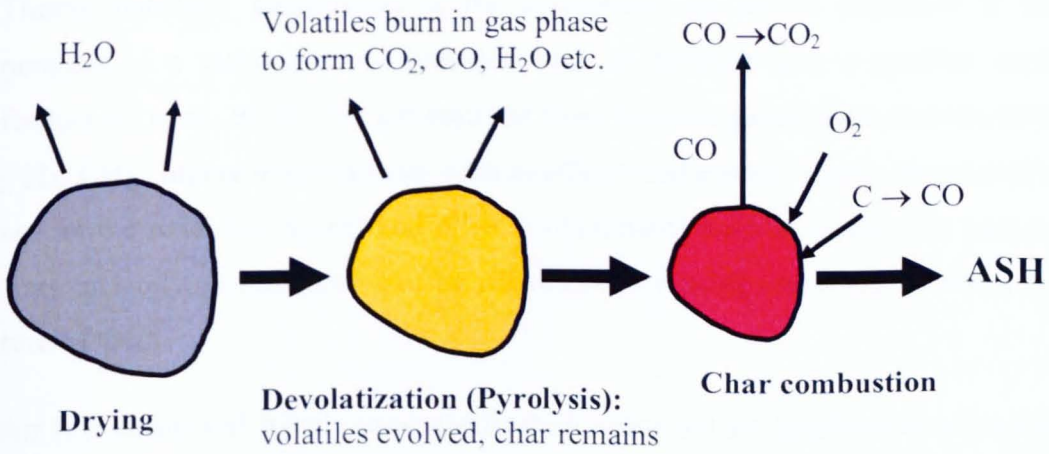

Figure 2.4 Three steps of biomass combustion(Liu H. 2011)

The combustion of a solid biomass material consists of three main steps as shown in Figure 2.4 (Liu H. 2011)

- The 1st step is drying, i.e. the evaporation of any water contained in the biomass material - this step does not produce energy but consumes energy.
- The 2nd step is the volatile release (devolatisation) and combustion step – the volatiles are released as a mixture of vapours (CO, CO_2, H_2, H_2O, C_xH_y

etc.) as the temperature of biomass materials rises; the combustion of volatile matter produces the flame seen around the burning solid fuel;

- The 3rd step is the char combustion step - the solid which remains after devolatisation consists of char (mainly carbon) and inert matter. The char burns to produce CO_2 whereas the inert matter becomes ash.

Direction combustion of biomass is widely practiced at all scales from domestic heaters to power plant boilers with specific combustion technologies including fixed - beds (e.g. stoker boilers), fluidized beds, and entrain-beds as well co-firing(Van Loo *et al.* 2008).

2.2.2. Biomass gasification

Thermo-chemical gasification is the conversion by partial oxidation at high temperature of a carbonaceous feedstock such as biomass into a gaseous energy carrier(Liu H. *et al.* 2010). The gas resulted from biomass gasification consists of CO, CO_2, H_2, CH_4, higher hydrocarbons such as ethane and ethene, water, nitrogen (if air is used as the oxidizing agent) and other contaminants such as small char particles, ash, tars and oils. Gasification can be carried out by using air, oxygen, steam or a mixture of them.

Air is a cheap and widely used gasification agent but air gasification of biomass produces a low calorific value gas (ca. 3 – 6 MJ/Nm^3) which is suitable for boiler, engine and turbine operation but not for pipeline transportation due to its low energy density(Liu H. *et al.* 2010). Oxygen gasification of biomass produces a medium calorific value gas (ca. 10 – 15 MJ/m_3) suitable for limited pipeline distribution and as synthesis gas for conversion, for example, to methanol and gasoline. Such a medium calorific value gas can also be produced by steam gasification.

There are many different designs of gasifiers including downdraft and updraft gasifiers, fluidized bed gasifiers and entrained flow gasifiers etc.(Knoef *et al.* 2005), but with the same set of main gasification reactions: those of hot steam and oxygen interacting with the biomass(Larkin S. *et al.* 2004). Similar to the combustion steps shown in Figure 2.4, the gasification process begins with the drying of the biomass to

evaporate moisture, followed by the release of the volatiles from the heated biomass, leaving the char. Volatiles and char in turn undergo partial oxidation reactions with steam and oxygen, resulting in the combustible gas.

Although biomass gasification has been practiced for over 100 years, so far it has had a very limited commercial impact on energy market due to competition from other energy resources. However small gasification plants (<300 kW) are now available commercially, often combined with gas engines driving small generators, and demonstration plants in the range 10-30 MW have been in operation since the mid-1990s(Larkin S. *et al.* 2004).

According to Renewable Energy Projects Handbook 2004 of World Energy Council(World Energy Council 2004), the modern biomass conversion technologies can be separated into three basic categories:

- Direct combustion processes
- Thermo chemical processes: Gasification
- Biochemical processes: Bio-fuel

Table 2.3 Summary of Biomass CHP Conversion Technologies

Biomass Conversion Technology	Common Fuel Types	Feed Size	Moisture Content	Capacity Range
Stoker grate, underfire stoker boilers	Sawdust, bark, chips, hog fuel, shavings, end cuts, sander dust	0.25–2 in.	10–50%	4 to 300 MW (many in the 20 to 50 MW range)
Fluidized bed boiler	Wood residue, peat, wide variety of fuels	< 2 in.	< 60%	Up to 300 MW (many in the 20 to 25 MW range)
Cofiring—pulverized coal boilers	Sawdust, bark, shavings, sander dust	< 0.25 in.	< 25%	Up to 1000 MW
Cofiring—stoker, fluidized bed boilers	Sawdust, bark, shavings, hog fuel	< 2 in.	10–50%	Up to 300 MW
Fixed bed gasifier	Chipped wood or hog fuel, rice hulls, shells, sewage sludge	0.25–4 in.	< 20%	Up to 50 MW
Fluidized bed gasifier	Most wood and agriculture residues	0.25–2 in.	15–30%	Up to 25 MW

Source: Based on Wright, 2006.

The principal categories of biomass conversion technologies for power and heat production are direct-fired and gasification systems. Within the gasification category, specific technologies include fixed bed gasifiers and fluidized bed gasifiers. Direct combustion remains the most common technique for deriving energy from biomass

resources for both electricity production and heat. Currently around 4.6% of UK's electricity comes from renewable energy resources in which Biomass has contributed around half of that supply(Defra UK *et al.* 2007). There are diversiform technologies in the world today for electricity generation from biomass. The typical capacity of existing biomass power plants ranges from 1 – 50 MW in size. Most of today's biomass power plants are direct-fired systems with steam-Rankine cycle. The biomass fuel is burned in a direct combustion boiler to produce high-pressure steam that is used to power a steam turbine-driven power generator. In many applications, steam is extracted from the turbine at medium pressures and temperatures and is used for process heat, space heating, or space cooling. Although technologies and processes to increase these efficiencies are being developed, due to the small size, energy conversion efficiencies are relatively low at about 15 – 25 percent. However, Steam cycle plants are often located at industrial sites, where the waste heat from the steam turbine is always recovered and used for meeting industrial process heat needs. Such combined heating and power (CHP), or cogeneration systems with direct biomass combustion provide higher levels of energy services per unit than systems that only generate power. The overall efficiencies of this biomass CHP system can be greater than 80%, which remains the most common technique for deriving energy from biomass. Furthermore, advanced combustion technologies, such as the application of fluidised bed combustion and advanced gas cleaning make great effort to the efficient production of electricity and heat in biomass combined heat and power installations. Within the range of about 50-80 MW_e, electrical efficiencies could possibly around 30-40% today. An alternative to the above-described direct combustion biomass technologies is biomass co-combustion with fossil fuels in existing boilers, which is considered as low-cost option for the nearest term. Successful demonstrations using biomass as a supplementary energy source in large high efficiency boilers have been carried out in many countries. Experiments showing that carefully control the range of biomass fuels at around 10–15 percent of the total energy input can minimal plant modifications and no impact on the plant efficiency and operation. Hybrid systems combining biomass with fossil fuel is proved feasible and environment friendly. Besides, it's also economical for the biomass fuels are lower cost than the fossil fuels.

Alternatively, biomass can be digested or fermented to produce biogas or bio-liquids. The resulting biogas or bio-liquids can be combusted for heat and electricity.

Another extensive use of bio-fuel in developed countries is producing petroleum-based fuels from biomass, which can be used as replacement of gasoline or kerosene (Herzog *et al.*).

2.3. Combined Heat and Power (CHP)

2.3.1. Background

Combined heat and power (CHP), which is also called cogeneration is the use of a heat engine or a power station to sequentially or simultaneously generate both electricity and useful heat. CHP is a well developed concept which can date back to the 1880s, when steam was a primary source of energy in industry and electricity was beginning to be used. On-site industrial power plants with cogeneration of power and heat were the main power systems in the early 19th. Then the development of large central power plants with higher efficiency and reliable utility grids, together with the low fuel costs and advances in technology, drove the electricity prices down and contributed to the decline of cogeneration. However, over the past decades, the increases in the world fossil energy price, the uncertainty with the fuel supplies, the deteriorating environment and the predicted global climate change have become serious problems to the entire human being and this results in CHP gaining attention again because of its potentials for fuel savings and low GHG emissions. Today, CHP represents a series of proven, reliable and cost-effective technologies that are already making an important contribution to meeting global heat and electricity demands. Due to the enhanced energy supply efficiency and utilisation of waste heat and low-carbon renewable energy resources, CHP, particularly together with district heating and cooling (DHC), is an important part of national and regional GHG emissions reductions strategies(Oliver 2006). The UK government has identified CHP as one of the key components of its CO_2 abatement program which represents the most significant individual measure in achieving the European Union's CO2 reduction targets (150Mt of a total of 800Mt)(European Commission 1997). The EU directive "on the promotion of cogeneration based on a useful heat demand in the internal energy market" states that(EU Cogeneration Directive 2004) :

- the potential for use of cogeneration as a measure to save energy is underused in the Community at present;

- promotion of high-efficiency cogeneration based on a useful heat demand is a Community priority given the potential benefits of cogeneration with regard to saving primary energy, avoiding network losses and reducing emissions, in particular of greenhouse gases;

- in addition, efficient use of energy by cogeneration can also contribute positively to the security of energy supply and to the competitive situation of the European Union and its Member States;

- it is therefore necessary to take measures to ensure that the potential is better exploited within the framework of the internal energy market'.

The overall efficiency of electricity generation has been improved over time, but the transition from primary energy such as fossil, biomass or nuclear fuels to electricity is still an inefficient process. According to the Second Law of Thermodynamics, thermal power systems inevitably reject heat into the environment and the thermal efficiency of a heat engine cannot be 100%. In fact, the maximum thermal efficiency of any heat engine cycle is the efficiency of a reversible Carnot heat engine(Cengel *et al.* 2006):

$$\eta_{Carnot} = 1 - T_L/T_H \tag{2.1}$$

Where T_H is the maximum temperature available (e.g. the metallurgical limit) and T_L is the lowest temperature available (e.g. cooling water temperature for the condenser of a steam-Rankine cycle-based power plant). Further, the power generation efficiency of most engines and power plants are much lower than the potential maximum efficiency. For instance, the power generation efficiency of gas turbines varies from 20% to about 40%, which indicates 60% to 80% of the heat supplied into gas turbines via burning of fuels is wasted. While some modem power plants can achieve nearly 60% power generation efficiency, most operate closer to 30% and smaller or older units may reach only 20% (International Energy Agency "Energy Balances of OECD Countries" 2010). Putting these percentages in another way, about 40% to 80% of all the primary energy input is always wasted with any power

generation units. Figure 2.5 shows that about 63% of the thermal input is wasted in the global electricity generation system (international Energy Agency 2007). The wasted energy from power plants emerges as heat and is dumped in different ways. Sometimes it ends up in cooling water, but most often it is dissipated into the atmosphere. This waste heat can be considered not only a large account of energy lost but also a form of pollution.

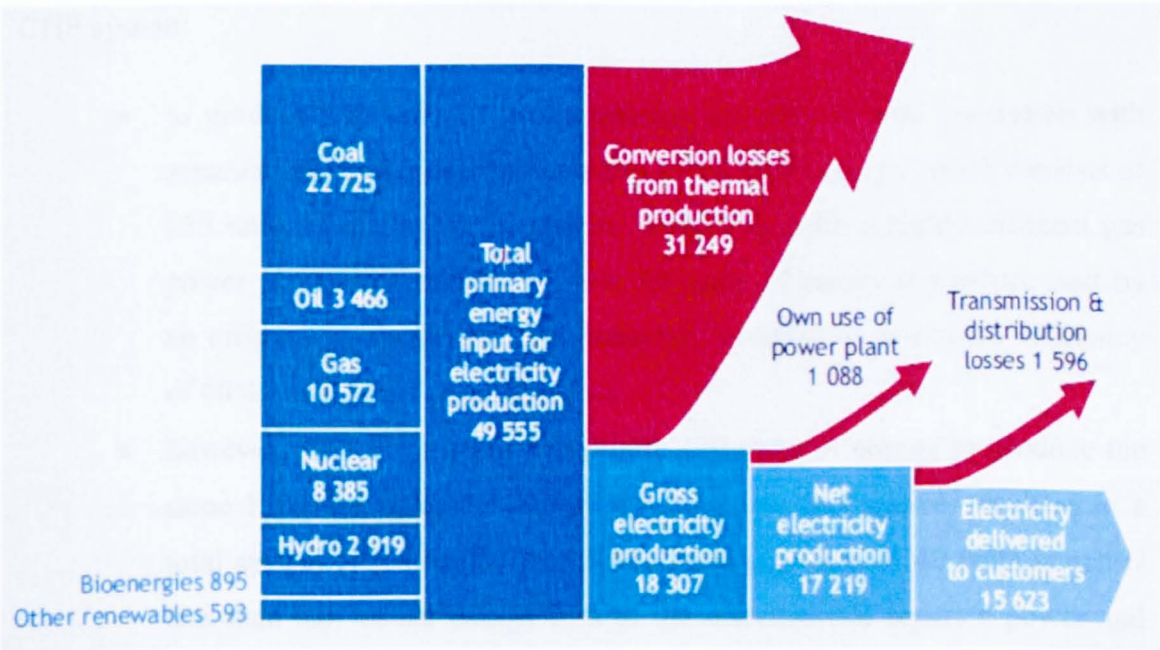

Figure 2.5 Energy flows in the global electricity system (TWh)(International Energy Agency "Combined Heat and Power- Evaluating the Benefits of Greater Global Investment" 2008)

With the CHP technology, most of this considerable amount of low-grade waste heat from an electricity generation process will not be wasted. Although the waste heat energy cannot be used to generate electricity, it can be used to produce hot water or for space heating or cooling. In this way, the waste heat from power generation replaces a high-grade energy resource such as gas, oil or even electricity that is used to generate thermal energy needed for hot water, space heating or cooling. Therefore, cogeneration represents a significant improvement in overall energy efficiency compared with conventional power generation plants. CHP systems can operate with an energy efficiency of up to 90%, leading to a major saving in fuel cost and a significant reduction in greenhouse gas emissions and other environmental pollutants.

CHP systems also reduce the network and transport losses because they are mostly sited near the end users.

The efficiencies of CHP systems may vary to some extent, mainly depending on the design of the systems, technologies and fuel sources. Figure 2.6 compares the overall efficiencies of an example CHP system and a conventional "separate heat and power" generation scheme. It illustrates the potential efficiency gains of a typical CHP system:

- to produce 130 units of useful energy, the conventional generation with separate heat and power systems use 215 units of energy which consists of 115 units of energy for electricity production with a highly efficient gas power plant (48% efficiency) and 100 units of energy to produce heat by an efficient gas boiler (80% efficiency), resulting in an overall efficiency of 60% and 85 units of energy loss.
- however, the CHP system needs only 170 units of energy to produce the same 130 units of useful energy from a single fuel source, resulting in a total system efficiency of 76.5% and an energy loss of 40 units which is less than half of the energy loss of the conventional separate power and heat generation.

While the benefits of CHP are widely recognised, the implementation of CHP remains low. Despite of the existence of various energy policies such as EU Cogeneration Directive 2004/8/EC (EU Cogeneration Directive 2004) which promote CHP in Europe, the United States, Japan and other countries, the share of CHP in global power generation has remained stagnant for the past several years at around 9% (International Energy Agency "Combined Heat and Power- Evaluating the Benefits of Greater Global Investment" 2008). The electricity generated by CHP schemes in the UK in 2009 was 27,777 GWh and this represents 7.47% of the total electricity generated (371,978 GWh) in the UK in 2009(Department of Energy & Climate Change "Digest of UK Energy Statistics 2010" 2010).

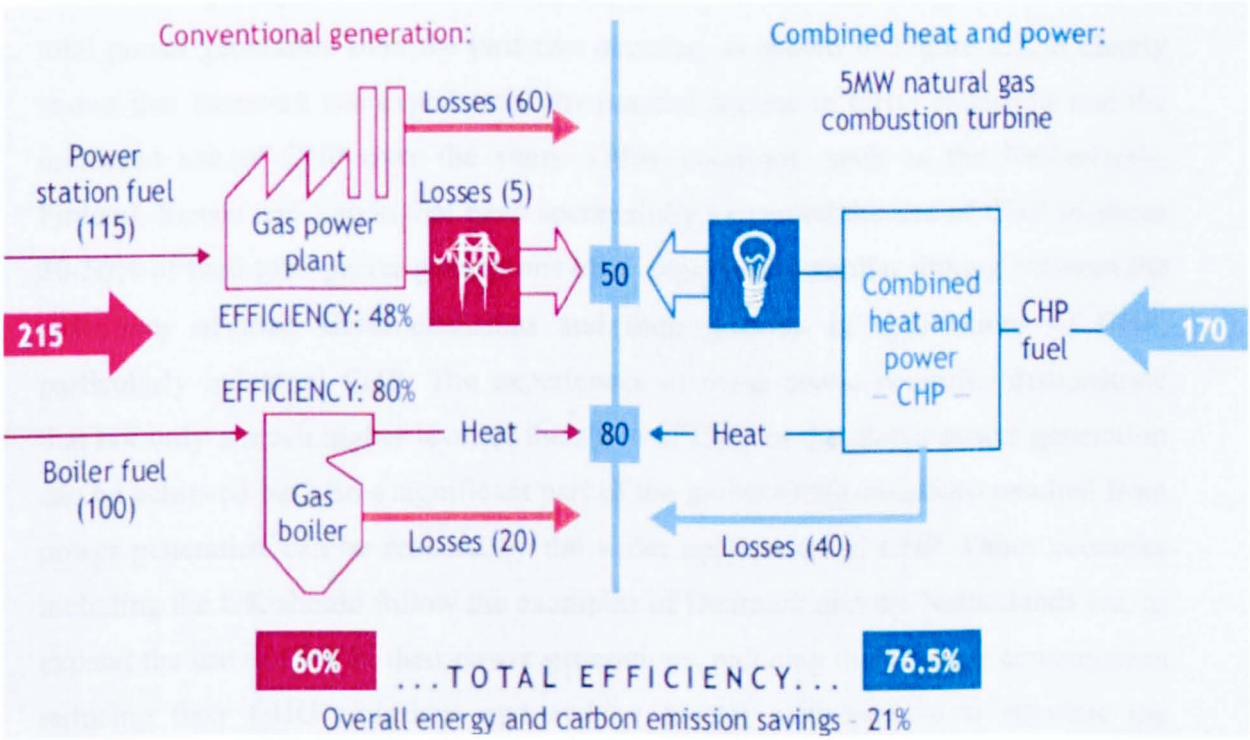

Figure 2.6 Efficiency gains of CHP vs. Conventional Generation (International Energy Agency "Combined Heat and Power- Evaluating the Benefits of Greater Global Investment" 2008)

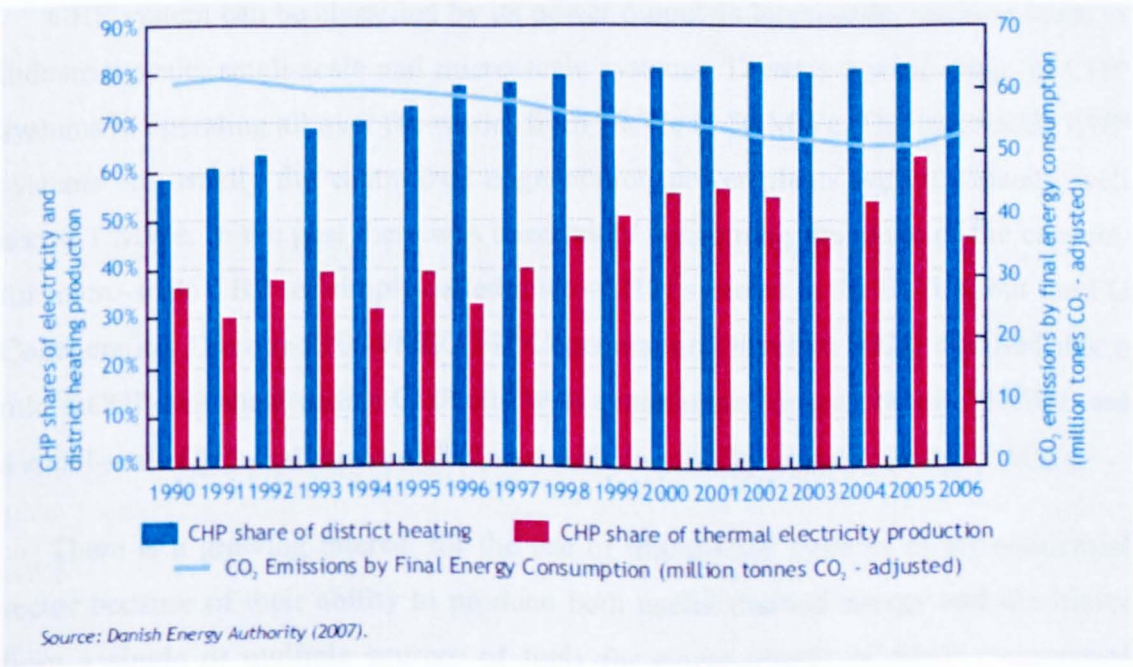

Figure 2.7 CHP/DHC growth and energy end-use carbon emissions in Denmark

However, Denmark has successfully expanded the use of CHP to over 50% of its total power generation over the past two decades, as shown in Figure 2.7. It clearly shows that Denmark has experienced the parallel decline in GHG emissions and the increased use of CHP over the years. Other countries, such as the Netherlands, Finland, Russia and Latvia that have successfully expanded the use of CHP to about 30-50% of their total power generations have experienced similar linking between the reductions of their GHG emissions and their growths in applications of CHP, particularly industrial CHP. The experiences of these above countries demonstrate that not only a much higher level of the share of CHP in the global power generation can be achieved but also a significant part of the global GHG emissions resulted from power generation can be reduced by the wider application of CHP. Other countries including the UK should follow the examples of Denmark and the Netherlands etc. to expand the use of CHP in their power generations, reducing their energy consumption, reducing their GHG emissions and making greater contributions to alleviate the problem of the global climate change.

2.3.2. CHP Technologies

CHP system can be classified by its power output as large-scale, medium-scale or industrial-scale, small-scale and micro-scale systems. There is a wide range of CHP systems in operating all over the world, from 1 kWe to 50 MWe. The large-scale CHP systems are usually the centralized cogeneration power plants with a capacity well above 1 MWe. In the past there was uncertainty concerning the range of the capacity for micro-scale CHP (or simply called micro-CHP) systems in the EU/UK but the EU Cogeneration Directive 2004/8/EC(EU Cogeneration Directive 2004) clarified that a micro-CHP unit shall mean a CHP unit with a maximum capacity below 50 kWe, and a small-scale CHP shall mean a CHP unit with an installed capacity below 1 MWe.

There is a growing interest for the use of micro-CHP systems in the residential sector because of their ability to produce both useful thermal energy and electricity from a single or multiple sources of fuels for single houses or small commercial buildings. Because the electricity generation efficiency of micro-CHP systems cannot compare with that of the highly efficient centralized electricity generation systems, a

micro-CHP system is often designed to mainly meet the thermal demand of a building with electricity as a by-product. When the electricity demand of the building is higher than the output of its micro-CHP system, the grid can be used as the back-up power to the CHP system which means the short supply of electricity is bought from the grid. On the other hand, if the electrical output from its micro-CHP system is more than the electricity demand of the building, the surplus of the electricity can be sold back to the grid as shown in Figure 2.8. (Marathon ecopower micro-CHP 2007).

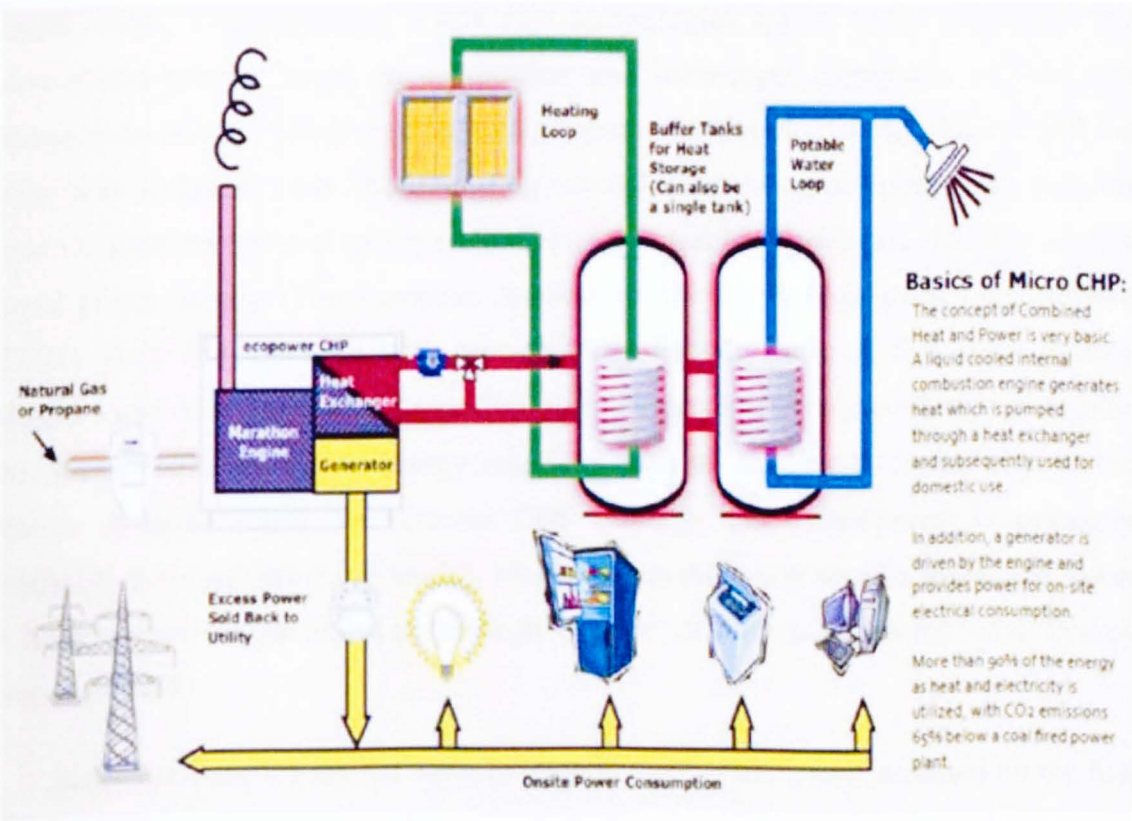

Figure 2.8 An example of micro-CHP system(Marathon ecopower micro-CHP 2007)

Theoretically, almost any fuel is suitable for micro-CHP, and they can work with a single or multiple sources of fuels. Although fossil fuels are currently widely used, other fuel resources such as biogas, landfill gas, municipal solid waste and biomass can also been used. With the depletion of fossil fuels and growing concerns for the environment and energy security, renewable energy resources such as biomass will become more important sources of fuels for CHP system in the future.

A typical CHP system consists of four basic elements: a prime mover (an engine or a drive system), an electricity generator, a heat recovery system, and a management and control system. Although each of these four elements can have significant impact on the performance of a CHP system, the prime mover is the most critical element of a CHP system.

There are a number of different technologies to convert fuels into useful forms of energy (mostly electricity and heat) that have been developed and researched for CHP applications. Although quite a few new technologies appear to be promising, the conversion process based on combustion and subsequent conversion of heat into mechanical energy, which then drives a generator for electricity production, is still the dominant technical route. Reciprocating internal combustion engines, steam turbines and combustion turbines which are based on this technical route are the most widely used prime movers (The European Association for the Promotion of Cogeneration 2001). New developments with prime movers include those of fuel cells, Stirling engines and micro-turbines. These CHP technologies has been considered as suitable to operate with renewable energy resources with an acceptable capital cost in the future (Maribu 2004). The current CHP research and development is primarily focused on improving performance, reliability, modular and smaller units, and lower GHG emissions (for example, through the use of biomass) (international Energy Agency 2007).

Although there are several ways to classify CHP system, such as based on the fuel used or the capacity range, they are generally classified by the type of the prime mover equipment which in some extent determine possibilities and availability of other related technologies. The technologies of the following prime movers will be discussed in this chapter, with specific respect to their ability to run as CHP: steam turbines, reciprocating engines, gas turbines, micro-turbines and fuel cells. A synopsis of the major parameters and performance of these prime movers is shown in Table 2.4. As the topic of the present PhD research is the development of a biomass-fired micro-scale CHP, the discussions below will also focus on the technologies related to micro-CHPs that are below 50 kWe, where possible.

Table 2.4 Comparison of Prime Mover Technologies

Technology	Fuel	Capacity MW	Electrical efficiency (%)	Overall efficiency (%)
Steam turbine	Any combustible	0.5-500	17-35	60-80
Reciprocating engines	Gaseous & liquid	0.003-10	25-45	65-92
Gas turbine	Gaseous	0.25-50+	25-42	65-87
Micro-turbines	Gaseous & liquid	0.03-0.25	15-30	60-85
Stirling engines	Any combustible	0.003-1.5	30-40	65-85
Fuel cells	Gaseous	0.003-3+	37-50	85-90

A: Steam turbines

Steam turbines are the most common power generation technology used in commercial electric power plants and industries. Usually, a fuel is combusted within a boiler, releasing heat which is used to generate high-pressure steam. The high pressure steam is transferred to the steam turbine, driving the turbine that is coupled with a generator to produce electric power. Because of steam turbine units have separate heat source and do not directly convert fuel to electric energy, they can operate with large variety of fuels with suitable combustion devices, from natural gas to solid waste, including all types of coal, wood, wood waste, and agricultural byproducts. The thermodynamic cycle of steam turbines are based upon the well known Rankine cycle. As illustrated in Figure 2.9, the working liquid (water) evaporates in the boiler when heated and then expands in the turbine to produce shaft work (Oliver 2006). The mechanical energy of the shaft work is turned into electricity with a generator. The exhaust vapor from the steam turbine passes through a condenser for condensation or a heat exchanger for heat extraction and then pumped back the boiler to complete the cycle.

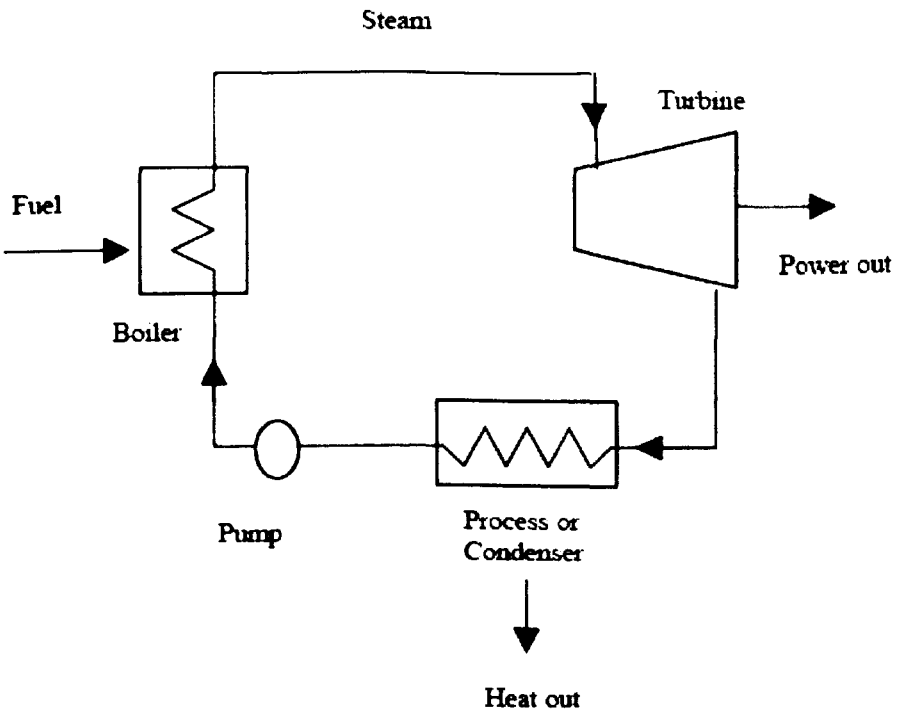

Figure 2.9 Simple Steam Turbine Power Cycle(Oliver 2006)

Depending on the exit pressures of the steam turbines, steam turbines fall into two types: backpressure turbines and condensing turbines.(Nishio *et al.* 1980) A backpressure turbine operates with an exit pressure equal or higher than atmospheric pressure, whereas a condensing turbine operates with an exit pressure lower than atmospheric pressure. Condensing turbines have the advantages of high power generation efficiency and being able to change electrical and thermal power independently when in cogeneration mode of operation. (Nishio *et al.* 1980)

Power generation using steam turbines is one of the oldest power generation technologies and still in commercial production. As a matter of fact, conventional steam turbine power plants currently generate most of the electricity around the world. The capacity of steam turbines ranges from a few hundred kW for small units to several hundred MW for large power plants. As steam turbines are more suitable for large-scale power generation, they are widely used for large-scale and industrial-scale CHP applications. Small-scale steam turbines have relatively low electrical

conversion efficiency, deteriorating rapidly with smaller capacity and therefore they are generally considered not suitable for micro-CHP applications. (Dong *et al.* 2009)

B: Reciprocating internal combustion engines

Reciprocating engines, also called internal combustion engines or endothermic engines are well known from cars. Reciprocating engines can operate on a wide range of liquid and gaseous fuels but not solid fuels. The reciprocating shaft power can produce either electricity through a generator or drive loads directly. The reciprocating engine CHPs are conventional internal combustion engines coupled with generators and heat exchangers to recover the heat of the exhaust gas and the cooling cycle. As a well-known and widespread technology, reciprocating engines are available for power generation applications in sizes ranging from a few kW to more than 10 MW and can be fired on a broad variety of fuels (Orlando 1996). In addition, reciprocating engines have high power generation efficiencies even in small sizes, making them suitable for small-scale CHP applications.(Oliver 2006)

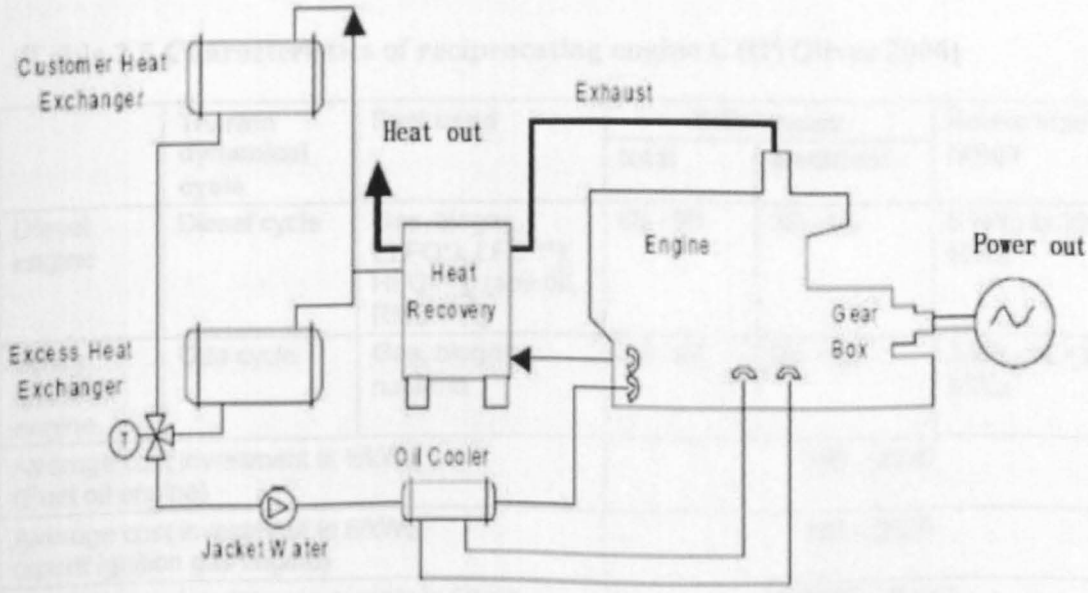

Figure 2.10 Closed-Loop Heat Recovery System for a Reciprocating IC Engine CHP(Oliver 2006)

Reciprocating IC engines are widely used in small power generating plants because they allow compact modular systems to suit various application needs. Besides, reciprocating engines are also well-proven technology that eases maintenance. Driven by economic and environmental pressures, reciprocating engine technology has improved dramatically with the development of engine research worldwide and heat recovery technology over the past decades. A typically reciprocating engine CHP is illustrated in Figure 2.10. Heat can be recovered not only from the exhaust, but also from the jacket water and the engine oil, which leads to notable increase of fuel efficiency and reduction of emissions (Environmental Analysis *et al.* 2007).

There are two basic types of reciprocating engines currently in use: Spark ignition engines and Compression engines (Simader *et al.* 2006). Spark ignition engines are operated mainly with natural gas as the preferred fuel, although biogas, gasoline, and landfill gas can also be used. The capacity of spark ignition engines ranges between 3 kWe and 6 MWe. Compression ignition engines, often called diesel engines, operate on petroleum diesel and biodiesel as well as other petroleum products such as heavy fuel oil [(Energy Nexus Group 2002).

Table 2.5 Characteristics of reciprocating engine CHP(Oliver 2006)

	Thermo dynamical cycle	Fuel used	Efficiencies		Power size range
			total	electrical	
Diesel engine	Diesel cycle	Gas, biogas, ELFO*), LFO **), HFO***), rape oil, RME ****)	65 - 90	35 - 45	5 kW_{el} to 20 MW_{el}
Spark ignition engine	Otto cycle	Gas, biogas, naphtha	70 - 92	25 – 43	3 kW_{el} to > 6 MW_{el}
Average cost investment in €/kW_{el} (Fuel oil engine)			340 – 2000		
Average cost investment in €/kW_{el} (spark ignition gas engine)			450 – 2500		
Operation and maintenance costs in €/kWh_{el}			0,0075 – 0,015		

*) Extra Light Fuel Oil, **) Light Fuel Oil, ***) Heavy Fuel Oil, ****) rapeseed methyl ester

Compression ignition engines can also be set up to run in a dual-fuel configuration that burns primarily natural gas or biogas with a small amount of diesel pilot fuel (Environmental Analysis *et al.* 2007). Compression ignition engine CHP presents a

higher power to heat ratio compared to spark ignition engine CHP, and has a large range of capacity from very small size of a few kWe for small systems to a power equivalent of some tens of MWe for large systems. **Error! Reference source not found.** summarises the characteristics both of diesel and spark ignition engine CHPs (Simader *et al.* 2006).

Although reciprocating engines have been proved to be suitable for numerous cogeneration applications in residential, commercial, institutional and small-scale industrial loads, they still have obvious drawbacks including relatively high vibration noises, a large number of moving parts and high cost for frequent maintenance. Moreover, compared to other CHP technologies, the relatively high emissions of reciprocating engines, particularly in nitrogen oxides and particulate matter, need to be reduced.

C: Gas (combustion) turbines and micro turbines

Combustion turbines, or gas turbines, have been used for power generation for decades and are now the frequently used prime movers in larger-scale cogenerations due to their high reliability and large range of power capacity. Comparing with the other two most widely used prime mover technologies (steam turbines and reciprocating engines), combustion turbines are easier to install with lower capital costs than steam turbines, and have lower costs in maintenance and lower emissions than reciprocating engines. (Simader *et al.* 2006)

A gas turbine is an internal combustion engine but operates with rotational motion rather than reciprocating motion. Observably, a gas turbine is only fuelled by a gaseous fuel such as natural gas or biogas. Gas turbines range in size from 30 kWe (micro turbines) to 250 MWe (large-scale power plant units) and can be used in a variety of power cycle configurations. CHP operation of a gas turbine is built up with a simple-cycle gas turbine and a heat recovery. Heat from the turbine exhaust is recovered and converted into useful thermal energy, mostly in the form of steam or hot water. However, because of the high temperature of combustion turbine exhaust gases - typically around 540°C, the exhaust gases can be used to support the combustion of additional fuel and this technology is called supplementary firing

(Oliver 2006)In some cases, high-pressure steam is generated from the recovered heat of the turbine exhaust and used to generate additional power with a steam turbine, and this can be called a combined cycle CHP system (Oliver 2006)

Micro turbines are the extension of combustion turbine technology, making the gas turbines smaller and more efficient units. The capacity of currently available micro turbines can be as low as 30 kWe. Micro turbines are primarily fuelled with natural gas, but now they are able to operate with wider variety of fuels, including diesel, gasoline and even biogas(Department of Trade and Industry 2006). Micro turbine devices have now achieved almost the same electrical efficiency as internal combustion engines. Additionally, they have environmental advantages, such as at lower emission levels of NOx and CO and less noise over an engine of comparable size.

The basic components of a micro turbine CHP are shown in Figure 2.11. The key part of a micro turbine CHP system is the compressor-turbine package, with single-shaft turbines commonly used on electric generators. The shaft of a micro turbine can work in high rotational speed up to 120,000 rpm. In a typical micro turbine CHP system, the inlet air is compressed and preheated in the recuperator with turbine exhaust heat. Then, the heated air mixed with fuel is sent into the combustor and ignited there. The hot combustion gas is then expanded in one or more turbine sections, producing rotating mechanical power to drive the compressor and the electric generator (Oliver 2006).

As a recently developed technology, micro turbines have started initial commercial service only from 1999. Hence at this stage there are few track records of this technology and they are offered by only a small number of suppliers. Besides, micro turbines are more expensive than internal combustion engines of equivalent sizes in capital costs. However, because it contains few moving parts, the operation and maintenance costs of a micro-turbine can be lower than that of an internal combustion engine. A micro turbine can be used in power-only generation or in a CHP system. With distributed generation applications it can be used by power producers and consumers, including industrial, institutional, commercial and even residential users in the future. Micro turbines' high outlet temperature (> 500 °C) is suitable for other high value applications, such as producing low-pressure steam or

hot water for on-site requirements; furthermore for cooling applications including absorption systems (Simader *et al.* 2006).

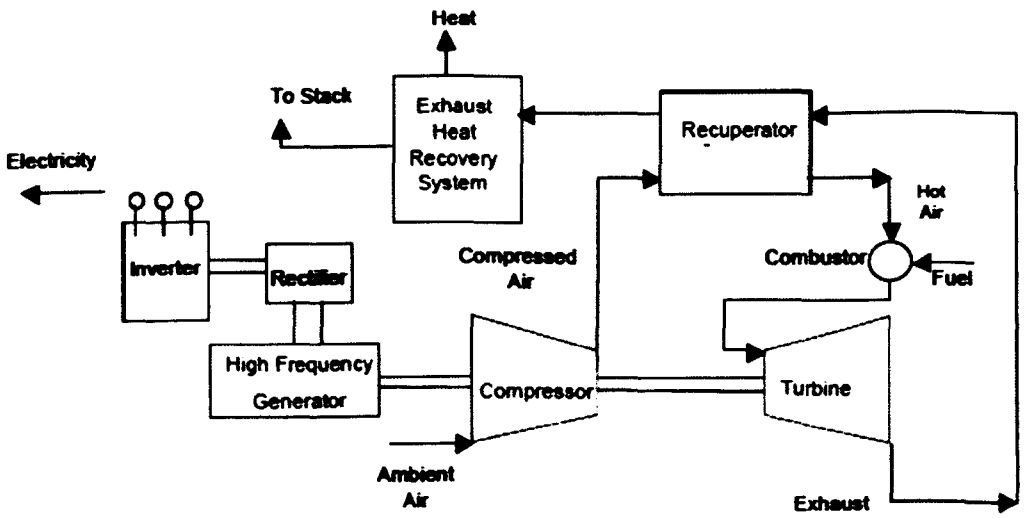

Source: Energy and Environmental Analysis. Inc., 2003.

Figure 2.11 A Typical Micro Turbine CHP System (Single-Shaft Design)(Oliver 2006)

D. Stirling engines

Compared to an conventional internal combustion engine, a Stirling engine is an external combustion device, which can produce either electricity through a generator or drive loads directly (Oliver 2006). As an external combustion engine, a Stirling engine generates heat externally in a separate combustion chamber. Due to this characteristic, Stirling engines can operate on almost any fuel. With external combustion that facilitates the control of the combustion process, Stirling engines have obvious advantages such as low noise and low air emission levels. Presently the electrical efficiency of Stirling engines can be as high as 40%, which is much higher than other prime movers' technologies, with 50% a possibility in the future, whereas the overall CHP efficiency of a Stirling engine cogeneration system is within in the range of 65–85% (Energy Nexus Group 2002). A Stirling cycle has the potential of achieving higher efficiency than Rankine cycle or Joule cycle as it more closely

approaches the Carnot cycle (Energy Nexus Group 2002). Besides, Stirling engines also have good capability to operate under part-load conditions. It is expected that while the full load electrical efficiency can be 35–50%, the electrical efficiency at 50% load can be expected to be in the 34–39% range (Onovwiona *et al.* 2006).

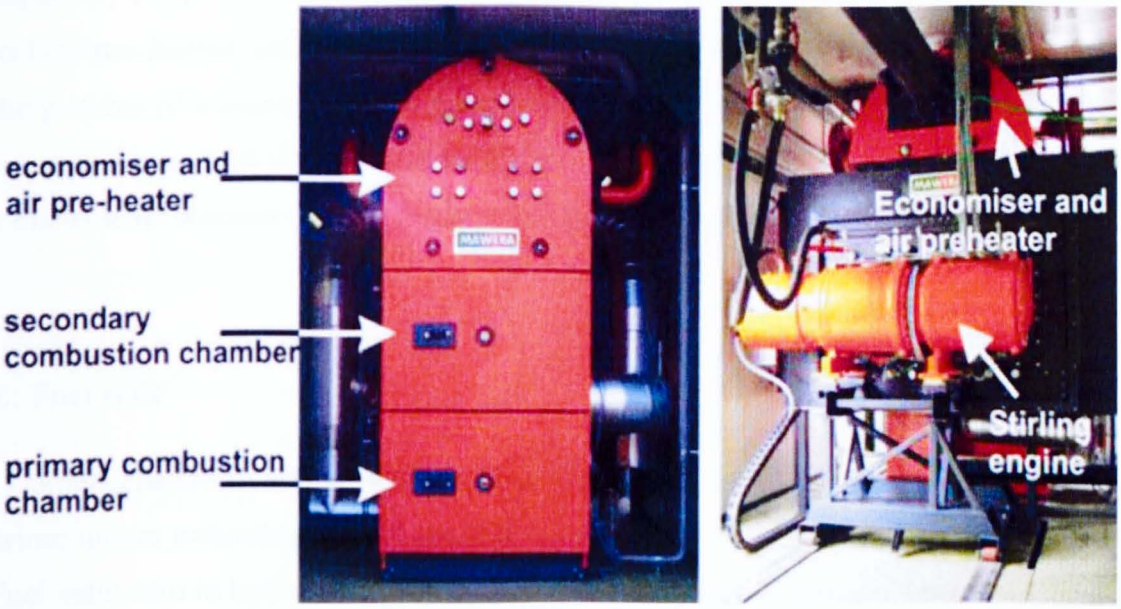

Figure 2.12 A biomass-fired CHP plant based on a Stirling engine, 75kWe and 475kWth(BIOS BIOENERGIESYSTEME GmbH)

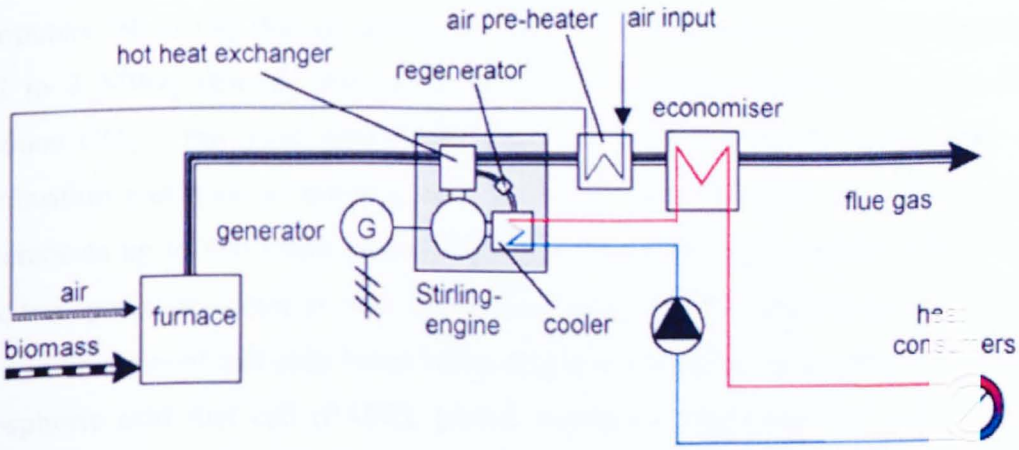

Figure 2.13 Schematic of a micro-scale biomass Stirling engine CHP (BIOS BIOENERGIESYSTEME GmbH)

Although there are some demonstrations of Stirling engine systems, they are still under development and not commercially available today, and for this reason almost no statistical data on reliability, availability or prices of Stirling engine systems are available. Nevertheless, because of their good performance at partial load and capability to operate with different fuels, Stirling engines are particularly well-suited to biomass-fuelled small-scale and micro-scale CHP applications. Figure 2.12 shows the pictures of a micro-scale biomass-fired CHP plant with a 35kWe Stirling engine, whereas Figure 2.13 (BIOS BIOENERGIESYSTEME GmbH)shows the schematic of a micro-scale biomass Stirling engine CHP system(Biedermann *et al.* 2004).

E: Fuel cells

Fuel cells are an entirely different technique to generate electricity than traditional prime mover technologies, and are still in the research and develop phase presently. Fuel cells take in hydrogen (or hydrogen-rich fuels) and oxygen to create electricity, heat, and water. Figure 2.14 shows the key system components of a fuel cell. Basically, a fuel cell consists of a stack of layers arranged around a central electrolyte: an anode at which the hydrogen is oxidized; a cathode at which the oxygen is reduced; and bipolar plates, which feed the gases, collect the electrons, and conduct the reaction heat. Fuel cells can be sized for a wide variety of applications - from laptop computers (50 to 100 We) to vehicles (50 to 85 kWe) and to central power generation (0.2 to 2 MWe) (Energy Nexus Group 2002). Hydrogen-fuelled fuel cells do not produce CO_2 – the main greenhouse gas in the atmosphere. Because there is no combustion and have no moving parts, fuel cells are quiet and can achieve electric efficiencies up to two times greater than internal combustion engines (Oliver 2006). The transportation sector is now the major market for the application of fuel cells. Four main types of fuel cells listed below appear to have the most attractive prospects: phosphoric acid fuel cell (PAFC), proton exchange membrane fuel cell (PEMFC), molten carbonate fuel cell (MCFC), and solid oxide fuel cell (SOFC). However, power generation seems to be another promising market in which fuel cells could be quickly commercialized. Typical performance and CHP characteristics of fuel cells based on natural gas fuel are shown in Figure 2.14 (Environmental Analysis *et al.* 2007).

PEMFC based residential CHP systems have reached demonstration stage, with a variety of FC developers reporting on their latest products, including Ebara Ballard's 1kWe stationary CHP system, Plug Power's GenSys 5C system (5 kWe, 9 kWth) and Hpower's 4.5 kW RCU [(Onovwiona *et al.* 2006). In addition, solid oxide fuel cells (SOFC) are suitable for residential CHP applications because they run efficiently at high temperatures, and have a favorable thermal/electric ratio. A 3.5 kWe SOFC CHP system for residential and commercial applications with an electrical efficiency of approximately 50% and overall CHP efficiency of approximately 80% has been developed by Hydrovolt, and a 2 kWe SOFC CHP system suitable for single family house applications with an overall efficiency of about 85% and a 10 kW SOFC system with an overall efficiency of about 85% have been developed by Global Thermoelectric, Inc. (Onovwiona *et al.* 2006).

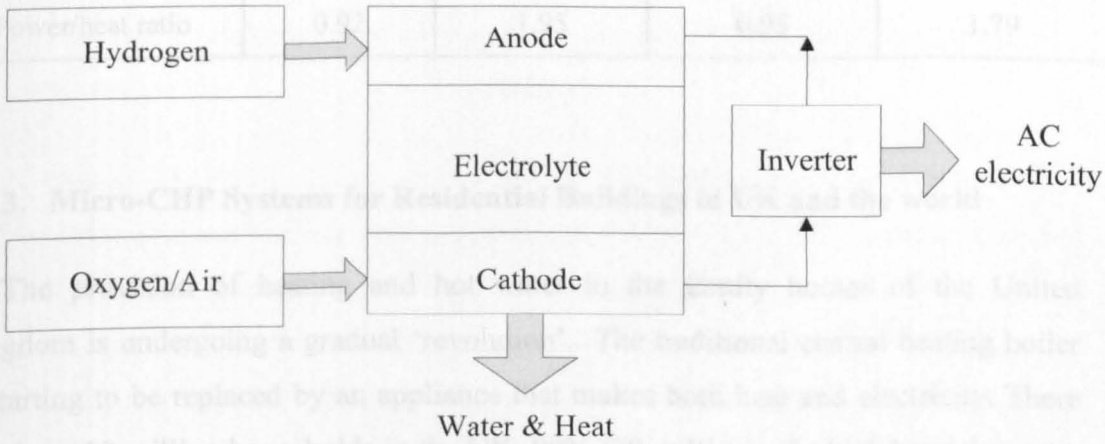

Figure 2.14 Basic construction of a fuel cell CHP system

Since fuel cells are still under research, development and demonstration, there are several disadvantages for their commercialization. Fuel cells are currently more expensive than internal combustion engines and also cost more on maintenance. There are only a handful of fuel cell installations on operating and therefore their long-term operational experience with fuels other than pure hydrogen such as natural gas and biomass-derived gaseous fuels are limited. Besides, relatively short lifetime of fuel cell systems is another main drawback(Simader *et al.* 2006). However, fuel cells' high electrical efficiencies, low noise during operation and low emissions make

them particularly suitable for residential, commercial and institutional building applications.

Table 2.6 Typical Performance Parameters of Fuel Cell CHPs (Oliver 2006)

Performance Characteristics				
Fuel cell type	PAFC	MCFC	PEM	SOFC
Nominal electric capacity (kW)	200	250	200	100
Commercial status	Commercial	Commercial	Demonstration	Demonstration
Electrical efficiency, HHV (%)	36	43	35	45
CHP Characteristics				
Total CHP efficiency, HHV (%)	75	65	72	70
Power/heat ratio	0.92	1.95	0.95	1.79

2.3.3. Micro-CHP Systems for Residential Buildings in UK and the world

The provision of heating and hot water in the family homes of the United Kingdom is undergoing a gradual 'revolution'. The traditional central heating boiler is starting to be replaced by an appliance that makes both heat and electricity. There are about 23 million households in the UK, 89% (20 million) of which have domestic central heating systems of different types. The majority of these were constructed prior to 1970 and consequently have relatively high heat loss of 0.05 kWh/m2/degree day (compared with Sweden's 0.038, Netherlands's 0.041 and Germany's 0.07)(Jeremy Harrison 2010). Average household floor area is 85m2 (Sweden (90), Germany (78)). Progressive improvements in Building Regulations since 1970, and the increasing number of smaller households is resulting in homes with significantly lower space heating demands, but with ever increasing domestic hot water usage.

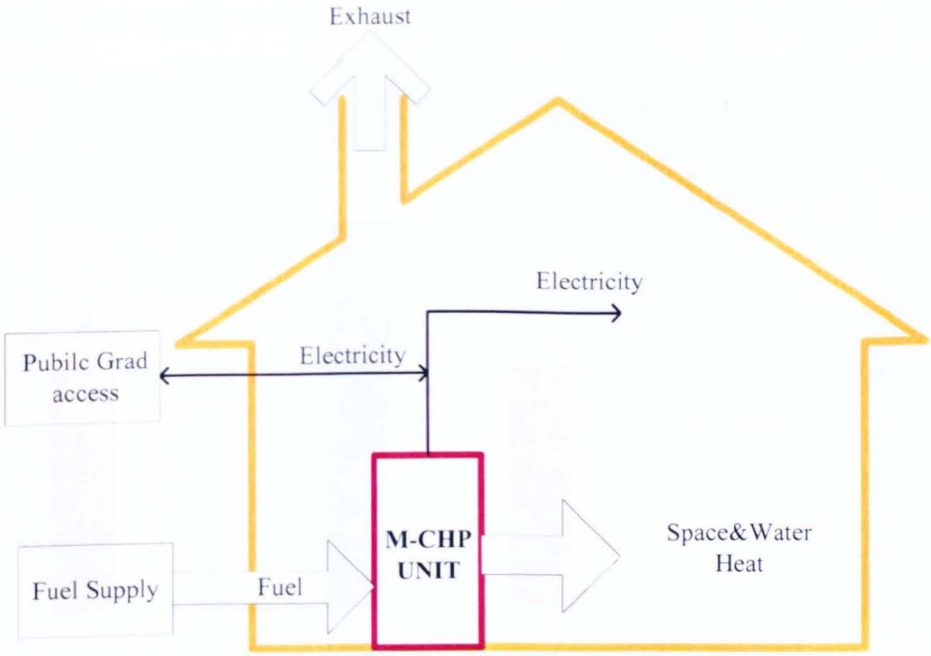

Figure 2.15 Schematic of energy flows in micro CHP system applied to a building

A typical UK family home with a gas central heating system requires around 18,000 kWh of space heating annually, together with 5000 kWh of water heating and 3,500 kWh of electricity consumption. The resulting heat to power ratio for the typical home thus aligns well with the characteristics of micro-CHP engine technology and the relatively low electrical efficiencies are in fact a benefit rather than a disadvantage as was earlier believed.

A micro-CHP system can be substantially more efficient than a SHP (separate heat and power) system of a central heating boiler and grid: the heat is used for space and water heating inside the building, whilst electricity is used within the building or fed into the public electricity grid as shown in Figure 2.15. This leads to lower household energy bills and reductions in energy use and carbon emissions.

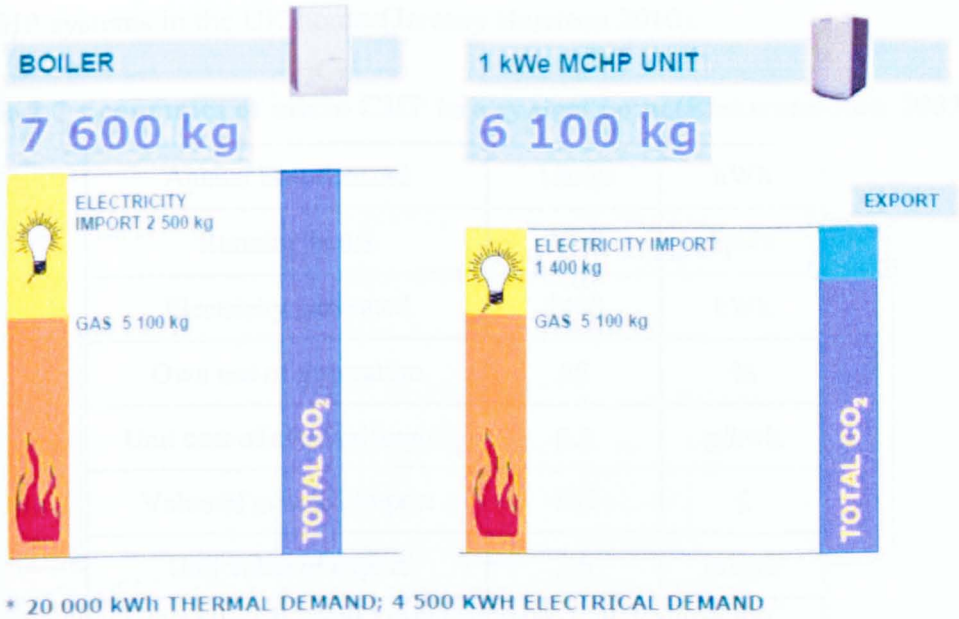

Figure 2.16 CO_2 Savings with Micro-CHP(Jeremy Harrison 2004)

Micro-CHP can help to meet a number of energy and social policy aims. The results of the Carbon Trust field trials on micro-CHP showed that micro-CHP units can make 12%-21% carbon savings in small commercial applications and 4%-14% carbon savings in houses with high heat demands (The Carbon Trust Ltd. 2011). As a result of its cool maritime climate, the UK has a significant heating season spread over several months. In addition, the majority of the UK housing stocks are not well insulated, with the demand for space heating ranging from 2,000 to 4,000 running hours. Although the 2000 to 4000 running hours might appear to be low compared with the requirements of industrial and commercial CHP installations with the anticipated hours of anything from 6,000 – 8,760, the higher unit value of electricity at the domestic level is able to compensate for this shortcoming (Jeremy Harrison 2010). Figure 2.16 compares the emissions of micro-CHP with those of SHP (conventional boiler with electricity from grid supply). It illustrates that an annual saving of 1.5 tonnes of CO_2 for a typical UK home(Jeremy Harrison 2004). Another reason to choose micro-CHP instead of traditional SHP is because of the economic benefit as micro-CHP systems have typical paybacks of 3-4 years as shown in Table 2.6 (Elektroteknisk 2003). The tendency to move home in the UK is every 7-8 years on average, which does not encourage long term investment in energy efficiency

measures, and therefore, short paybacks are essential for successful applications of micro-CHP systems in the UK homes(Jeremy Harrison 2010).

Table 2.7 Economics of micro CHP in a typical home(Elektroteknisk 2003)

Annual heat demand	18000	kWh
Running hours	3000	hours
Electricity generated	2400	kWh
Own use of generation	85	%
Unit cost of avoided import	6.5	p/kwh
Value of avoided import	133	£
Unit value of export	2.5	p/kwh
Value of export	9	£
Total value of generation	142	£
Additional gas cost	0	£
Marginal cost of unit	500	£
Simple payback	3~4	years

In addition to a reduction of greenhouse gas emissions from energy supply, micro-CHP systems also increase decentralisation of energy supply which improves energy security, avoids energy losses from electricity transmission and distribution networks, and potentially reduces energy cost to consumers (Wolfe 2008). The report of the Carbon Trust field trials on micro-CHP(The Carbon Trust Ltd. 2011) also indicates that if the costs can be reduced and performance continues to improve, the market of micro-CHP for the UK homes can be well above 4 million. It has also been reported that micro-CHPs have the potential to achieve over 15% of UK electricity demand by 2050.

As the development of micro-CHP systems for residential applications has the potential to provide significant benefits to users, customers, manufacturers and suppliers of such systems and, in general, benefit to the nation as a whole, in various countries, micro-CHP is considered as one potential building block in a more

sustainable energy system, although the installed units of micro-CHP are still in low level currently. In addition to the UK, other countries are also particularly active in the research and introduction of micro CHP systems such as Japan, Germany and the Netherlands (Brown *et al.* 2007).

Germany has taken a strategic decision to position itself as a leader in micro-CHP. By 2003, over 8000 micro-CHP units with a capacity of 5 kWe had been installed in German businesses and large homes by one of the main developers. The German government anticipated to increase its residential fuel cell to a number as high as 850,000 units, which is about 5% of the total number of German household. In 2004, there were only 60 MWe of micro cogeneration capacity installed in Germany. However, this share could increase to 3.3 GW_e or 3% of the projected German electricity demand in 2050. A major reason for the rather low percentages of micro-CHP for Germany is the competing trend towards larger district heating installations. The Germany government recently established a €500 million National Innovation Programme for hydrogen and fuel cells(Ren *et al.* 2010). Germany's fuel cell applications are divided into four segments: transport, portable, industrial (>100 kWe) and "house energy" (1-10 kWe). €125-150 million of project funding is earmarked for stationary applications (including CHP)(International Energy Agency "CHP/DHC Country Scorecard: Germany" 2009).

In Japan, the power to most residential buildings is supplied from centralized power generation plants, 60% of which are fossil fuel fired with a mean efficiency of about 45%. Therefore, in recent years, the introduction of some distributed sustainable energy systems is strongly recommended to residential buildings among other residential conservation options. Besides the grid-connected photovoltaic (PV) system, another timely example of the distributed residential energy supply technology is the micro-scale combined heat and power generation, with a maximum electrical output capacity between roughly 1 kWe and 10 kWe(Ren *et al.* 2010). Although micro-CHP systems with gas engines were only starting to be commercialized in 2003, the Japanese gas companies have installed over 60000 micro-CHP systems in residential applications. However, more recently, instead of gas engine CHP systems which were developed earlier, the residential fuel cell systems have received more attention from both the government and the developers. Over 3000 fuel cell gas engine CHP systems

of 5kWe, 6kWeand 9.9kWe had been installed as of March 2007(International Energy Agency "CHP/DHC Country Scorecard: Japan" 2009). The Japanese government had set ambitious goals to introduce 1.2 million units of fuel cell CHP systems in the residential sector by the year 2010 when the total number of households is estimated to be around 50 million (Ren *et al.* 2010). However, Japan remains the only market where micro-CHP can be considered commercial, with annual sales of Honda's ECOWILL levelling at around 20,000(Dijkstra 2010).

Likewise, in the Netherlands, by 2006 CHP provides about 50% of national electricity production, mainly in industry and in greenhouses. Because of the use of cogeneration and natural gas, electricity production has been relatively clean in the Netherlands. In addition, the share of sustainable electricity is growing, with large-scale wind and the use of biomass and waste in power stations accounting for much of this growth. (Albert Faber *et al.* 2008). There are more than 6 million houses have gas central heating appliances, and 400,000 gas boilers are sold each year. Early 2007 the three main energy companies Nuon, Essent and Eneco have signed a covenant together with Gasterra, aiming to promote the application of domestic gas-based technologies in general, specifically micro- CHPs. The covenants had sold and installed 10,000 units in the Netherlands, and use these for large scale testing of performance and grid stability by 2009(Dijkstra 2010).

2.4. Micro-CHP with Organic Rankine cycle

From the analysis performed in previous chapters, a micro-CHP system operating on renewable energies shows extraordinary advantages compared to those conventional heating systems in both energy saving and environment protection etc. In this section, a micro-CHP based on an Organic Rankine cycle system will be represented briefly.

The interest for low grade heat recovery has been growing for the last decades, due to the increasing concern over energy shortage and global warming. Among the proposed solutions, the Organic Rankine Cycle (ORC) system is the most widely used.

This ORC process is similar to the cycle of a conventional steam turbine, except for the working fluid that drives the turbine, which is a high molecular mass organic fluid. The ORC system involves parts of the same components as conventional steam power system: work-producing expansion device, condenser and pump. However, there always is an evaporator in replacement of a boiler to vaporize working fluid in relatively lower evaporating temperatures, as shown in Figure 2.17a.

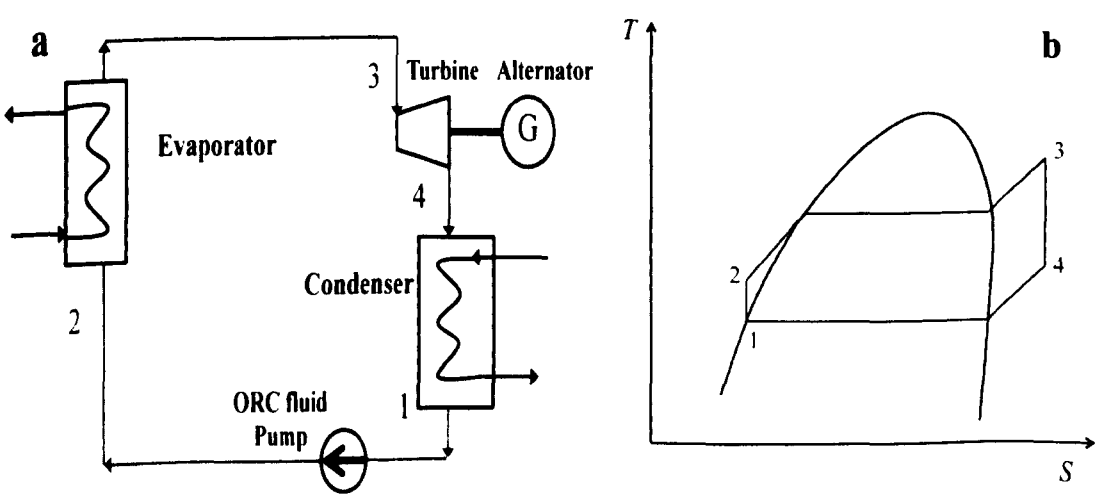

Figure 2.17 ORC system diagram and T–S process diagram: (a) ORC system diagram and (b) a typical T–S process diagram for the investigated ORC system

The pump supplies the working fluid to the evaporator, where the working fluid is heated and vaporized by the exhaust heat. The generated high pressure vapour flows into the turbine and produces power there, and then, the low pressure vapor is led to the condenser and condensed by air. The condensed working fluid flows into the receiver and is pumped back to the evaporator, and a new cycle begins. The heating and cooling sources are not directly in contact with the working fluid or with the turbine. For high temperature applications like combined heat and power biomass-powered plants, high temperature thermal oil is used as a heat carrier and a regenerator is added, to further improve the cycle performance. The typical T-S process for the investigated ORC system is as shown in Figure 2.17b.

Due to different working fluids can be chosen depending on the level of heat resource temperature, it is possible to generate electrical energy from waste heat, geothermal sources, combustion of biomass or solar thermal sources. The ORC process can also produce electricity in a wide range of power outputs (from few kW up to 3 MW electric power per unit)(Simader *et al.* 2006).

The ORC system has technical benefits as high cycle efficiency and high turbine efficiency, low mechanical stress of the turbine, low RPM of the turbine allowing the direct drive of the electric generator without reduction gear, no erosion of the turbine blades, due to the absence of the moisture in the vapour nozzles and Very long operational life of the machine etc. furthermore, it also have practical advantages, such as simple start-stop procedures, quiet operation, minimum maintenance requirements, and good part load performance.

However, the characteristic and principle of Organic Rankine cycle will be farther discussed in the following Chapter with modelling.

2.5. Conclusions

This chapter presents a detailed explanation of biomass fuel as renewable energy resource, mainly including the contributions of biomass to the world primary energy saving and categories and characteristics of biomass materials. Besides, as biomass materials can be converted to various useful forms of energy such as heat, electricity and liquid fuels, the conversion technologies of convent biomass fuel into modern energy carriers – electricity, gas, and liquid bio-fuels were discussed.

The capability and benefits of combined heat and power (CHP) technology were described within this chapter. Furthermore, a survey of the different micro-CHP technologies on the market was mentioned, especially micro turbines that converted and adapted to operate with renewable energy. The basic principle of Organic Rankine cycle work with low grade heat resources was also mentioned, and the further discussion will be made in the following chapter with the modelling.

It was shown that micro-CHP system based on Organic Rankine Cycle (ORC) operating on renewable energies presents many advantages compared to conventional cogeneration systems, since they could operate with renewable energies (mostly present as low grade heat resources) while achieving high primary energy savings and reducing significantly CO_2 emissions.

As the aim of the project is to develop and evaluate a novel, first-of-its-kind, micro-scale biomass fired CHP system, a special care has to be taken when designing and operating the micro-CHP system. Therefore, a modelling analysis of the proposed biomass fired micro-CHP system with Organic Rankine cycle will be presented in the next chapter before the laboratory testing.

Chapter 3. Thermodynamic Modelling of the Proposed Biomass-Fired Micro-Scale CHP System

3.1. Introduction

Modelling is a powerful tool for many technological investigations. It can not only provide useful insights and feasibility to new technological inventions but also save time and cost by eliminating unnecessary experimental trials. Therefore, a thermodynamic modelling study had been carried out prior to the full experimental investigation of the proposed biomass-fired micro-scale CHP system.

In this Chapter, the thermodynamic modelling of the proposed biomass-fired micro-scale CHP system with organic Rankine Cycle (ORC) is presented. The main aims of the thermodynamic modelling were to investigate the effects of changing operating conditions, recuperating heat with an internal heat exchanger (IHE), superheating and subcooling the organic working fluid on the performance of the micro-scale CHP system. Three environmentally friendly organic refrigerants have been selected as the working fluids: HFE7000, HFE7100 and n-pentane. The selection of these working fluids used in the modelling is not only according to their thermo-physical properties but also limited by the available database of the refrigerants with the simulation software EES (McGraw-Hill's Engineering Equation Solver(F-Chart Software), which is to be described later in this chapter). The proposed micro-scale CHP system is supposed to be able to generate both electricity and heat by using the hot water produced from a biomass boiler.

Different simulation routines were created to model different types of organic Rankine cycles with the micro-scale CHP. With each simulation routine, a simple Pinch-Point analysis based on temperature profiles in the condenser was carried out to calculate the temperature at which the water in the heating loop was leaving the condenser.

The effects on the electrical and thermal energy outputs of the micro-scale CHP system of the following four types of variables were investigated with the thermodynamic modelling:

i. Changing operating conditions with each of the three ORC fluids. The modelling was carried out with the maximum system temperature in the range of 110-140°C and the minimum system temperature in the range of 30-50°C.
ii. Recuperating energy with an Internal Heat Exchanger (IHE)
iii. Superheating the working fluid
iv. Sub-cooling the working fluid

A brief review of the organic Rankine cycle principles is given below, which is followed by the further details on the proposed micro-scale CHP system with ORC, the discussion on the ORC fluid selection and the analysis of the thermodynamic modelling results.

3.2. Principle of Micro-CHP System with ORC

As discussed in the previous chapters, the greenhouse gases, particularly carbon dioxides from fossil fuels' consumption have been regarded as the main reason of global warming and other environmental problems over the past decades. The interest for low grade heat recovery has been growing for the last decade or so with a large number of new solutions being proposed to generate electricity from low temperature heat sources. Among the proposed solutions, CHP has been considered to be the major evolvement of traditional power generation systems(Denntice d'Accacia M 2003), which can make significant energy saving and environmental conservation. On the other hand, energy use in various buildings accounts for nearly half of the UK's delivered energy consumption and half of the UK's CO_2 emissions. Many believe that micro-scale CHP is the most effective way to satisfy the energy demands and to reduce CO_2 emissions of domestic and light commercial buildings such as small office buildings. The heating and power demands of typical domestic buildings and small commercial buildings can be fully met by micro-scale CHP systems within the size range of 1kWe to 10 kWe. Currently, micro-scale CHP systems within the size range of 1kWe to 10 kWe are undergoing rapid development, and are emerging on the market with promising prospects for the near future commercialisation. However, to drastically reduce the CO_2 emissions, the energy demands of the buildings have to be

supplied by renewable energy-based systems, such as building integrated wind turbines, solar PV, solar thermal and biomass-fuelled micro-scale CHP systems. The key aim of the present PhD research project is to develop and evaluate a biomass-fuelled micro-scale CHP system. A micro-CHP system operating on renewable energies has significant advantages compared to fossil fuel energy supply systems of either SHP (separate heating and power) or CHP in both energy saving and environment protection.

3.2.1. Power Generation with Organic Rankine cycle

The Rankine cycle was developed in the early 19th century by a Scottish engineer and physicist William John Macquorn Rankine(Rankine). Rankine developed a complete theory of the steam engine and indeed of all heat engines. The Rankine cycle was usually based on water as a working fluid. Applications of the cycle with different working fluids started to appear in the late 19th century, such as the Naphtha boats(Naphtha launch). In 1883 Frank Ofeldt developed the first Organic Rankine Cycle: the Naphtha Launch with which an organic fluid (naphtha) had replaced steam as the working fluid(Naphtha launch). Today, Rankine Cycle with organic working fluid is a well-known and widely spread form of energy production, mostly in low-grade heat resources such as geothermal and biomass applications, but great rises in solar and heat recovery applications also being expected. Environmental concern over climate change and rising oil prices are powerful reasons supporting the explosive growth of this efficient, clean and reliable technology of producing electricity.

The interest for low grade heat recovery has been growing for a few decades and the ORC system is the most widely used among the proposed solutions for low grade heat recovery,

An ORC system is very similar to a steam Rankine cycle system. However, for an ORC system, the working fluid is an organic fluid characterized by a lower boiling temperature than water and thus allowing its evaporation at a reduced temperature. Since different working fluids can be chosen according to the temperature levels of the available heat sources, it is possible to generate electrical energy by use of an ORC system from waste heat, geothermal, combustion of biomass and solar thermal

sources. ORC is also applicable to a wide range of power outputs (from few kW up to 3 MW electric power per unit)(Simader *et al.* 2006).

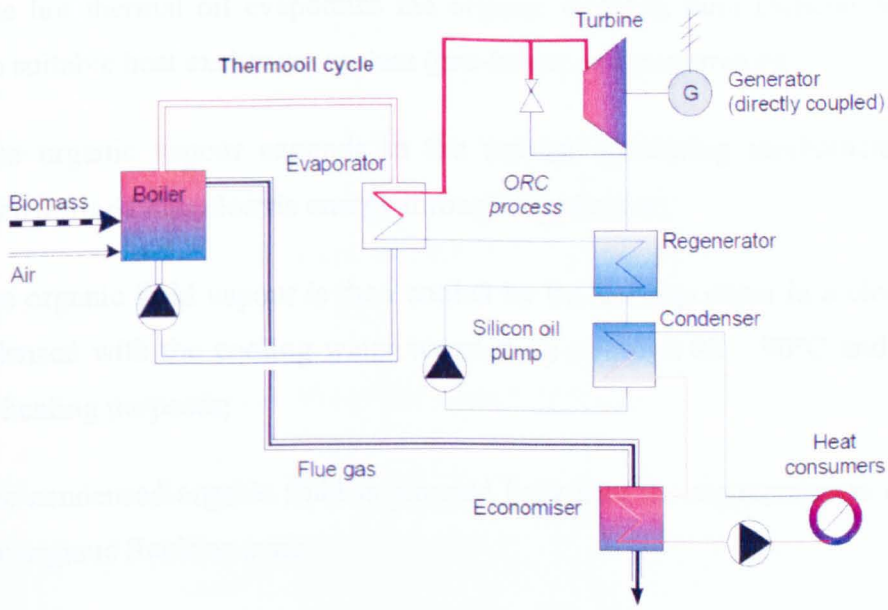

Figure 3.1 Principle of a biomass-fired CHP with an ORC process(Oliver 2006)

As mentioned before in chapter 2.5, an ORC system has the same types of components as a conventional steam Rankine cycle system: boiler (evaporator), work-producing expansion device (turbine), condenser and pump. However, there always is an evaporator to vaporize the working fluid at a relatively low evaporating temperature. The organic working fluid is vaporized by application of a heat source in the evaporator. The organic fluid vapor expands in the turbine, producing mechanical energy which can be transformed to electrical energy via a generator, and is then condensed using a flow of coolant such as water in a shell-and-tube heat exchanger. The condensate is pumped back to the evaporator thus closing the thermodynamic cycle. Heating and cooling sources are not directly in contact with the working fluid or with the turbine. For high temperature applications such as biomass-fired CHP power plants (as shown in Figure 3.1), a high temperature thermal oil can be used as a heat carrier and a regenerator can be added, to further improve the cycle performance.

The biomass-fired CHP power plant with an ORC process shown in Figure 3.1 consists of three closed loop cycles - the thermal oil cycle, the organic Rankine cycle and the cooling water cycle:.

1. The biomass boiler as a heat source heats thermal oil to a high temperature, typically about 300°C, in a closed cycle;

2. The hot thermal oil evaporates the organic working fluid (Silicon oil) of the ORC in a suitable heat exchanger system (pre-heater and evaporator);

3. The organic vapour expands in the turbine, producing mechanical energy, further transformed into electric energy through a generator;

4. The organic fluid vapour is then cooled by the cooling water in a closed cycle and condensed with the cooling water warmed up at about 80 - 90°C and used for different heating purposes;

5. The condensed organic fluid is pumped back into the regenerator to close and restart the organic Rankine cycle.

The main technical benefits of ORC systems are (Minea 2007):

• High cycle efficiency and high turbine efficiency (up to 85%)

• Low mechanical stress of the turbine, due to the low peripheral speed

• Low RPM of the turbine allowing the direct drive of the electric generator without reduction gear

•No erosion of the turbine blades, due to the absence of the moisture in the vapour nozzles

•Very long operational life of the machine due to the characteristics of the working fluid, that is, unlike steam, non-eroding and non-corroding for valve seats tubing and turbine blades.

ORC systems also have practical advantages, such as simple start-stop procedures, quiet operation, minimum maintenance requirements, and good part load performance.

Partly due to the above listed technical benefits and practical advantages, organic Rankine cycle has become one of the main power generation concepts that has been applied to biomass-fuelled CHP systems, in particular with those within the size range of 200 kWe to 1.5 MWe. ORC manufacturers have been present on the market since

the beginning of the 1980's. They provide ORC solutions in a broad range of power and temperature levels, as shown in Table 3.1. These manufacturers now offer various biomass-fired ORC power generation and CHP systems which have been successfully demonstrated and become commercially available with typical electrical efficiency of 15 - 20%. For instance, ADORATEC in German offers CHP systems with ORC in the power range between 300 and 2.400 kWe, fuelled by biomass, waste heat or geothermal heat (ADORATEC). Turboden based on Northern Italy offers different standard models for CHP cogeneration with ORC generally within the range of 400 kWe and 2 MWe (TURBODEN Ltd.).

Table 3.1 Non-exhaustive list of the main ORC manufacturers(Quoilin 2009)

Manufacturer	Applications	Power range	Heat source temperature	Technology
ORMAT, US	Geothermal, WHR, solar	200 KWe – 72 MWe	150° - 300°C	Fluid : n-pentane
Turboden, Italy	CHP, geothermal	200 KWe – 2 MWe	100 - 300°C	Fluids : OMTS, Solkatherm Axial turbines
Adoratec, Germany	CHP	315 – 1600 KWe	300°C	Fluid: OMTS
GMK, Germany	WHR, Geothermal, CHP	50 KWe – 2 MWe	120° - 350°C	3000 rpm Multi-stage axial turbines (KKK) Fluid: GL160 (GMK patented)
Koehler-Ziegler, Germany	CHP	70 – 200 KWe	150 – 270°C	Fluid: Hydrocarbons Screw expander
UTC, US	WHR, geothermal	280 KWe	>93°C	
Cryostar	WHR, Geothermal	n/a	100 – 400 °C	Radial inflow turbine Fluids: R245fa, R134a
Freepower, UK	WHR	6 KWe - 120 KW	180 - 225 °C	
Tri-o-gen, Netherlands	WHR	160 kWe	>350°C	Turbo-expander
Electratherm, US	WHR	50 KWe	>93°C	Twin screw expander
Infinity Turbine	WHR	250 KWe	>80°C	Fluid: R134a Radial Turboexpander

*Sources: Manufacturers websites; Citrin, 2005; Gaia, 2006; Lorenz, 2006; Holdmann, 2007; Schuster, 2009

3.2.2. The proposed biomass-fired CHP system with organic Rankine Cycle

As stated above, the principle of the ORC-based power generation is similar to that of the steam-driven Rankine turbine cycle, except that the working fluid (which is not water) has favourable thermodynamic properties (the boiling point, the critical point, the latent heat, the slope of the saturation vapour T-s line, the maximum stability temperature, etc.), is used as the working medium for the turbine(Hung *et al.* 1997). The ORC-based power generation has been widely applied to the power generation from low temperature heat sources, such as the recovery of industrial waste heat, geothermal heat and solar heat, with the size of the generator as small as a fraction of a kWe(Hung *et al.* 1997). An ORC turbine is more economical than a steam-driven turbine in terms of capital and maintenance costs due to the use of non-eroding, non-corrosive and low temperature working fluid vapour. In addition, the ORC-based power generation offers advantages in electricity generation efficiency over the steam Rankine cycle power generation at small- and micro-scale systems. Over the past decade, the Department of Architecture and Built Environment, University of Nottingham, UK, has carried out a series of research projects which focus on the ORC-based micro-scale power generation for residential and small commercial building applications. Different heat sources have been chosen such as solar energy(Yagoub *et al.* 2006) and gas-fired boiler(Nguyen *et al.* 2001) etc. Results from these previous research projects have indicated that the ORC-based power generation can be successfully applied to micro-scale CHP systems using various heat sources including hot-water generated from biomass boiler.

The originally proposed biomass-fired micro-scale CHP system of this project is schematically shown in Figure 3.2. It consists of two main cycles: the hot water cycle and the organic Rankine cycle. The heat released from the combustion of biomass inside the biomass boiler is used to heat the water via the boiler heat exchanger, while the hot water is used as the heating source of the organic Rankince cycle. The ORC working fluid is closely circulating within the organic Rankine cycle: the condensed ORC working fluid is pumped through the evaporator where it is heated by the circulating hot water to generate organic working fluid vapour which expands in the turbine to generate electricity via a generator; the working fluid at the turbine exhaust is condensed in the condenser and flows back to the circulation pump to begin a new

cycle. Cooling water is used to recover the heat of the working fluid after the turbine exhaust. Depending on the ORC working fluid used and the operating conditions of the micro-scale CHP system, the heat recovered by the cooling water can be used for hot water supply or under floor heating etc.

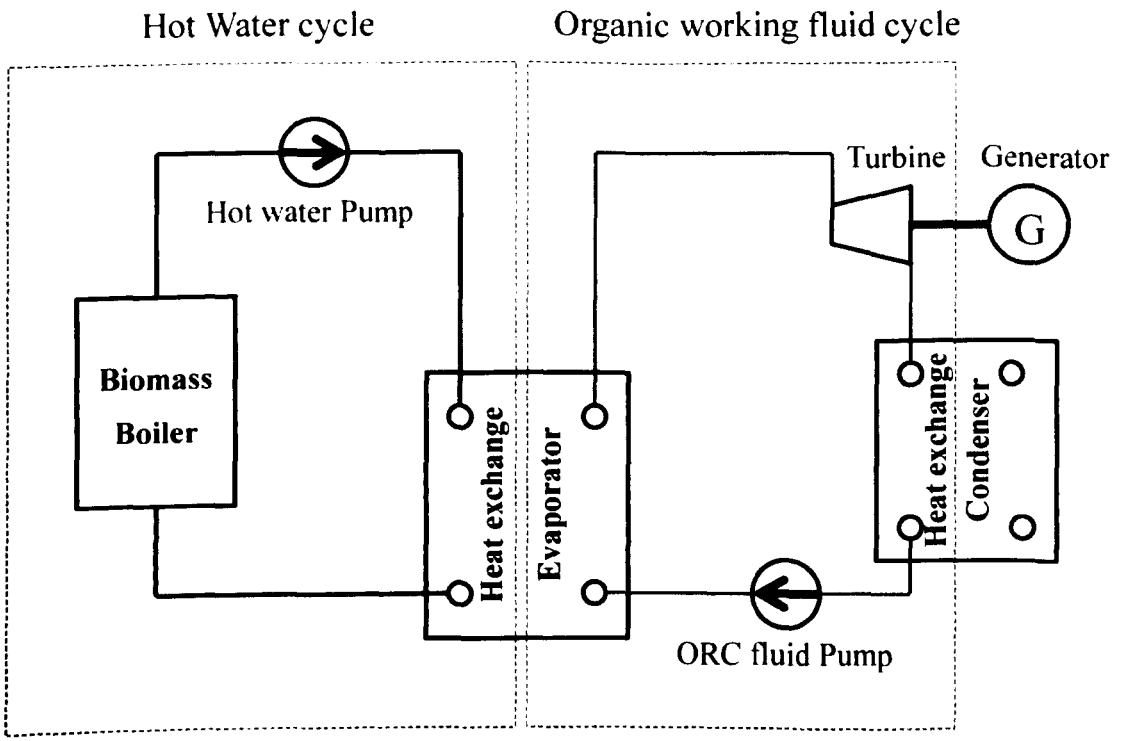

Figure 3.2 Schematic of the originally proposed biomass-fired CHP system

3.3. Working fluid selection for a low temperature ORC

3.3.1. Introduction

For micro-scale organic Rankine cycle, the design and its energy performances are strongly depend on the properties of the working fluids. Organic fluids present lots of advantages compared with water, particularly for low power outputs, as a result of utilizing low grade energy as heat input. In this section, the required characteristics of ideal working fluids will be discussed. An ideal organic fluid needs to fulfil several requirements, such as environmental, safety, and suitable thermodynamic and thermo-physical properties that can match the design requirements of the proposed Rankine cycle components.

3.3.2. Review of previous studies on ORC working fluids

The use of organic Rankine cycle for micro-scale power generation is not a new concept and many investigations have been carried out. There are micro-CHP units based on Rankine cycle operating with organic fluids which are named as organic Rankine cycle micro-CHP(Yamamoto *et al.* 2001). The ORC technology offers the opportunity to operate these micro engines with renewable energy resources and low-temperature heat sources. The ORC technology has been used in the previous years with different configurations in energy recovery from low-grade waste heat applications and geothermal applications as reported, amongst others, by Liu et al (2004) and Saleh et al (2007), and is now seen as one of the favourable technologies to be used in micro-CHP and solar energy applications. A number of investigations have been carried out to study the types and properties of ORC working fluids. Amongst them, Saleh et al. (2007), Liu et al. (2004), Drescher and Brüggeman (2007), Hung et al. (1997) and Mago et al. (2008) have, in particular, investigated the role and performance of dry fluids for ORC.

Saleh et al. (2007) screened a number of fluids for geothermal applications of ORC such as alkanes, fluorinated alkanes, ethers, and fluorinated ethers, with operating temperatures between 100° C (source) and 30° C (sink). They had studied different cycle configurations depending on the shape of the saturated vapour line in

the T-S diagram which was used to distinguish the different types of organic working fluids. They also studied the effect of superheating organic working fluids on ORC efficiency and concluded that the characteristics of the heat carrying fluid had to be considered when determining the optimal fluid for an application(Saleh *et al.* 2007). Borsukiewicz- Gozdur et al. (2007) who studied the power output of an ORC-based geothermal power plant concluded that there was an optimum evaporation temperature for an ORC working fluid(Borsukiewicz-Gozdur *et al.* 2007). Hung et al. (1997) shows that the slopes and the shapes of the saturation vapour curve of the fluids have a primary effect on the performance of the ORC where the "isentropic" fluids seem to be the most suitable type of the selected working fluid for recovering low temperature waste heat(Hung *et al.* 1997). Liu et al. (2004) analysed the performance of several working fluids of ORC adapted to waste heat applications. They concluded that wet fluids are not the best option for low temperature ORCs and that cycle efficiency increases as the temperature of the heat source increases, and decreases if the fluids with lower critical temperature are used(Liu *et al.* 2004). Further discussion on the three categories of ORC fluids, i.e. the 'dry fluids', the 'wet fluids' and the 'isentropic fluids' will be given in Section 3.3.3.

Hung (2001) had shown that the efficiency of the ORC heavily depends on two factors: working conditions of the cycle and thermodynamic properties of the working fluids. Different working fluids had been compared including benzene, toluene, p-xylene, R-113, and R-123. Among these fluids p-xylene shows the highest efficiency while benzene shows the lowest. The study also showed that p-xylene presents the lowest irreversibility's when recovering high temperature waste heat, while R-113 and R-123 present a better performance in recovering low-temperature waste heat(Hung 2001). Mago et al. (2008) investigated the benefits of using a regenerative ORC with dry organic fluids to convert waste heat to power from low-grade heat sources. The different working fluids studied were R-113, R-245ca, R-123, and isobutene. It was found that using the regenerator could lead to a higher thermal efficiency and lower irreversibilities. It was also found that the boiling point temperature of the ORC working fluid had a significant effect on the cycle thermal efficiency and the authors concluded that the organic fluids should be operated at saturated conditions(Mago *et al.* 2008). Wei et al. (2007) conducted a performance analysis and optimization of an organic Rankine cycle system using HFC-245fa as working fluid driven by exhaust

heat to maximize its recovery in order to improve the system output net power and both the electricity and overall efficiency(Wei *et al.* 2007). Angelino et al. (2000) investigated the use of working fluids such as aromatic hydrocarbons, siloxane, and siloxane mixtures straight chain hydrocarbons, and aromatic per-fluorocarbons for waste heat recovery from molten carbonate fuel cell plant. The performance of energy recovery cycles using different fluids was evaluated by means of optimization software for different operating conditions and cycle configurations(Angelino *et al.* 2000). Chen et al. (2006) conducted a comparative study of the CO_2 trans-critical cycle with an organic Rankine cycle and using R-123 as working fluid in waste heat recovery. The results show that the CO_2 trans-critical cycle represents a higher performance than R-123 when operating with low-grade waste heat(Chen *et al.* 2006).

Marciniak et al. (1981) conducted a comparative study of seven working fluids (water, methanol, R-11, R-113, 2-methypyridine/H_2O, Fluorinol 85, and toluene) on the design of an ORC power system in the range of 600–2400 kW. The author pointed out the disadvantage of using water as the working fluid for operating temperatures below 371° C where it becomes less efficient and too expensive. However, other working fluids such as organic compounds can be economically attractive at lower temperatures(Marciniak *et al.* 1981). Cong et al. (2005) carried out a detail analysis for producing mechanical work by an ORC operating on solar energy using R-123 or isobutene as the working fluid and studied the effect of the thermodynamic properties of the two working fluids on the operating conditions(Cong *et al.* 2005). McMahan et al. (2006) studied the use of ORC for electricity production by means of compound parabolic collectors. The effect of the selection of working fluids and the configuration of the ORC on the system performances had been discussed and an economic optimization methodology for solar-thermal ORC power plants had been presented(McMahan 2006).

Studies have also been carried out to investigate electricity and heat production by means of ORC from solid biomass combustion over the past years. For example, Drescher and Brüggeman (2007) had tested some isomeric hydrocarbons such as alkybenzenes for biomass ORC applications and showed that the ORC efficiency increased if the minimum temperature process was lowered, the maximum process

temperature increased, and the vaporization enthalpy to enthalpy input increased (i.e. very low degrees of superheating and subcooling) (Drescher *et al.* 2007).

The different studies summarised above have shown that the selection of the ORC working fluids needs to take account of many parameters such as those related to the heating source and the working fluids themselves. The ORC fluid will affect not only the efficiency of the ORC process but also the design of the ORC main components.

3.3.3. Working fluids selected for the project

Organic working fluids can be divided into three different categories - the 'wet fluids', the 'dry fluids' and the 'isentropic fluids', depending on their vapour saturation curve types (see Figure 3.3) in the temperature-entropy (T-S) diagram. Saturation vapour curve is the most crucial characteristic of the working fluid in an ORC. It affects the fluid applicability, cycle efficiency, and component design in an ORC power generation system. The derivative (dT/ds) is primarily a function of the vapour specific heat capacity and, as a consequence, is directly related to the molecule structure of the fluid. The heat capacity ratio (or adiabatic index) is the ratio of the heat capacity at constant pressure (C_P)to heat capacity at constant volume(C_V). It is denoted by(γ):

$$\gamma = \frac{C_P}{C_V} \tag{3.1}$$

For simple molecules, the value of heat capacity ratio (γ) is relatively high. Those fluids exhibit a negative slope of the saturated vapour line in the T-S diagram and are known as the 'wet fluids'. As the complexity of the molecule increases, the heat capacity ratio (γ) decreases, tending to one and the slope of the saturated vapour line becomes positive and become one of the 'dry fluids'). For an ideal working fluid, (dT/ds) tends to the infinity; then the fluid saturation vapour curve tends to be vertical in the T-S diagram, so the name of "isentropic" fluids. This feature affects the ORC fluid applicability, operation and cycle efficiency(Liu *et al.* 2004).

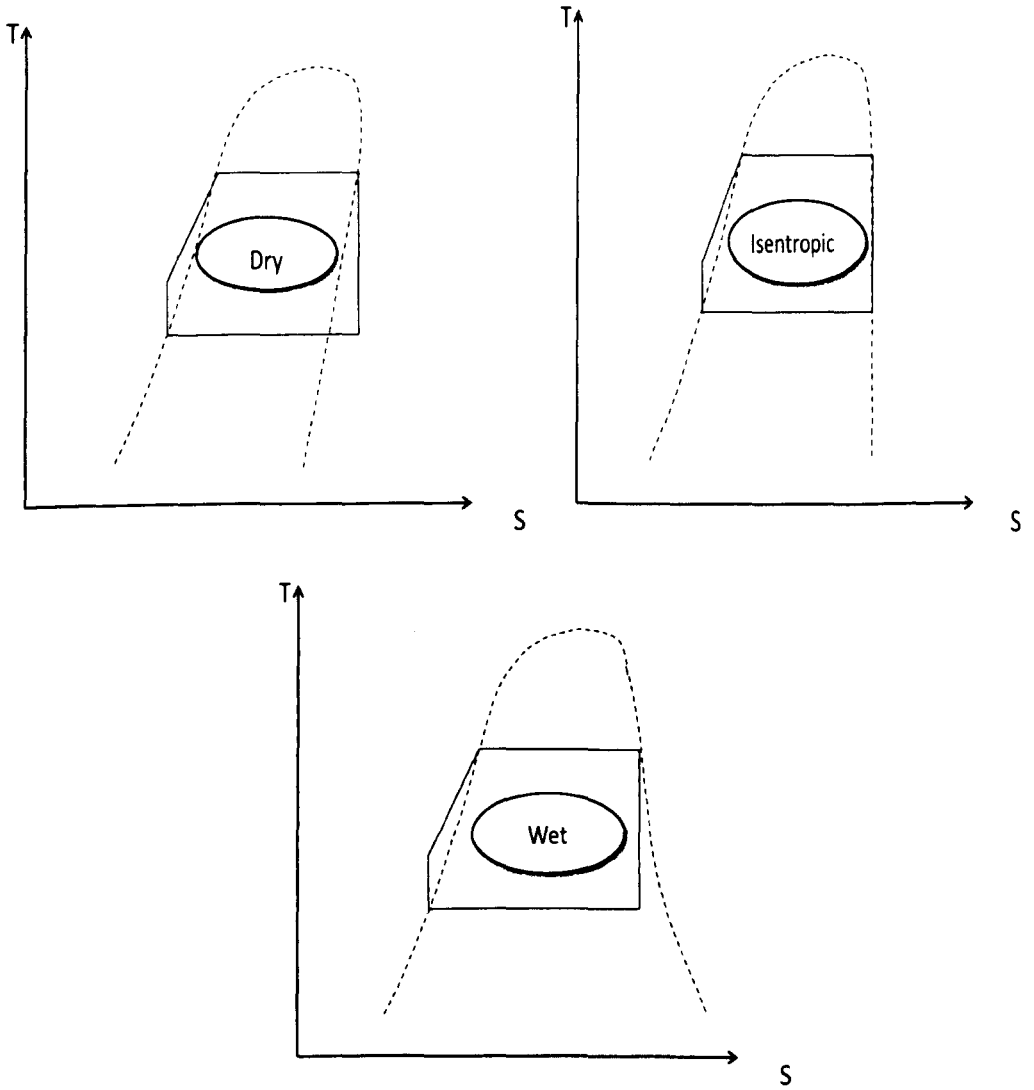

Figure 3.3 Schematic representation of dry, isentropic and wet fluids

The choice of the working fluid for a given ORC application is a key-issue and has been treated with great care in numerous studies reviewed in the above section. Generally, the characteristics of an ORC fluid should fulfil the following requirements:

1. Thermodynamic performance: the efficiency and/or output power should be as high as possible for the given heat source and heat sink temperatures. This generally involves low pump power consumption and appropriate boiling and critical temperatures.

2. Positive or isentropic saturation vapour curve, i.e. dry or isentropic fluids. A negative saturation vapour curve, i.e. a 'wet fluid', leads to droplets at the end of the

expansion(Quoilin 2009). The vapour must therefore be superheated at the turbine inlet in order to avoid turbine damages, which decreases cycle performance (Yamamoto *et al.* 2001). In the case of positive saturation vapour curve, i.e. with a dry fluid, a recuperator can be used in order to increase cycle efficiency.

3. High vapour density: this parameter is of key importance, especially for fluids showing a very low condensing pressure (e.g. silicon oils). A low density leads to very large equipments at the expander and condenser level.

4. Acceptable pressures: as already stated with water, high pressures usually lead to higher investment costs and increasing complexity.

5. High stability temperature: unlike water, organic fluids usually suffer from chemical deteriorations and decomposition at high temperatures. The maximum heat source temperature is therefore limited by the chemical stability of the working fluid. The working fluids should be thermally and chemically stable at all operating temperatures and pressures.

6. Low environmental impact and high safety level: the main environmental factors that need to be taken into account are the Ozone Depleting Potential (ODP), the Greenhouse Warming Potential (GWP), the toxicity and the flammability. The working fluid should be non-toxic, and preferably non-flammable.

7. The working fluids should be non-corrosive to the more common engineering materials used for the different components of the ORC such as pipes, turbine, heat exchangers, and seals.

8. Availability and cost: The fluid selected should be commercially available with acceptable cost.

In general, the screening method for working fluids depends on different criteria such as environment, safety, performance, and economic issues. In this project, the working fluid selection was also limited by the available database of the refrigerants with the simulation software EES (McGraw-Hill's Engineering Equation Solver, to be described later).

Some of the organic working fluids used in previous investigations of ORC processes, such as Freons, CFCS, are ozone depleting substances and hence detrimental to the environment. HCFCs and HFCs have great Global Warming Potentials (GWP) and are either phasing-out or facing the calls of phase–out - on Friday, September 21, 2007, representatives of 191 countries met in Montreal and agreed to accelerate phase-outs of HCFCs from 2009, with developed countries agreeing to reduce production and consumption 10 years earlier than previously promised, with final phase out in 2020(Montreal protocol 2007). Even though HFC refrigerants remain to be 'the best option to meet many needs', HFCs will face the calls for phase-out because of their great GWPs. There are many environment-friendly working fluids, such as hydrofluoroethers (HFEs) and n-pentane, which can be used in ORC-based processes. Tsai et al. (2005) did an environment risk assessment of hydrofluoroethers (HFEs) and indicated that some HFEs such as HFE-7000, HFE-7100, HFE-7200 and HEF-7500 could be considered to replace HCFCs, and HFCs in order to reduce the greenhouse gases emission and become environmentally friendly(Tsai 2005).

In this project two different HFEs are taken into consideration, HFE7000 (also known as HFE347mcc and RE347mcc) and HFE7100 (also known as HFE449mccc), which are also included in the database of the software (EES) used for the modelling. Their boiling points, 35.24°C and 60.04°C respectively, and critical temperatures, 164.6°C and 195.3°C respectively, indicate that they are the suitable working fluids for micro-CHP systems delivering heat to domestic heating systems such as under floor heating and domestic hot water. One potential advantage of using these fluids is that the pressure in the condenser can be kept near to the region of 1 atm, thus reducing maintenance costs due to system leaking, using vacuum pumps or pressurizing the cycle. The critical temperatures of these two fluids are higher than the maximum process temperature - the evaporation temperature which is designed to be at 160°C.

In addition to HFE7000 and HFE7100, an alkane, n-pentane, has also been selected as the working fluid for the modelling. The thermophysical properties, of n-pentane are very similar to those of HFE7000 and HFE7100 and are also included in the database of the modelling software - EES. n-pentane has low ODP and GWP

values, low toxicity, and is relatively stable(Saleh *et al.* 2007). But n-pentane is flammable and therefore proper safety measures have to implement if it is used in practice.

Table 3.2 Properties of selected fluids

	HFE7000	HFE7100	n-pentane
Molecular formula	n-$C_3F_7OCH_3$	$C_4F_9OCH_3$	C_5H_{12}
Boiling Point (°C)	35.23	60.03	35.87
Critical Temperature (°C)	164.6	195.3	196.5
Critical Pressure (kPa)	2478	2229	3364
Enthalpy of Vaporisation (kJ/kg)*	132.4	111.5	357.8
Ozone Depletion Potential	0	0	0
Global Warming Potential	450	410	3

*The enthalpy of vaporisation is obtained at the substance normal boiling point

All the three fluids selected for modelling, HFE7000, HFE7100 and n-pentane selected for modelling are dry fluids. As definition, the slope of the saturated vapour line of a dry fluid is positive (Figure 3.3) and hence when it enters the turbine as a saturated vapour, it will exit from the turbine in the superheated vapour region. This means no superheating before the turbine is needed to avoid damage to the turbine blades due to droplets. This characteristic is particularly favourable in applications with low-temperature heat sources. The properties of the three selected fluids are shown in Table 3.2, with the enthalpy of vaporisation being obtained at the substance normal boiling point. For modelling consistency, all thermophysical properties of the selected fluids were calculated by using the database of the modelling software - EES, although their values may slightly differ from those presented by other researchers(Sekiya *et al.* 2000).

3.4. Modelling Software

The software used in this ORC model is McGraw-Hill's Engineering Equation Solver, which is named as EES in this thesis for short(F-Chart Software). EES is a general equation-solving program that can numerically solve thousands of coupled non-linear algebraic equations. The program can also be used to solve differential and integral equations, do optimization, provide uncertainty analyses, perform linear and non-linear regression, convert units, check unit consistency, and generate publication-quality plots. A major feature of EES is the high accuracy thermodynamic and transport property database that is provided for hundreds of substances in a manner that allows it to be used with the equation solving capability(F-Chart Software).

A major difference between EES and other existing equation solving programs, such as BACKONE (BACKONE Equations of State), is the many built-in mathematical and thermophysical property functions which EES provides. For example, the steam tables are implemented such that any thermodynamic property of steam can be obtained from a built-in function call in terms of any two other properties. Similar capability is provided for many other fluids, e.g., ammonia, nitrogen, methane, propane, all common CFC refrigerants, R-134a and including all three ORC fluids selected for this project: HFE7100, HFE7000 and n-pentane. Hence, all thermodynamic properties of the ORC fluids in this thermodynamic modeling study were obtained by use of EES. EES also allows professional plotting (2-D, contour, and 3-D) T-s, P-h and P-V diagrams with automatic updating. Fluid properties such as temperature, pressure, enthalpy and entropy could be calculated by the programme with a good degree of accuracy and then directly be linked to the set of equations representing the various processes of the Organic Rankine Cycle (F-Chart Software).

EES has another very useful feature called parametric tables. In such tables, selected variables appear on the columns, while the lines represent different cases; each case has an unique combination of independent variables (IV) values; the user can input different IV values on different lines, therefore avoiding having to change those values in the routine code every time the value of an IV changes. Calculations yielding the values of the dependent variables for all cases are then completed all at once, saving a significant amount of time(F-Chart Software).

However, EES still has some shortcomings, such as the list of fluids included in the software database is neither particularly large nor up to date. The refrigerants included are mainly CFCs, HCFCs, HFCs, and hydrocarbons(F-Chart Software). The number of environmentally friendly fluids which could be used for ORC applications such as this project was quite small. In particular, only two hydrofluoroethers (HFEs), HFE7000 and HFE7100 were included in the list and could be used in the modelling of this study. The presence of the phased-out refrigerants and those of facing phasing-out is anyway useful, for it allows comparing the performances of new fluids with the ones used before the implementation of Kyoto Protocol and Montréal Protocol.

In the case of HFE7000, and HFE7100, the correlations, used in the software of EES to calculate the fluid state properties were fit to data supplied by the manufacturer 3M(3M Ltd.). In the case of n-pentane, correlations and basic data were taken from existing literature(F-Chart Software).

EES applied in mechanical engineering thermodynamics and heat transfer can be great help for the researcher to work problems. However, much of the time and effort would be saved to solve problems results from looking up property information and solving the appropriate equations. Besides, EES is particularly useful for design problems in which the effects of one or more parameters need to be determined. Just like this case. The program provides this capability with its Parametric Table, which is similar to a spreadsheet. The modelling process and appropriate equations will be described in the following sector. The variables will be identified and are independent by entering their values in table cells. Then the EES will calculate the values of the dependent variables in the table. The relationship of the variables in the table can then be displayed in publication-quality plots.

However, it has to be noted that just some functions of EES were used in this project, and therefore this section does not aim at giving an exhaustive description of the software capabilities and limits, that go far beyond what has been mentioned above

3.5. Organic Rankine Cycle Modelling

3.5.1. Modelling Simplifications and Assumptions

The modelling and analysis of the organic Rankine cycles have been conducted according to the First Law of Thermodynamics, that of energy conservation, to find both the work inputs and outputs, and heat added and rejected are all under steady state conditions. The ORC modelling described in this chapter is part of the overall research project tasks which is ideally to be done at the cycle design stage. Due to time restrictions, the ORC modelling has been carried out concurrently with some of the experimental activities. Nevertheless, the modelling results have been used to guide the experimental activities of the project wherever possible. There are a number of simplifications that have been adopted with the modelling:

- The modelling of some of the cycle components is a simplistic one with assumed generic thermal efficiencies. In particular, this is true for the evaporator and condenser which represent a generic ability of the components to transfer heat from the warm side to the cold side.
- Heat transfer simplifications: Heat transfer coefficients which should be related to a number of factors such as velocity, density, viscosity, boundary layers of the fluid and dimensions of the heat exchangers, were not taken into account with the modelling. Instead, a default assumption that 'the required amount of heat can be transferred from the warm side to the cold side' is adopted with the modelling.
- Pressure drops in the heat exchangers and in the pipes were ignored with the modelling. In addition, the heat losses through all the pipe walls of the cycle have been assumed to be equal to zero. The heat losses through heat exchangers are taken into account by use of assumed thermal efficiencies detailed below.

Furthermore, a number of parameters (as show in Table 3.3) have been set to be constants throughout the whole modelling process:

- According to the size of the biomass boiler used in this project, the nominal thermal input of the biomass boiler is taken as 20 kWe. The

thermal efficiency (η_{boiler}) of the biomass boiler is set to be 85% (based on the low heating value of the biomass fuel), which is specified by the manufacturer and confirmed by the testing on the biomass boiler. The boiler thermal efficiency is expected to decrease slightly when the hot water temperature is higher than the nominal operating temperature (95 ^{0}C) specified by the manufacturer. However, this has been neglected with the modeling studies reported in this chapter.

- A well-insulated SWEP compact heat exchanger is used as the evaporator of the ORC fluid and hence its heat loss to the surrounding is expected to be small. The thermal efficiency of evaporate (η_{evap}) is assumed to be 0.96. The isentropic turbine efficiency ($\eta_{turb,IS}$) is assumed to be 85% following Saleh et al.(Saleh *et al.* 2007)
- The heat loss factor of the condenser thermal is assumed to be 0.98, another well-insulated SWEP compact heat exchanger is used as the condenser and hence its heat loss is expected to be small. Because of its lower operation temperature than the evaporator.
- The isentropic pump efficiency ($\eta_{pump,IS}$) is assumed to be 85%
- The efficiency of the alternator (η_{alt}) is set to be 90% although the value can vary considerably depending on the type and size of the alternator. Any uncertainty in the performance of this element can affect greatly the electrical efficiency of the system.
- The inlet temperature of the cooling water of the condenser can vary considerably from season to season, which can alter the thermal efficiency of the system. Nevertheless, for the laboratory test is starting in the winter of 2009, it is assumed to be 13 ^{0}C which is the average temperature of the tap water used in the test then.

Although in real experimentation, the turbine, pump, alternator, boiler and heat exchangers efficiencies will change depending on different organic working fluid type, working temperature and pressure, size and design of components etc., the thermodynamic modelling will not try to analyse the effects of the changing efficiencies on the performance of the system. Instead, the modelling will focus on the comparative analyses of system performance with different organic working fluids

and different cycle configurations, with or without internal heat recuperations, which will be detailed later within this chapter.

Table 3.3 Values of Assumed Parameters

Boiler thermal input	Q_{in}	25	kW_{th}
Pump Isentropic Efficiency	$\eta_{pump,IS}$	85	%
Evaporator Heat thermal efficiency	η_{evap}	96	%
Turbine Isentropic Efficiency	$\eta_{turb,IS}$	85	%
Internal Heat Exchanger thermal efficiency	η_{IHE}	97	%
Condenser Heat Loss Factor	η_{cond}	98	%
Boiler Thermal Efficiency	η_{boiler}	85	%
Alternator Efficiency	η_{alt}	90	%
Cold water inlet temperature	$T_{cooling\_w}$	13	°C

3.5.2. Cycle Configurations and thermal efficiency of ORC

The basic Organic Rankine cycle configuration to be modelled in this project involves four processes as shown in Figure 3.4:

- Pumping process of the organic working fluid (between states 1-2),
- Evaporation process (between states 2-3),
- Expansion process in a turbine (between states 3-4),
- Condensation process (between states 4-1).

According to the basic ORC configuration described above, an ideal, basic organic Rankine cycle can be depicted on a T-s diagram as Figure 3.5. This ideal Rankine cycle does not involve any internal irreversibility and these four processes can be summarised as the following:

- Isentropic compression in the pump(between states 1-2)

- Constant pressure heat addition in the evaporation (between states 2-3)
- Isentropic expansion in a turbine (between states 3-4)
- Constant pressure heat rejection in a condenser (between states 4-1)

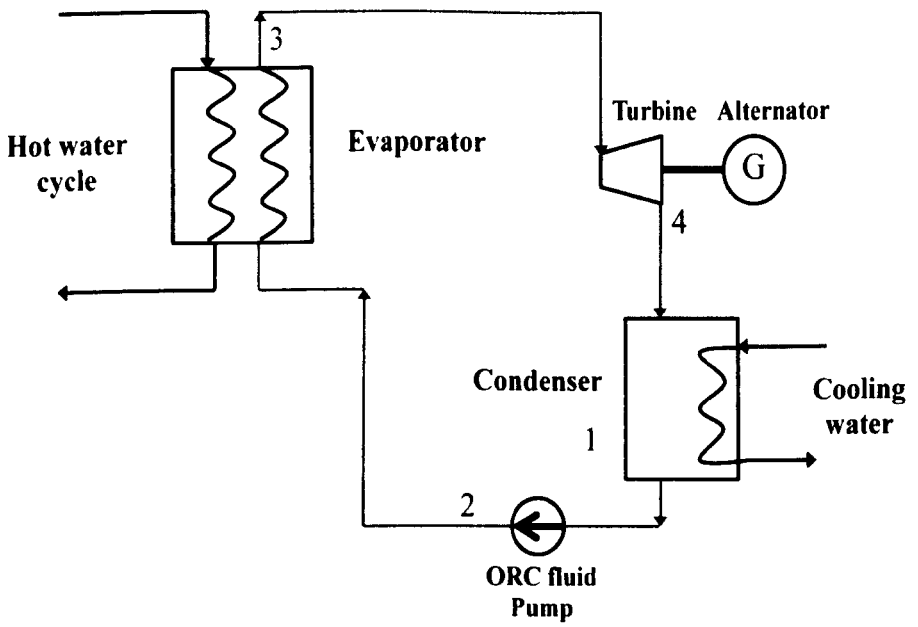

Figure 3.4 A Basic Organic Rankine cycle

The working fluid enters the pump at state 1 as saturated liquid and is compressed isentropically to the operating pressure of the evaporator. The working fluid temperature increases somewhat during this isentropic compression process due to a slight decrease in the specific volume of the fluid. Then, the working fluid enters evaporator as a compressed liquid at state 2 and leaves as a saturated or superheated vapour at state 3. The evaporator here is basically a large heat exchanger where the heat of hot water originating from the combustion of biomass is transferred to the organic working fluid essentially at constant pressure. After that, the saturated or superheated vapour at state 3 enters the turbine, where it expands isentropically and produces work by rotating the shaft connected to an electric generator. The pressure and the temperature of working fluid drop during this process to the values at state 4, where the working fluid enters the condenser. At this state, the working fluid is usually a superheated vapour as only dry working fluids are used with the proposed system. Finally, the working fluid is condensed at constant pressure in the condenser, which is also basically a heat exchanger, by rejecting heat to a cooling water system. The working fluid leaves the condenser as a saturated liquid or a sub-cooled liquid

which denotes the liquid temperature is lower than the corresponding saturated liquid temperature and enters the pump, completing the cycle.

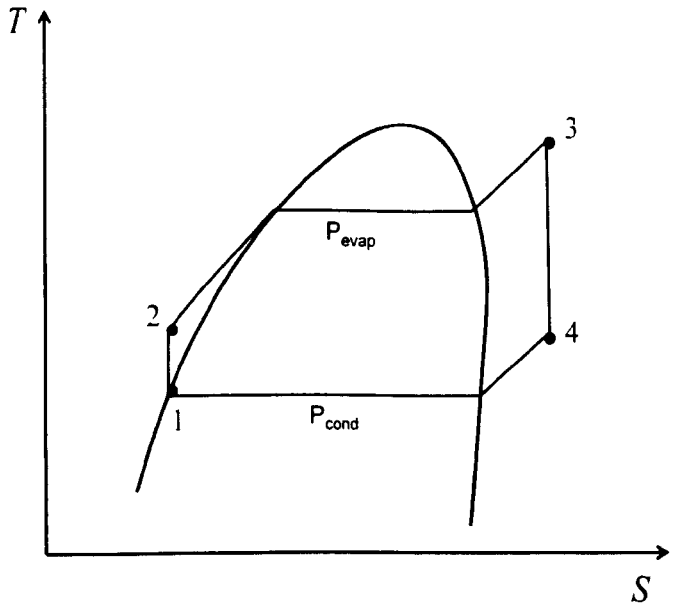

Figure 3.5 T-s diagram of a ideal basic ORC

All four components associated with the basic organic Rankine cycle (the pump, boiler, turbine, and condenser) are assumed to be steady-flow devices, and thus all four processes that make up the organic Rankine cycle can be analyzed as steady-flow processes. The kinetic and potential energy changes of the fluid/vapour are usually small relative to the work and heat transfer terms and are therefore neglected with the modelling. Applications of the conservation of mass and the first law of thermodynamics lead to the expressions for the work per unit of mass flowing of the turbine (W_{turb}) and that of the pump (W_{pump}), the net work (W_{net}), the heat transfer into the system per unit of mass flowing(q_{in}), the heat transfer out of the system per unit of mass flowing(q_{out}) and the efficiency (η_{Rank}). Theoretically speaking, the work input into the system (w_{pump}) should be defined as positive work, the work output of the system (w_{turb}) as negative work. However, during the following calculate, for net work output of the cycle is expressed as numerical positive value, the sign of works may be differ from their thermodynamic definition.

The work of the turbine and work of the pump can be expressed as:

$$w_{pump} = h_2 - h_1 \tag{3.2}$$

$$w_{turb} = h_3 - h_4 \tag{3.3}$$

The net work output of the cycle can be expressed as:

$$w_{net} = w_{turb} - w_{pump} = (h_3 - h_4) - (h_2 - h_1) \tag{3.4}$$

The heat transfer supplied by the evaporator is

$$q_{in} = h_3 - h_2 \tag{3.5}$$

The thermal efficiency of the Rankine cycle can be expressed as the net work of the system divided by the heat input into the system.

$$\eta_{Rank} = \frac{w_{net}}{q_{in}} \tag{3.6}$$

$$\eta_{Rank} = \frac{(h_3 - h_4) - (h_2 - h_1)}{h_3 - h_2} \tag{3.7}$$

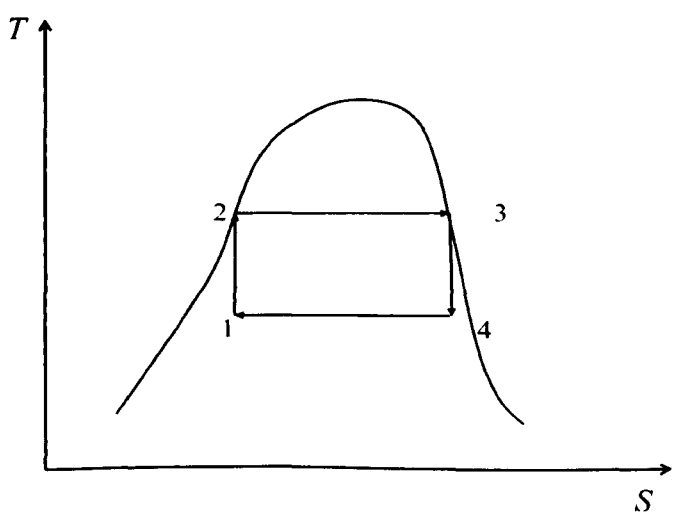

Figure 3.6 T-s diagram of a Carnot cycle

Consider a steady-flow Carnot cycle executed within the saturation of working fluid, as shown in Figure 3.6. This ideal Carnot cycle does not involve any internal irreversibility and these four processes can be summarised as the following:

The fluid is compressed isentropically by a compressor (pump) to the initial state (process 1-2), and then heated reversibly and isothermally in a boiler (evaporator) (process 2-3), expanded isentropically in a turbine (process 3-4), condensed reversibly and isothermally in a condenser (process 4-1). The thermal efficiency of a Carnot cycle operating between high temperature (T_{max}) and low temperature (T_{min}) reservoirs is given by

$$\eta_{Carnot} = 1 - \frac{T_{min}}{T_{max}} \tag{3.8}$$

The maximum temperature of the heat source (T_{max}) depends on the type of energy source (hot water generated from combustion of biomass for this project) and the energy transfer efficiency of evaporator, whereas (T_{min}) depends on the available cooling water temperature and the heat transfer efficiency of the condenser. As none of the cycles operating between temperatures (T_{max}) and (T_{min}) can exceed the efficiency of a Carnot cycle, (η_{Rank})should always be smaller than (η_{Carnot}) .

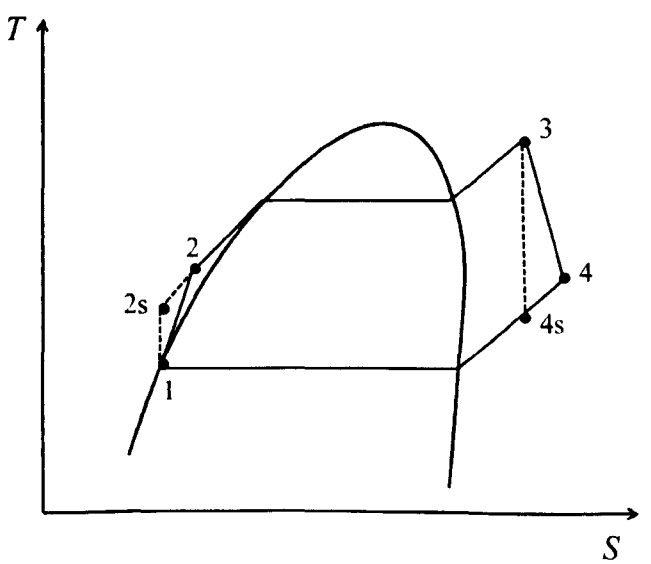

Figure 3.7 T-s diagram of a real basic ORC

A real, basic organic Rankine cycle will involve some internal irreversible processes, particularly the turbine expansion process and the pumping process which are to be represented by an isentropic efficiency of the turbine and an isentropic

efficiency of the pump in the modelling. As shown in Figure 3.7. This will be further discussed in the next section.

In addition to the basic Organic Rankine cycle configuration shown in Figure 3.4, other ORC configurations have been investigated in this modelling which include those with and without Internal Heat Exchanger (IHE), and those with and without superheating and subcooling.

In an ORC with an Internal Heat Exchanger (Figure 3.8), some heat contained in the vapour after the turbine exhaust is recuperated, before the vapour is condensed, and is used for pre-heating the organic working fluid. The modified Rankine Cycle stages therefore become:

- pumping the fluid (process 1-2)
- preheating the fluid with the recuperated heat (2-2a)
- evaporation (2a-3)
- expansion(3-4)
- release of the heat to be recuperated (4-4a)
- condensation (4a-1)

The controlled variable of the IHE (such as at a design stage) is the temperature drop on the warm side, (ΔT_{IHE}) in this modelling, it has been varied between 0 and 30K, according to the fluid and operating conditions.

Three types of organic Rankine cycle for the selected 3 ORC fluids which belong to the category of dry working fluids have been modelled:

Type I: saturated cycle,

Type II: cycle with superheating,

Type III: cycle with subcooling.

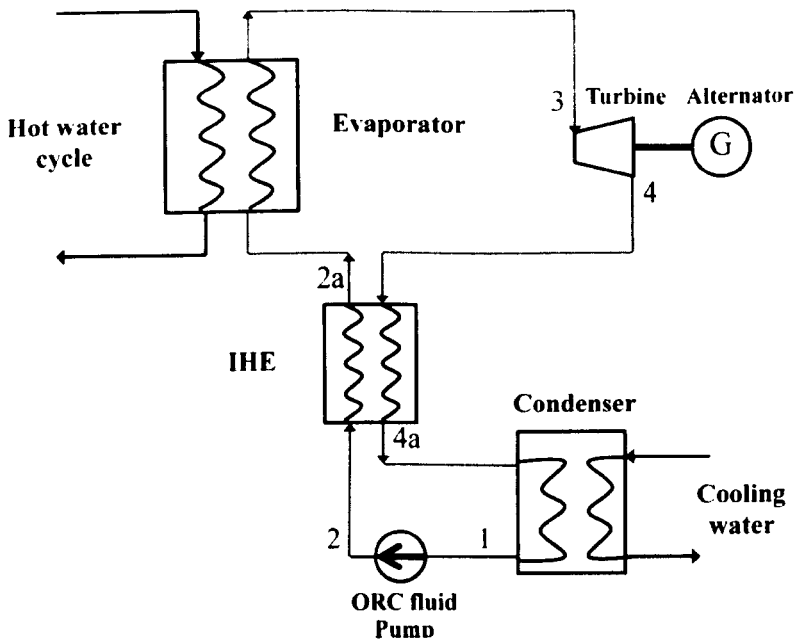

Figure 3.8 Organic Rankine cycle with IHE

These three types of cycles are further described below:

- Type I cycle:

This type of ORC is shown in the T-s diagram in Figure 3.9. The working fluid leaves the condenser as saturated liquid (state point 1). Then it is compressed in the pump to evaporator pressure (state point 2) with isentropic pump efficiency$(\eta_{pump,IS})$. After that, the fluid is heated at constant pressure and achieves the cycle maximum temperature (state point 3) till it becomes saturated vapour. Then it enters the turbine and expands to state point 4 where it reaches as superheated region with isentropic turbine efficiency$(\eta_{turb,IS})$. In the end of the cycle, the working fluid enters the condenser and removes heat at constant pressure till it becomes a saturated liquid (state point 1).

- Type II cycle:

This type of ORC is represented in the T-s diagram in Figure 3.10. The state point 1, 2 and 4 are same as Type I cycle. The working fluid is heated from state point 2 till it becomes saturated vapour and thereafter it is superheated (state point 3). Type B cycle will be referred as 'superheating' because 'state point 3' is in superheated state.

- Type III cycle:

This type of ORC is represented in the T-s diagram in Figure 3.11. The process steps in this cycle are similar to Type I cycle with only difference that the state point 1 lays in the compressed liquid region. Type III cycle will be referred as 'sub-cooling' because the temperature of state point 1 is below the saturation temperature.

With each of the three types of ORC shown in Figure 3.9– Figure 3.11, state points 2a and 4a are used to denote the potential presence of an IHE.

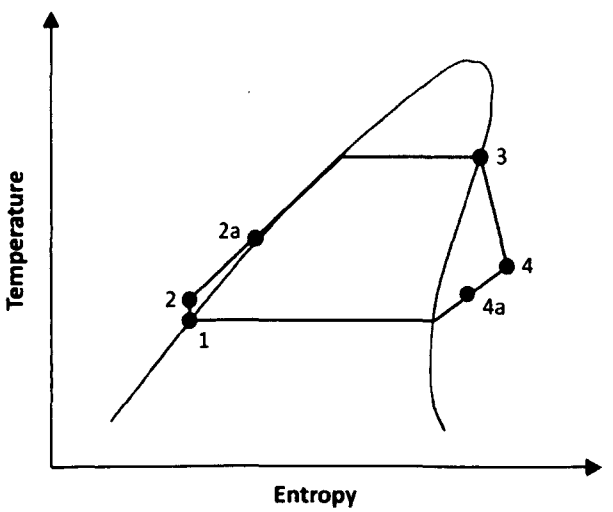

Figure 3.9 T-s diagram of Type I cycle

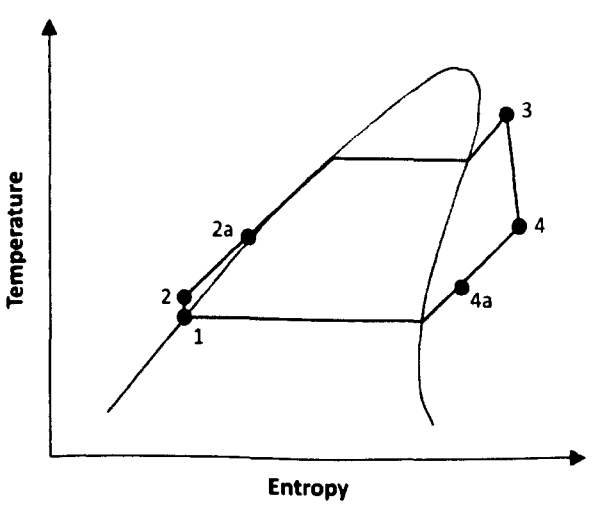

Figure 3.10 T-s diagram of Type II cycle: with superheating

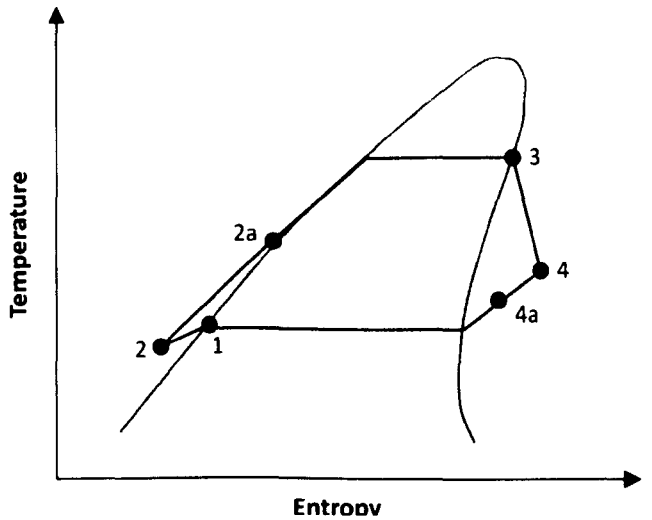

Figure 3.11 T-s diagram of Type III cycle: with subcooling

The thermal efficiency of each type of ORC (Type I, II or III) can be calculated by using equation (3.6) providing that the actual enthalpy of the ORC at each state point is used in the calculation. Other efficiencies of the CHP system can also be calculated with the above listed simplifications and assumptions. The actual equations involved in the calculations of efficiencies for the basic ORC configuration (Figure 3.4) may be different from those for the ORC configuration with IHE (Figure 3.8). All of the relevant equations needed for the modelling will be detailed in the next subsection (3.5.3).

The saturated and superheating/subcooling routines created for the modelling dealt with (ΔT_{IHE}); if such variable was set to 0 K, there was no Internal Heat Exchanger in the cycle: this meant that no special routine was needed to simulate the use of the IHE. Three different modelling routines were created to model each of the three types of ORC.

In the configurations with superheating and subcooling, the number of processes is the same as in the saturated configuration; however, for computational reasons, different routines for superheating and subcooling had to be created. In fact, for the saturated configuration, the software needs, as input value, not only the fluid saturated pressure (or, alternatively, the temperature), but also the quality x of the liquid/vapour mixture at states 3 and 1 (x=1 and x=0 respectively). In the superheating and subcooling configurations, on the other hand, the state of the fluid is solely determined by its pressure and temperature.

In all types of routines, a simple "pinch-point type" analysis, based on the temperature profiles of the two sides of the heat exchanger, has been carried out for the two sides of the condenser. The minimum temperature difference between the two sides was set to 5 K. In a real application, a low temperature difference across the two sides of a heat exchanger means that a very large heat exchanger may have to be used for effective heat transfer. The simple analysis adopted with this modelling determines the flow and the outlet temperature of the cooling fluid used in the thermal process of the CHP (in this case, the water to be used as the domestic hot water supply or space heating).

3.5.3. Modelling of the proposed micro-CHP with a real ORC

As pointed out above, a real organic Rankine cycle will be different from that of an ideal organic Rankine cycle (shown in Figure 3.5). In this section, Figure 3.12 illustrates the deviation of a real ORC from the ideal ORC, as a result of the presence of the various irreversibilities in the cycle processes. However, fluid frictions and heat losses to the surroundings are the two common sources of irreversibilities.

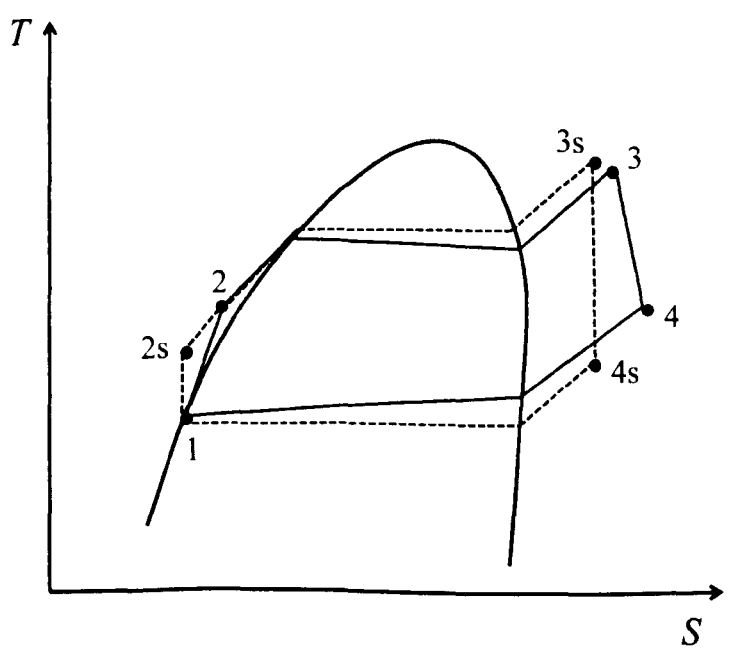

Figure 3.12 Deviation of a real ORC from the ideal ORC

Fluid frictions cause pressure drops in the evaporator, the condenser, and the piping between various components. As a result, the working fluid leaves the evaporator (state point 3) at a somewhat lower pressure than state point 3s. Also, the pressure at the turbine inlet is somewhat lower than that at the boiler exit due to the pressure drop in the connecting pipes. The pressure drop in the condenser is usually very small. To compensate for these pressure drops, the working fluid must be pumped to a sufficiently higher pressure than the ideal cycle calls for. This requires a larger pump and larger work input to the pump.

A. Pumping process: state point 1-state point 2

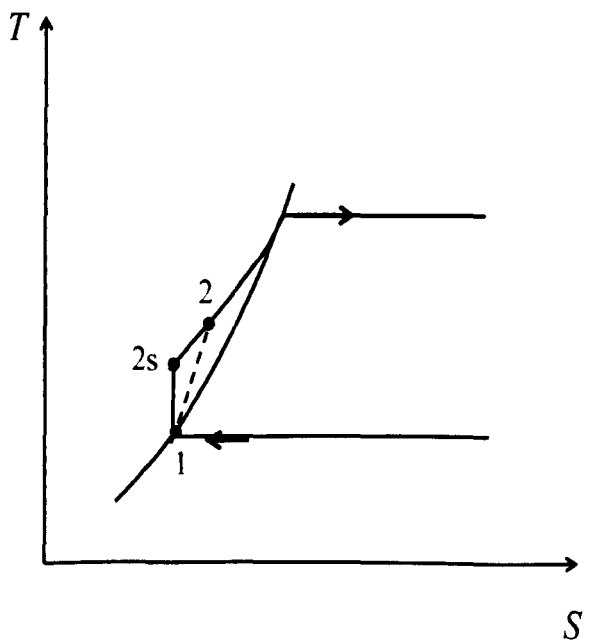

Figure 3.13 Irreversibility with the ORC fluid pumping process

In the pumping process, the pressure of the fluid, at a liquid stage, is increased from the minimum process pressure to the maximum process pressure (Figure 3.13). On the T-s diagram, the state point 1 and state point 2 representing the state points before and after the pumping are very close and located in the same isobar. To enhance the clarity, all the vertical distance between states 1 and 2 on the T-s diagram of Figure 3.13 is greatly exaggerated.

The pressure at point 1 is the fluid saturated pressure corresponding to the given condensing temperature; similarly, the pressure at point 2 is the fluid saturated pressure corresponding to the given evaporating temperature. As mentioned in above section 3.51, the pump has an isentropic efficiency $(\eta_{pump\ ,IS})$ of 85%. The deviation of actual pump work from the isentropic one can be accounted for by utilizing isentropic efficiencies, defined as:

$$\eta_{pump} = \frac{W_{pump\ ,ID}}{w_{pump}} \tag{3.9}$$

Therefore the work input required by the pump is defined by:

$$w_{pump} = \frac{W_{pump\ ,ID}}{\eta_{pump\ ,IS}} \tag{3.10}$$

$W_{pump\ ,ID}$ is the ideal pump work if the process were isentropic. The ideal pump work is calculated as the enthalpy flow difference between points 2s and 1; the fluid entropy (see Figure 3.13) and mass flow rate (it is a closed cycle) at state 2s is the same as at state 1:

$$W_{pump\ ,ID} = \dot{H}_{2s} - \dot{H}_1 = \dot{m} \cdot (h_{2s} - h_1) \tag{3.11}$$

$\dot{m}$ is the ORC mass flow rate here and h_2 and h_1 indicate the enthalpy values at state 2 and 1 respectively.

The work done by the pump increases the enthalpy *h* of the fluid; therefore:

$$W_{pump} = \dot{m} \cdot (h_2 - h_1) \tag{3.12}$$

B: Heating/Evaporation process (state point 2 – state point 3 for basic ORC configuration (Figure 3.4) & state point 2a – state point 3 for ORC configuration with IHE (Figure 3.8)

For the proposed micro-CHP system shown in Figure 3.2, the heat to drive the CHP is supplied by combusting biomass in the boiler. However, the modelling of combustion and heat transfer inside the biomass boiler is beyond the scope of the

thermodynamic modelling of ORC described in this chapter. Instead, the heat for the ORC is assumed to be transferred from the hot water generated from the biomass boiler to the working fluid in the evaporator. The evaporator considered with the modelling can be a series of heat exchangers. A Pinch Point analysis (Saleh *et al.* 2007) for the evaporator has not been carried out because the temperatures on the boiler side of the evaporator have been assumed to be much higher than those on the ORC side; thus, the changes in heat transfer rates are considered to be negligible. Also, for the sake of simplicity, no pressure losses have been accounted for in the evaporator, although small pressure losses do occur in reality.

The amount of heat supplied to the evaporator is defined as (Q_{evap}). It is dictated by the efficiency of the boiler and the heat losses within the evaporator which have been taken into account, as shown below. The use of compact heat exchangers such as SWEP's stainless steel copper-brazed heat exchangers in the actual experimental system is expected to avoid the excessive heat losses. As specified in section 3.5.1, the biomass boiler efficiency is set to 85% and the evaporator efficiency is 96%, therefore the amount of heat that is supplied to the evaporator can be calculated as follows:

$$Q_{evap} = Q_{boiler,nominal} \cdot \eta_{boiler} \cdot \eta_{evap} \tag{3.13}$$

The heat supplied by the hot water side increases the enthalpy of the working fluid but the initial enthalpy of the working fluid at the inlet of the evaporator depends on the ORC configuration. In the basic ORC configuration as shown by Figure 3.4, the organic working fluid comes from the ORC feed pump (without IHE) and hence,

$$Q_{evap} = \dot{m} \cdot (h_3 - h_2) \tag{3.14}$$

Whereas in the configuration with IHE as shown by Figure 3.8, the organic working fluid comes from the internal heat exchanger (i.e. recuperator) and therefore,

$$Q_{evap} = \dot{m} \cdot (h_3 - h_{2a}) \tag{3.15}$$

The organic working fluid can exit the evaporator as either saturated vapour or superheated vapour. For modelling purposes, the boiler thermal input (Q_{boiler}), boiler

thermal efficiency (η_{boiler}) and the evaporator heat lost factor are assumed to be constant as specified in Table 3-3, therefore the heat supply rate for the evaporation of organic working fluid (Q_{evap}) is also constant but the organic working fluid mass flow rate ($\dot{m}$) in the ORC loop will depend on not only the ORC types (shown in Figure 3.9– Figure 3.11) but also the ORC configurations, i.e. if IHE is used.

C. Turbine expansion process: state point 3 – state point 4

In this process, the working fluid vapour at state point 3 enters the ORC turbine, where it expands to produce mechanical energy or shaft power which can be converted to electricity by connecting the turbine to an electric generator (e.g. an alternator). The ORC vapour pressure drops from the maximum process pressure to the minimum process pressure during its expansion in the turbine. The expansion process of the working fluid vapour in the ORC turbine is non-isentropic process which is characterized by the turbine's isentropic efficiency specified as a constant (85%) in Table 3.3. There is also some energy loss with the conversion of the turbine's mechanical energy or shaft power to electrical energy by the alternator, with the conversion efficiency assumed to be 90% (Table 3.3).

If ($W_{turb,ID}$) is used to denote the ideal work output of the turbine with an isentropic expansion process, then the actual work output of the turbine can be calculated as:

$$W_{turb} = W_{turb,ID} \cdot \eta_{turb} \tag{3.16}$$

where ($\eta_{turb,IS}$) is the turbine isentropic efficiency. The electrical output from the turbine/alternator combination, (W_{el}) is the, product of the actual turbine work output, and the alternator efficiency(η_{alt}).

$$W_{el} = W_{turb} \cdot \eta_{alt} \tag{3.17}$$

The isentropic expansion process of the organic working fluid is described by the T-s diagram of Figure 3.14. The ORC fluid entropy and mass flow rate at state point

4s are the same as those at state point 3. Therefore, the ideal work output of the ORC turbine, $(W_{turb\ ,ID})$ can be calculated as:

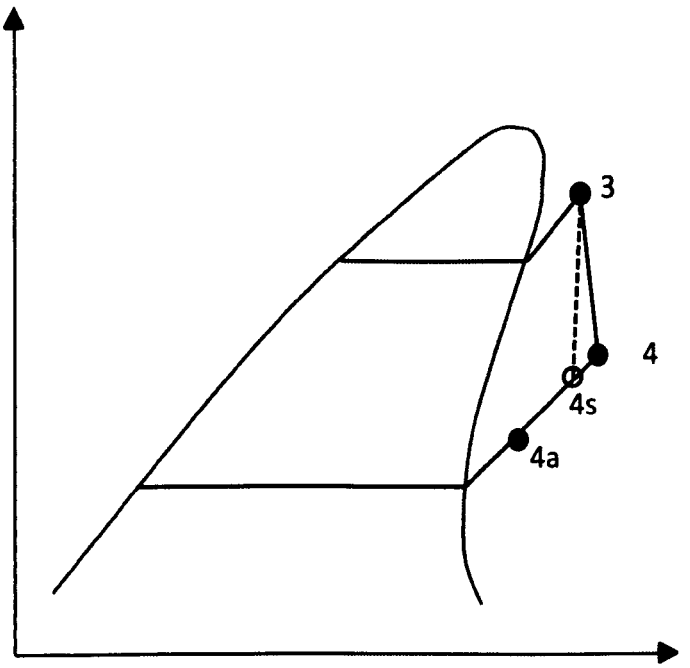

Figure 3.14 Irreversibility with the turbine expansion process

$$W_{turb\ ,ID} = \dot{m} \cdot (h_3 - h_{4s}) \tag{3.18}$$

The actual work output or the mechanical energy of the turbine produced by the working fluid vapour expansion in the turbine can be related to the working fluid enthalpy drop and mass flow rate as follows:

$$W_{turb} = \dot{m} \cdot (h_3 - h_4) \tag{3.19}$$

As only dry working fluids are considered by the modelling study of this project, the working fluid at the exit of the ORC turbine, i.e. after the expansion in the turbine, state point 4, will always be within the superheated vapour region.

D. Condensing process: state point 4 – state point 1 for basic ORC configuration (Figure 3.4) & state point 4a – state point 1 for ORC configuration with IHE (Figure 3.8)

In this process, the working fluid vapour is condensed in the condenser, and useful heat is recovered by an open loop cooling water system. Counter-current flows between the hot side fluid and the cold side fluid are beneficial to the heat transfer process between the fluids and therefore are adopted for all heat exchangers including the evaporator, the condenser and the recuperator. Cold water from the main water tap which is assumed to be at 13 °C (as measured) enters the condenser at the same end as the outlet of the ORC fluid, whereas the heated tap water exits at the same end as the inlet of the ORC fluid.

Because the temperatures on the two sides of the condenser heat exchanger are similar and the temperature difference between the hot side and the cold side cannot be too small, otherwise very large number of plates would be needed to complete the required heat transfer. A simple Pinch Point analysis (Saleh *et al.* 2007)of the temperature profiles with the condenser heat exchanger is carried out with the assumed the minimum temperature difference between the two sides of the heat exchanger, (ΔT_{PP}), fixed at 5K in the model. Figure 3.15 illustrates the temperature profiles of the condenser heat exchanger for ORC with subcooling. The heat transfer from the hot side (the ORC fluid side) to the cold side (the cold water side) of the condenser takes place in three phases:

(1) A sensible heat transfer when the ORC fluid vapour is in the superheated region (state point 4 – state point 5 for the basic ORC configuration, Figure 3.4 or state point 4a – state point 5 for the ORC configuration with IHE, Figure 3.8). The steady-state energy flow heat transfer equation for each of the two ORC configurations are as follows:

For the basic ORC configuration (Figure 3.4, without IHE):

$$\dot{m} \cdot (h_{4a} - h_5) \cdot \eta_{cond} = \dot{m}_{water} \cdot (h_{10} - h_9) \tag{3.20}$$

For the ORC configuration with IHE (Figure 3.8):

$$\dot{m} \cdot (h_4 - h_5) \cdot \eta_{cond} = \dot{m}_{water} \cdot (h_{10} - h_9) \tag{3.21}$$

Where ($\dot{m}_{water}$) is the cooling water flow rate of the condenser.

(2) A latent heat transfer when the ORC fluid is condensed (state point 5 – state point 6). The heat transfer equation is:

$$\dot{m} \cdot (h_5 - h_6) \cdot \eta_{cond} = \dot{m}_{water} \cdot (h_9 - h_8) \tag{3.22}$$

(3) A sensible heat transfer when the ORC fluid is further cooled (from the saturated liquid state point 6 to subcooled liquid state point 1). The heat transfer equation is:

$$\dot{m} \cdot (h_6 - h_1) \cdot \eta_{cond} = \dot{m}_{water} \cdot (h_8 - h_7) \tag{3.23}$$

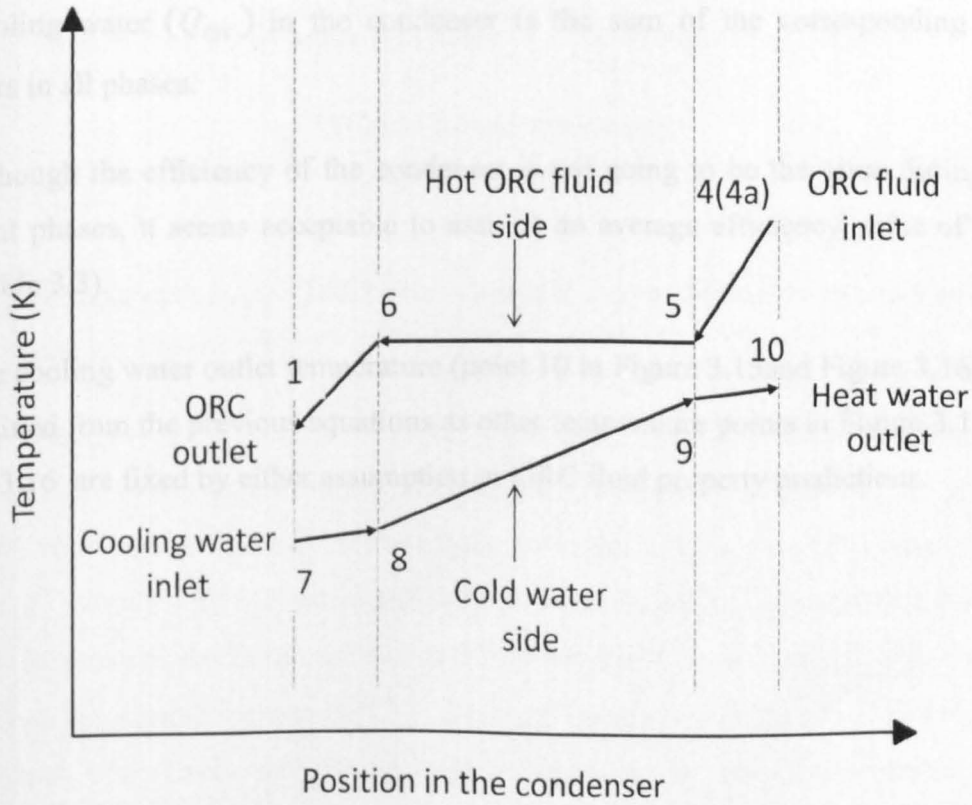

Figure 3.15 Temperature profiles of the two sides of the condenser

(ORC with subcooling)

Figure 3.15 illustrates the temperature profiles of the condenser for organic Rankine cycles without subcooling. The heat transfer from the hot side (the ORC fluid side) to the cold side (the cold water side) of the condenser takes place in two phases:

(1) The sensible heat transfer when the ORC fluid vapour is in the superheated region. The same equations as (3.20) & (3.21) shown above can be used to calculate the energy balance/heat transfer.

(2) The latent heat transfer when the ORC fluid is condensed. The associated heat transfer equation is:

$$\dot{m} \cdot (h_5 - h_1) \cdot \eta_{cond} = \dot{m}_{water} \cdot (h_9 - h_7) \tag{3.24}$$

With each of the equations 3-21 to 3-24, the left-hand side of the equation is the heat released by the ORC fluid, while the right-hand side is the heat received by the cooling water. The total heat released by the ORC (Q_{cond}) and total heat received by the cooling water (Q_{cw}) in the condenser is the sum of the corresponding heat transfers in all phases.

Although the efficiency of the condenser is not going to be the same during the different phases, it seems acceptable to assume an average efficiency value of 98% (see Table 3.3).

The cooling water outlet temperature (point 10 in Figure 3.15and Figure 3.16) can be obtained from the previous equations as other temperature points in Figure 3.15and Figure 3.16 are fixed by either assumption or ORC fluid property predictions.

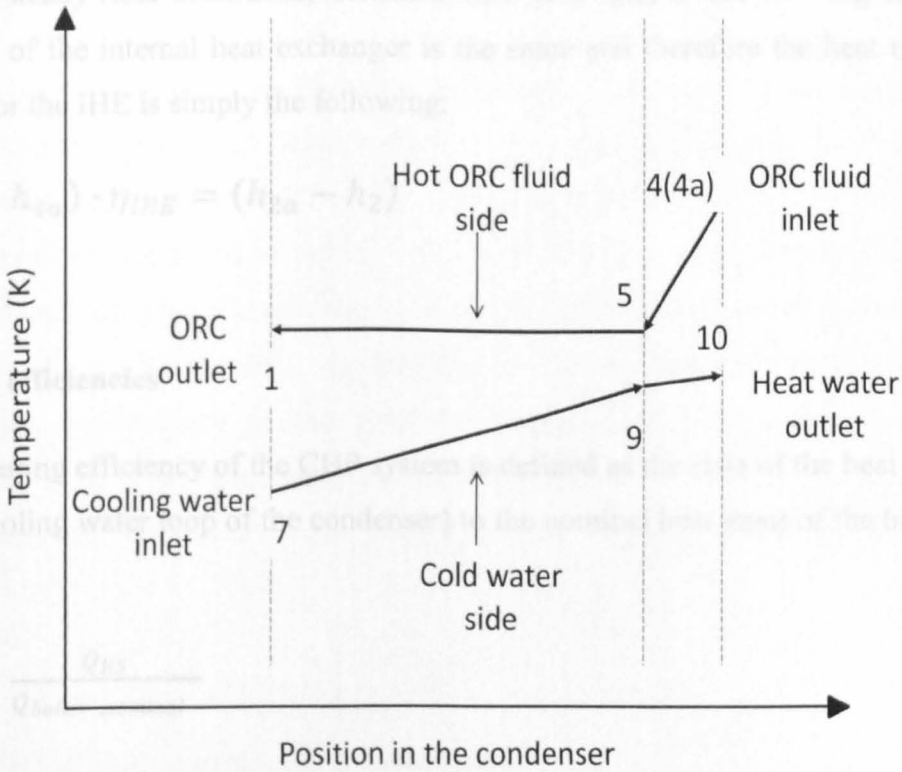

Figure 3.16 Temperature profiles of the two sides of the condenser

(ORC without subcooling)

E. Internal heat exchanger (IHE) (State point 2 – state point 2a and state point 4 – state point 4a, Figure 3.8):

The Internal Heat Exchanger recuperates heat from the ORC fluid after the turbine outlet which is in the superheated vapour state and releases it to the ORC fluid after the ORC fluid pump which is in the liquid state (see Figure 3.8). The temperature difference across the IHE sides is assumed to be sufficiently large and therefore no pinch point analysis has been carried out. The inclusion of an IHE will lead to a slight decrease in the overall system (CHP) efficiency because additional heat losses from the Internal Heat Exchanger are expected. However, the use of a compact heat exchanger such as a well-insulated SWEP compact heat exchanger will minimize the heat losses.

Under steady-state conditions, the mass flow rate ($\dot{m}$) of the working fluid on both sides of the internal heat exchanger is the same and therefore the heat transfer equation for the IHE is simply the following:

$$(h_4 - h_{4a}) \cdot \eta_{IHE} = (h_{2a} - h_2) \tag{3.25}$$

F. System efficiencies

The heating efficiency of the CHP system is defined as the ratio of the heat output (via the cooling water loop of the condenser) to the nominal heat input of the biomass boiler:

$$\eta_{th} = \frac{Q_{HS}}{Q_{boiler\ ,nominal}} \tag{3.26}$$

The electrical efficiency of the CHP system is defined as the ratio of the electrical output to the nominal heat input of the biomass boiler:

$$\eta_{el} = \frac{W_{el} - W_{pump}}{Q_{boiler\ ,nominal}} \tag{3.27}$$

The overall CHP efficiency is defined as the total energy output (heat plus electrical) divided by the nominal heat input of the biomass boiler. This is equivalent to the sum of the heating efficiency and the electrical efficiency:

$$\eta_{ov} = \frac{Q_{HS} + W_{el} - W_{pump}}{Q_{boiler\ ,nominal}} = \eta_{th} + \eta_{el} \tag{3.28}$$

The organic Rankine cycle efficiency of the basic ORC configuration (Fig.3.4) is calculated by equation (3.7), whereas for the ORC configuration with IHE, equation (3.29) must be used:

$$\eta_{Rank} = \frac{(h_3 - h_4) - (h_2 - h_1)}{h_3 - h_{2a}} \tag{3.29}$$

3.6. Thermodynamic Modelling Results and Discussion

This section presents and discusses the results of thermodynamics modelling studies of the proposed micro biomass-fired CHP system with organic Rankine cycle (ORC). Three environmentally friendly refrigerants, HFE7000, HFE7100 and n-pentane have been modelled as the ORC fluids. It is worthwhile to reiterate the main aims of the modelling were to investigate the effects of changing operating conditions, recuperating heat with the IHE, superheating and subcooling the organic working fluid on the performance of the proposed micro-scale CHP system. Particular attention has been given to the electrical efficiency of the micro-scale CHP system as low electrical efficiency is one of the main problems for micro-scale biomass-fuelled CHP systems(Dong *et al.* 2009)

3.6.1. Effect of changing operating conditions

Different operating conditions of the proposed micro-scale CHP system with ORC have been modelled. In particular, a range of evaporator temperatures and condenser temperatures have been modelled with all three ORC fluids (HFE7000, HFE7100, n-pentane):

Evaporator temperatures: 100 °C, 110 °C, 120 °C, 130 °C, 140 °C

Condenser temperatures: 20 °C, 30 °C, 40 °C, 45 °C, 50 °C

Figures 3.17 – 3.19 show the electrical efficiency (η_{el}) of the proposed biomass-fired micro-scale CHP system against the ratio of the condenser temperature to the evaporator temperature (the ratio of the heat sink temperature to the heat source temperature), for the three ORC fluids, respectively. These modelling results were obtained with Type I cycle only (i.e. no superheating or subcooling) but with both the basic ORC configuration (Figure 3.4) indicated by 'no IHE' and the ORC configuration with IHE (Figure 3.8) indicated by 'IHE = 10 ^{0}C'. For each ORC fluid,

the predicted electrical efficiency of the CHP system decreases with the ratio between the condenser temperature and the evaporator temperature with both temperatures expressed as absolute temperatures in Kelvin. This is as expected if we recall the maximum theoretical efficiency, the Carnot efficiency, of a heat engine:

$$\eta_{\text{Carnot}} = 1 - \frac{T_{min}}{T_{max}} \tag{3.30}$$

Where (T_{min}) denotes the temperature on the steam side of the condenser(T_C) of the ideal Rankine cycle; and (T_{max}) denotes the average temperature of heat addition at the evaporator(T_E).

The comparisons of the predicted ORC efficiencies (η_{Rank}) with the Carnot cycle efficiency (η_{Carnot}) are shown in Figure 3.20 with HFE7000 as the ORC fluid, in Figure 3.21 with HFE7100 as the ORC fluid, and in Figure 3.22 with n-pentane as the ORC fluid, with the condenser temperature fixed at 293K, 303 K, 313 K and 323 K. These figures show that the predicted ORC efficiency is well below the Carnot cycle efficiency for each of the ORC fluids. However, the ORC efficiency decreases as the evaporator temperature decreases (if T_C is fixed, a decrease in T_E means an increase of T_C/T_E), but not linearly.

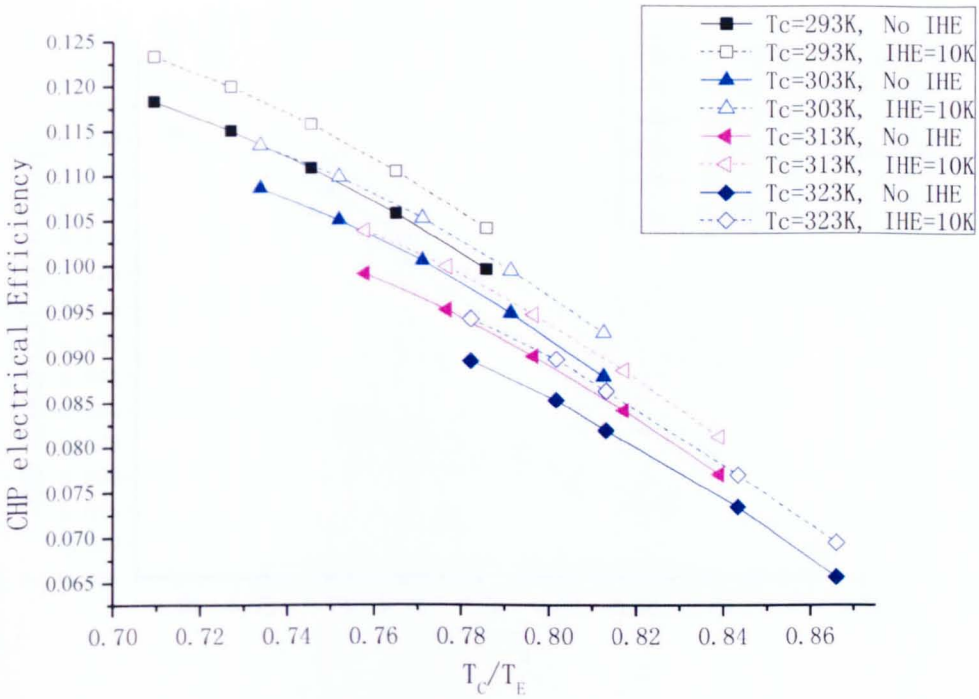

Figure 3.17 CHP electrical efficiency vs. T_C/T_E), (fixedT_CHFE7000)

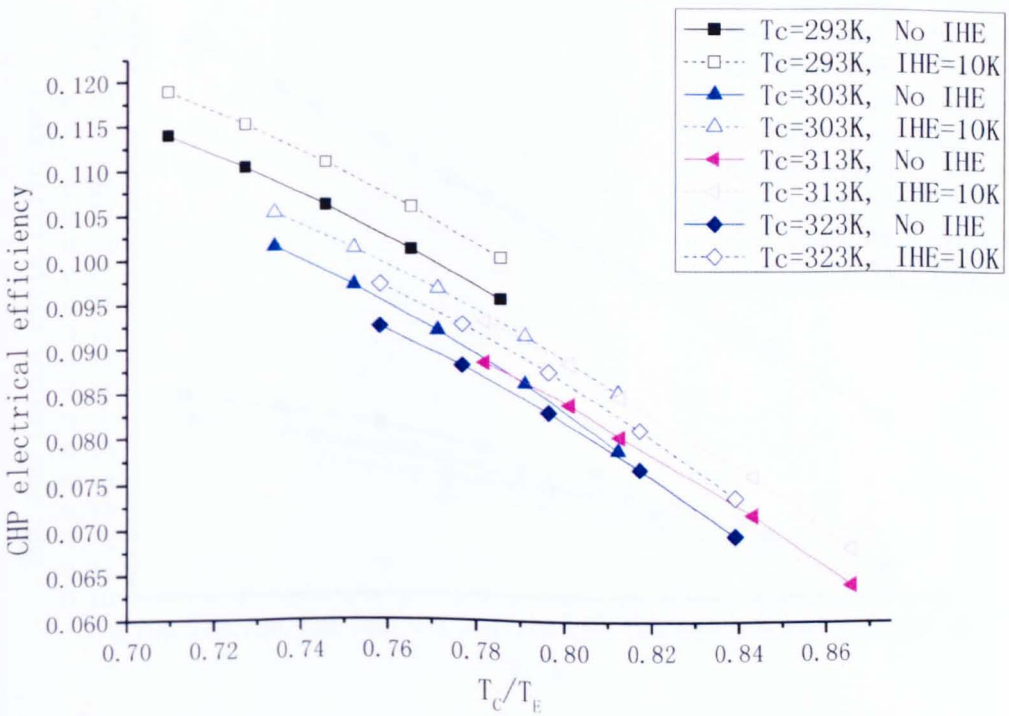

Figure 3.18 CHP electrical efficiency vs. T_C/T_E (fixed T_C, HFE7100)

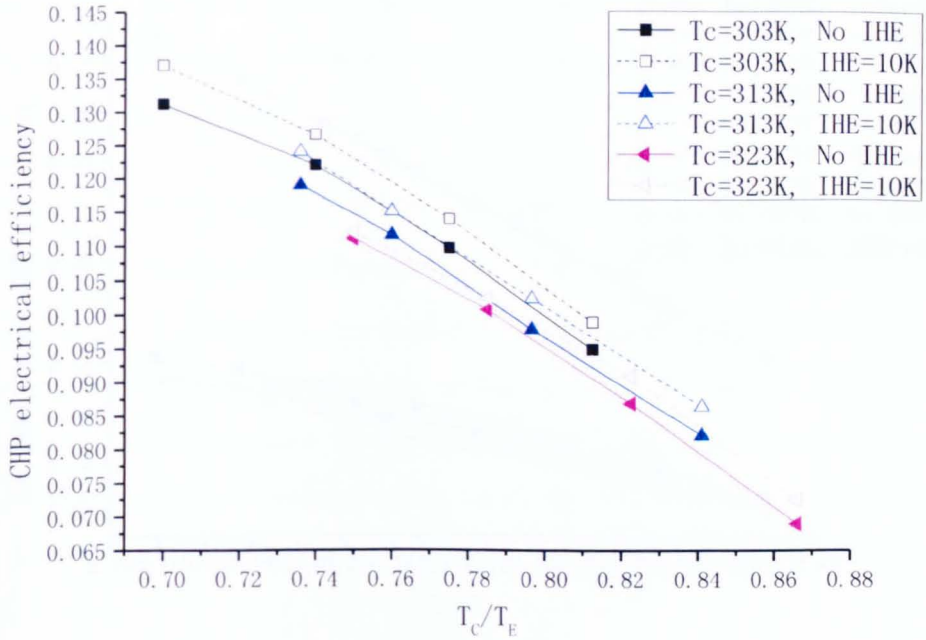

Figure 3.19 CHP Electrical efficiency vs. T_C/T_E (fixed T_C, n-pentane)

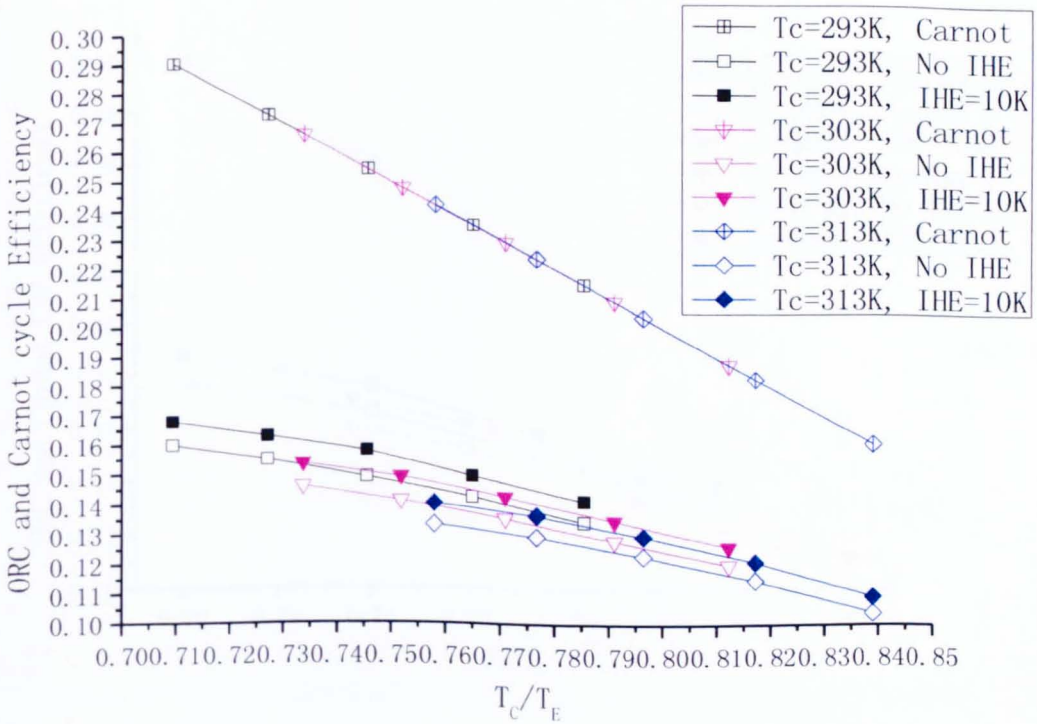

Figure 3.20 ORC and Carnot efficiency vs. T_C/T_E (fixed T_C, HFE7000)

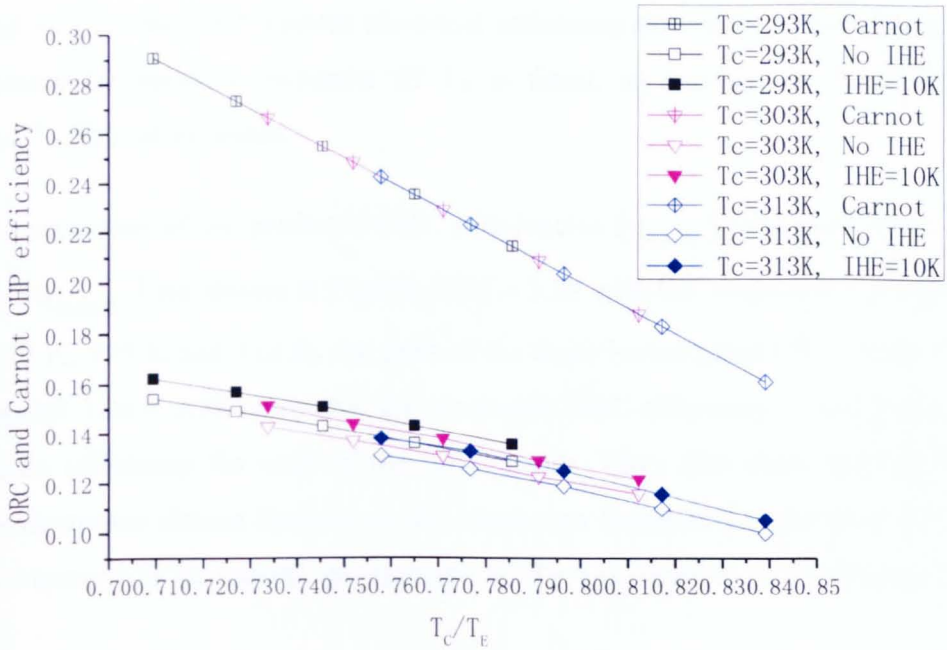

Figure 3.21 ORC and Carnot efficiency vs. TC/TE), (fixed TC, HFE7100)

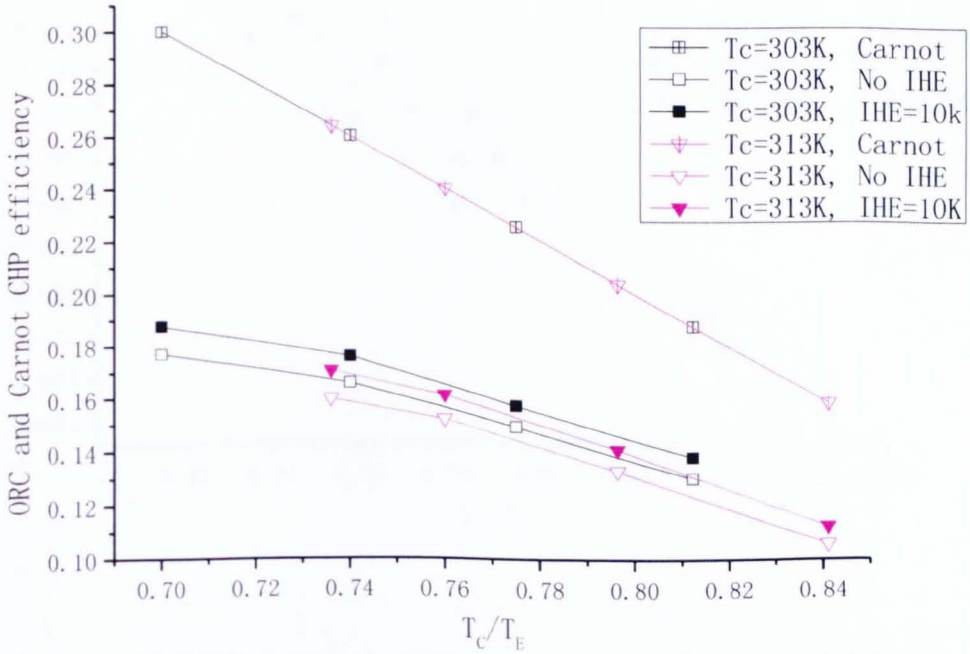

Figure 3.22 ORC and Carnot efficiency vs. T_C/T_E (fixed T_C, n-pentane)

Figures 3.23 - 3.25 show that with evaporator temperatures fixed at 373 K, 383K, 393 K and 413 K, the CHP system electrical efficiency decreases almost linearly as the condenser temperature increases (if T_E is fixed, an increase in T_C means an increase of T_C/T_E), as expected.

The comparisons of the predicted ORC efficiencies (η_{Rank}) with the Carnot cycle efficiency (η_{Carnot}) are shown in Figures 3.26 – 3.28 with the evaporator temperature fixed at 373 K, 393 K and 413 K, for each of the three investigated ORC fluids. Once again, Figures 3.26 – 3.28 show that the predicted ORC efficiency is well below the Carnot cycle efficiency for each of the ORC fluids. They also show that the ORC efficiency decreases almost linearly as the condenser temperature increases (if T_E is fixed, an increase in T_C means an increase of T_C/T_E), similar to the Carnot cycle efficiency.

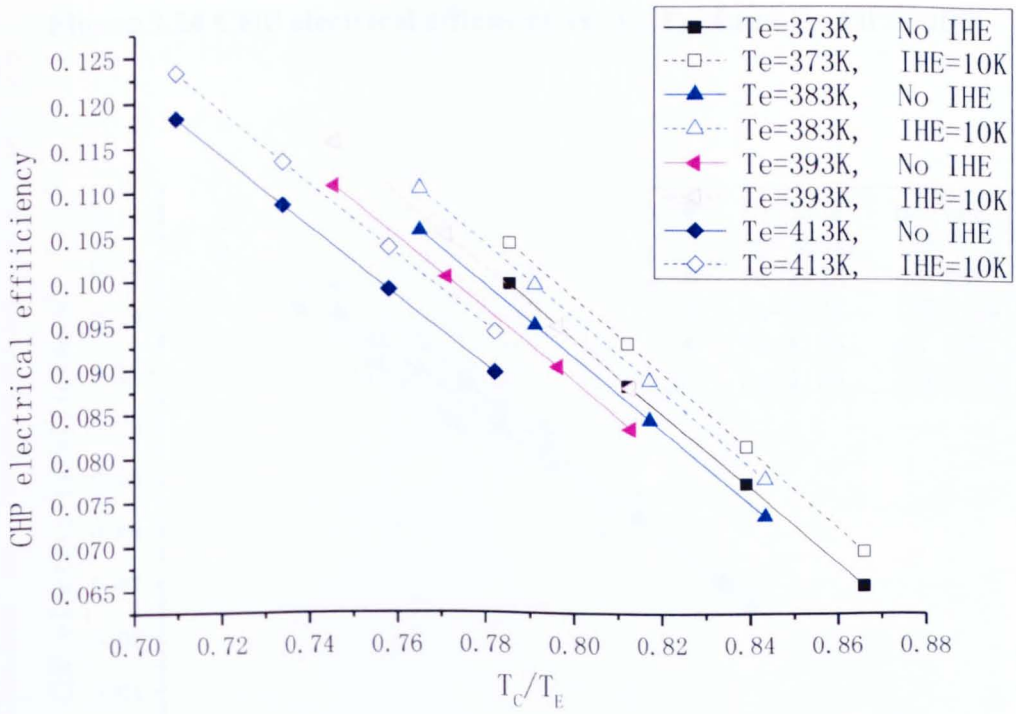

Figure 3.23 CHP electrical efficiency vs. T_C/T_E (fixed T_E, HFE7000)

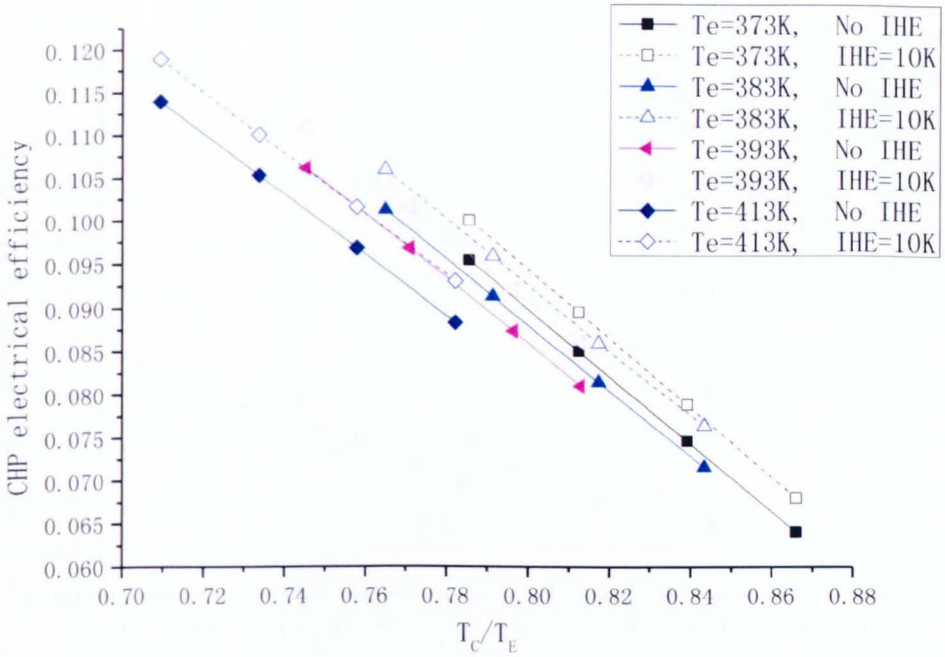

Figure 3.24 CHP electrical efficiency vs. T_C/T_E (fixed T_E, HFE7100)

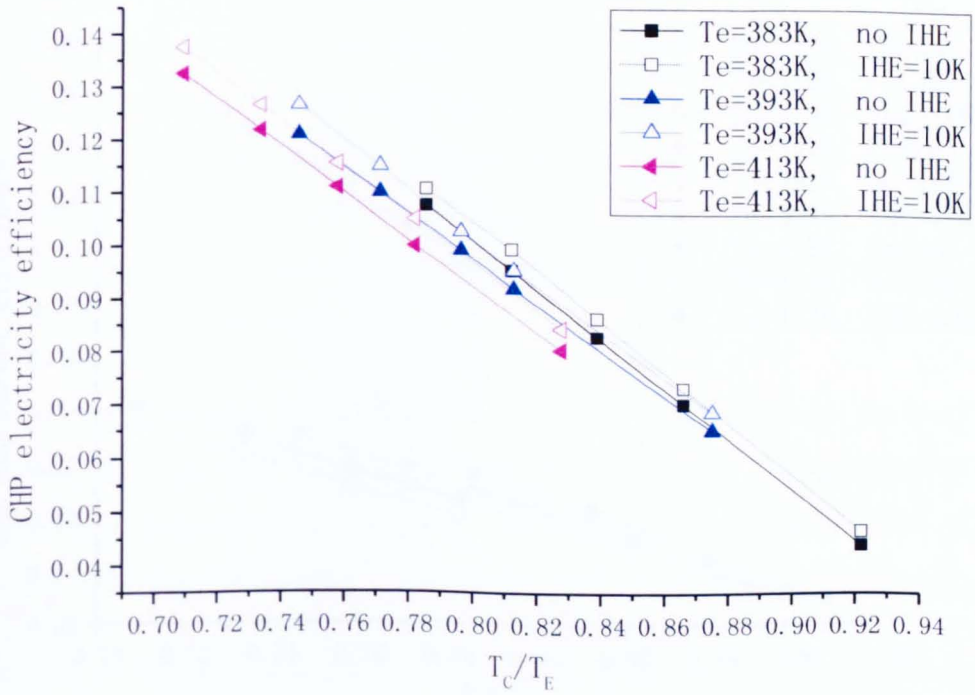

Figure 3.25 CHP electrical efficiency *vs.* T_C/T_E fixed T_E n-pentane

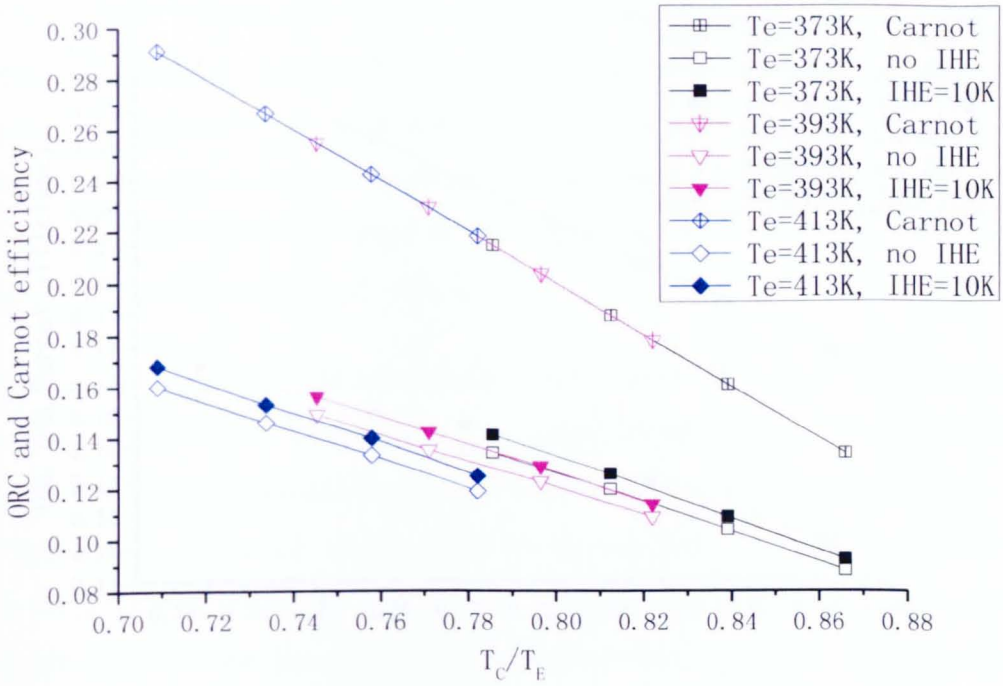

Figure 3.26 ORC and Carnot efficiency vs. T_C/T_E fixed T_E, HFE7000)

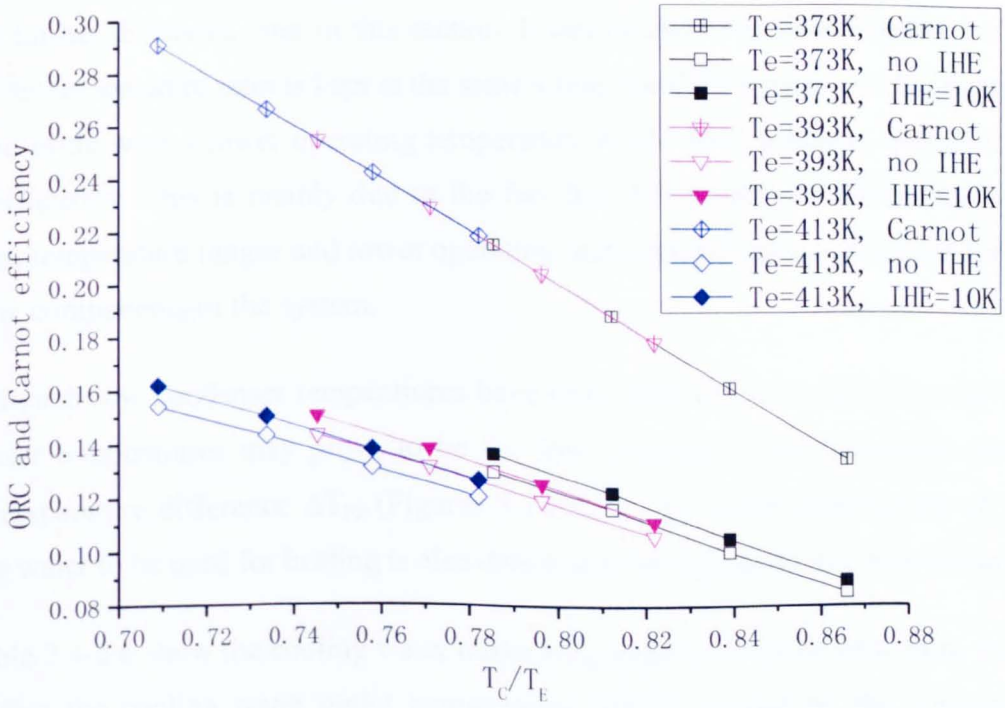

Figure 3.27 ORC and Carnot efficiency vs. T_C/T_E (fixed T_E, HFE7100)

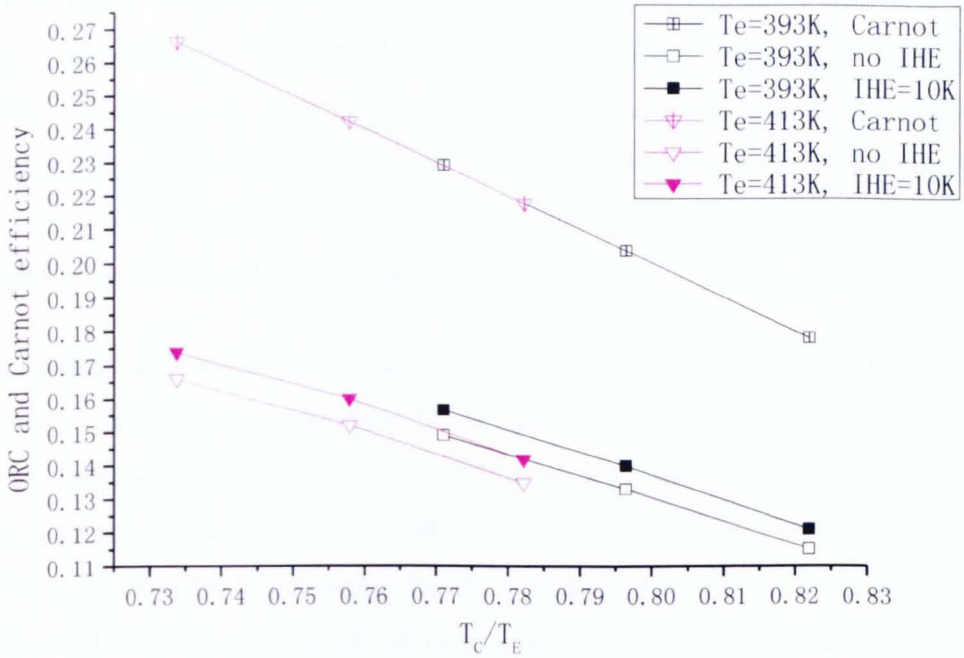

Figure 3.28 ORC and Carnot efficiency vs. T_C/T_E (fixed T_E, n-pentane)

The results shown in Figures 3.17 to 3.28 indicated by 'IHE = 10 ^{0}C' represent the modelling results of the ORC cycles with the Internal Heat Exchanger (Figure 3.8) will be further discussed later in this section. It can be observed from Figures 3.17 – 3.28 if the temperature ratio is kept at the same value, the CHP system and the organic Rankine cycle with a lower operating temperature would have a higher electrical or ORC efficiency. This is mainly due to the fact that fluids perform differently over different temperature ranges and lower operating temperatures have lower heat losses from the components of the system.

Although low condenser temperatures have been used in the model, some of the condenser temperatures may prove to be too low. Because of the minimum pinch point temperature difference ΔT_{PP} (Figures 3.14-3.15), the outlet temperature of the cooling water to be used for heating is also determined by the condenser temperature.

Table 2.4-2.6 show the cooling water outlet temperature. It can be seen from these tables that the cooling water outlet temperatures mainly depend on the condenser temperature and to a much less degree on the evaporator temperatures. It can also be seen that he cooling water outlet temperatures are too low for any heating purposes if

the condenser temperature is set at 293K. Results in Figures 3.17 – 3.28 already showed that lower temperature ratios between the condenser temperatures and the evaporator temperatures are needed for higher electrical efficiencies and ORC efficiencies. Therefore, to generate higher electrical outputs, and at the same to produce useful thermal energy for heating, the proposed micro-CHP system needs to have the hot water supplied at high temperatures and the condenser operating at temperatures higher than at least 30 – 40 ^{0}C.

The proposed micro-scale biomass-fired ORC-based CHP system of this project uses hot water generated in the biomass boiler, instead of thermal oil which is used by medium to large-scale biomass-fired ORC-based CHP systems (Oliver 2006) to deliver heat to the evaporator of the ORC. However, if the temperature of the hot water to be generated by the biomass boiler is higher than 373 K, then pressurised water is needed. This can be achieved by using suitable boiler heat exchanger and evaporator materials to cope with the required high pressure operation. The required hot water temperature is expected to be higher than the evaporator temperature modelled which ranges from 373 K to 413 K. Similar simple pinch analysis to that of condenser can also be applied to the evaporator but this has not been included in the present thermodynamic modelling.

Table 3.4 Cooling water outlet temperature (Type I Cycle, no IHE, HFE7000)

Working fluid	T_{evap} [K]	T_{cond} [K]	T_{cond_out} [°C]
HFE7000	373	293	15.53
HFE7000	383	293	15.61
HFE7000	393	293	15.67
HFE7000	403	293	15.73
HFE7000	413	293	15.8
HFE7000	373	303	27.93
HFE7000	383	303	28.38
HFE7000	393	303	28.79
HFE7000	403	303	29.23

HFE7000	413	303	29.59
HFE7000	373	313	39.84
HFE7000	383	313	40.32
HFE7000	393	313	41.48
HFE7000	403	313	41.46
HFE7000	413	313	42.99
HFE7000	373	323	51.15
HFE7000	383	323	52.4
HFE7000	393	323	53.65
HFE7000	403	323	54.76
HFE7000	413	323	55.92

Table 3.5 Cooling water outlet temperature (Type I Cycle, no IHE, HFE7100)

Working fluid	T_{evap} [K]	T_{cond} [K]	T_{cond_out} [°C]
HFE7100	373	293	15.69
HFE7100	383	293	15.79
HFE7100	393	293	15.88
HFE7100	403	293	15.98
HFE7100	413	293	16.07
HFE7100	373	303	28.82
HFE7100	383	303	29.48
HFE7100	393	303	30.02
HFE7100	403	303	30.59
HFE7100	413	303	31.23
HFE7100	373	313	41.33

HFE7100	383	313	42.4
HFE7100	393	313	43.62
HFE7100	403	313	44.74
HFE7100	413	313	45.93
HFE7100	373	323	53.43
HFE7100	383	323	54.82
HFE7100	393	323	56.54
HFE7100	403	323	57.7
HFE7100	413	323	60.3

Table 3.6 Cooling water outlet temperature (Type I Cycle, no IHE, n-pentane)

Working fluid	T_{evap} [K]	T_{cond} [K]	T_{cond_out} [°C]
n-pentane	373	293	15.29
n-pentane	393	293	15.38
n-pentane	413	293	15.46
n-pentane	373	303	26.63
n-pentane	393	303	27.17
n-pentane	413	303	27.69
n-pentane	373	313	37.75
n-pentane	393	313	38.78
n-pentane	413	313	39.77

3.6.2. Effect of Internal Heat Exchanger

The results shown in Figures 3.17 to 3.28 indicated by 'IHE = 10 ^{0}C' represent the modelling results of the ORC cycles with the Internal Heat Exchanger which recuperates heat from the ORC fluid which is in the superheated vapour region and releases it to the ORC fluid which is in the liquid region. With the inclusion of athe IHE, heat that would be released in the condenser is used to pre-heat the ORC fluid after the pumping process. The variable controlled in the thermodynamic modelling is the temperature drop in the warm side of the internal heat exchanger. The values for the temperature drops in the IHE always refer to this parameter. Therefore, 'IHE = 10 ^{0}C' indicates that the heat transfer between the hot ORC fluid vapour and the cold ORC fluid liquid has resulted in a temperature drop of the hot ORC fluid by 10 ^{0}C. The value for the temperature drop lies within 0 K (no IHE) and a maximum value depending on the organic Rankine cycle operating conditions and types (I, II, III).

The IHE leads to higher electrical efficiency and ORC efficiency. But it does not lead to an increase in the overall CHP efficiency as the heat released in the condenser is assumed to be used for heating purposes and not wasted. Because there is a small heat loss from the IHE, the addition of the IHE will actually result in a slight decrease of the overall CHP efficiency.

Figures 3.17 – 3.28 have showed that the inclusion of an IHE (with a temperature drop of 10 K) always leads to increases in the electrical efficiency of the CHP system and ORC efficiency. The explanation to this observation can be found from the definitions of the CHP system's electrical efficiency and ORC efficiency. Because the enthalpy increase between state points 2a and 3 is smaller than that between state points 2 and 3, whereas the heat supply from the biomass boiler is kept at a constant level, a greater mass of ORC fluid can be circulated in the CHP system. The increased mass flow rate of the ORC fluid means that a greater amount of work is done by the ORC fluid in the turbine, therefore more work output and hence more electricity is produced. With an increased flow of ORC fluid, more pump power is required to pump the increased mass flow of ORC fluid, but this additional pump power input is far smaller than the resulting extra work output. Because the heat input from the boiler is kept constant, this means an increase in the CHP system's electrical output.

Figures 3.25 – 3.27 show the change in the system electrical efficiency over the temperature drop in the internal heat exchanger with selected operating conditions for the three fluids. It can be clearly seen from these figures that decreasing the condenser temperature and/or increasing the evaporator temperature increase the CHP system's electrical efficiency.

Figures 3.27 – 3.29 show that the increase in the electrical efficiency of the CHP system over the temperature drop in the IHE follows an almost linear pattern. The electrical efficiency increase rates, which can be defined as the percentage increase of the efficiency per degrees of temperature drop, of HFE7000 and HFE7100 are similar and slightly higher than with n-pentane; however, when n-pentane is used as the working fluid, the electrical efficiency is the highest amongst the three ORC fluids modelled. The increase in the electrical efficiency of the CHP system as a result of the inclusion of the IHE lies between 0.4-0.5% per 10 K of temperature drop in the IHE for the three fluids modelled.

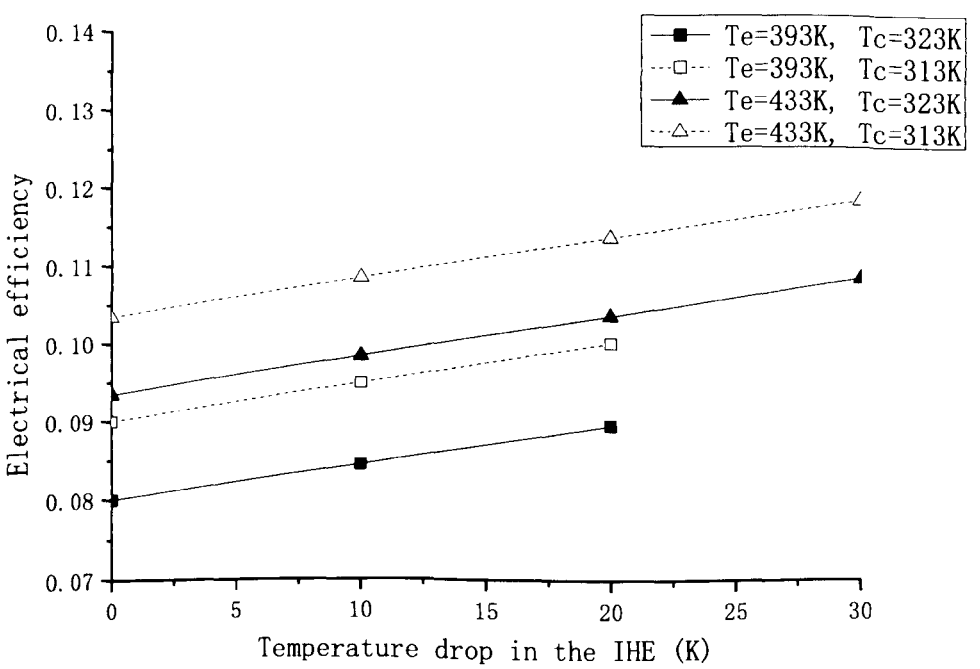

Figure 3.29 Electrical Efficiency vs. Temperature drop in the IHE (Type I cycle, HFE7000)

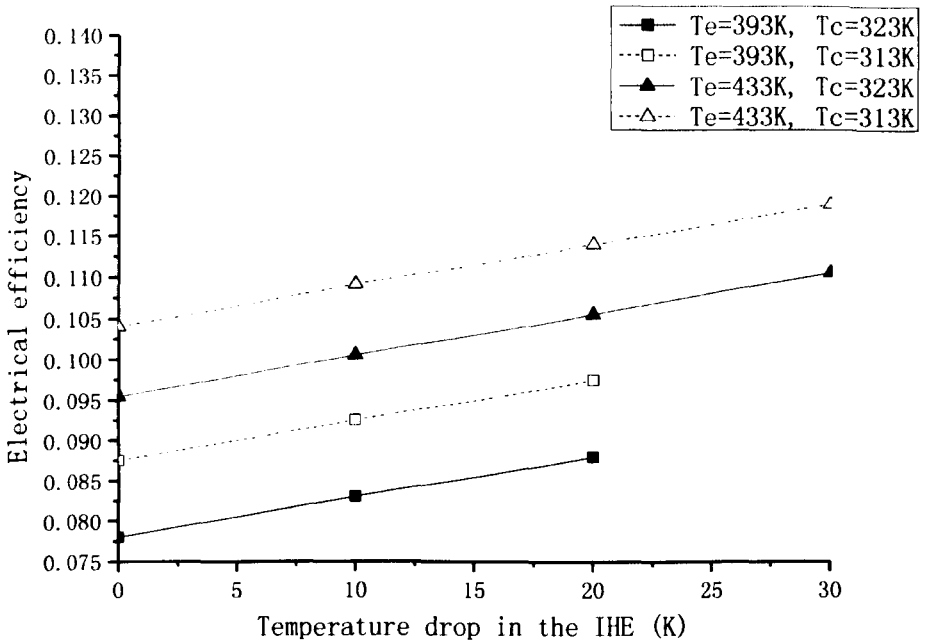

Figure 3.30 Electrical Efficiency vs. Temperature drop in the IHE (Type I cycle, HFE7100)

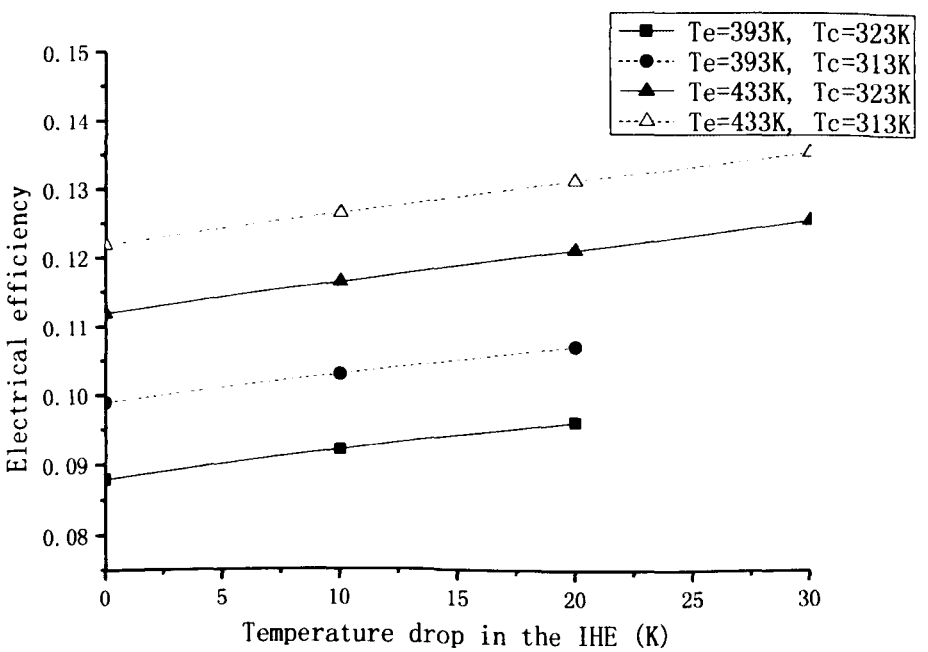

Figure 3.31 Electrical Efficiency vs. Temperature drop in the IHE (Type I cycle, n-pentane)

3.6.3. Effect of superheating

The reason for why superheating is a parameter often considered in the Rankine Cycle analysis, is that wet fluids (such as steam) might need superheating to avoid condensation in the turbine. Condensation of wet fluids in the turbine is detrimental to the turbine blades which are usually rotating at high speeds and hence can be damaged by the liquid droplets. However, in this project, the effects of superheating the fluids are somewhat expected to be known as the three selected ORC working fluids are dry fluids. As explained in Section 3.3.3, the slope of the saturated vapour line of each of the three ORC working fluids is positive; therefore after the expansion in the turbine, the ORC working fluid will always be in superheated vapour region. Therefore, superheating of the working fluid is not needed for the reasons of safety regarding the turbine as there will be no liquid drops to be formed in the turbine which can cause damage to the turbine blades. In addition, the modelling results in Figures 3.32 -3.34 show that superheating has negative effects on the CHP system's electrical efficiency for any of the three investigated ORC working fluids. This means that when HFE7000, HFE7100 or n-pentane is used as the ORC fluid, superheating is detrimental to the ORC efficiency, which is in agreement with Saleh et al. (Saleh *et al.* 2007)who found a decrease of the thermal efficiency by superheating dry fluids. As the heat output from the biomass boiler is kept at a constant level with the modelling, superheating the ORC working fluid means reducing the ORC working fluid mass flow rate in this case. Since the superheating process is carried out along the isobaric curve, the pressure difference across the turbine will be the same and the increase in the enthalpy drop between the turbine inlet and outlet will be small. Therefore, the total turbine work output will decrease due to the decreased fluid mass flow rate. With a constant boiler output constant, the electrical efficiency of the CHP system will decrease. The results in Figures 3.28 – 3.30 indicate that the same detrimental effect of superheating on the CHP system's electrical efficiency can be observed for the basic ORC configuration (Figure 3.4) and the ORC configuration with IHE (Figure 3.8). Therefore, it can be concluded that superheating dry ORC fluids is not only unnecessary but also detrimental to the electrical efficiency.

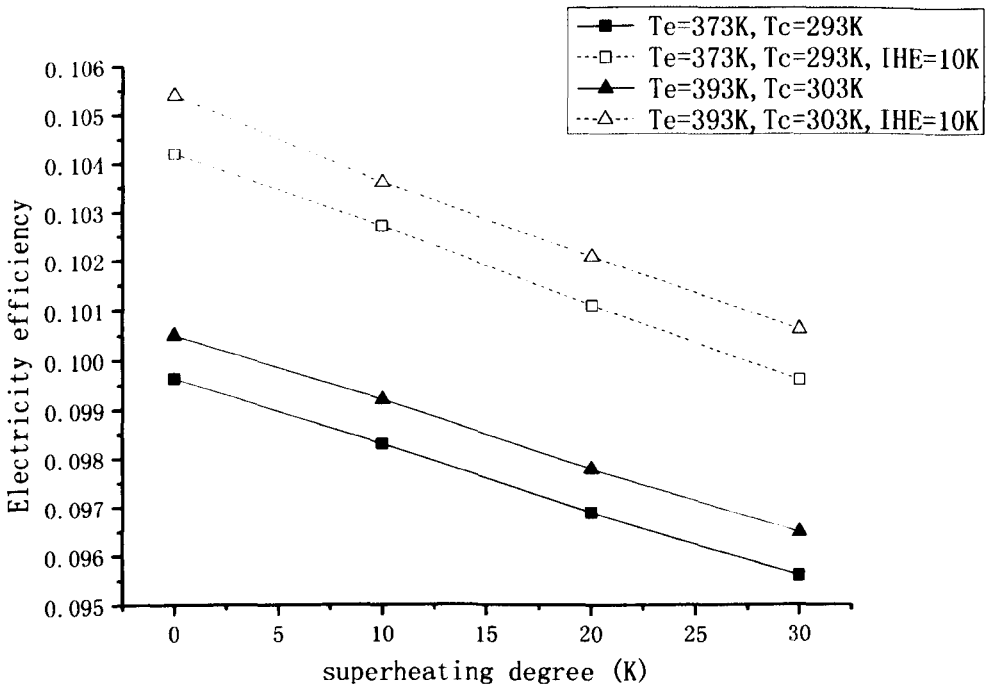

Figure 3.32 Electrical Efficiency vs. Degree of Superheating (HFE7000)

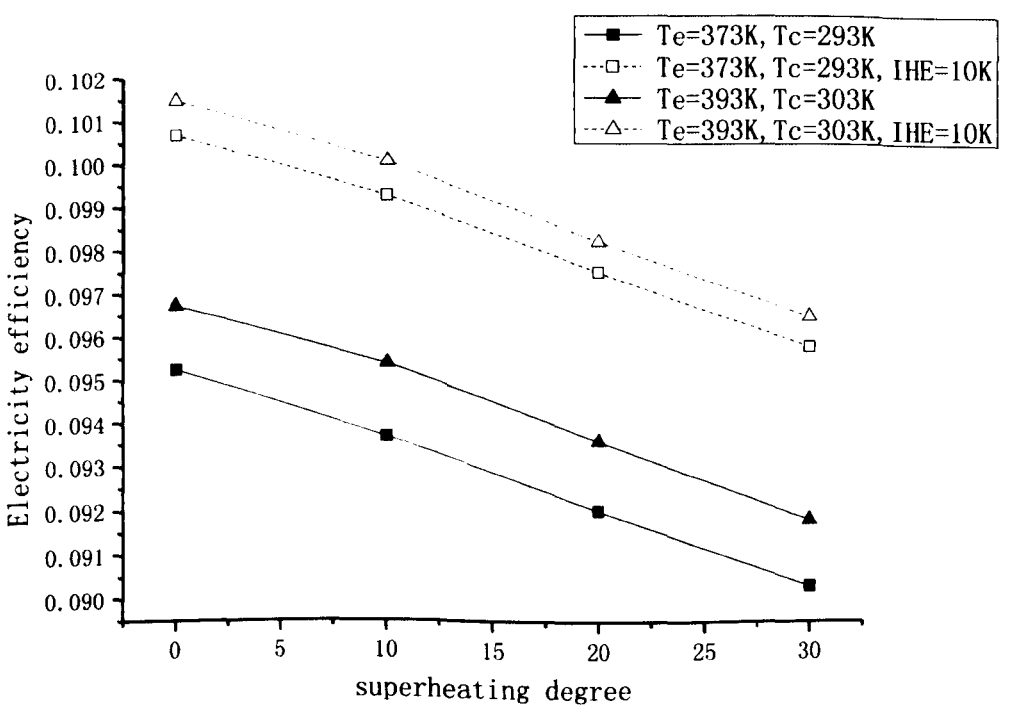

Figure 3.33 Electrical Efficiency vs. Degree of Superheating (HFE7100)

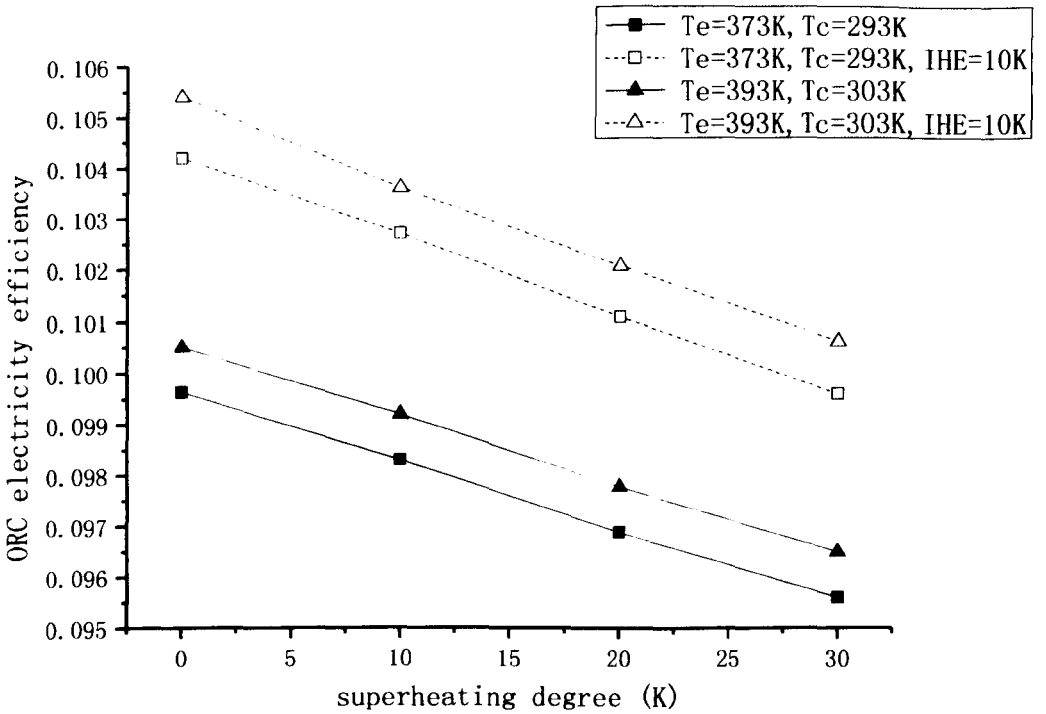

Figure 3.34 Electrical Efficiency vs. Degree of Superheating (n-pentane)

3.6.4. Effect of sub-cooling

Subcooling means that the ORC fluid is not only condensed to liquid in the condenser but also further cooled down to a temperature below the saturation temperature of the condenser, corresponding to the minimum operating pressure. This procedure is often used to avoid damage to the ORC fluid pump, which requires the ORC fluid to enter as a liquid, rather than a mixture of liquid and vapour. As it is virtually impossible to achieve the saturated liquid state, subcooling the fluid by a few degrees can be used to ensure that no vapour enters the pump.

However, subcooling the ORC working fluid has a negative effect on the electrical efficiency of the CHP system, as demonstrated by Figures 3.31 – 3.33. When the ORC working fluid is subcooled, the enthalpy of the fluid after the pumping process become smaller, this means that the enthalpy difference across the evaporator increases, more thermal input is needed to raise the ORC fluid to the state point 3,

and consequently a smaller fluid mass flow rate of the ORC working fluid is used as the total thermal input from the biomass boiler is fixed. As the pressure difference across the turbine remains the same and so is the turbine work output per kg of the ORC working fluid, the CHP system electrical efficiency decreases. The results in Figures 3.35 – 3.37 indicate that the same detrimental effect of subcooling on the CHP system's electrical efficiency can be observed for the basic ORC configuration (Figure 3.4) and the ORC configuration with IHE (Figure 3.8). Therefore, it can be concluded that although subcooling the ORC working fluid is necessary for the protection of the ORC fluid pump, subcooling will lead to lower electrical efficiency and hence should be minimised.

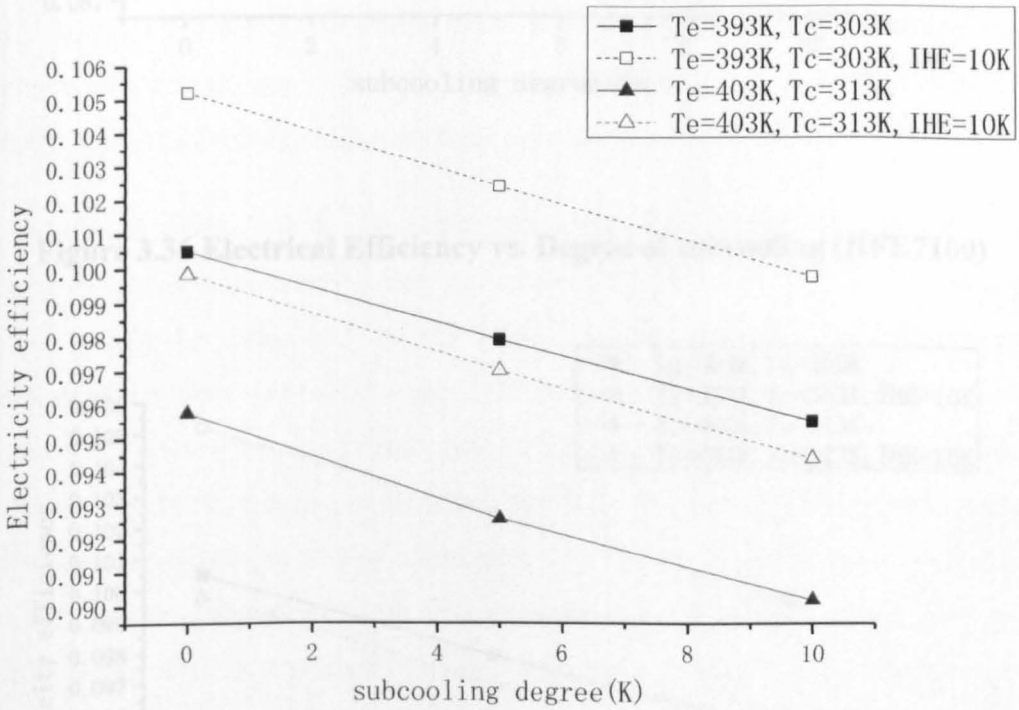

Figure 3.35 Electrical Efficiency vs. Degree of subcooling (HFE 7000)

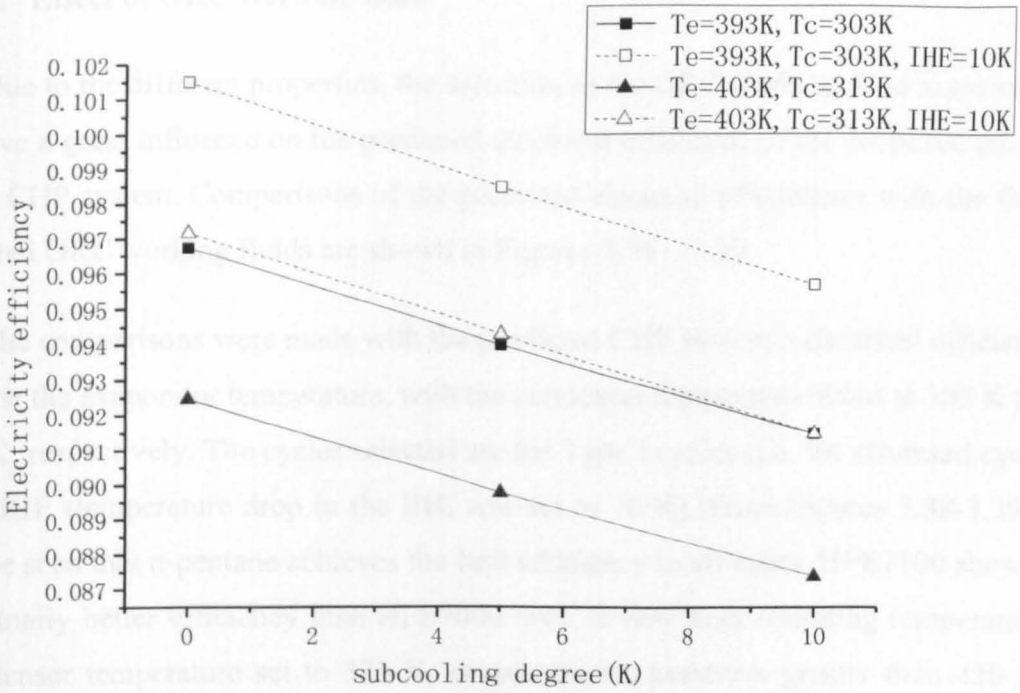

Figure 3.36 Electrical Efficiency vs. Degree of subcooling (HFE7100)

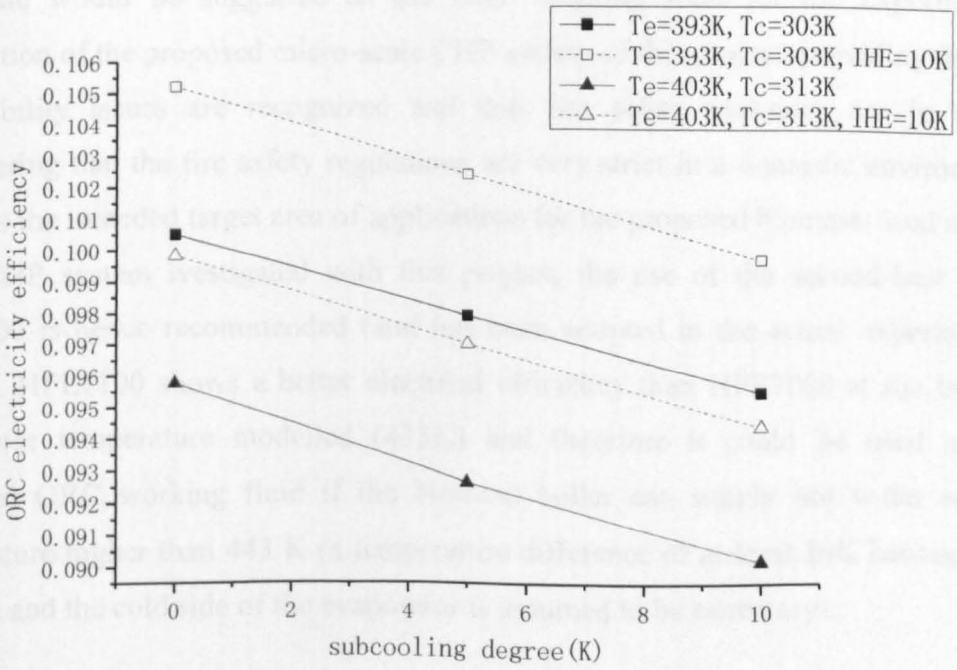

Figure 3.37 Electrical Efficiency vs. Degree of subcooling (n-pentane)

3.6.5. Effect of ORC working fluid

Due to the different properties, the selection of the ORC working fluid is expected to have a great influence on the predicted electrical efficiency of the proposed micro-scale CHP system. Comparisons of the predicted electrical efficiencies with the three selected ORC working fluids are shown in Figures 3.38 – 3.39.

The comparisons were made with the predicted CHP system's electrical efficiency against the evaporator temperature, with the condenser temperature fixed at 303 K and 323 K, respectively. The cycles selected are the Type I cycles (i.e. the saturated cycles) with IHE (temperature drop in the IHE was set to 10 K). From Figures 3.38-3.39, it can be seen that n-pentane achieves the best efficiency in all cases; HFE7100 shows a marginally better efficiency than HFE7000 only at very high operating temperatures (condenser temperature set to 323 K, evaporator temperatures greater than 430 K), although it has the advantage of lower fluid pressures (see Table 3.7).

Generally speaking, under the same modelling conditions, the predicted ORC efficiency follows the following order: n-pentane > HFE7000 > HFE7100. Therefore, n-pentane would be suggested as the ORC working fluid for the experimental verification of the proposed micro-scale CHP system of this project, providing that the flammability issues are recognized and that fire safety measures are in place. Considering that the fire safety regulations are very strict in a domestic environment which is the intended target area of applications for the proposed biomass-fired micro-scale CHP system ivestigated with this project, the use of the second-best fluid, HFE7000 is hence recommended (and has been adopted in the actual experimental testing). HFE7100 shows a better electrical efficiency than HFE7000 at the highest evaporator temperature modelled (433K) and therefore it could be used as the preferred ORC working fluid if the biomass boiler can supply hot water with a temperature higher than 443 K (a temperature difference of at least 10K between the hot side and the cold side of the evaporator is assumed to be necessary).

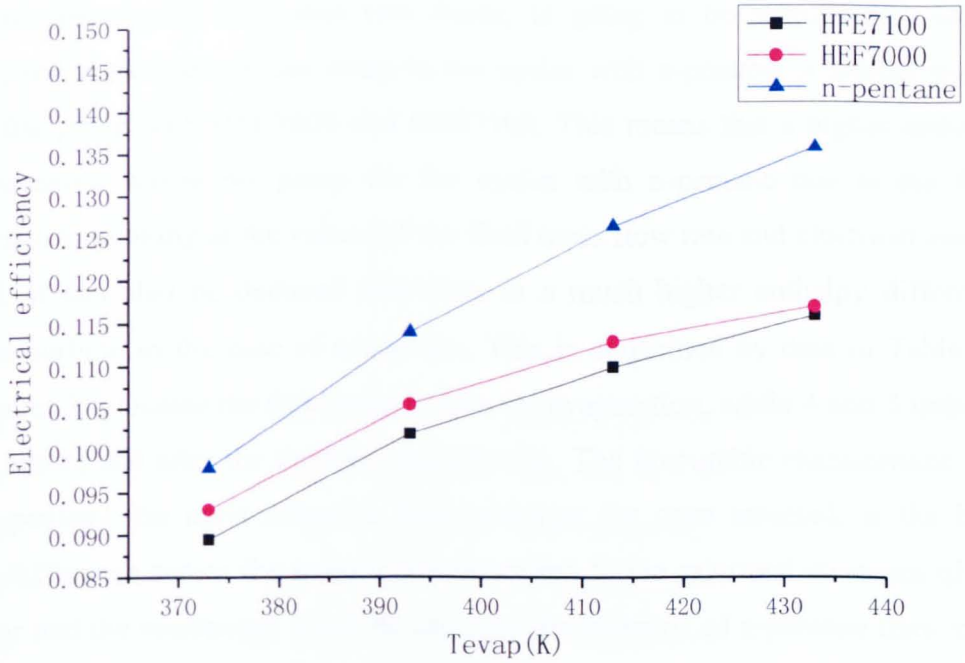

Figure 3.38 Comparisons of the predicted electrical efficiencies of the three selected ORC working fluids (Type I cycle, IHE = 10 K, Tcond=303K)

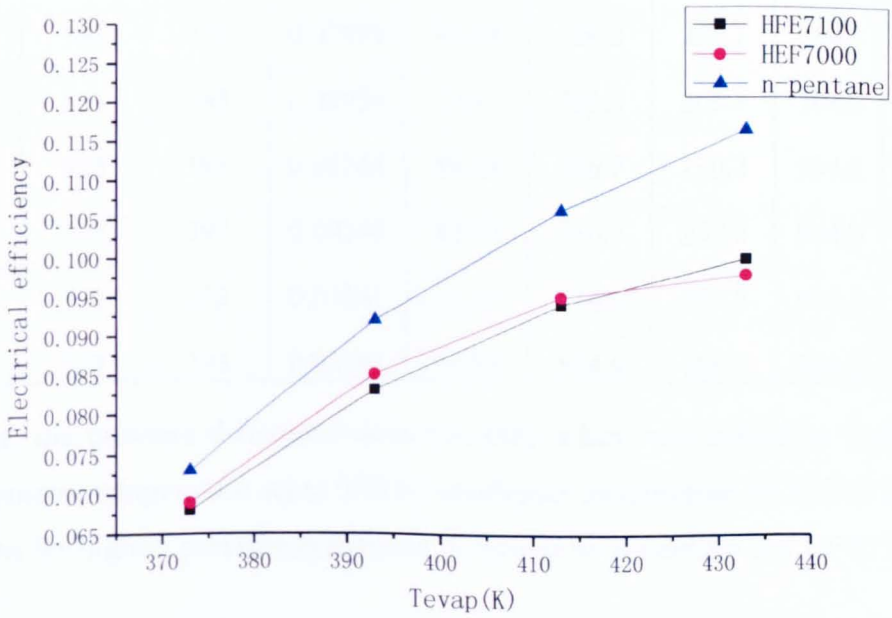

Figure 3.39 Comparison of the predicted electrical efficiencies of the three selected ORC working fluids (Type I cycle, IHE = 10 K, Tcond=323K)

Because the enthalpy of vaporisation is higher for n-pentane, the fluid mass flow rate, as compared with the other two fluids, is going to be substantially lower. However, the work done by the pump in the cycles with n-pentane is similar to that done by the pump with HFE7000 and HFE7100. This means that a higher enthalpy difference exists across the pump for the cycles with n-pentane due to the fluid characteristics. Looking at the values of the fluid mass flow rate and electrical energy produced, it can also be deduced that there is a much higher enthalpy difference across the turbine in the case of n-pentane. This is confirmed by data in Table 3.7 (The number 2 indicates the fluid state before the evaporation, while 4 and 5 indicate the state before and after the turbine, respectively). The favourable characteristic that makes n-pentane the most effective fluid amongst the ones selected, is the high enthalpy difference across the isobars corresponding to the saturated pressures of the evaporator and the condenser; it can be said that the enthalpy of n-pentane rises more than the other fluids as the temperature or pressure increases.

Table 3.7 Comparison of enthalpy and pressure differences across the turbine

Working Fluid	T_{cond} [°C]	T_{evap} [°C]	m [kg/s]	h[2] [kJ/kg]	h[4] [kJ/kg]	h[5] [kJ/kg]	P[4] [kPa]	P[5] [kPa]
HFE7000	303	393	0.07989	81.94	286.2	257.1	1042	83.82
HFE7000	323	393	0.08959	104	286.2	265.3	1042	166.8
HFE7100	303	393	0.08265	59.23	256.7	230.2	504.2	34.15
HFE7100	323	393	0.09346	82.07	256.7	237.6	504.2	72.42
n-pentane	303	393	0.03241	11.11	514.6	437.5	904.3	82.62
n-pentane	323	393	0.03581	58.83	514.6	458.7	904.3	159.8

However, the pressure difference does not play a key role indeed as Table 3.7 shows (evaporator temperature set to 393 K, condenser temperature set to 313 K) that HFE7000 has the highest pressure difference, followed by n-pentane and HFE7100.

The higher enthalpy of vaporisation of n-pentane also explains the system behaviour, with regard to the electrical efficiency. In Section 3.6.2 it is observed that the increase in efficiency due to the IHE for n-pentane is smaller; In Section 3.6.3 and 3.6.4 it is observed that the decrease in efficiency due to superheating and subcooling

is also lower. Because n-pentane has a high enthalpy of vaporisation, the reduction (in the case of IHE) and increase (in the case of superheating and subcooling) in enthalpy difference across the evaporator are proportionally smaller in comparison with the other two fluids.

3.7. Conclusions

The proposed biomass-fired micro-CHP system with organic Rankine cycle has been thermodynamically modelled with three selected dry organic working fluids, namely HFE7000, HFE7100 and n-pentane. The modelling results show that the electrical efficiency of the micro-CHP system depends on not only the modelling conditions but also the ORC fluid. A comparison of the three fluids shows that n-pentane exhibits the best electrical efficiency, follows the following order: n-pentane > HFE7000 > HFE7100. But as n-pentane is a flammable fluid, the use of n-pentane in a domestic Micro-CHP system might not be straightforward. Consequently, HFE7000 is recommended as the preferred working fluid of the proposed micro-CHP system for the experimental testing stage. HFE7100 can yield a better efficiency than HFE7000 at the highest modelled evaporator temperature (433K) and therefore if the biomass boiler can produce a hot water with a minimum temperature of 443K, HFE7100 can be used as the preferred ORC working fluid for experimental testing.

The modelling results also show that using an Internal Heat Exchanger improves the CHP electrical efficiency. An IHE will increase the system electrical efficiency, whilst keeping the overall efficiency nearly the same. Under the system operating conditions assumed in the model, the efficiency curve almost follows a linear pattern; the efficiency increase can be estimated to be 0.4-0.5% for every 10 K of temperature drop in the internal heat exchanger. The increase rate for n-pentane is slightly lower than those for HFE7000 and HFE7100.

Superheating has a negative effect on the predicted electrical efficiency. As only dry fluids are to be used with the proposed micro-CHP system, superheating is not required for safety reasons with regard to turbine blades. The additional heat input required for superheating does not increase the pressure difference across the turbine,

and therefore the work output will almost the same as that with no superheating and hence leads to a lower electrical efficiency.

Subcooling is used to prevent vapour from going into the pump; therefore a low degree of subcooling is acceptable. However, subcooling the working fluid has a negative effect on the system electrical efficiency, for the same work output in the turbine, more heat is needed to bring the fluid to the evaporator temperature.

Chapter 4. Experimental Set-Up for the Investigation of the Proposed Biomass-Fired ORC-Based Micro-CHP System

HFE7000 and HFE7100 have been selected as the ORC working fluids for the experimental testing of the proposed biomass-fired micro-CHP system described in Chapter 3. Although the results of thermodynamic modelling detailed in Chapter 3 have indicated that n-pentane is a better ORC working fluid than either HFE7000 or HFE7100 as far as the CHP system's electrical efficiency is concerned, no guarantee of safety regarding the flammable n-pentane which may be leaked via various components of the experimental CHP system including the turbine, ORC fluid pump, connecting pipes etc. has led to the exclusion of this potentially efficient ORC fluid for experimental testing. The setup and components of the operating CHP system with ORC for this project are to be detailed in this chapter.

A range of laboratory experiments were carrying out in the University of Nottingham with the following objectives:

- to prove the feasibility of the proposed biomass-fired micro-CHP system with ORC;
- to evaluate the electrical efficiency of the micro-size biomass-fired Organic Rankine cycle system with varying operating parameters;
- to investigate gas emissions of the biomass boiler under different CHP operation modes;
- to provide experimental data or trends for comparisons with those of thermodynamic modelling describe in Chapter 3.

In order to improve the system performance, the selection of the different components of the CHP system requires advanced technical assessments to identify the most suitable technologies that can be easily modified if necessary and integrated into the CHP system. Different operating conditions of the CHP system with the

organic Rankine cycle need to be taken into account when selecting the technologies and components of the CHP system.

This chapter starts with a brief review of previous experimental investigations on biomass-fuelled micro-CHP and ORC, followed by an overview of the experimental setup, experimental procedures and detailed descriptions of the main components of the experimental CHP system.

4.1. Previous Experimental Investigations on Biomass-Fuelled Micro-CHP and ORC

The following gives a brief review on the experimental investigations of micro-CHP operating on biomass energy and/or organic working fluids for different applications.

G. Friedl et al.(Friedl *et al.* 2009) have developed Wood pellet combustion units as a comfortable, full automatic and low emission solution for the provision of space heating in small scale applications. The thermoelectric power production method was chosen from a number of technologies and the first development step was the implementation of a Prototype with a fuel heat input of 10 kW and a nominal electrical power of 200 W. The central point of the implementation was the integration of a thermo-generator in a pellet combustion unit and the subsequent evaluation of the system concept. The integrated system implemented in the prototype confirms the feasibility of the combination of these technologies. The electrical efficiency of the thermo-generator was found to be in accordance with the target value of 4%, corresponding to a produced nominal electric power of 200 W.

The Viking gasification plant at the Technical University of Denmark(Ahrenfeldt *et al.* 2006) was built to demonstrate a continuous combined heat and power operation of a two-stage gasifier fuelled with wood chips. The nominal thermal input of the gasifier is 75 kW. The operation validate that the Viking two-stage gasification CHP plant can be operated at stable conditions, continuously, and unmanned. The plant produces a gas with a very stable composition suitable for gas engine operation. Multiple measurements of the tar content, carried out by three independent groups,

showed that only minor amounts of naphthalene (0.1 mg/Nm3) could be detected in the raw producer gas. The energy balance for the plant shows a fuel to gas efficiency of 93%, a gas to electricity efficiency of 29%, and an overall wood to electricity efficiency of 25%.

An ORC has been designed and tested by Yamamoto et al.(Yamamoto *et al.* 2001). The ORC system has been designed to operate with low-grade heat. The working fluids tested are HCFC-123 and water. The experimental test bench was composed of a shell-and-tube heat exchanger for the condenser, electrical heaters for heat generation, and an impulse micro-turbine designed for the study. The maximum cycle efficiency was 1.25% with HCFC-123. This poor efficiency is due to the poor efficiency of the turbine prototype. A micro-CHP system driven by solar and natural gas has been installed and tested for a small-scale application. Two fluids, HFE-301 and pentane, were considered as potential working fluids for this system. Results show that HFE-301 performed better than pentane in terms of actual electrical efficiencies, i.e.7.6% and 5%, respectively. The prototype was composed of: evacuated glass tube (Thermomax Ltd), brazed-plate heat exchangers (condenser and boiler), an electrical pump with an explosion proof motor was used for HFE-301 and a double diaphragm pump for pentane. The turbine/generator was designed to deliver 1.5 kWel, the operating rotation speed was 60 000 rpm, and propelled by the radial flow of vapour.

4.2. An Overview of the Experimental CHP System Setup and Testing Procedures

4.2.1. An overview of the experimental CHP system

The experimental setup of the proposed biomass-fired micro-CHP system with ORC of this project is overviewed in this section and the general testing procures are explained. The overall aim of the experimental programme is to setup and evaluate a first of its kind biomass-fuelled micro-scale CHP system with organic Rankine cycle, particularly the capability of the CHP system to generate electricity. During the experimental testing period of the project, a number of available improvements have

been performed with each component in order to achieve better system performance and efficiencies. The experimental micro-CHP system can be divided into several parts according to their functions:

- Biomass combustion unit which mainly includes the biomass fuel, the biomass boiler, and the flue gas analysis system;
- Electricity generating system which mainly includes the micro-turbine, the alternator and the electric output circuit;
- Heat exchangers and Pumps;
- Data acquisition system.

The details of the main components of the experimental micro-CHP system will be described in the following sections of 4.3 – 4.6. The initial setup of the experimental micro-CHP system was based on the experiment setup of Daminao (Daminabo Ferdinand 2009), in which a 9kW electric boiler was applied to drive a micro-CHP system. For this work, the original experimental setup of Daminabo (2009) has been greatly modified and expanded. Almost every component of the original electric boiler derived system has been replaced during the experimental testing period, for example two biomass pellet boilers (25 kW and 50 kW) were used to replace the 9kW electric boiler. In addition, more components such as gas analysis system have been added into the experimental system. The improved experimental system has much greater capacity than that of Daminabo (2009) and is a truly 'biomass-fired micro-CHP with ORC' experimental system.

The current experimental micro-CHP system is schematically shown in Figure 4.1. Some components may differ from those shown in Figure 4.1 during the experimental testing period that last for two years as replacements and improvements to various components of the system happened at different times during the experimental testing period.

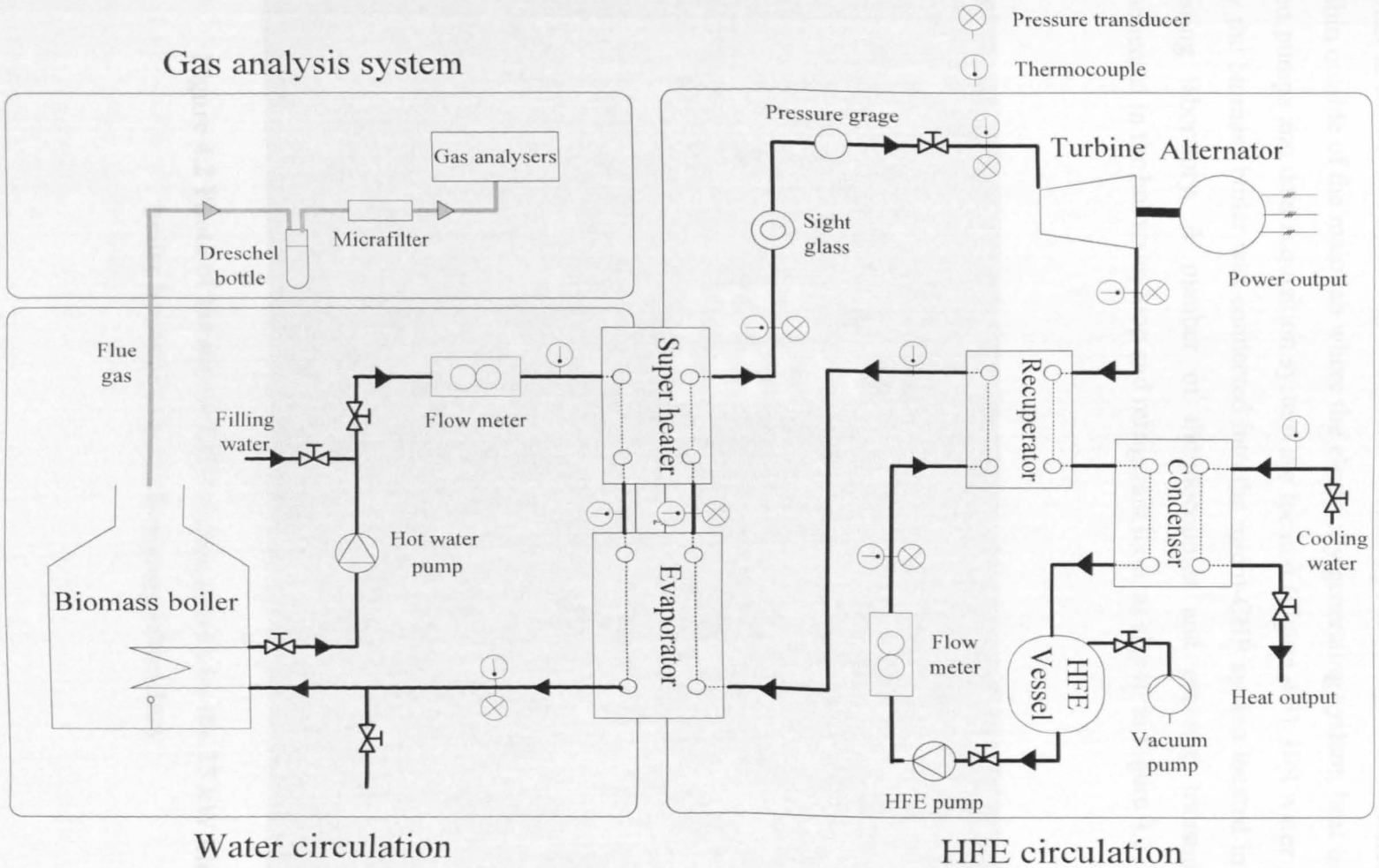

Figure 4.1 Layout of the Biomass fired CHP system

A test rig photo of the micro-CHP system driven by the 25 kW biomass pellet boiler is shown in Figure 4.2. The 25kW biomass pellet boiler was installed in a log cabin outside of the main lab where the electricity generating system, heat exchangers and pumps and data acquisition system are located (Figure 4.3). Hot water generated by the biomass boiler was connected into the micro-CHP system located in the main testing laboratory. A number of thermocouples and pressure transmitters are connected in the hot water loop and refrigerant loop, as shown in Figure 4.2.

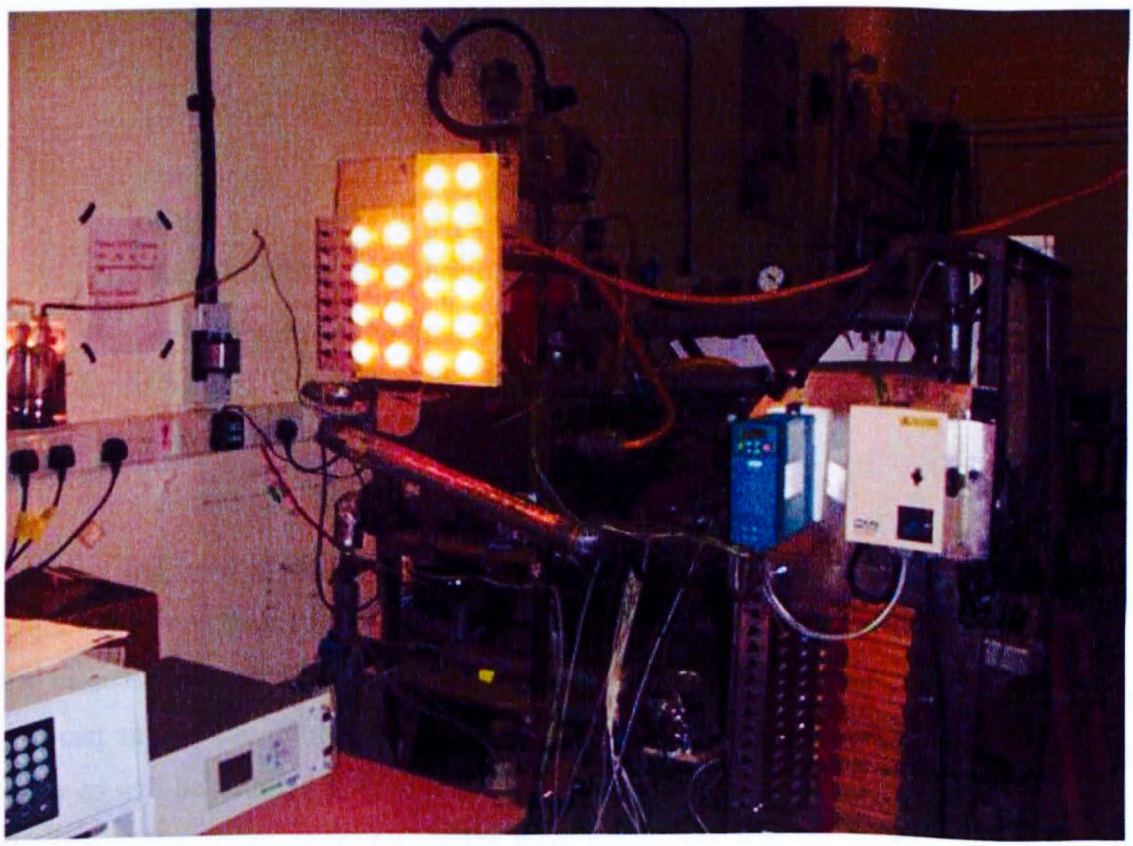

Figure 4.2 Photo of the micro-CHP system driven by the 25 kW biomass boiler housed in the main testing laboratory

Figure 4.3 Photo of the 25 kW biomass pellet boiler housed in a log cabin outside the main testing laboratory

After the testing phase with the 25 kW biomass pellet boiler, a 50 kW biomass pellet boiler was used to drive the micro-CHP system as shown in Figure 4.4. The 50 kW biomass pellet boiler can not only supply more heat to the micro-CHP system but also can supply the hot water at higher temperature than the 25 kW biomass pellet boiler as will be detailed later in this chapter. During the testing phase with the 50 kW biomass pellet boiler, more DC bulbs were connected into the micro-CHP system's electrical circuit as the power generated by the micro-CHP system was much greater than that achieved with the 25 kW biomass boiler. Both of the 25 kW and 50 kW biomass pellet boilers were designed and manufactured by Ashwell Engineering Services Limited(Ashwell Ltd) with further information given in the next section of this chapter.

Flue gas composition and emissions of the boiler were monitored by the gas analysis system, also to be detailed in the next section, during these two phases of tests.

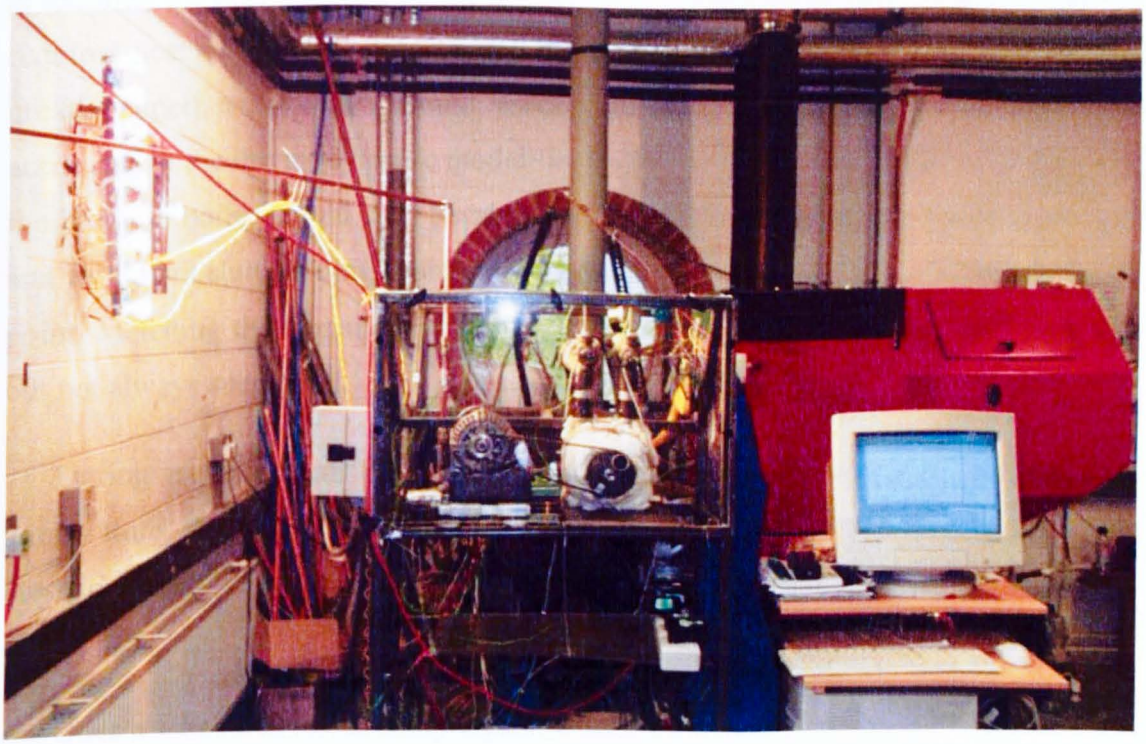

Figure 4.4 Photo of the CHP system driven by the 50 kW biomass boiler

4.2.2. An overview of the testing procedures

Each test starts with the automatic start-up of the biomass boiler after setting up the required hot water temperature at the boiler control panel which can be as high as 120 ^{0}C for the 25 kW biomass boiler and 140 ^{0}C for the 50 kW biomass boiler. Wood pellets are burned in the combustion furnace of the boiler to heat up the water via a hot water heat exchanger located inside the boiler furnace. Once the hot water temperature reaches the set value, the testing of the CHP system can be started. Firstly, the refrigerant pump is switched on with a given load which can be changed from 1% to 100% of the pump capacity via the pump load control box. The load of the HFE pump restricts the heat energy transferred into the HFE loop and hence the rotation speeds of the turbine. During a test, the pump load can be steadily increased, which results in increases in the turbine rotation speed and the power output of the CHP system. If moisture of ORC fluid is seen by the sight glass at the inlet of the turbine, this means the heat energy received from the evaporator and super heater (supplied by the hot water of the biomass boiler) cannot match the need of HFE fluid vaporisation. Then the CHP testing can be stopped. On the other hand, if the ORC fluid pump load

is too low, the heat supplied by the hot water of the biomass boiler would exceed the required heat of the HFE fluid vaporisation. In this case, the HFE fluid can become greatly superheated which would reduce the CHP system's electrical efficiency according to the thermodynamic modelling results described in Chapter 3. In addition, the biomass boiler would stop burning once its set hot water temperature is reached and would not start burning again until the hot water temperature is 2 ^{0}C below the set point. Matching the demand and supply of heat has always been tried with each test but not always successful.

During each test, all of the measured process parameters, such as pressures, temperature, flow rates and output data such as the overall voltage and current of the electrical loads are recorded by the data acquisition system (to be described in section 4.6).

Once a scheduled test is completed, the biomass boiler is switched off but the HFE working fluid pump is kept on for some time with reduced loads so that the residual heat of the biomass boiler can be dissipated for safety reasons. Similarly, the hot water pump will not be switched off until the next day.

4.3. Biomass Combustion Unit

4.3.1 Wood pellet boilers

According to the types of fuel charging, the biomass combustion boilers can be divided into two categories: those with discontinuous/manual fuel charging and those with automatic fuel charging. For micro-CHP systems, the discontinuous/manual fuel charging boilers are very inconvenient to the users and hence mostly disregarded. Ideally, micro-CHP systems used in residential and small commercial buildings should operate in fully automated mode which can keep running for a long period without the need of user interventions. There are many commercially available small-scale and micro-scale biomass boilers suitable for integration with the proposed micro-CHP system of this project. These boilers are usually very efficient and can burn a variety of biomass fuels such as wood pellets and wood chips with high efficiency and low pollutant emissions.

Figure 4.5 The 25kW wood pellet boiler and its fuel hopper and combustion furnace

Two wood pellet boilers (25 kW and 50 kW) manufactured by a UK company - Ashwell Engineering Services Ltd(Ashwell Ltd) are used in this study. The Ashwell Green-tec series of domestic biomass boilers are highly efficient automatic boilers with the overall net efficiency in excess of 85%. They satisfy the current EU regulation (EN 303-05) on the emissions of domestic biomass boilers. Figure 4.5 shows the 25kW wood pellet boiler with its integrated fuel hopper and combustion furnace.

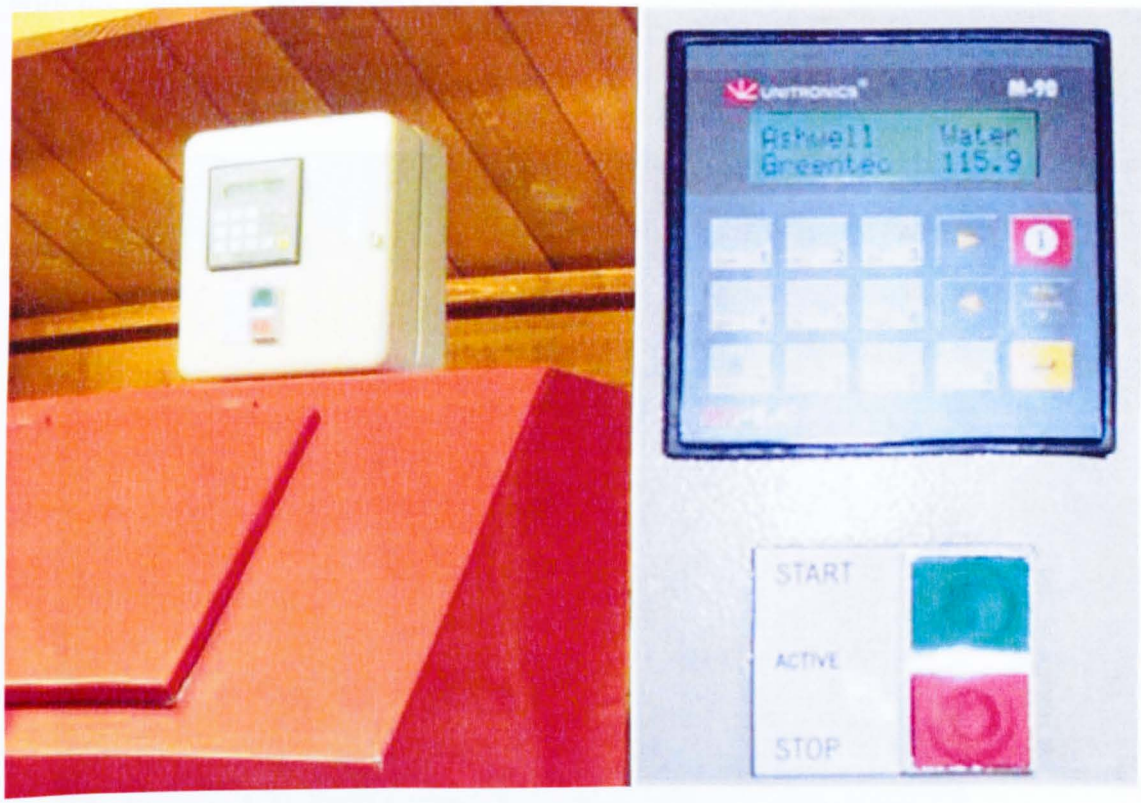

Figure 4.6 Control panel of the 25kW wood pellet boiler

The 25 kW boiler has the capabilities of auto-ignition and automatic control of the hot water temperature via its control panel Figure 4.6. The 25 kW boiler was originally designed to supply hot water for domestic heating purposes and therefore the maximum hot water temperature was set at 95 ^{0}C. Thermodynamic modelling results shown in Chapter 3 have showed that higher water temperature would lead to the micro-CHP system having higher electrical efficiency. Therefore, ideally the boiler should supply the hot water at temperatures as high as possible. After discussing with the manufacture of the boiler – Ashwell Engineering Services Ltd, it

was understood that the pressure testing of the boiler's integrated water heat exchanger was conducted at 3 bar (gauge pressure) and therefore, in theory, the boiler should be able to supply hot water at a maximum temperature corresponding to water's boiling point at 3 bar (gauge pressure) which is about 143 ^{0}C. But safety to the boiler and the more importantly to the personnel was a major concern to the boiler manufacturer and the research team members of the project. Eventually, modifications had been made to the boiler's control panel so that the boiler could supply hot water with the maximum temperature of 120 ^{0}C.

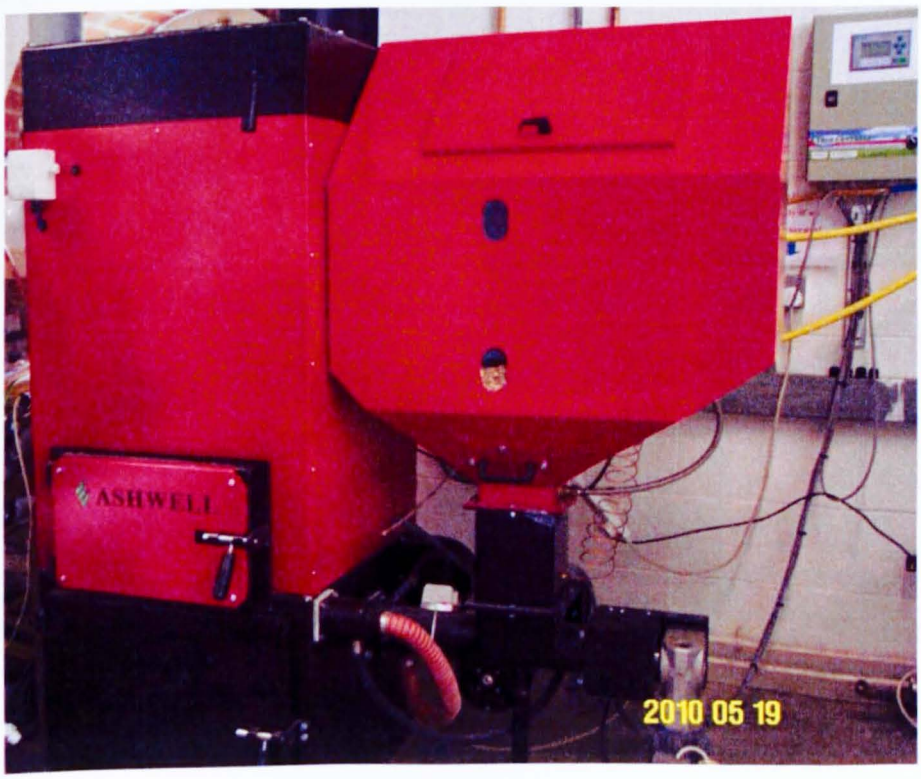

Figure 4.7 The 50 kW wood pellet boiler

The 50 kW biomass boiler was also designed and manufactured by Ashwell Engineering services Ltd (Figure 4.7). In addition to having a bigger capacity, the 50 kW was also specifically designed for the present research project and the maximum hot water temperature was designed to 180 ^{0}C. But as will be shown in Chapter 5, the maximum hot water temperature achieved was much lower than the designed value - about 140 ^{0}C only. Main reason for this was believed to be the design of the heat exchanger. Another major difference with the 50 kW boiler is the air supplies to the

combustion furnace – combustion air has been split to primary air and secondary supplies to control the formation of nitrogen oxides via the mechanism of air staging (NIMMO *et al.* 2010).

Figure 4.8 shows the details of the 50 kW wood pellet boiler furnace – the primary air is supplied through the small holes at the bottom of the fuel bed, whereas the secondary air is supplied by the four pipes above the fuel bed.

Figure 4.8 The 50 kW wood pellet boiler combustion furnace

Both the 25 kW and the 50 kW wood pellet boilers are equipped with self cleaning underfeed stoker as illustrated in Figure 4.9. Ash formed from the combustion process is collected by the ash pan which is directly below the combustion chamber as shown in Figure 4.10.

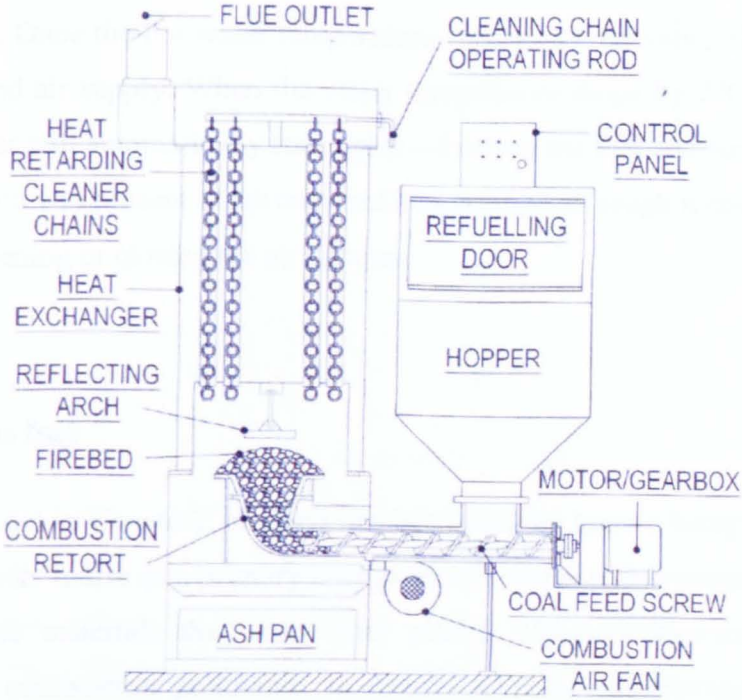

Figure 4.9 Configuration of the boiler with self cleaning underfeed stoker

Figure 4.10 Ash collection pan of the 50 kW wood pellet boiler

After the hot water temperature is set to a desired value (e.g. 115°C), the boiler automatically starts its ignition and then increases its load to the designed value to heat the water. Once the hot water temperature reaches its set value, the boiler stops fuel feeding and air supply. When the water temperature drops by 2°C below the set value, the boiler will automatically start again—feeding the fuel and supplying the air. The air/fuel ratio was present at the commissioning stage although it could be adjusted anytime via opening or closing the air damper.

4.3.1. Biomass fuel

As pointed out in Chapter2, biomass has been used by human being for thousands of years and ranks fourth as a primary energy source worldwide currently. Biomass is C-based organic materials that stem from plants. Although biomass combustion releases some combustion pollutants, it absorbs CO_2 by photosynthesis when the plants grow up. Biomass is renewable due to the very little net CO_2 emissions to the atmosphere(Liu H. 2011). Owing to the low sulphur and low nitrogen contents of many biomass materials, substituting biomass for fossil fuels, particularly coal, can reduce SO_x and NO_x emissions. Compared with other renewable resources such as wind energy and solar energy, Biomass energy has a significant advantage of continuity and reliability.

The calorific value of a biomass fuel varies greatly, depending on the fuel type and the moisture content. Apart from the calorific value, the ash content is also very important. Wood contains about 0.5% of ash; but straw contains up to 6% of ash. The difference in ash contents leads to different calorific values. Table 4.1 shows values characterizing biomass fuels including a comparison to coal(Strehler 2000).

Table 4.1 Typical analysis and calorific value of wood and selected biomass fuels

Fuel	Volatiles (%)	LHV (MJ/kg)	Ash (%)	C (%)	O (%)	H (%)	N (%)	S (%)
Straw	80.3	14.2	4.3	44	35	5	0.5	0.1
Wood	85	15.3	0.5	43	37	5	0.1	-
Charcoal	23	30.1	0.7	71	11	3	0.1	-
Peat	70	13.5	1.8	47	32	5	0.8	0.3
Mineral coal	26	29.5	1-15	73	5	4	1.4	1

The combustion process of a solid biomass fuel depends mainly on its moisture content and chemical characteristics as well as its calorific value and density. Solid biomass fuels often need to be dried, preferably using natural resources such as solar energy, in order to reduce the moisture content and ensure a good storage with little energy losses. Thus, biomass fuels with low moisture contents are the basis of a high combustion quality especially in small furnaces. Besides, combustion of biomass is also depending on the physical structure of the biomass materials. The physical structure of a biomass fuel can be influenced by different processing techniques, like milling, cutting, compaction, baling, or pelletizing.

The biomass fuel used in this project is the wood pellets supplied by Balcas Limited (Balcas Ltd.). The wood pellets are made from nature wood without additives or artificial binding agents. During the pellet making process the natural resin or lignin present in the wood naturally moves to the surface of the pellet creating a protective coating which helps the pellet keep its structure (see Figure 4.11). The proximate and elemental analyses of the wood pellets are shown in Table 4.2. The wood pellets have been measured to have a diameter of 6 mm and a length of 5–20 mm, and a calorific value 17 500 kJ/kg.

Figure 4.11 Brites wood pellets

Table 4.2 Proximate and elemental analyses of the wood pellets used in tests

Proximate analysis (wt %, as received)			
Moisture	**Ash**	**Volatile matter**	**Fixed carbon***
7.48	0.83	75.92	15.77

Elemental analyses (wt % as received)						
C	**H**	**N**	**S**	**M**	**Ash**	**O***
47.40	5.99	0.13	<0.1	7.48	0.83	38.17

* By difference

4.3.2. Flue gas and flue gas analysers

Combustion is the most mature conversion technology used for biomass resource. However, biomass combustion releases some combustion pollutants such as CO and NOx etc., which need to be controlled(Liu *et al.* 2002). The chemical and physical properties of biomass fuels affect not only the combustion characteristics but also the emissions of various pollutants such as SO_x, NO_x, CO and particulates(Liu *et al.* 2003). Table 4.2 has shown that biomass fuels contain much more volatiles than coal but have low energy densities (i.e. heating values). In an ideal case, biomass combustion

should represent the complete oxidation of the solid organic part of the biomass into the gases of CO_2 and H_2O. However, the actual biomass combustion process also results in the formation of various pollutants (CO, NO_x, etc.).

The combustion of the wood pellets in the boiler furnaces of this project is usually very stable and trouble-free under normal operating conditions. No visible smoke has been observed from the chimney when in normal operation (Figure 4.12a). But there is some smoking that can be clearly seen from the chimney when the boiler is working in an 'idle' state, which means the residual fuel is burning in the furnace with no forced air supply in the furnace after the preset hot water temperature has been reached (Figure 4.12b). As pointed in the above section, once the hot water temperature of the boiler reaches its set value, the boiler stops both of fuel feeding and air supply, i.e. entering the 'idle' phase. When the water temperature drops by 2°C below the set value, the boiler will automatically start again—feeding the fuel and supplying the combustion air, ending the 'idle' phase.

Figure 4.12 Flue gas from the 25 kW wood pellet chimney

Both of the 25 kW and 50 kW wood pellet boilers used in this project have been certified to satisfy the current EU regulation (EN 303-05) on the emissions of domestic biomass boilers. However, the certification only applies to the emissions under normal operation conditions and does not apply to 'idle' conditions. During the experimental testing period of this project, the emissions of the boilers have been closely monitored under both normal operation and 'idle' conditions.

There are two sets of gas analyzers used in this project. One is the VS-3000 Multi-component Analyzer, including a gas sampling unit, of Horiba Limited (HORIBA Ltd.) as show in Figure 4.13 on the left and the other is the EL3000 continuous Gas Analysis of ABB Limited (ABB Ltd.) as show in Figure 4.13on the right.

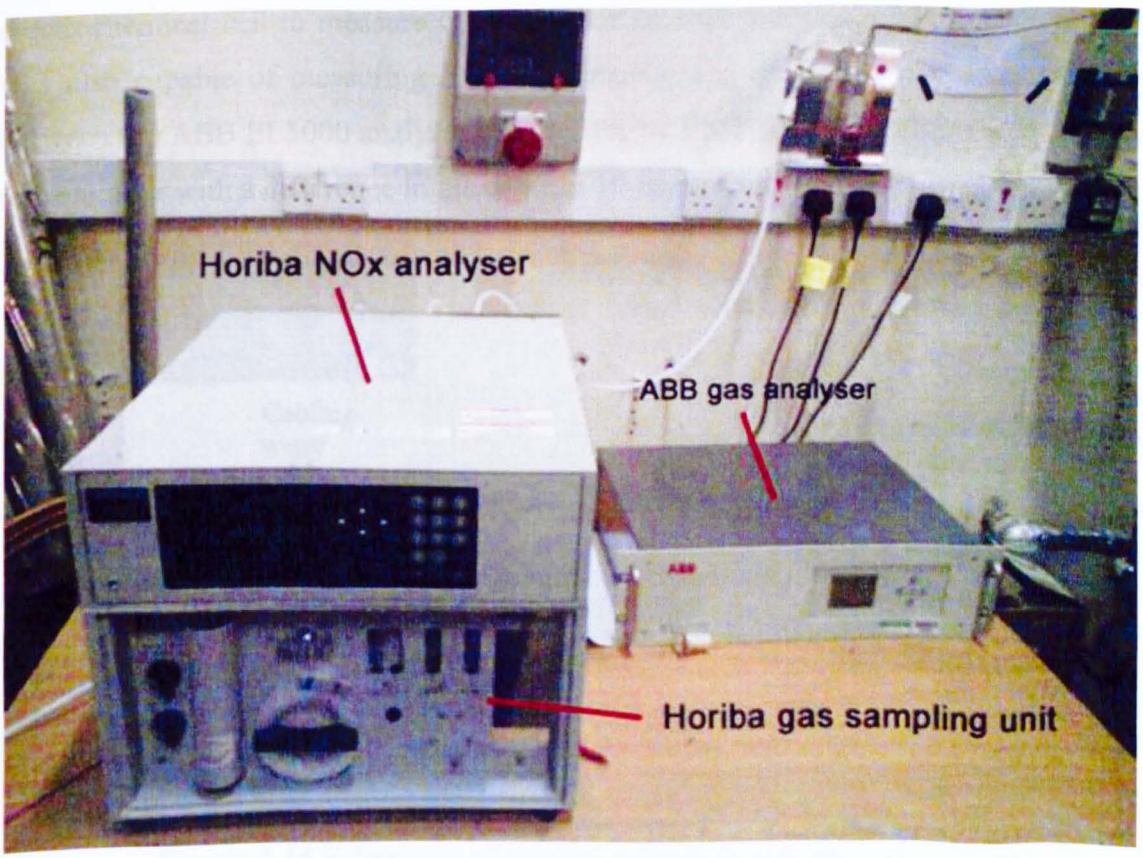

Figure 4.13 Gas analysers

The VS-3000 Multi-component analyzer is the versatile gas analyzer that has the capable of measuring a wider selection of gas components utilizing many different types of sensor technology. Non-dispersive infrared (NDIR) modules are available to measure gases such as CO, CO_2, O_2, NOx, N_2O, CH_4, SO_2 and others gases. The actual module used in the current project is the Horiba VS-3000 chemiluminescent NO_x analyser connected to a Horiba gas sampling unit for the measurement of NO/NO_x emissions.

The Horiba VS-3000 sampling unit (Figure 4.13) is equipped with a gas sampling pump which is capable of providing two channels of gas samples for both gas analysers. The main composition of the flue gas (CO_2, O_2, CO) was continuously measured by the ABB EL3000 continuous gas analyser equipped with a non-dispersive infrared (NDIR) gas photometer (Uras26) to measure CO_2 and CO, and an electrochemical cell to measure O_2. The ABB EL3000 analyser's NDIR photometer was also capable of measuring NO continuously, and the measured values of NO between the ABB EL3000 analyser and the Horiba VS-3000 NO_x analyser were found to be similar with a difference in the order of 10 ppmv.

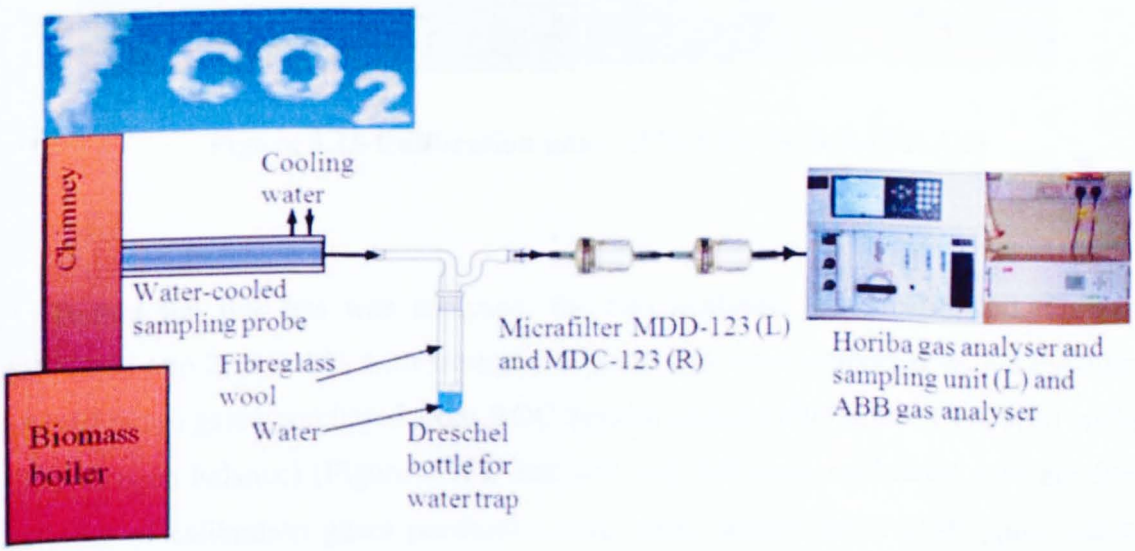

Figure 4.14 Schematic of the gas sampling and analysis system

Figure 4.14 shows a schematic of the gas-sampling and analysis system. A stainless water-cooled sampling probe was made and used to sample flue gases at the exit of the boiler, i.e. at the inlet of the chimney after the water heat exchanger of the

boiler. To protect the gas analysers, quartz wool was placed at the inlet of the probe serving as the first barrier of particles, and a water trap and two further particle filters were also used in the sampling line.

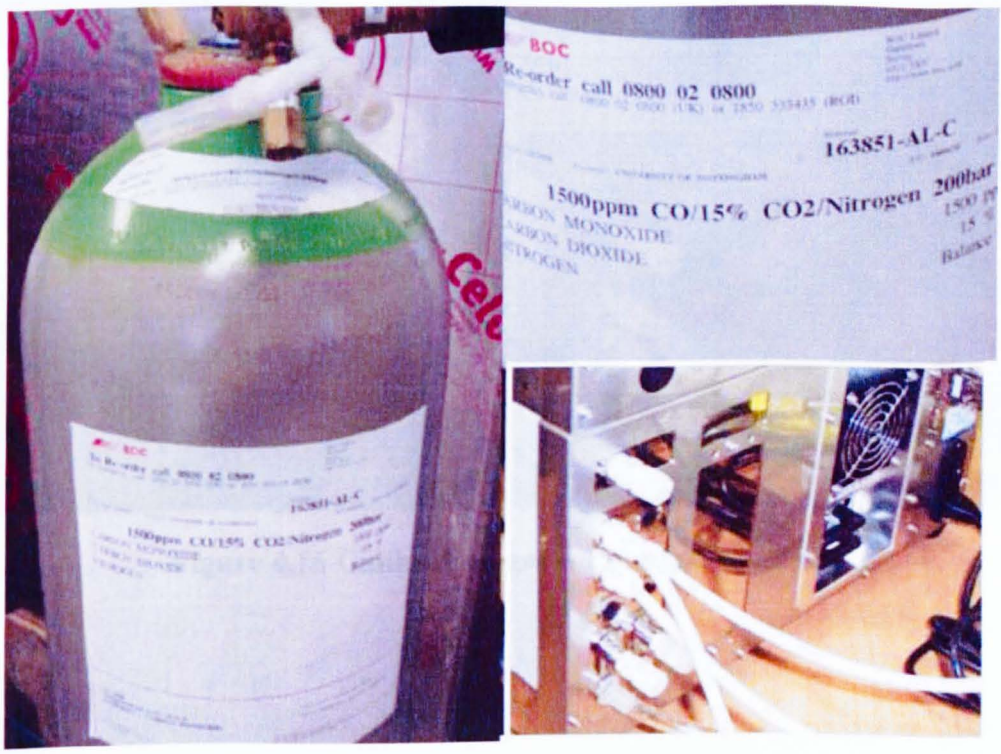

Figure 4.15 Calibration gas – 15% CO_2 % & 0.15% CO

Before the flue gas was analysed, the two analysers were calibrated. O_2 was calibrated into 20.9 vol % with fresh air. CO and CO_2 were calibrated with a cylinder of calibration gases purchased from BOC Special Gases (1500 ppmv CO/15.00 vol% CO_2/nitrogen balance) (Figure 4.15), and NO_x and NO were calibrated with another cylinder of calibration gases purchased from BOC special gases (150 ppmv nitric oxide/nitrogen balance) (Figure 4.16). Ambient air has been used to calibrate the zero points of NOx and CO, whereas the zero point of CO_2 and O_2 has been calibrated by the NO calibration gas.

Figure 4.16 Calibration gas – 150 ppm Nitric oxide

4.4. Electricity generating system

The electricity generating system mainly consists of the ORC micro-turbine, the alternator and the electric output circuit.

4.4.1. ORC micro-turbine

The ORC turbine is a key component of the micro-CHP system, shown in Figure 4.1, developed and evaluated by the present research project. A turbine is a kind of rotary machine which converts the kinetic energy in a stream of fluid (gas or liquid) into mechanical energy by driving the stream through a set of blades. However, as the micro-scale organic Rankine cycles are mostly working with low-grade heat resources which have low temperature and pressure, turbine expanders instead of the steam turbines are often used. Various expanders can be used as the Rankine cycle turbines, such as turbines, screw machines, scroll machines and reciprocal piston engines,. Compared the two types of expanders, velocity-type (e.g. axial turbine expanders) and volume-type expanders (e.g. expanders, scroll expanders and reciprocal piston expanders), the latter are more appropriate to the micro-CHP units with ORC as they are characterized by lower flow rates, higher expansion ratios and much lower rotational speeds compared with the velocity-type expanders(Badami *et al.* 2009). Moreover, the volume-type expanders have an acceptable performance over a wide range of operations, such as work in two-phase conditions which may appear at the end of the expansion in some cases.

However, market search proved that there were no commercially available micro-scale expanders that could be used with the micro-CHP system with ORC of this project. After enquiries with industrial suppliers and discussions within the research team, modified air motors were selected for the micro-scale biomass CHP system with ORC in this project, as the expanders. Air motors are rotary vane machines originally designed to compress air and then drive the rotors. Compared with other expander concepts, the rotary vane expander has simpler structure, easier manufacturing and lower cost. But these air motors are not designed to work with organic working fluids and hence the leaking of the organic working fluid is a difficult problem to overcome when modified and used as the ORC expander.

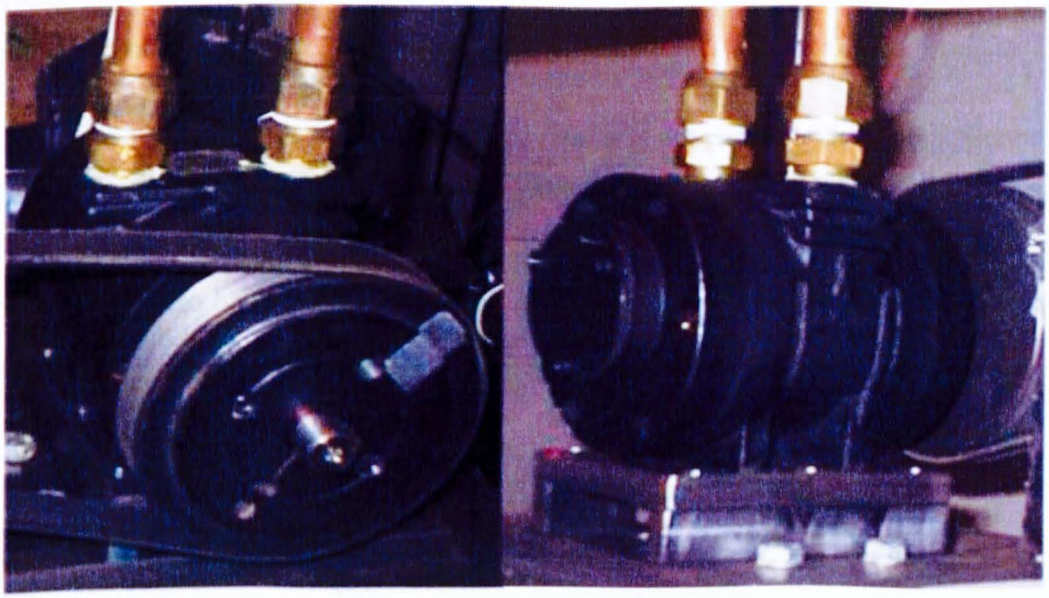

Front view Back view

Figure 4.17 Non-lubricated air-motor as the ORC micro-turbine

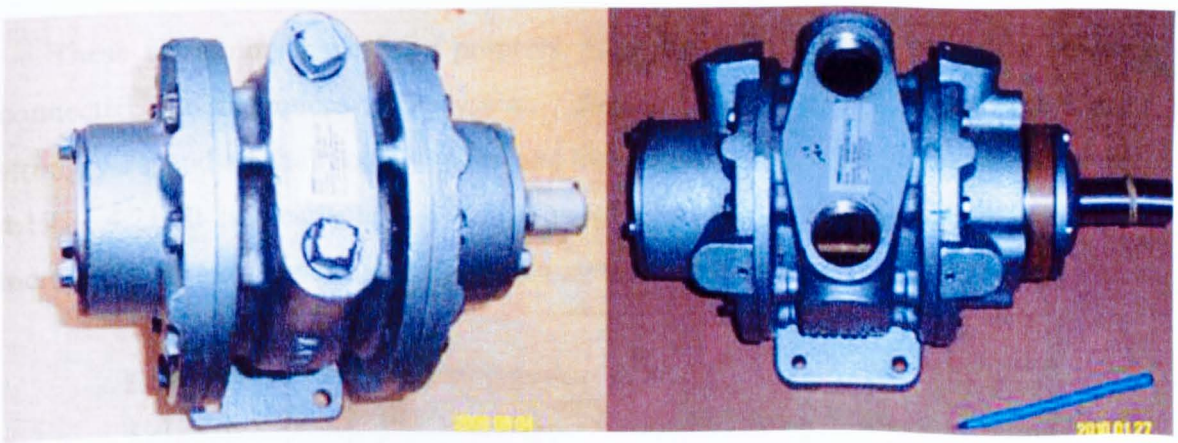

Figure 4.18 Lubricated air motors as the ORC micro-turbines (left – model 8AM-FRV-2B, right - model 16AM-FRV-2)

The air motors that have been evaluated as the turbine expander of the micro-CHP system in the project include a non-lubricated air motor (model NL52-NCW-2: 4 vanes, clock-wise rotation) and two lubricated air motors (model 8AM-FRV-2B - 4 vanes, reversible and model 16AM-FRV-2: 6 vanes, reversible) from GAST

Limited(Gast Ltd.), as show in Figure 4.18 – 4.19. The operating data of these selected air motors are listed in below.

The non-lubricated air motor was mainly tested with the 25 kW wood pellet boiler, whereas the bigger lubricated air motor (model: 16AM-FRV-2) was mainly tested with the 50kW wood pellet boiler. The smaller lubricated air motor (model: 8AM-FRV-2B) was also briefly tested with the 25 kW wood pellet boiler but its testing was abandoned after serious leaking of ORC fluid was found.

Table 4.3 Air Motor Operating Data

Model	Max.Speed (rpm)	Output Power (hp/kW)	Maximum Pressure (bar, gauge)
NL52-NCW-2	2000	2.50/1.86	5.5
8AM-FRV-2B	2500	5.25/3,9	7
16AM-FRV-2	2000	9.5/7.1	7

These air motors have been properly modified and carefully sealed up before connected into the micro-CHP system. The output power of the air motors are strongly depend on the rotation speed and the supply air pressure, as show in Figure 4.19 – 4.21. It is clearly to see that the output power rises significantly with the increase of air motor speed and the supply air pressure.

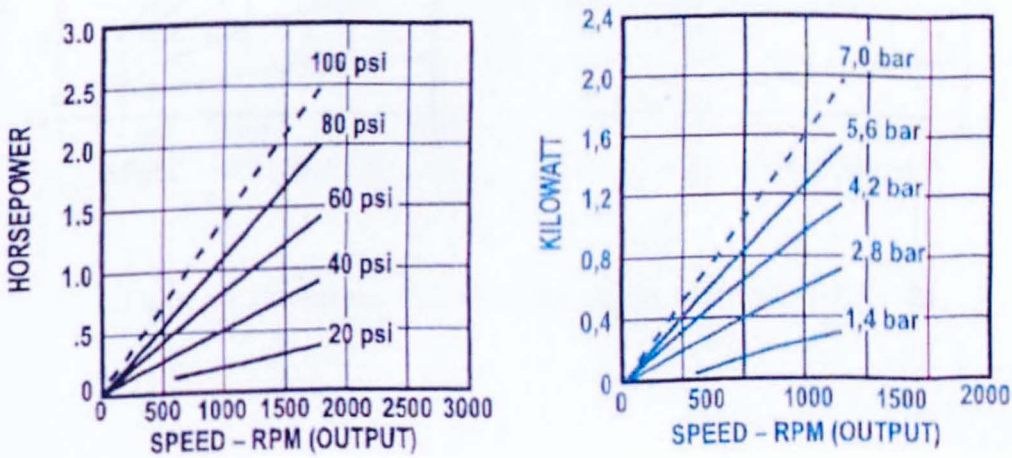

Figure 4.19 Output Power vs. Speed (model NL52-NCW-2)

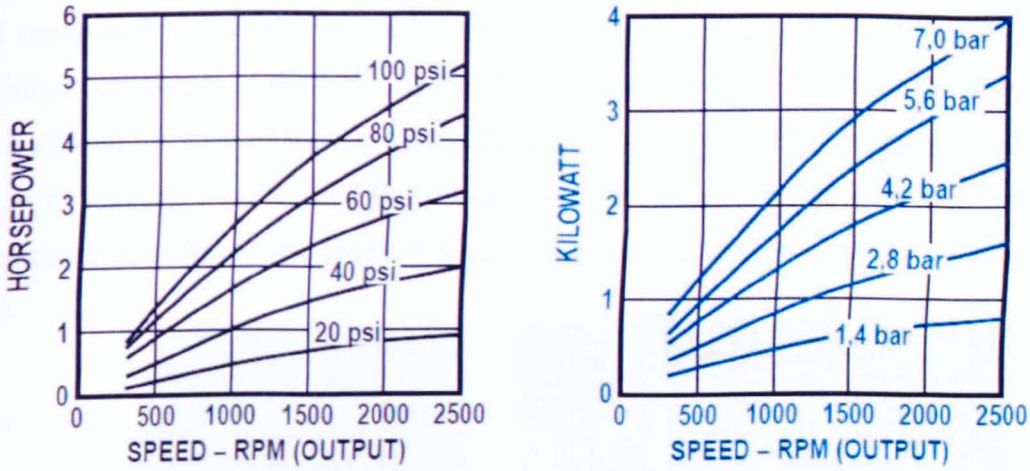

Figure 4.20 Output Power vs. Speed (model 8AM-FRV-2B)

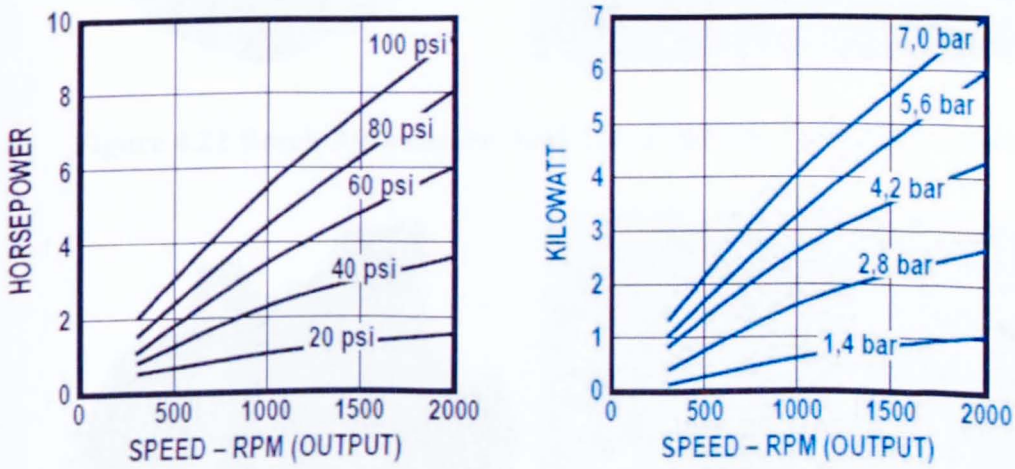

Figure 4.21 Output Power vs. Speed (model 16AM-FRV-2)

4.4.2. Alternator

An alternator is an electromechanical device that converts mechanical energy to electrical energy in the form of alternating current. In this project, a reliable, efficient and inexpensive alternator is needed to work with the micro-scale turbine as one of the key components of the CHP electricity generating system. Automotive alternators were chosen because of their great availability, low cost and easy couplings with the micro-turbine via a pulley and belt assembly. Four different kinds of alternators with different rated voltages and currents have been tested with the micro-CHP system.

Figure 4.22 Bosch Alternators: 14V, 100 A (left) & 14 V, 140A (right)

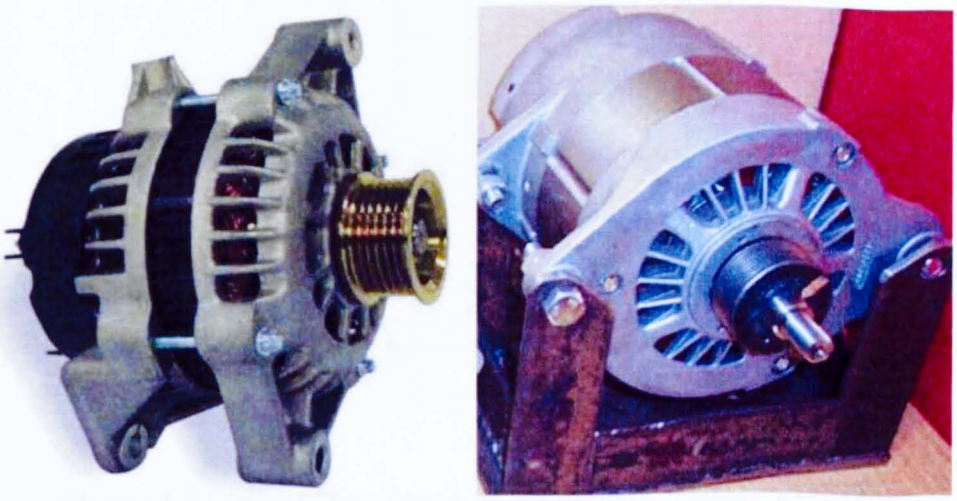

Figure 4.23 Unipoint (12V, 100A) (left) and Prestolite Alternator (12V, 100A) (right)

The four alternators that have been tested include two Bosch car alternators (Bocsh Ltd.) (14V, 100 A & 140A) as shown in Figure 4.22, a Unipoint (Unipoint Ltd.) ALT series car alternator (12V, 100A) as shown in Figure 4.22on the left and a prestolite(Prestolite Ltd.) 4000 Series alternator for emergency vehicles (12V, 200A), as shown in Figure 4.22on the right.

The output power of an alternator is obviously depending on the alternator rotation speed as illustrated by Figure 4.24-4.25. Figures 4.24-4.25 show that the cutting-speeds, i.e. the minimum alternator RPM when there is an output current, of these alternators are in the region of 800 – 1100 RPM. Therefore, these alternators should operate with alternators' RPM above their respective cutting-in speeds and ideally above 2000 – 3000 RPM. However, all the alternators tested were mostly working at low RPM (just above 1000 RPM but well below 2000 RPM) as a result of relatively low turbine speed during the tests.

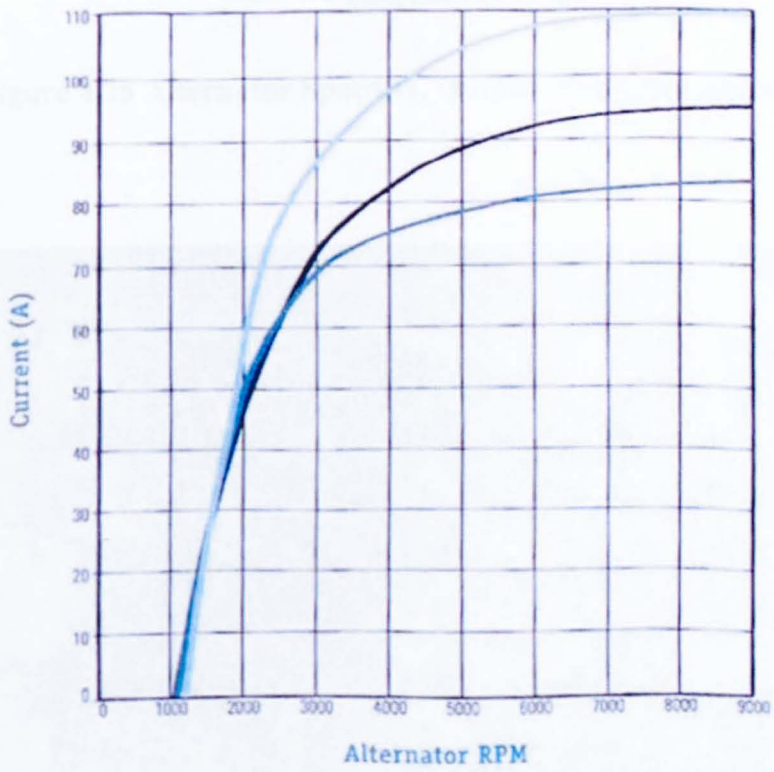

Figure 4.24 Alternator Speed vs. Output (Unipoint alternator)

Figure 4.26 shows the coupling of the turbine and alternator of the micro-CHP system in the testing laboratory. The turbine (on the right) is connected to the alternator (on the left) by the pulley and belt assembly.

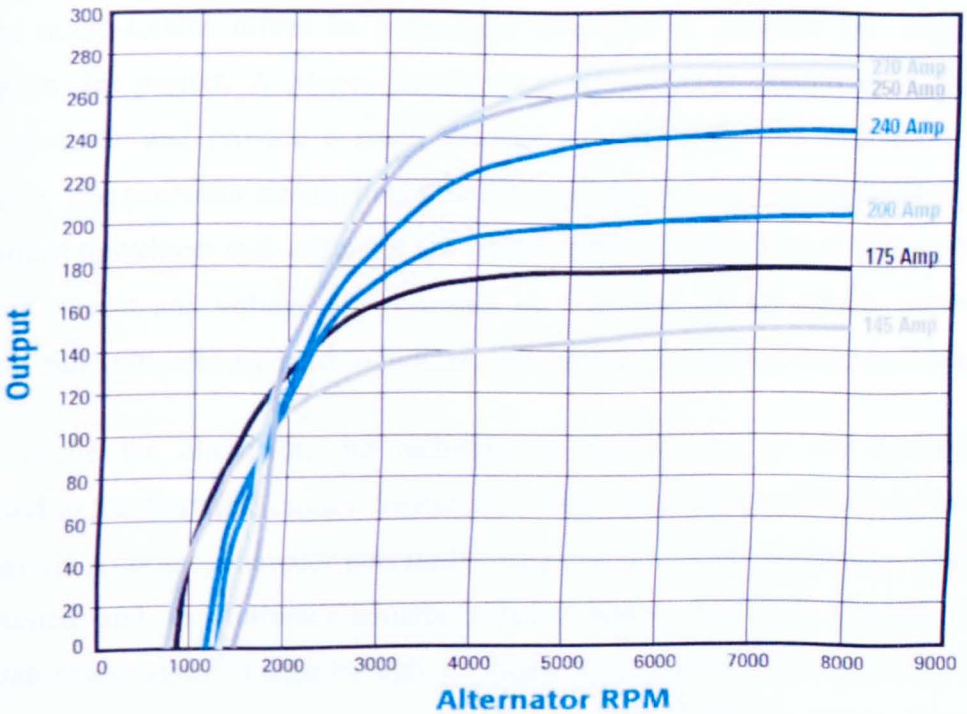

Figure 4.25 Alternator Speed vs. Output (Prestolite alternator)

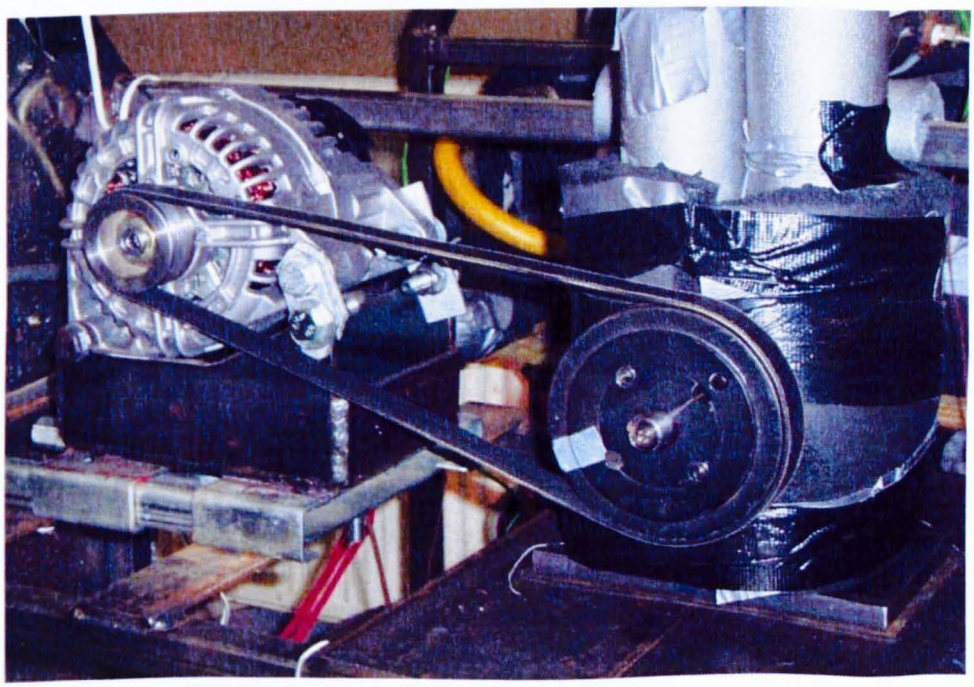

Figure 4.26 Coupling of the turbine and alternator

4.4.3. Electric output circuit and load

The micro-turbine drives an automotive alternator to generate DC current and voltage in this project. A proper electrical output circuit is needed to connect the electrical loads and provide a small amount of current for the excitation of the alternator. The alternator circuit diagram of this project is shown in Figure 4.27. The DK current transducer and voltmeter are connected to the datataker DT80 so that the transient current and voltage are recorded by computer. A set of the mechanical ammeter and voltmeter are used to indicate the current and voltage values during tests.

To excite the alternator, the rechargeable electric cell (a car battery) was connected in the electrical circuit. Switch #2 is kept on at first, and then switch #1 is switched on. After the alternator gets initial magnetic field from the battery, alternator gets excited and the turbine/alternator rotation speed decreases sharply. If the turbine/alternator speed is high enough, i.e. higher than the cutting-in speed indicated by the alternator output and speed curves (Figures 4.24-4.25), the turbine/alternator will generate DC voltage and current continuously.

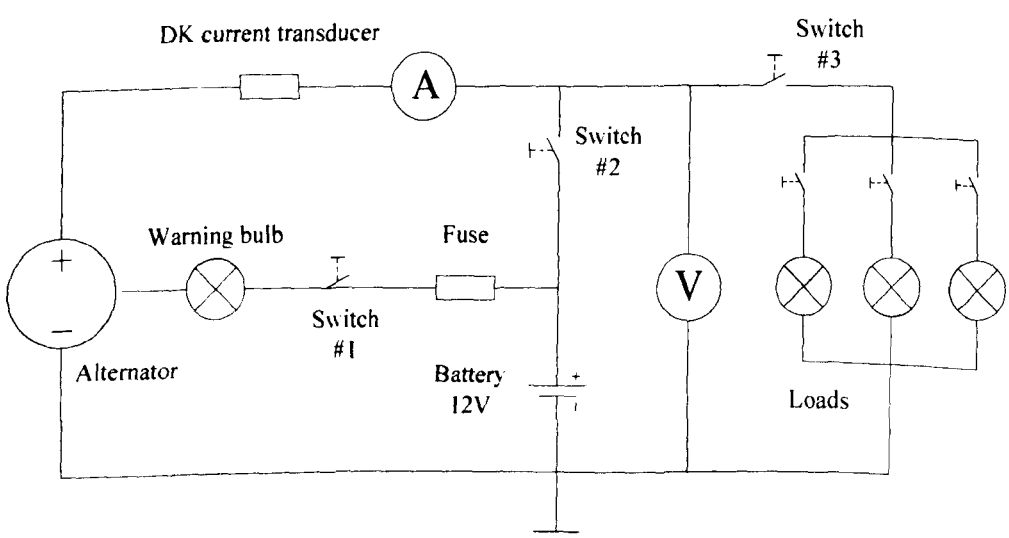

Figure 4.27 Electric output circuit diagram for the micro-CHP

More cases for the states of the electric switches are listed in Table 4.4. During the operation, the alternator generates electricity and loads can work properly.

Table 4.4 Excitation and power output of the alternator

Switch name	Switch #2	Switch #3	Switch #1	Switch of loads
Alternator excitation	On	Off	On	off
Battery charging	On	Off	Off	Off
Load output	Off	On	Off	On
Batter charging & load output	On	On	off	On

Various loads have been tried with the experimental system during different stages of the tests, such as small fans of several watt, resistances (150 Watt HS150), and finally DC bulbs (12V 20W) as shown in Figure 4.28. The DC bulbs were considered to be the best choice as they are not only visual but also easy to add on or take off from the amount of loads. If all other experimental conditions (e.g. the biomass boiler load, the ORC fluid pump load etc.) are fixed, the total current output will increase with the loads but the voltage decreases. An optimal match of the current and voltage can lead to the maximum electric power output as the electric power output is the product of the current and voltage. Figure 4.29 shows a photo of electrical generation test - the light bulbs of the board are powered by the ORC micro-CHP system.

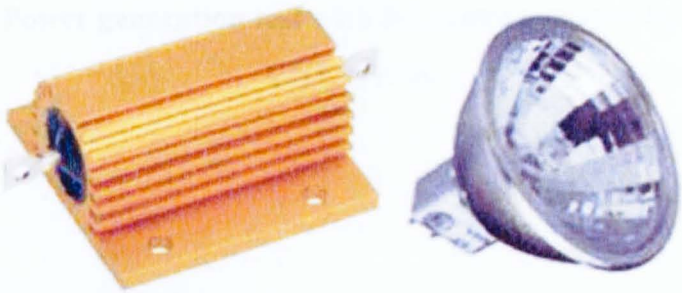

Figure 4.28 HS150 resistance (left) and DC bulb (right)

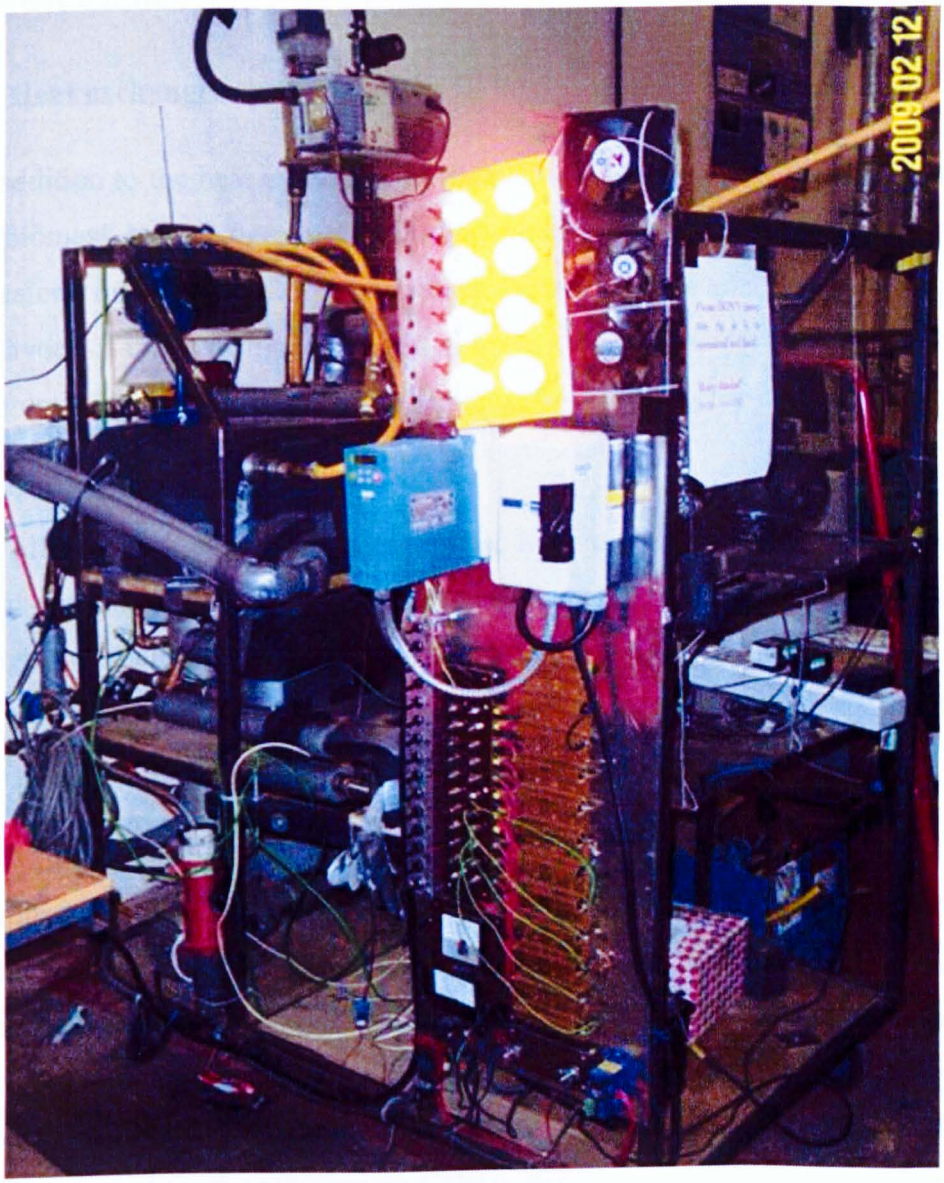

Figure 4.29 Power generation test with DC bulbs powered by the ORC micro-CHP system

4.5. Heat exchangers and Pumps

4.5.1. Heat exchangers

In addition to the heat exchanger in the biomass boiler which is an integrated part of the biomass boiler, there are four other heat exchangers used as the evaporator, superheater, condenser, and a recovery heat exchanger (named recuperator) as shown in the layout of the investigated system (Figure 4.1). The selection of these four heat exchangers takes into consideration the specific operating conditions of each heat exchanger.

For all heat exchangers, compactness and high heat exchange coefficients are two essential criteria for their selection. The evaporator and condenser have to be able to hold high volumetric flow rates of working fluids that can be operating at different pressures. The recuperator is designed to transfer efficiently the heat from a working fluid in gas phase to a working fluid in liquid phase, having similar mass flow rate but different heat capacities and heat transfer coefficients.

Compact heat exchangers (CHEXs) offer high heat transfer coefficients and large surface areas with a small size that making them to be the most suitable to the project. There are different technologies of CHEXs such as plate heat exchangers, plate-fin heat exchanger, micro-channel heat exchangers, etc. After taking the operating conditions, efficiency and cost into consideration, the brazed plate heat exchangers have been selected for the ORC micro-CHP system.

Brazed plate heat exchangers consist of a pack of pressed-plate brazed together, thus completely eliminating the use of gaskets, as shown in Figure 4.30. These heat exchangers have heat transfer capacities up to 600 kW. Plate materials are usually made of stainless steel. Copper brazed units are available for temperatures up to 225°C and a maximum operating pressure of 3 MPa, but copper braze may produce an incompatibility with some working media. Nickel brazed units are available for temperatures up to 400°C and maximum operating pressures of 1.6 MPa.

The brazed plate heat exchangers using in this project are chosen from SWEP Limited (SWEP Ltd.) and Alfa Laval Limited (Alfa Laval Ltd.): Evaporator - SWEP B25X30, Super heater - Alfa Laval CB76-30H, Recuperator - SWEP

B120TH*60/1P-SC-S and Condenser – SWEP B120TH*80/1P-SC-S.(Figure 4.30) shows the recuperator, condenser and evaporator connected in the CHP experimental system.

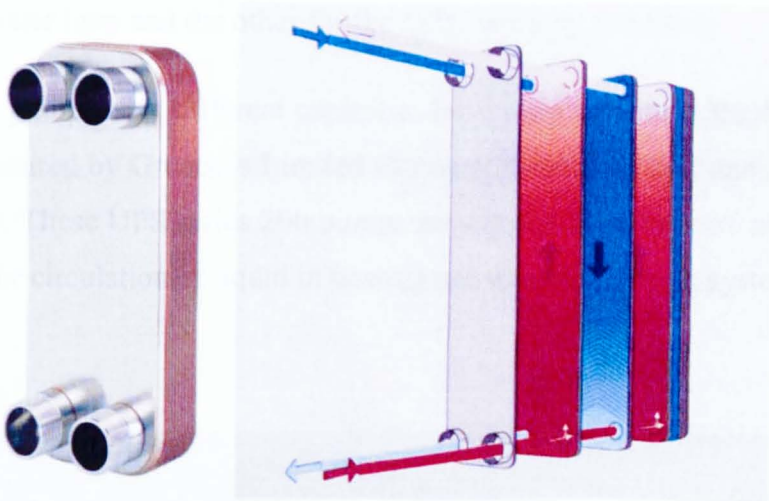

Figure 4.30 Brazed plate heat exchanger

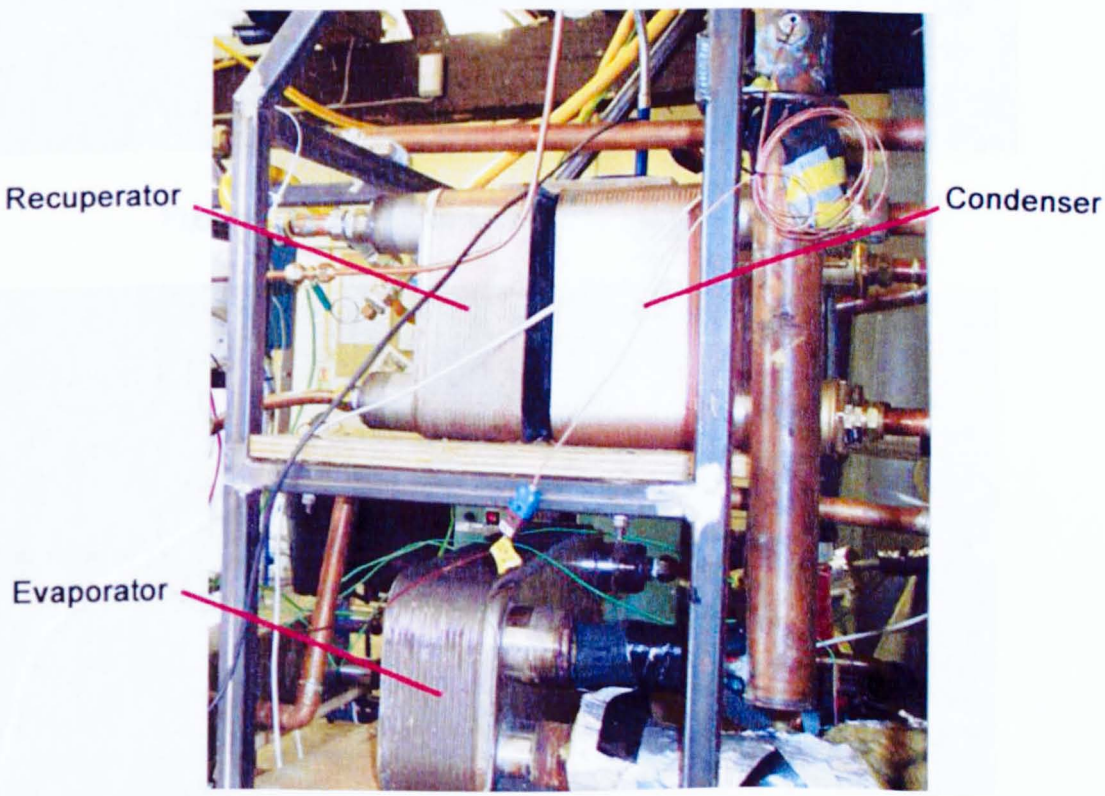

Figure 4.31 Recuperator, Condenser and Evaporator of the CHP system

4.5.2. Pumps

A wide variety of pumps is available on the market and their selection depends on the application. Two kinds of pumps are need in the micro-CHP testing of this project – one for the hot water loop and the other for the ORC working fluid loop.

Two hot water pumps with different capacities have been used with the hot water loop, both manufactured by Grundfos Limited Germany(Grundfos Ltd.) and shown in Figure 4.32 – 4.33. These UPS series 200 pumps are canned-rotor type of circulation pumps, designed for circulation of liquid in heating and air-conditioning systems.

Figure 4.32 Grundfos UPS 32-80 hot water pump

Figure 4.33 Grundfos UPS 40-120F hot water pump

The technical data of the UPS Series 200 pumps are given in Table 4.5 and Figure 4.34

Table 4.5 Technical data of the UPS Series 200 pumps

Flow rate	max 70 m^3/h
Head	max 18 m
Liquid temp	-10 °C to +120 °C (Peak temp: 140 °C)
Operate pressure	max 10 bar

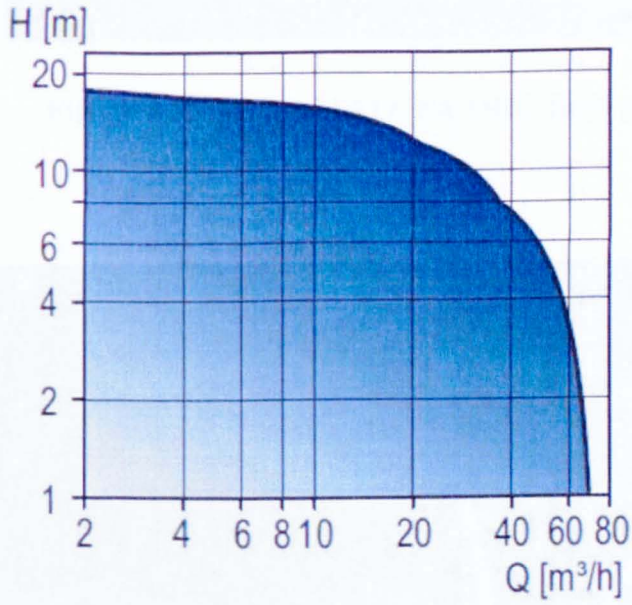

Figure 4.34 Water head vs. Flow rate

The ORC fluid pump should be leaking proof, suitable for the pumping of the selected ORC fluids and long time continuous operation. It should also be capable of providing the desired volumetric flow rate with the corresponding pressure ratio and the required operating outlet pressure, ideally with low power consumption. AEG limited (AGE Ltd.) pumps were selected as the ORC fluid pump for the micro-CHP testing system as shown in Figure 4.35 - 4.36. The technical data of the AGE pumps are listed in Table 4.6. To provide ORC fluid pump load variations, a separate ORC pump load control has been connected to the ORC fluid pump power supply – the

ORC fluid pump load control box can be seen in Figure 4.29 (the blue box below the DC bulbs).

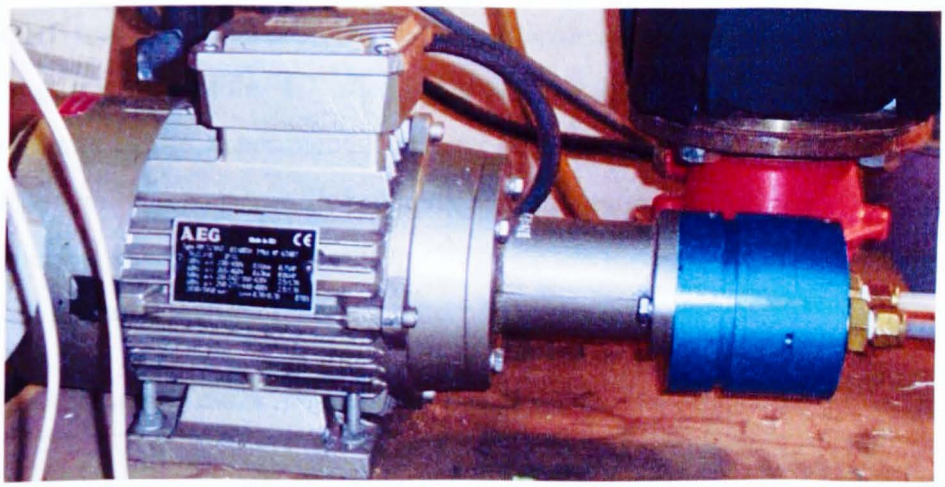

Figure 4.35 AEG AM 71Z BA ORC fluid pump

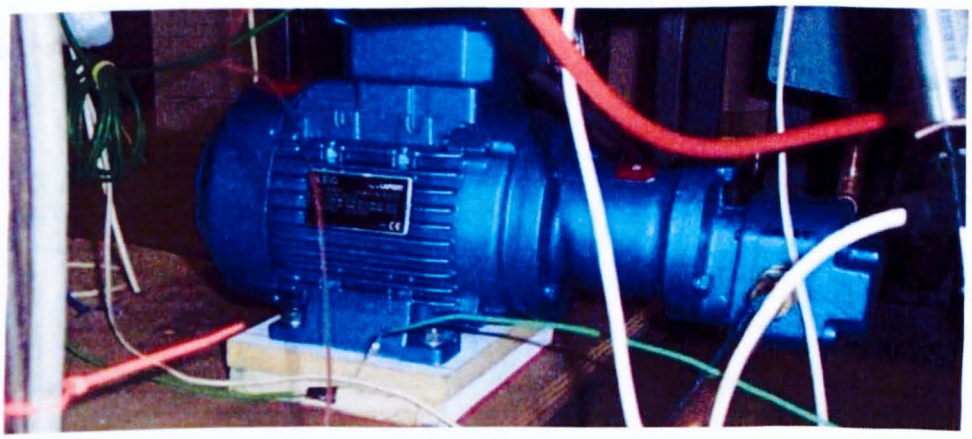

Figure 4.36 AGE AM 80Z BA ORC fluid pump

Table 4.6 Technical data of the AGE pumps

Type	kW	HP	min-1	η		
				50%	75%	100%
AM71ZBA	0.55	0.75	2830	57.0	64.0	71.0
AM80ZBA4	1.1	1.5	2810	72.1	75.0	75.3

4.6. Data acquisition and precision

Data acquisition is an essential part of any experimental investigations. The whole micro-CHP test rig of this project is equipped with various measuring transducers and displaying meters. Table 4.7 shows the list of main categories of instrumental measurements of the experimental test rig: standard K-type thermocouples, pressure transmitters, voltage, current, flow meters and gas analysers. All measured parameters except the few manually recorded (e.g. RPM of the turbine, boiler load and flow rate of ORC fluid) are recorded by a computer via a data logger.

Table 4.7 List of main instrumental measurements

Name	Description	Unit
Hot water loop	Water pressure at the evaporator inlet	bar
	Water temperature at the evaporator inlet	°C
	Water pressure at the superheater outlet	bar
	Water temperature at the superheater outlet	°C
	water volumetric flow rate	l/m
HFE loop	HFE pressure at the superheater outlet	bar
	HFE temperature at the superheater outlet	°C T
	HFE pressure at the turbine inlet	bar
	HFE temperature at the turbine inlet	°C
	HFE pressure at the turbine outlet	bar
	HFE temperature at the turbine outlet	°C
	HFE pressure at the recuperator inlet	bar
	HFE temperature at the recuperator outlet	°C
	HFE pressure at the receiver vessel inlet	bar

	HFE temperature at the receiver vessel outlet	°C
	HFE volumetric flow rate	l/m
Cooling system	Water temperature at the condenser inlet	°C
	Water temperature at the condenser outlet	°C
Alternator output power	Alternator output voltage	V
	Alternator output current	Amp

Tables 4.8 – 4.10 show the detailed specifications of the main parameter sensors – thermocouples, pressure sensors, current and voltage meter. Where possible, these sensors have been directly calibrated (e.g. thermocouples by using boiling water) or cross-checked with other types of sensors (e.g. pressure sensor against mechanical pressure gauge, current and voltage meter against mechanical current and voltage meters).

Table 4.8 Detailed specifications of standard K-type thermocouples

Thermocouple type	Type K
Temperature measurement range	-40°C to +1100°C (operating temp=-50°C ~200°C)
Accuracy - Class 1	±1.5 between −40 °C and 375 °C ±0.004×T between 375 °C and 1000 °C
+Ve arm	Nickel/Chromium
- Ve arm	Nickel/Aluminium
Wire diameter	0.2mm

Table 4.9 Detailed specifications of pressure transmitters

Model	RS pressure transmitter,0-40bar 4-20mA
Output Span	16mA ±0.5%
Output Zero	4mA ±0.5% of span
Non Linearity, Hysteresis & Repeatability (NLH)	±0.1% of span (best fit straight line)
Compensated Temp Range	-20°C to 125°C

Thermal Zero Shift	0 to 100°C, ±0.01% of span / °C <0°C & >100°C, ±0.015% span / °C
Thermal Span Shift	±0.015% reading/ oC typical
Long Term Stability	0.1% / 12 months typical
Loop Resistance	1.1k Ω max @32Vdc supply

Table 4.10 Detailed specifications of digital-multimeter

Model	Fluke 87-V DMM Ex
Current Accuracy	ac: ±1%;dc: ±0.2%
Maximum Current	100A
Maximum Voltage Measurement	1000 Vac/dc
Safety	EN 61010-1 CAT III 1000V, CAT IV 600V
Series	FL87V
Specific Application	Industrial
Voltage Accuracy	ac: ±0.7%;dc: ±0.05%

The data logger - DataTaker DT80 (DataTaker Ltd.) used in the project is a smart data logger that provides an extensive array of features allowing it to be used across a wide variety of applications. As DataTaker DT80 has only 12 digital channels, a compatibles extension (DataTaker CEM20) was connected with DataTaker DT80, as shown in Figure 4.37, so that together they could provide enough digital channels needed for the measurements listed in Table 4.7.

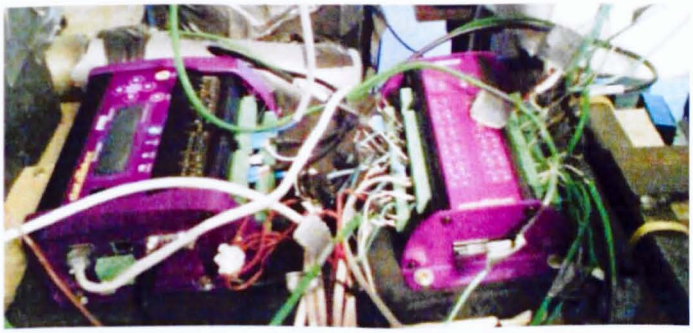

Figure 4.37 DataTaker DT80 (left) connected with its compatible extension module CEM20 (right)

4.7. Conclusions

This chapter has presented the main features of the equipment used in the experimental investigation of the proposed biomass-fired micro-CHP with ORC and the processes of test operations. Each of the following main components of the biomass-fired micro-CHP system with ORC has been introduced and discussed:

- Biomass combustion unit which mainly includes the biomass fuel, the biomass boiler, and the flue gas analysis system;
- Electricity generating system which mainly includes the micro-turbine, the alternator and the electric output circuit;
- Heat exchangers and Pumps;
- Data acquisition system.

Experimental results obtained with the experimental micro-CHP system described in this chapter will presented and analysed in the next chapter.

Chapter 5. Experiment Results and Discussion

5.1. Introduction

In the previous chapter, the experimental set-up and system components were described. This chapter presents the results and analysis of the tests conducted during the period between Jan 2009 and July 2010. A total of over 50 CHP tests had been conducted during the above period in order to evaluate the performance of the biomass-fired micro-CHP system with ORC. These tests were conducted with two different wood pellet boilers which can operate with different maximum hot water temperatures, various turbines and alternators. The electrical efficiency and CHP system overall efficiency have been calculated for different operating conditions. Besides, the flue gas emissions of the two biomass boiler under are also analysed and presented in this chapter.

The 25kW wood pellet boiler system operated with the non-lubricating turbine (as shown in Figure 4.17) to drive the Bosch alternator (12Volts, 100Amps, as shown in Figure 4.22) is selected as a good example of the CHP test with this particular boiler. The results of another test with the same boiler, turbine but a different alternator (Prestolite Alternator, 12Volts, 100Amps, as shown in Figure 4.23 were also presented for comparison. The flue gas emissions of the 25 kW wood pellet boiler have been analysed qualitatively and quantitative. A noticeable characteristic of the 25kW boiler testing system was that the heat produced by the boiler was more than that could be absorbed by the refrigerant loop as a result of small heat exchangers being used as the evaporator and the superheater at the time. Consequently, the boiler stopped burning when reaching the setting water temperature and re-started burning after the hot water temperature dropping by 2^0C below the setting water temperature. This led to some unstable and significantly fluctuating measured parameters such as water temperatures, flue gas compositions and emissions etc.

The 50kW wood pellet boiler system operated with the bigger lubricating turbine (Figure 4.18) to drive the Bosch alternator (14 Volts, 140Amps, as shown in Figure 4.22 is selected as a good example of the CHP test with this bigger boiler. The testing results with the same combination of boiler and turbine but with a different alternator

(Prestolite Alternator, 14Volts, 200Amps, Figure 4.23) were included for comparison. The flue gas emissions of this boiler have also been analysed qualitatively and quantitatively. For the micro-CHP system tested with the 50kW boiler, the heat produced by the boiler could be matched and absorbed by the refrigerant loop during the main CHP and power generation tests – several modifications to the micro-CHP testing system had been carried out by the time including replacing the small heat exchangers with the large heat exchangers and replacing the 15mm diameter connecting pipes with 22 mm diameter pipes etc.. Therefore, the 50 kW wood pellet boiler worked continuously at the constant load and there were no obvious large fluctuations with the measured parameters.

5.2. Experimental Results with the Micro-CHP System Driven by the 25 kW Wood Pellet Boiler

The test on 14 Sep. 2009 is selected as a good example of the 25 kW_{th} biomass boiler-based CHP test as it produced the best power output in the test history of this biomass boiler. The non-lubricating turbine was applied on the system to drive the Bosch alternator (12Volts, 100Amps) with the pulley diameter ratio of 1:2. Refrigerant HFE7000 was used as the working fluid with a flow rate measured to be up to 6.5kg/min. The initial setting of the boiler hot water temperature was chosen as 115^0C but was later increased to 120^0C during the CHP/electricity generation test as the moisture of HFE7000 was observed frequently at the micro-ORC turbine inlet observation glass window. The hot water flow rate was measured to be around 30.9 l/min and the cooling water temperature from the tap was found to about 15.5 ^{0}C with a flow rate of 9.0 l/min.

The hot water flow rate is a key parameter for the calculation of the biomass boiler thermal output and hence the thermal input of the ORC loop. The mechanical flow meter for the hot water was calibrated by weighing collected tap water in buckets and the reading of the flow meter and linearity of the readings were considered acceptable as shown in Figure 5.1.

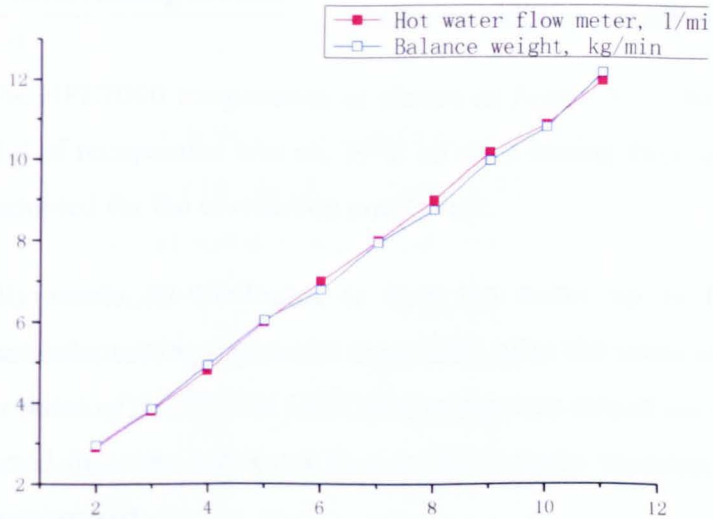

Figure 5.1 Calibration for hot water flow meter

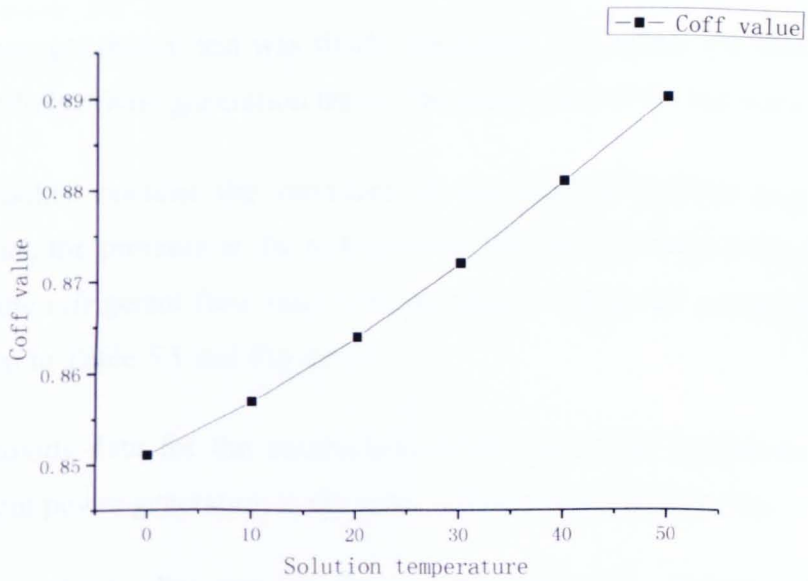

Figure 5.2 Calibrating water flow rate into HFE7000 flow rate

HFE7000 flow rate was also measured by a volumetric-type of water flow meter – but it was converted to HFE7000 flow rate by using the following correlation to considering the difference in density between HFE7000 and water: kg/min=

$\frac{\text{LPL MH waterflow meter reading in l/min}}{\text{coff}}$, where correlation coefficient (Coff) slightly varies with the HFE7000 temperature as shown in Figure 5.2. The HFE7000 temperature at the inlet of recuperator was ca. 35^{0}C on most testing days and hence a value of 0.8765 was adopted for the correlation coefficient.

The boiler usually needs 30-40minutes to heat tap water up to the setting temperature. In the particular testing day on 10 Sept 2009, after the water temperature reached the initial set point of 115^{0}C, the HFE7000 pump was turned on so that the heat could be transferred from the hot water loop to the Organic working fluid loop and the test could be progressed.

5.2.1. Non-power generation test

A non-power generation test was firstly conducted (i.e. before the alternator was excited for CHP/electricity generation tests). The main aims of the test were

- to quickly examine the variations of the main parameters (e.g. RPM of turbine, the pressure at the turbine inlet, the pressure drop over the turbine and the refrigerant flow rate) with increasing refrigerant pump capacity, as shown in Table 5.1 and Figure 5.1;
- to provide data for the comparison of the parameter variations with and without power generation at the same refrigerant pump capacity.

Therefore, without alternator excitation, the HFE7000 pumping load was increased from 28% to 60 %. With the maximum hot water temperature set at 115 ^{0}C, the moisture of HFE7000 would always appear when the pumping load was set to be higher than 60%, which would decrease the turbine RMP sharply. Each pumping load was operating for over 10 minutes to make sure the system become quasi-steady. It was difficult to operate the system under 'steady-state' conditions as the biomass-boiler heat output via the hot water did not exactly match the heat demand of the HFE7000 loop, especially at low HFE pumping loads and therefore the system was operating under 'quasi-steady' state conditions, i.e. with little variations of most measured parameters.

Figure 5.3 – 5.5 show that the alternator RPM, refrigerant flow rate and turbine inlet pressure increase with increasing HFE pump load.

The other parameters such as temperatures, pressures, the organic working fluid flow rate, are mostly increasing with the HFE pump load, as shown in Table 5.1. However, although the boiler hot water temperature was staying around the setting point of 115^{0}C, the actual maximum hot water temperature that was measured was still a few degrees below 115^{0}C. The temperatures and pressures of HFE7000 loop were seen to increase with the increase of HFE pumping load. The cooling water inlet temperature remained at around 15.5^{0}C and the cooling water outlet temperature increased with the HFE pumping load. The turbine pressure ratio between the inlet and the outlet was also showing a visible increase with the HFE pump load. These indicate more heat had been transferred from the hot water loop to the HFE loop as the HFE pump load increased – this was exactly expected as higher flows in the HFE7000 sides of the evaporator and superheater heat exchangers would lead to greater heat transfer from the hot water to the working fluid (HFE7000).

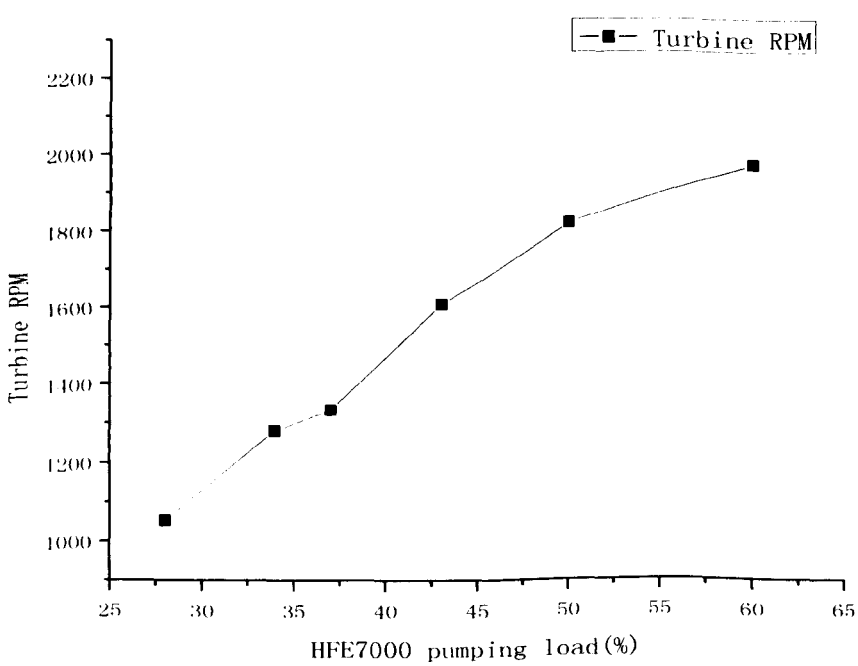

Figure 5.3 HFE7000 pumping load (%) vs. Turbine RPM

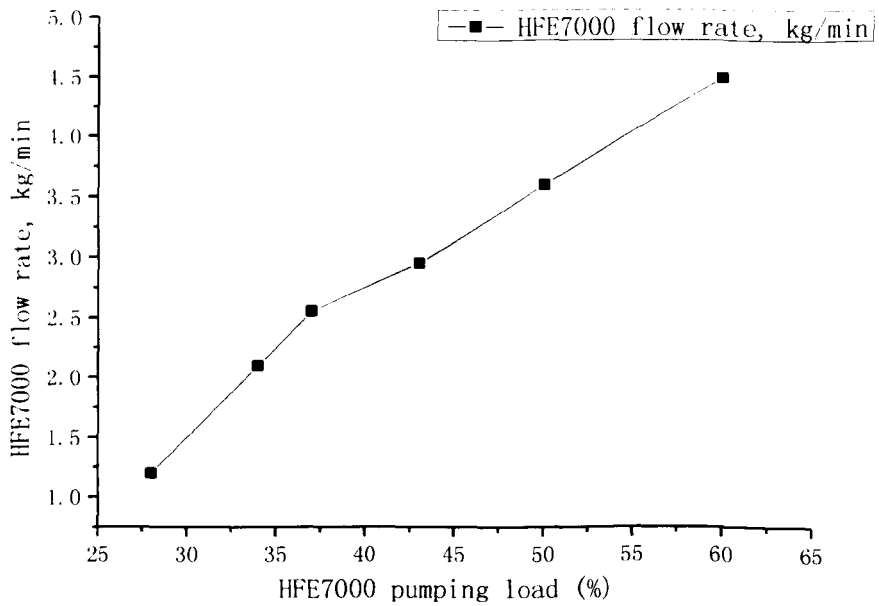

Figure 5.4 HFE7000 pumping load (%) vs. HFE7000 flow rate, kg/min

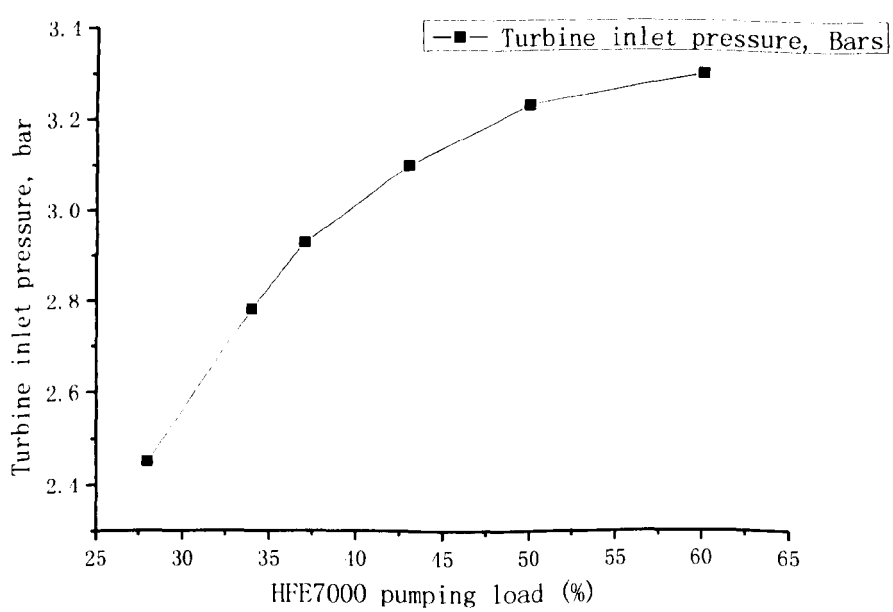

Figure 5.5 HFE7000 pumping load (%) vs. Turbine inlet pressure (bar)

Table 5.1 Typical variations of parameters with various HFE pump loads (25 kW biomass boiler without power generation)

HFE pump load %	28	34	37	43	50	60
Turbine RPM	1053	1278	1333	1611	1820	1970
Alternator RPM	2106	2556	2666	3222	3640	3940
HFE7000 flow rate $\dot{m}$ (kg/min)	1.2	2.3	2.55	2.96	3.6	4.5
Boiler inlet water T (^{0}C)	108.6	104.3	104.4	105.3	104.3	104.1
Boiler outlet water T (^{0}C)	113.1	111.8	110.1	111.3	111.1	113.2
Turbine inlet HFE7000 T (^{0}C)	108.1	105.6	106.3	107.8	108.1	112.2
Turbine outlet HFE7000 T (^{0}C)	96.4	95.4	97.4	98.3	99.2	99.9
Evaporator inlet HFE7000 T(^{0}C)	23.5	25.7	26.8	28.7	37.3	55.4
Superheater outlet HFE7000 T(^{0}C)	82.5	105.3	105.9	107.4	107.6	108.6
Condenser inlet water T (^{0}C)	15.9	15.2	15.3	15.4	15.5	15.6
Condenser outlet water T (^{0}C)	27.6	39.8	42.5	46.5	50.4	52.4
Turbine inlet HFE7000 P_{t_in} (bars)	1.96	2.4	2.62	2.72	2.82	3.17
Turbine outlet HFE7000 P_{t_out} (bars)	1.05	1.28	1.44	1.34	1.2	1.29
Turbine pressure ratio, P_{t_in}/P_{t_out}	1.87	1.87	1.92	2.03	2.35	2.46

5.2.2. CHP/power generation test

As discussed in Chapter 4, to generate electricity and conduct CHP testing, the alternator needs to be excited. After the alternator was excited, the alternator RPM would decrease and stabilize at a lower RPM than that achieved without excitation. The micro-CHP system generated Direct Currents from the mechanical energy of the turbine via the alternator. When a load was connected, the power output could be determined by measuring the DC current and voltage. A power generation and CHP test of the micro-CHP system could take several hours each time, usually with the biomass boiler continuously operating (with a hot water temperature set point of 120 ^{0}C) and the organic working fluid pump operating with different loads. Figure 5.6 – 5.7 show the variations of the main temperatures and pressures for the system during a selected period of time. As explained in Chapter 4, the control panel of the 25 kW biomass boiler had not been designed to moderate the fuel consumption rate of the boiler and therefore the heat supplied by the hot water of the boiler could not exactly match the heat absorb rate by the HFE7000 loop of the micro-CHP system. Therefore, during the test hours, the boiler kept on stopping burning after the temperature of the hot water at the outlet of the boiler heat exchanger reaching its set point (120 ^{0}C), and re-starting burning again after the hot water temperature dropping by 2^{0}C below the set point (118 ^{0}C in this test). Because of this 'stop & re-start' cycle, there were obvious water/ORC fluid temperature fluctuations during CHP testing as shown clearly in all Figures 5.6 – 5.7.

During the power generation and CHP testing, different electric loads can be connected to the output of the alternator, and with the test conducted on 14 Sept 2009 20W-rated DC bulbs were used as electric loads. The bulbs were added to the electric circuit carefully one after another with the increase of the HFE pumping load. The maximum electric power output of 344.6W (13.63V, 25.28A) had been achieved with the electric loads of 15 of 20W-rated DC bulbs connected in parallel.

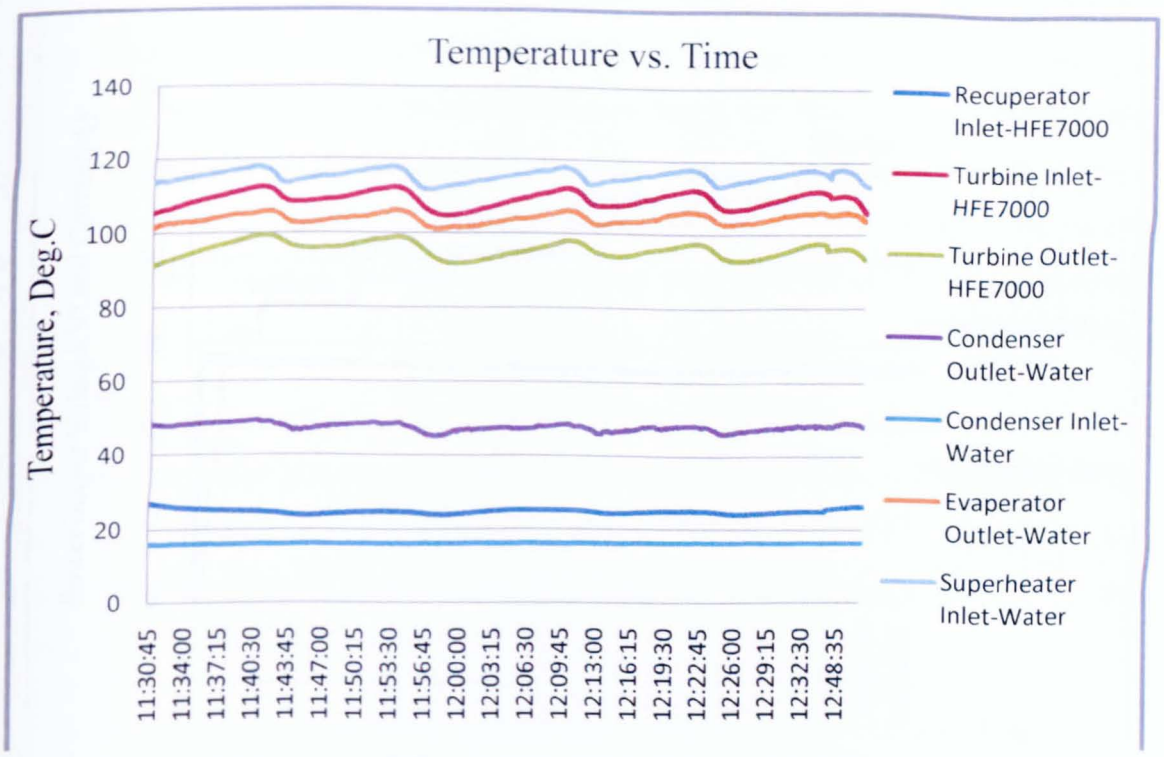

Figure 5.6 Variations of main temperatures of the micro-CHP system (14/09/2009)

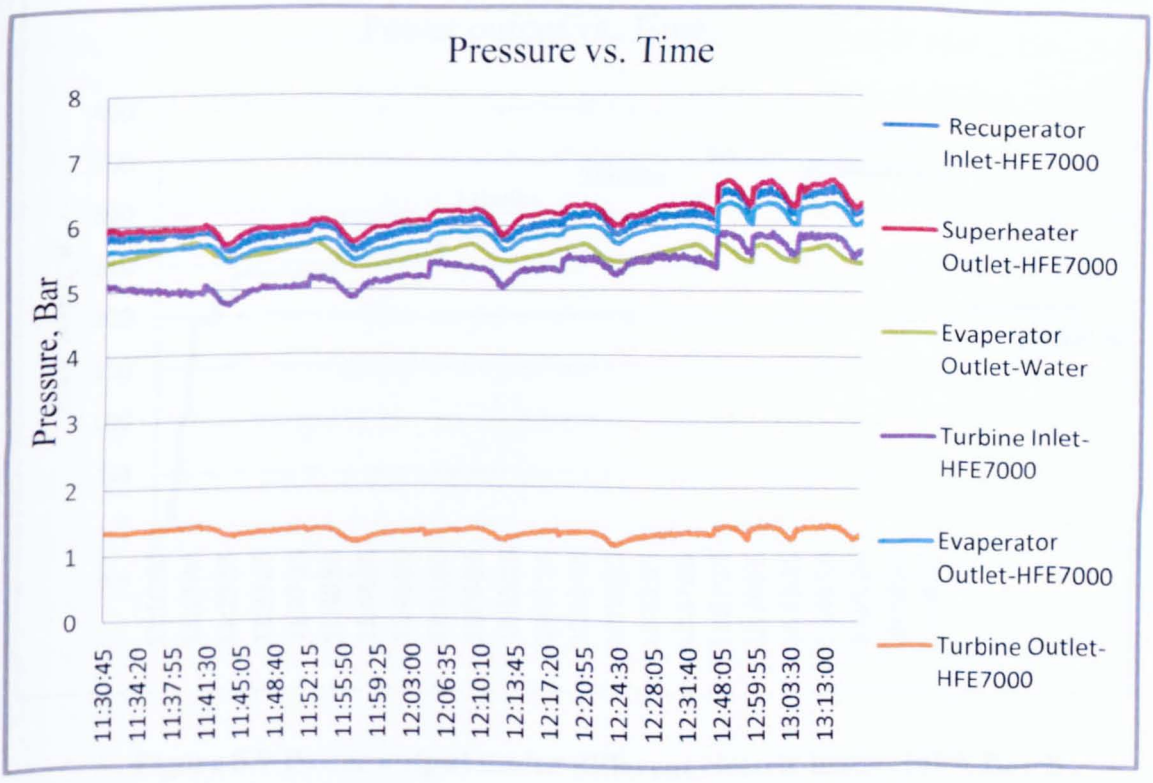

Figure 5.7 Variations of the main pressures of the micro-CHP system (14/09/2009)

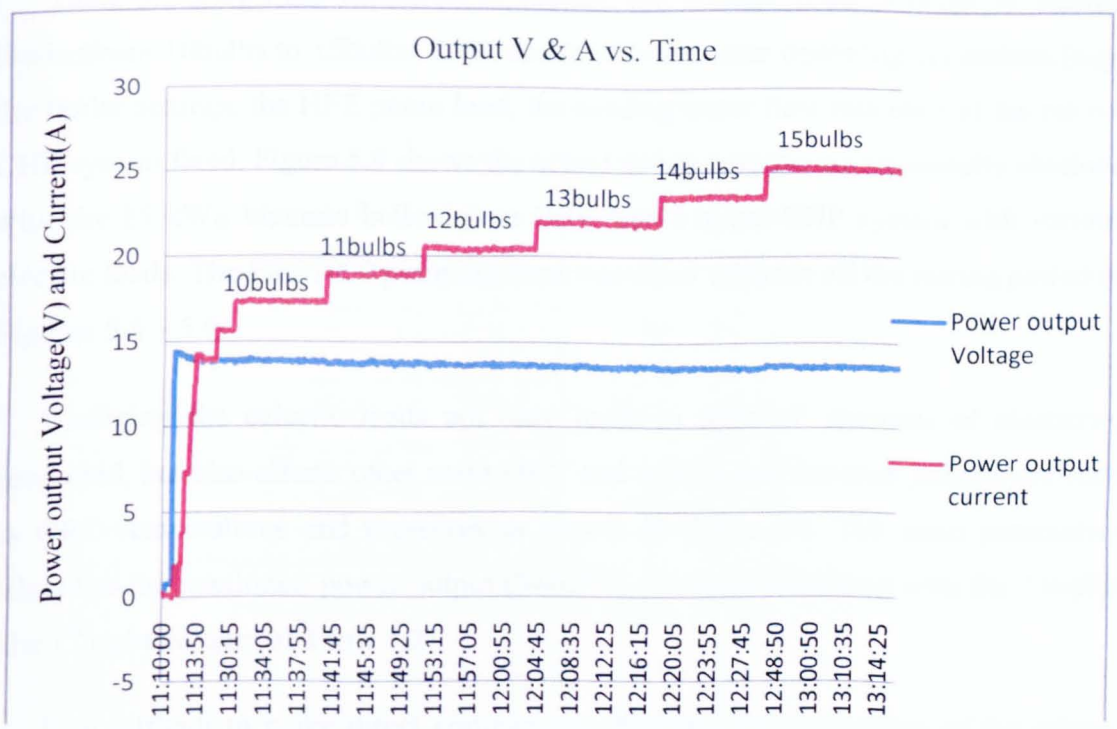

Figure 5.8 Measured DC currents and voltages with different electric loads (140A Bosch Alternator, 20W-rated DC bulbs, 14/09/2009)

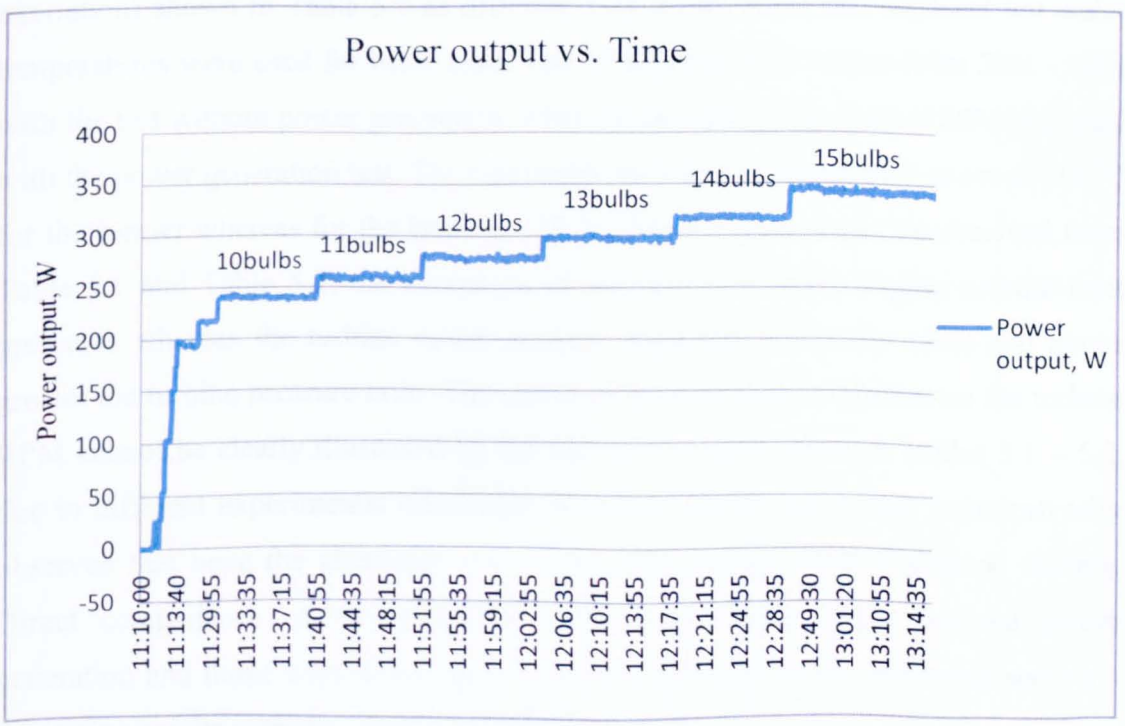

Figure 5.9 Power output under different electric loads (140A Bosch Alternator, 20W-rated DC bulbs, 14/09/2009)

Table 5.2 shows the variations of current and voltage under 6 different electric loads (from 10bulbs to 15bulbs, 20W each) with the other operating conditions (e.g., the boiler settings, the HFE pump load, the cooling water flow rate etc.) of the micro-CHP system fixed. Figure 5.9 shows the actual power outputs experimentally obtained with the 25 kW_{th} biomass boile-driven ORC-based micro-CHP system with various electric loads. The HFE7000 pumping load was set at 80% for all the testing period of Figures 5.8 – 5.9.

Changing the eclectic loads not only leads to different amounts of electricity generated, but also affects other main ORC and system performance parameters such as ORC temperatures and pressures as shown in Table 5.2. The main parameters related to the maximum power output (344.5W) are those measured with the 15bulbs (the 1st right column of Table 5.2).

It is difficult to make direct comparisons between the parameters of the micro-CHP system measured without power generation (i.e. without the alternator excitation) shown in Table 5.1 and those measured with power generation (i.e. with alternator excitation) shown in Table 5.2 as different HFE pump loads and different hot water temperatures were used for these tests. The HFE pump load ranged from 28% - 60% with the test without power generation, whereas the HFE pump load of 80% was used with the power generation test. The maximum hot water temperature was set at 115 ^{0}C for the former whereas for the latter at 120 ^{0}C. Nevertheless, it can be observed from Table 5.1 and Table 5.2, the excitation of the alternator led to higher turbine inlet pressures whereas the turbine outlet pressure remained nearly the same and hence greater the turbine pressure ratio. The effect of the alternator excitation on the turbine RPM cannot be clearly illustrated by the measured values shown n Tables 5.1 – 5.2, due to different experimental conditions described above, but it was experimentally observed that once the alternator was excited, the turbine RPM decreased sharply. Direct comparisons of the measured parameters between those without power generation and those with power generation will be made in the following section – the testing results with the 50kW biomass boiler.

Table 5.2 Variations of the main parameters of the micro-CHP system under different electric loads (25 kW biomass boiler with power generation, HFE pump load 80%)

Electric loads	10 bulbs (20W each)	11 bulbs (20W each)	12 bulbs (20W each)	13 bulbs (20W each)	14 bulbs (20W each)	15 bulbs (20W each)
Turbine RPM	2010	1940	1720	1629	1588	1593
Alternator RPM	4020	3880	3440	3258	3176	3186
HFE7000 flow rate $\dot{m}$ (kg/min)	6.03	6.31	6.36	6.22	6.3	6.6
Boiler inlet water T (^{0}C)	115.4	114.6	114.8	115.1	115	117.8
Turbine inlet HFE7000 T (^{0}C)	108.9	108.5	107.4	107.9	110.7	111
Turbine outlet HFE7000 T (^{0}C)	95.4	96.1	93.6	94.1	97.1	95.8
evaporator inlet HFE7000 T(^{0}C)	63.8	61.9	62.5	61.5	64.2	95.8
superheater outlet HFE7000 T(^{0}C)	109.3	108.9	107.8	108.3	110.9	110.7
Condenser inlet water T (^{0}C)	15.9	15.9	16.1	16.1	16.1	16.2
Condenser outlet water T (^{0}C)	48.5	46.9	47.3	46.7	47.9	48
Turbine inlet HFE7000 P_{t_in} (bar)	5.02	4.99	5.12	5.36	5.34	5.7
Turbine outlet HFE7000 P_{t_out} (bar)	1.35	1.3	1.32	1.3	1.27	1.32
Turbine pressure ratio, P_{t_in}/P_{t_out}	3.72	3.83	3.9	4.12	4.2	4.38

To investigate the effect of the alternator on the amount of power generated , the Prestolite alternator (12Volts, 100Amps) was connected into the micro-CHP ORC system to replace the original Bosch alternator (12Volts, 100Amps) in the afternoon of the same testing day afternoon. Other experimental conditions were kept the same as those of the test with the 100A Bosch Alternator and the same 20W-rated DC bulbs were used as electric loads for the Prestolite alternator (12V, 100A). However, with the same experimental conditions, the Prestolite alternator had a lower RPM and could only operate with as many as 11 bulbs. The HFE pumping load was the same 80% and the HFE7000 flow rate was observed to be slightly smaller than the system with the 100A Bosch alternator. The maximum electric power output with the Prestolite alternator was achieved with the electric load of 11 of 20W-rated DC bulbs connected in parallel but was only 249.9W (13.36V,18.71A) which is about 95 W smaller than that achieved with the 100A Bosch Alternator. Figure 5.10 shows the variations of the DC currents and voltages under 6 different loads and Figure 5.11 shows the electric power output of this micro-CHP system with the Prestolite Alternator. The differences in electrical generation performance and weight between the two alternators are most likely to be responsible for the observed difference in power output. The Prestolite Alternator is more than two times heavier than the 140A Bosh Alternator. The Prestolite Alternator has the potential to generate greater power than the 140A Bosch Alternator if both have high RPM (e.g. 5000 RPM) as shown by their respective performance curves (Figure 4.24 And Figure 4.25). Unfortunately both alternators were running at a speed much lower than 5000 RPM. Heavy weight of the Prestolite Alternator led to a lower RMP than the 100A Bosch Alternator and hence the lower power output.

Some power generation/CHP tests had also been carried out with the 100A Bosch Alternator (Figure 4.22), especially during the early months of 2009. The 100A Bosch Alternator is very similar to the 100A Bosch Alternator (Figure 4.22), except its current rating. However, under otherwise identical conditions, the 140A Bosch Alternator always led to higher power output than the 100A Bosch Alternator. Therefore, it can be concluded that the 100A Bosch Alternator was the best Alternator which led to the highest power output under the experimental conditions of the micro-CHP system driven by the 25 kW biomass boiler.

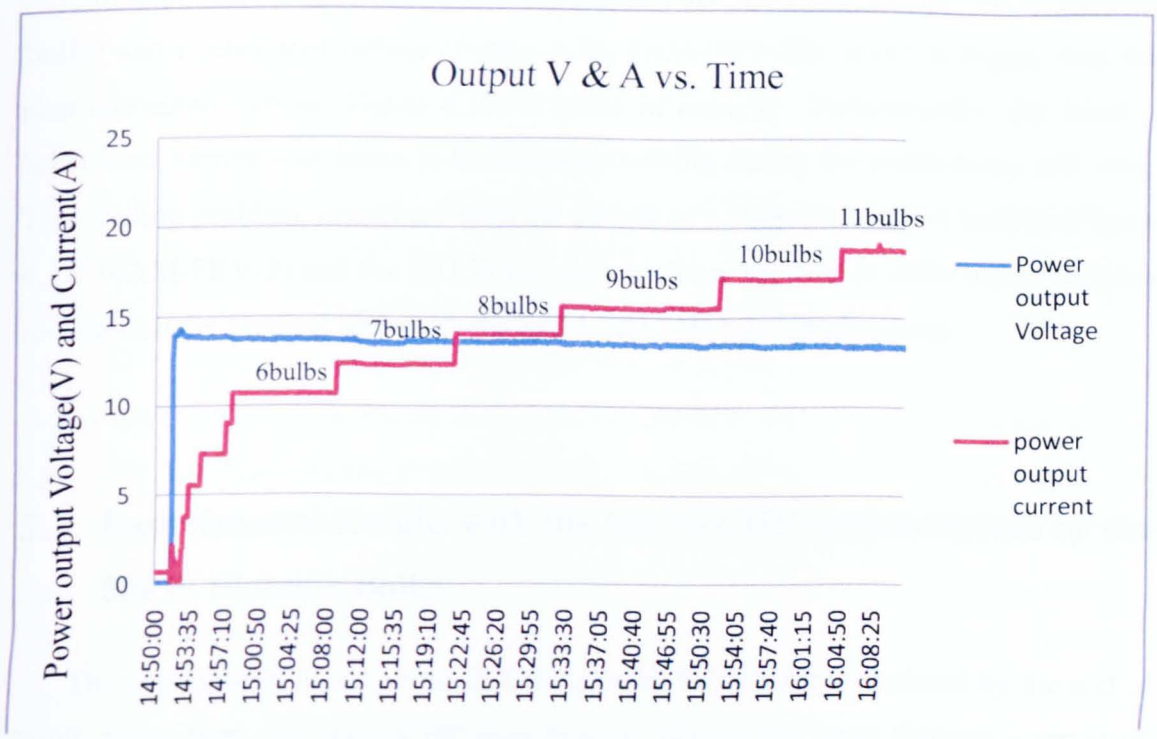

Figure 5.10 Current and voltage with different electric loads (Prestolite Alternator, 20W-rated DC bulbs, 14/09/2009)

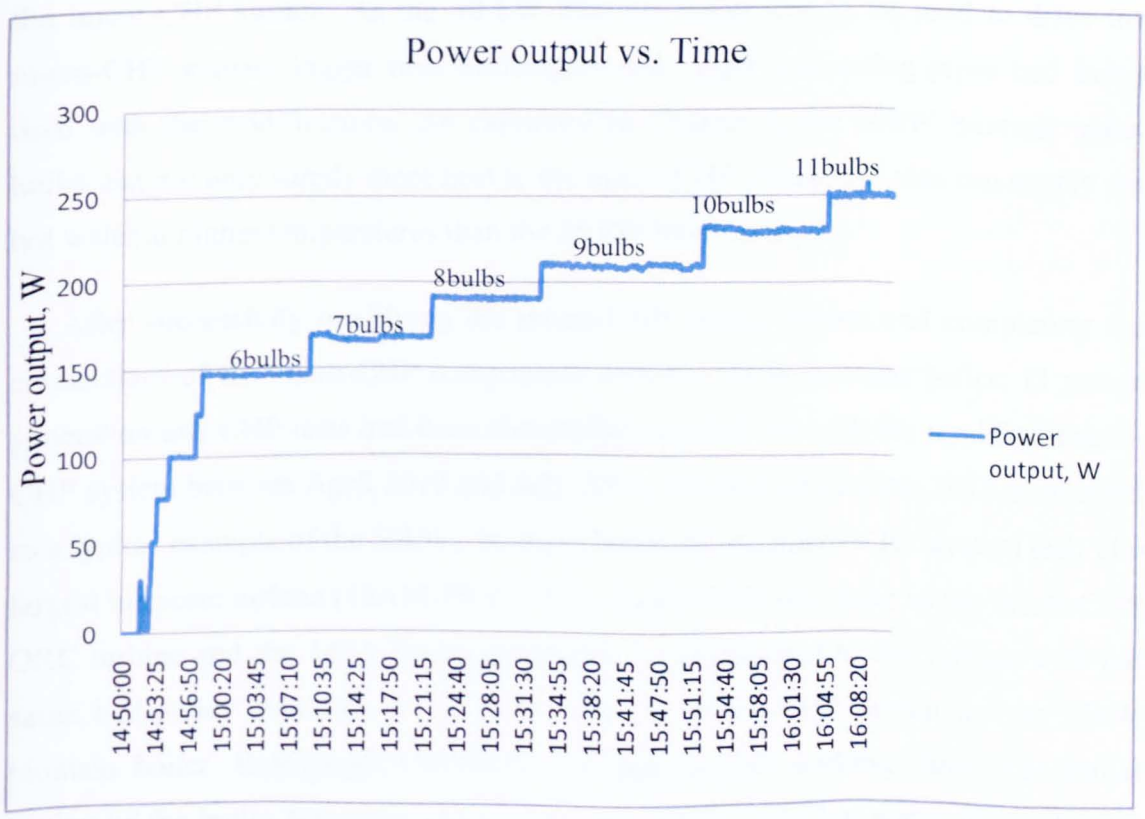

Figure 5.11 Power output under different electric loads (Prestolite Alternator, 20W-rated DC bulbs, 14/09/2009)

Attempts had been made to test the micro-CHP system with the 25kW biomass boiler and a lubricated turbine (Figure 4.18, 8AM-FRV-2B) which is bigger than the non-lubricated turbine (Figure 4.17) in terms of capacity. Unfortunately, the 8AM... lubricated turbine was found to be seriously leaking during the preliminary trial runs. The leaking problem, combined with the arrival of a bigger lubricated turbine (Figure 4.18 16AM-FRV-2) and the 50 kW biomass boiler at the end of 2009 led to decision to abandon the planned tests with the 8AM-FRV-2B lubricated turbine.

5.3. Experimental Results with the Micro-CHP System Driven by the 50kW Biomass Boiler

The experiments based on the 25kW biomass boiler were completed by the end of 2009. Since then, the micro-CHP experimental system had gone through a series of modifications including the replacements of the heat exchangers used as the evaporator and the superheater and the connecting pipes between the components of the micro-CHP system. As the 50 kW biomass boiler was to be used to drive the micro-CHP system, bigger heat exchangers and bigger connecting pipes had being used with the modifications. As explained in Chapter 4, the 50kW biomass pellet boiler can not only supply more heat to the micro-CHP system but also can supply the hot water at higher temperatures than the 25 kW biomass boiler.

After successfully modifying the micro-CHP testing system and completing the connections of the micro-CHP components with the 50kW biomass boiler, 11 power generation and CHP tests had been successfully carried out with the modified micro-CHP system between April 2010 and July 2010. The test on 22 June 2010 is selected as a typical example of the 50kW$_{th}$ biomass boiler-driven micro-CHP system test. The largest lubricate turbine (16AM-FRV-2-NU, Figure 4.18) was used as the micro-CHP ORC turbine and the 140A Bosch Alternator was connected to the turbine with the same belt-pulley assembly as the tests with the micro-CHP driven by the 25kW biomass boiler. Refrigerant HFE7000 was used as the working fluid. The initial setting of the boiler hot water temperature was 130^{0}C. The hot water flow rate was measured to be around 27.5 l/m and the cooling water for the condenser was the tap water with a temperature of about 16 ^{0}C and a flow rate of 19.0 l/m.

5.3.1. Non-power generation test

The test procedures for the 50 kW biomass boiler-driven micro-CHP system are the same as those adopted for the 25kW biomass boiler-driven micro-CHP system. Before the alternator was excited, a non-power generation test was conducted to examine the system performance, in particular, the variations of the main parameters such as the RPM of the turbine, the pressure at the turbine inlet, the pressure drop over the turbine and the refrigerant flow rate at various HFE pump loads. As the 50kW biomass boiler produces more heat energy than the 25kW biomass boiler, the HFE pumping load can reach 100% without causing the appearance of the HFE7000 moisture at the turbine inlet. The HFE pump load was set at 60%, 70%, 80%, 90% 95% and 100% in this particular test. The comparisons of the parameter variations with and without power generation (i.e. alternator excitation) at the same HFE pump load were made. Each pumping load was again operating for over 10 minutes to make sure the system become quasi-steady.

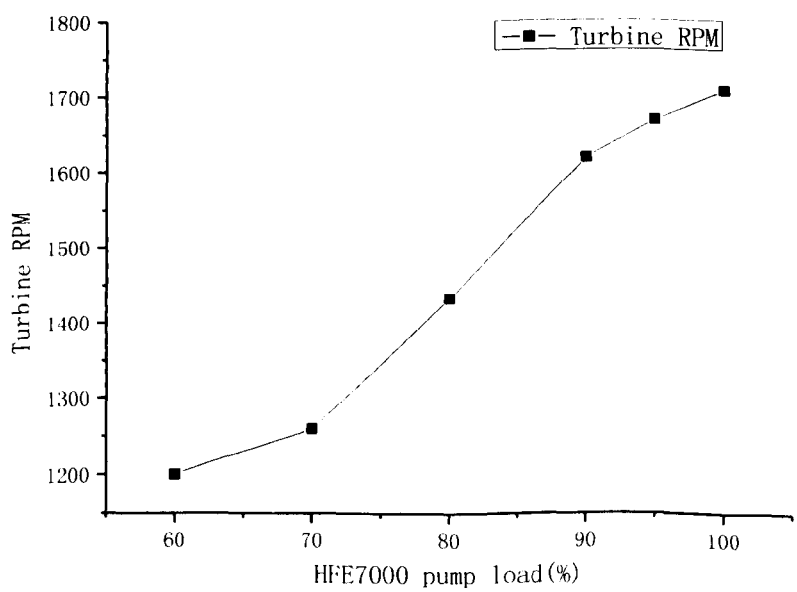

Figure 5.12 HFE7000 pumping load (%) vs. Turbine RPM

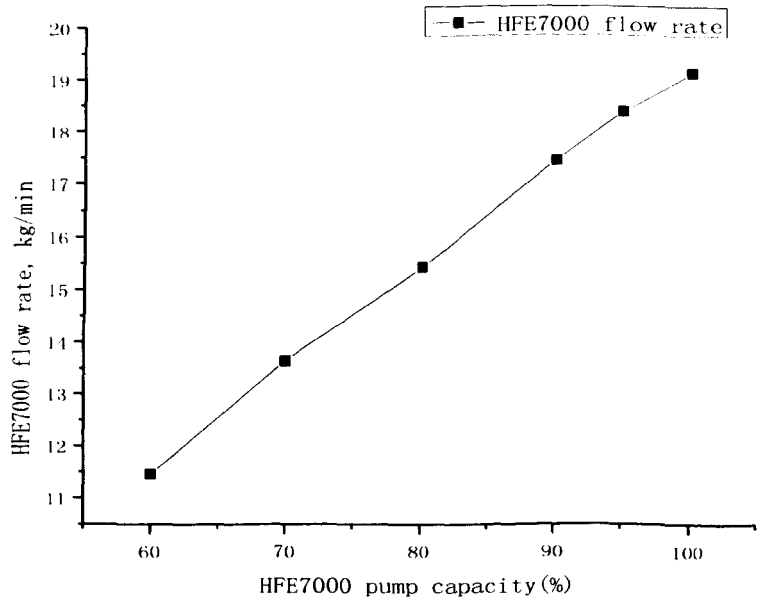

Figure 5.13 HFE7000 pumping load (%) vs. HFE7000 Flow rate, kg/min

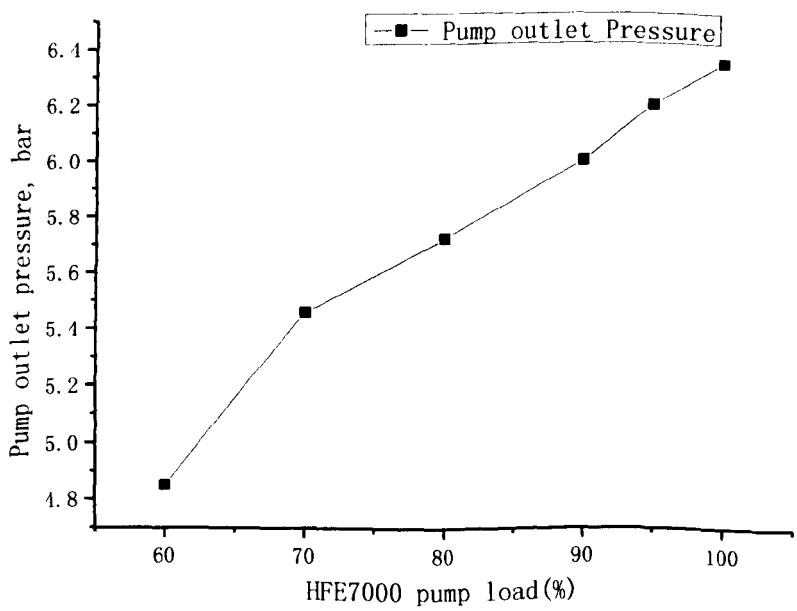

Figure 5.14 HFE7000 pumping load (%) vs. Pump outlet HFE7000 pressure (bar)

Figure 5.12-Figure 5.14 show that the alternator RPM, HFE7000 flow rate and turbine inlet pressure increase with the HFE pump load.

Table 5.3 Typical variations of main parameters with HFE pump load (50kW biomass boiler without power generation)

HFE pump load %	60	70	80	90	95	100
Turbine RPM	1200	1228	1433	1655	1670	1710
Alternator RPM	2400	2456	2866	3310	3340	3420
HFE7000 flow rate $\dot{m}$ (kg/min)	11.46	13.65	15.47	17.5	18.44	19.2
Boiler inlet water T (^{0}C)	90.1	99.8	101.2	100.3	98.7	96.6
Boiler outlet water T (^{0}C)	113.1	123.5	127.8	128.8	128.1	126.6
Turbine inlet HFE7000 T (^{0}C)	112.7	121.6	125.6	126.3	125.3	123.2
Turbine outlet HFE7000 T (^{0}C)	105.4	116.7	121.9	123.3	122.6	120.6
evaporator inlet HFE7000 T(^{0}C)	72.1	78.6	80.3	80.6	81.4	81.4
superheater outlet HFE7000 T(^{0}C)	114.2	122.7	127.1	127.8	127	125.3
Condenser inlet water T (^{0}C)	10.9	11.2	11.3	10.4	10.5	10.6
Condenser outlet water T (^{0}C)	40.3	44.5	47.6	47.1	48	48.6
Turbine inlet HFE7000 P_{t_in} (bars)	3.78	4.15	4.18	4.19	4.43	4.42
Turbine outlet HFE7000 P_{t_out} (bars)	3.33	3.54	3.46	3.31	3.37	3.47
Turbine pressure ratio, P_{t_in}/P_{t_out}	1.16	1.17	1.22	1.26	1.27	1.28

The other parameters such as the temperatures, pressures and the flow rate of the organic working are changing with the HFE pump load, as shown in Table 5.3. The actual maximum boiler outlet water temperature was a few degrees below the setting point at 130^{0}C. The temperatures and pressures of the HFE7000 loop were seen to mostly increase with the increasing of the HFE pumping load. The turbine pressure

ratio was also having a visible increase with the HFE pump load. However, the cooling water temperature remained as the cooling water temperature increased.

5.3.2. CHP/power generation test

The procedures for the power generation/CHP test of the 50kW biomass boiler-driven micro-CHP were almost the same as those of the 25kW biomass boiler-driven micro-CHP system. With the continuous operations of the biomass boiler and the HFE pump, the alternator was excited following the steps described in Chapter 4. The alternator RPM was seen to decrease and stabilize at a lower RPM. The CHP system generated DC current from the mechanical energy of the turbine via the alternator. When loads were connected, the power outputs were measured.

Each CHP test with the 50kW biomass boiler also takes several hours to complete, usually with the biomass boiler continuously operating with a hot water temperature set point of 130 ^{0}C and the organic working fluid pump operating with different loads. Figure 5.15 and Figure 5.16 show the variations of main temperatures and pressures of the micro-CHP system in the selected time period on the testing day of 22 June 2010. Comparing Figures 5.15 – 5.16 with Figures 5.6 – 5.7, it can be seen that the variations of temperatures and pressures for the 50kW biomass boiler-driven system are much smaller than those for the 25kW biomass boiler-driven system. This is mainly due to the notable difference in the way of combustion/operation between the two biomass boilers. With the modified micro-CHP system, all of the heat supplied by the hot water of the 50kW biomass boiler was absorbed by the HFE7000 loop of the micro-CHP system during the power generation/CHP test. Therefore, during this test, period, the boiler kept on burning wood pellet fuel at the 100% of its design load consistently, The hot water temperature of the boiler was always slightly below the set temperature point at about 128^{0}C. Therefore, there was no 'idle' combustion period for the 50kW biomass boiler which was observed with the 25kW biomass boiler during its power generation/CHP tests. Because of this, there were no 'shoulders' of variations in Figures 5.15 – 5.16, which were common features of variations observed with the 25kW biomass boiler-driven micro-CHP system as shown in Figure 5.6 and Figure 5.7.

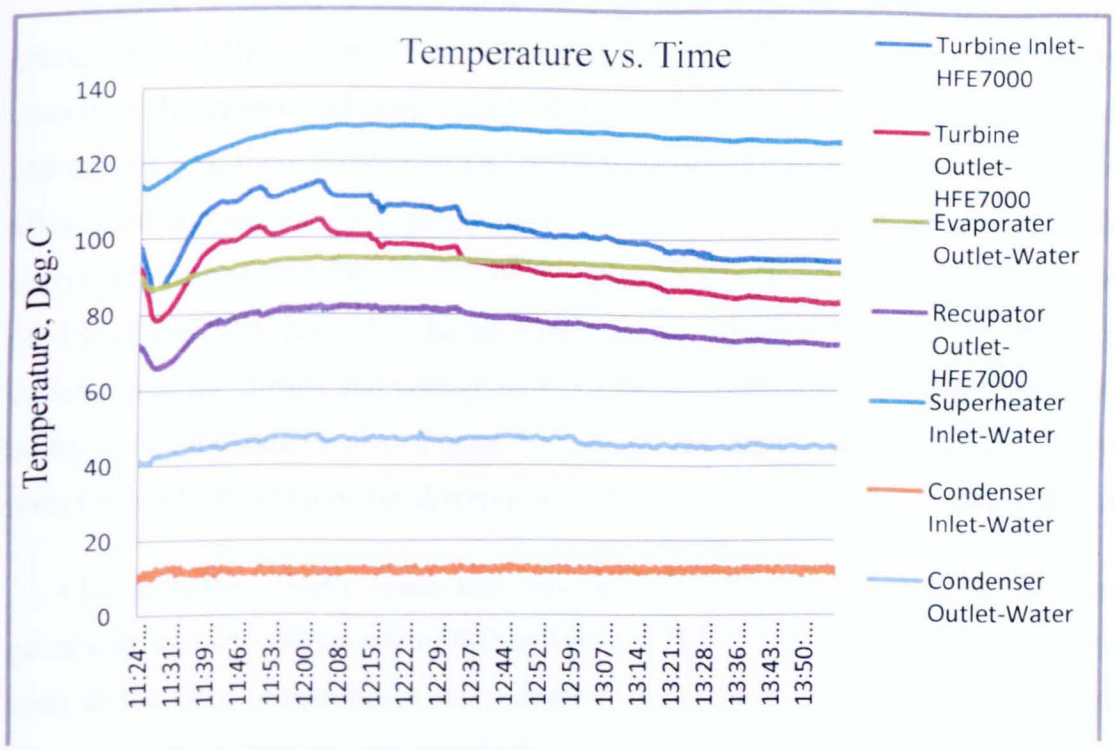

Figure 5.15 Variations of the main temperatures of the 50kW biomass boiler-driven micro-CHP system (22/06/2010)

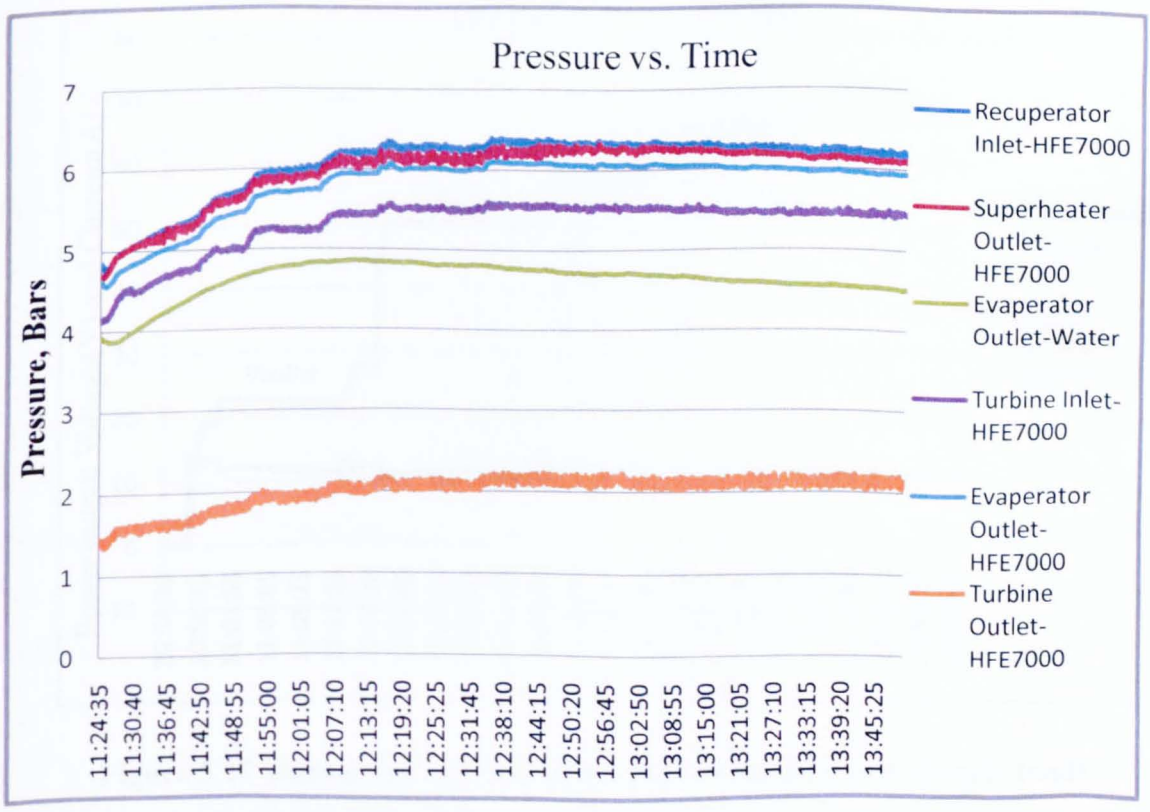

Figure 5.16 Variations of the main pressures of the 50kW biomass boiler-driven micro-CHP system (22/06/2010)

As more electricity is expected to be generated from the 50kW biomass boiler-driven micro-CHP system, 20 of 50W-rated DC bulbs had been wired into the load circuit of the system and connected to the output of the alternator as electric loads. During the test, these 50W-rated DC bulbs were added into the circuit carefully one after another with the HFE pump load set at 95%. The maximum electric power output of this test, 748.6W (11.0V, 68.07A) had been achieved with the electric load of 18 of the 50W-rated DC bulbs connected in parallel. Figure 5.17 shows the variations of the current and voltage with 5 different electric loads (from 9 50W-rated bulbs to 18 50W-rated bulbs). Figure 5.18 shows the electric power outputs achieved with the 50kW biomass boiler-driven micro-CHP system with different electric loads.

Changing the eclectic loads not only leads to different amounts of electricity generated, but also affects other ORC and micro-CHP system performance parameters such as the ORC temperatures and pressures, as shown in Table 5.4 which includes the operating conditions corresponding to the maximum power output (748.6W, 18bulbs).

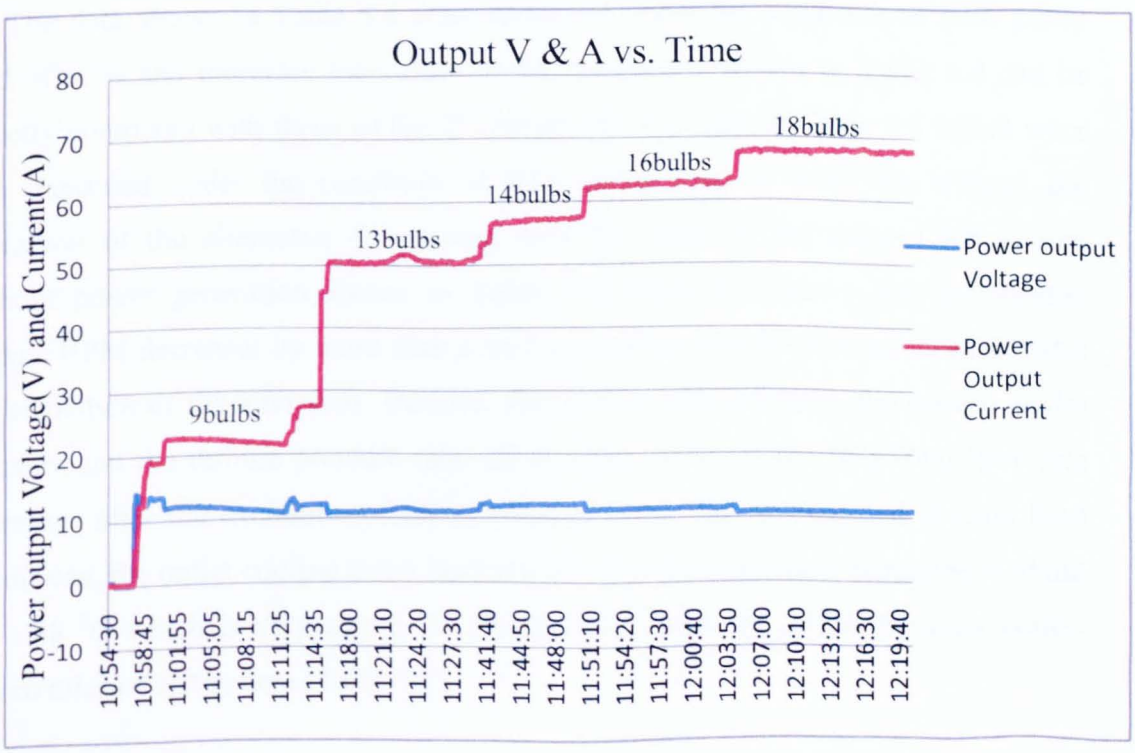

Figure 5.17 Output DC current and voltage with different electric loads (140A Bosch Alternator, 50W-rated DC bulbs, 22/06/2010)

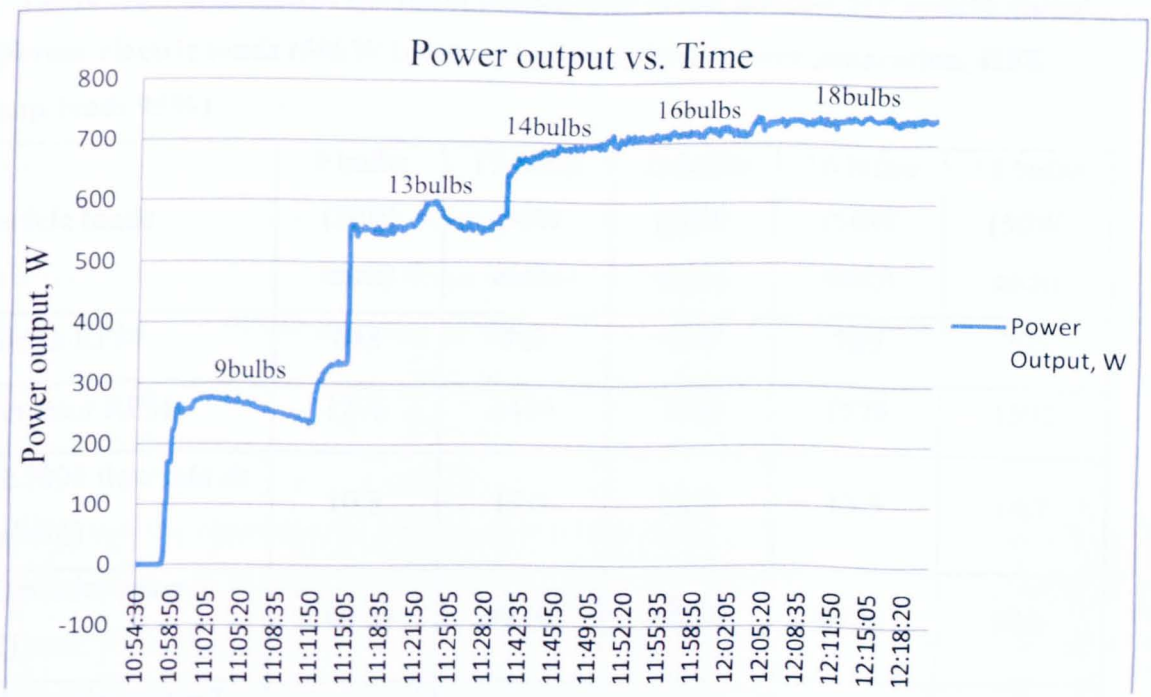

Figure 5.18 Power output with different electric loads (140A Bosch Alternator, 50W-rated DC bulbs, 22/06/2010)

The data shown in Table 5.4 were measured under the condition of HFE pump load of 95% and therefore the values of the parameters shown in Table 5.4 can be directly compared with those of the 2nd column on the right of Table 5.3 which were also measured under the condition of HFE pump load of 95% but without the excitation of the alternator. Comparing with the cases of the micro-CHP system without power generation shown in Table 5.3, Table 5.4 shows that the excited turbine RPM decreases by more than a half, compared with the turbine RPM without the excitation of the alternator. Besides, the turbine inlet pressure, the turbine outlet pressure and the turbine pressure ratio all increase, whereas the HFE7000 flow rate decreases after the excitation of the alternator. Under the investigated electric load conditions, the outlet cooling water temperature after the condenser remained at about 46 – 48 ^{0}C which is very similar to that achieved with the 25kW biomass boiler-driven micro-CHP system (Table 5.2).

Table 5.4 Variations of the main parameters of the micro-CHP system under different electric loads (50kW biomass boiler without power generation, HFE pump load: 95%)

Electric loads	9 bulbs (50W each)	13 bulbs (50W each)	14 bulbs (50W each)	16 bulbs (50W each)	18 bulbs (50W each)
Turbine RPM	648	707	778	789	796
Alternator RPM	1296	1414	1556	1578	1592
HFE7000 flow rate $\dot{m}$ (kg/min)	10.8	12.3	12.8	13.5	14.7
Boiler inlet water T (^{0}C)	100.34	99.01	93.34	94.51	94.6
Boiler outlet water T (^{0}C)	131.05	130.44	127.01	128.9	129.68
Turbine inlet HFE7000 T (^{0}C)	124.33	121.47	112.5	113.8	108.54
Turbine outlet HFE7000 T (^{0}C)	116.42	113.77	102.41	103.6	98.37
evaporator inlet HFE7000 T(^{0}C)	81.396	81.46	45.64	81.41	81.69
superheater outlet HFE7000 T(^{0}C)	126.35	123.35	113.44	115.03	108.47
Condenser inlet water T (^{0}C)	11.129	10.15	12.61	12.5	11.83
Condenser outlet water T (^{0}C)	47.59	46.4	46.15	47.02	46.96
Turbine inlet HFE7000 P_{t_in} (bar)	4.97	4.57	4.98	5.25	5.53
Turbine outlet HFE7000 P_{t_out} (bar)	2.59	1.65	1.82	1.92	2.03
Turbine pressure ratio, P_{t_in}/P_{t_out}	1.66	2.09	2.11	2.13	2.15

For comparison purpose, the Prestolite alternator (14Volts, 200Amps) was connected into the 50kW biomass boiler-driven micro-CHP system to replace the original Bosch alternator (14Volts, 140Amps) and tested on 23 June 2010. The same lubricated turbine (16AM-FRV-2-NU, Figure 4.18) and the same pulley-belt assembly connecting the turbine and the alternator were used on 23 June 2010. Other operating conditions such as the set point of the biomass boiler hot water temperature and the HFE pump load remained the same as those of the power generation/CHP test on 22 June 2010. The same 50W-rated DC bulbs were also used as the electric loads for the Prestolite alternator.

Although the experimental conditions were the same as those of the 140A Bosch Alternator test on 22 June 2012 and the micro-CHP system with the Prestolite Alternator could operate with as many as 19 of 50W-rated bulbs, the electric power output was found to be somewhat lower than that of the micro-CHP system with the 140A Bosch Alternator. The maximum electric power output for the Prestolite Alternator-based system was around 700W, first achieved with the electric loads of 14 of 50W-rated DC bulbs. After that, more 50W-rated bulbs were added, the micro-CHP system was still working properly, although the value of current kept on increasing with electric loads and the value of voltage was decreasing steadily. As a result, there was no obvious increase in electric power output when the electric loads were increased from 14bulbs to 19 bulbs, as shown by Figures 5.19 – 5.20. The peak value of electric power output was found to be 707.8W (11.79V, 60,01A) achievedwith 14 bulbs.

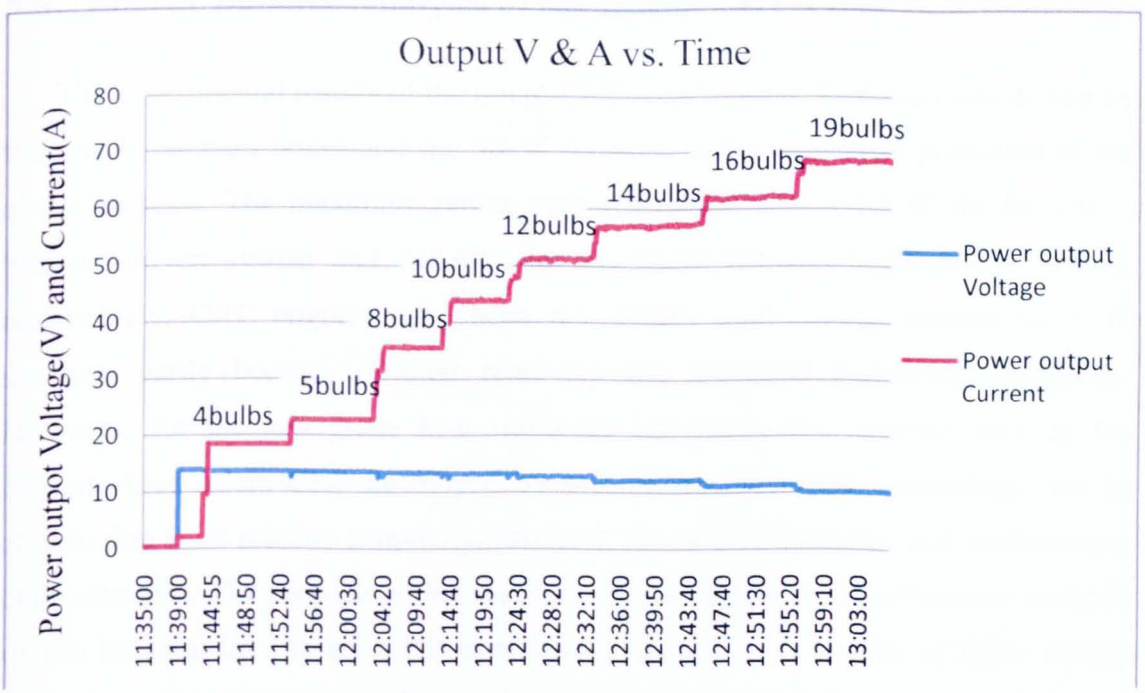

Figure 5.19 DC current and voltage under different electric loads (Prestolite Alternator, 50W-rated DC bulbs, 23/06/2010)

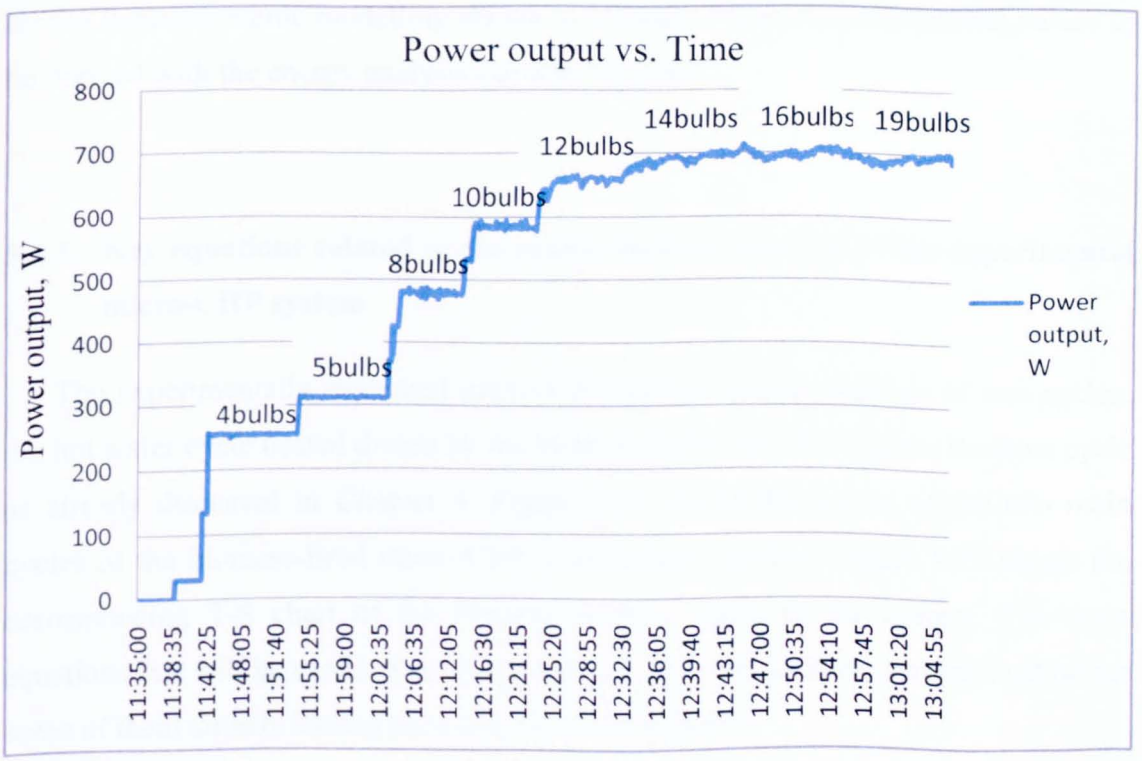

Figure 5.20 Power output under different electric loads (Prestolite Alternator, 50W-rated DC bulbs, 23/06/2010)

5.4. Energy Balance Analysis of the Micro-CHP Tests

The experimental results of the micro-CHP with Organic Rankine cycle driven by the 25kW biomass boiler and the 50kW biomass boiler have been presented in the above sections. The maximum power output achieved was 344.5 W for the 25kW biomass-driven system and 748.6W for the 50kW biomass boiler-driven system, respectively. ORC engines have been not widely used among commercial CHP systems, partly because of their relatively low electrical conversion efficiency. However, for the low grade heat resources and micro-size systems such as the biomass-fired micro-CHP developed by this project, the ORC technology has be chosen due to its relative simplicity, low cost, favourable durability and performance characteristics. The purpose of this section is to carry out the energy balance analyses of the biomass-fired micro-CHP experimental system. The results of these energy balance analyses can not only quantify the energy performance of the evaluated experimental system but also reveal which components of the system should be improved in the future. Direct comparisons of the efficiencies between those predicted by the thermodynamic modelling shown in Chapter 4 and the experimental values to be derived with the energy analysis can also be made.

5.4.1. Key equations related to the energy balance analysis of the experimental micro-CHP system

The experimentally evaluated micro-CHP system mainly consists of two cycles: the hot water cycle heated driven by the biomass boiler and the organic Rankine cycle as already discussed in Chapter 4. Figure 5.21 shows the layout of the two main cycles of the biomass-fired micro-CHP experimental system. Figure 5.22 shows the corresponding T-S chart of the Organic Rankine cycle of the system. The main equations that will be used in the energy balance analyses are to be summarized below, some of them already having been discussed in Chapter 3.

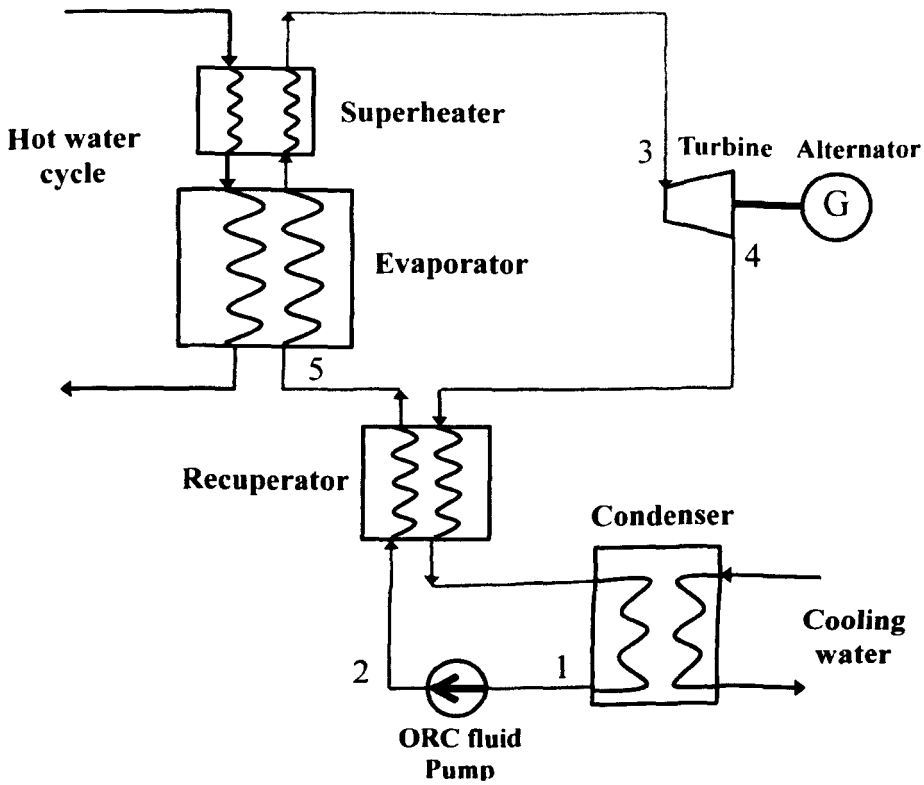

Figure 5.21 Layout of the two cycles of the experimental biomass-fired micro-CHP system

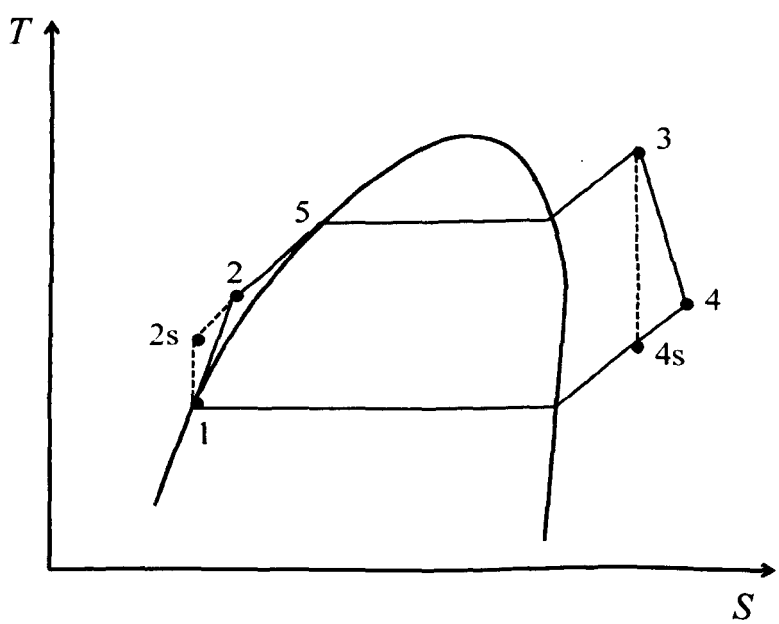

Figure 5.22 T-S chart of the organic Rankine cycle of the experimental biomass-fired micro-CHP system

As shown in Figure 5.21, the organic Rankine cycle is a closed loop cycle, mass conservation of working fluid and the first law of thermodynamics can be applied to the ORC analyses. The ideal work output of the turbine $(W_{turb,ID})$ (process 3-4s) can be expressed as

$$W_{turb,ID} = \dot{m} \cdot (h_3 - h_{4s}) \tag{5.1}$$

As the process in the turbine is not an isentropic expansion process, the actual work output of the turbine (W_{turb}) (process 3-4) is

$$W_{turb} = \dot{m} \cdot (h_3 - h_4) \tag{5.2}$$

Where $\dot{m}$ is the working fluid mass flow rate (kg/s) measured by the HFE flow meter. There are pressure transducers and thermocouples before the inlet and after the outlet of turbine to measure the pressures and temperatures in the experimental micro-CHP system. Therefore, with the known pressures (P_3, P_4) and temperatures (T_3, T_4), the thermodynamic properties of state point 3 and point 4, in particular the enthalpy of point 3 (h_3) and point 4 (h_4) can be solved out by use of the Thermodynamics Engineering Equation Solver (EES)(F-Chart Software). The actual work output of the turbine (W_{turb}) can then be calculated by use of Equation (5.2). Besides, as shown in the T-S chart (Figure 5.22), process 3-4s is an isentropic expansion process; the entropy value of point 4s should be equal to point 3, which has been solved within the step to calculate the actual turbine work output(W_{turb}). Noting the pressure of state point 4s is the same as that of state point 4 as they are on the same isobaric line of Figure 5.22. With the known values of pressure and entropy, the enthalpy value (h_{4s}) of the state point 4s can be found via the EES(F-Chart Software). The ideal work output of the turbine $(W_{turb,ID})$ can then be calculated by use of Equation (5.1).

The isentropic efficiency of the turbine (η_{turb}) can then be calculated as the ratio between the actual work output of the turbine (W_{turb}) and the ideal work output of the turbine $(W_{turb,ID})$, i.e. Equation (5.3).

$$\eta_{turb} = \frac{W_{turb}}{W_{turb,ID}} = \frac{h_3 - h_4}{h_3 - h_{4s}} \tag{5.3}$$

The generator (i.e. alternator) efficiency (η_{alt}) can be expressed as the measured power output (W_{el}) divided by the actual work output from the turbine(W_{turb}).

$$\eta_{alt} = \frac{w_{el}}{w_{turb}} = \frac{w_{el}}{\dot{m}\cdot(h_3-h_4)} \tag{5.4}$$

Similarly, the ideal work input by the HFE pump $(W_{pump,ID})$ (Figure 5.22) can be expressed as

$$W_{pump,ID} = \dot{m}\cdot(h_{2s} - h_1) \tag{5.5}$$

Again, the process of the HFE pumping process cannot be an isentropic compression process, the actual work input by the HFE pump (W_{pump}) (process 1-2 of Figure 5.22) is

$$W_{pump,} = \dot{m}\cdot(h_2 - h_1) \tag{5.6}$$

The pressure at point 1 equals to the pressure of point 4 as the fluid saturated pressure, whereas the temperature and pressure at point 2 are measured at the outlet of the superheater. Therefore the enthalpy of point 1 (h_1) and point 2 (h_2) can be obtained by use of EES(F-Chart Software).

The net work of the ORC (W_{net}) is the difference between the actual work output of the turbine (W_{turb}) and the actual pump work input(W_{pump}):

$$W_{net} = W_{turb} - W_{pump} = \dot{m}\cdot[(h_3 - h_4) - (h_2 - h_1)] \tag{5.7}$$

The heat transfer supplied by the biomass boiler via the evaporator and the superheater is

$$Q_{in} = \dot{m}\cdot(h_4 - h_5) \tag{5.8}$$

The thermal efficiency of the ORC can be expressed as the net work output of the ORC divided by the heat input into the ORC as below.

$$\eta_{ORC} = \frac{W_{net}}{Q_{in}} \tag{5.9}$$

For the hot water loop, the biomass boiler efficiency can be defined as the ratio between the heat released by the hot water through the evaporator and the thermal input to the boiler.

$$\eta_{boiler} = \frac{Q_{water}}{Q_{burn}} = \frac{\dot{m}_{water}\,(h_{sph\_in} - h_{evap\_out})}{Q_{burn}} \tag{5.10}$$

Where ($\dot{m}_{water}$) the measured hot water is flow rate (h_{sph_in}) and (h_{evap_out}) are the hot water enthalpies at the inlet of the superheater and outlet of the evaporator, respectively. The thermal input to the biomass boiler (Q_{burn}) can be calculated from the wood pellet consumption rate of the biomass boiler, ($\dot{M}_{burn}$) and the calorific value (CV) of the biomass fuel:

$$Q_{burn} = \dot{M}_{burn} * \text{CV} \tag{5.11}$$

As the boiler efficiency is to be evaluated on low heating value (LHV), the CV in the above equation is replaced with LHV.

For the cooling water cycle, the heat absorbed by the cooling water in the condenser (Q_{cond_w}) is

$$Q_{cooling\_w} = \dot{m}_{cooling\_w}(h_{cond\_out} - h_{cond\_in}) \tag{5.12}$$

where ($\dot{m}_{cooling\_w}$) is the cooling water flow rate; h_{cond_out} and h_{cond_in} are cooling water enthalpies at the outlet and inlet of the condenser, respectively.

Therefore, the electrical efficiency(η_{el}), thermal efficiency (η_{th}) and total CHP efficiency (η_{CHP}) can be assessed as

$$\eta_{el} = \frac{W_{el}}{Q_{burn}} \tag{5.13}$$

$$\eta_{th} = \frac{Q_{cooling\_w}}{Q_{burn}} \tag{5.14}$$

$$\eta_{CHP} = \eta_{el} + \eta_{th} = \frac{W_{el} + Q_{cooling\_w}}{Q_{burn}} \tag{5.15}$$

The electrical efficiency (η_{el}) and the total CHP efficiency (η_{CHP}) are the most important parameters of the biomass-fired micro-CHP system developed and evaluated with the present research project.

5.4.2. Results of energy balance analyses and discussion

According to the various equations shown in above subsection, the efficiencies of the biomass-fired micro-CHP with ORC experimental system have been be calculated and presented in the tables below.

Table 5.5 Results of energy balance analysis of the power generation/CHP test (25kW biomass boiler-driven micro-CHP system, 14 Sept 2009)

Electric Loads	11bulb (20W each)	12bulb (20W each)	13bulb (20W each)	14bulb (20W each)	15bulb (20W each)
Turbine RPM	1940	1720	1629	1588	1593
Alternator RPM	3880	3440	3258	3176	3186
Power output(W)	259.55	278.76	287.56	317.28	344.55
Turbine efficiency (%)	49.51	48.59	51.37	52.68	51.78
Alternator efficiency (%)	46.54	50.14	48.07	50.25	54.63
ORC efficiency (%)	2.20	2.36	2.55	2.62	2.85
Electrical efficiency (%)	0.87	0.96	0.99	1.07	1.17
Thermal efficiency (%)	80.95	80.76	79.34	80.37	85.05
CHP efficiency (%)	81.82	81.72	80.33	80.44	86.22

Table 5.5 shows the energy balance analysis of the power generation/CHP test conducted on 14 Sep. 2009 which was selected as a good example of the 25kW biomass boiler-driven micro-CHP tests. The non-lubricating turbine was applied on the micro-CHP system to drive the 140A Bosch alternator. As pointed out, the test achieved the best power output at 344.6W (13.63V, 25.28A) with the 25kW biomass boiler-driven micro-CHP sysytem.

Table 5.6 shows the results of the energy balance analysis of the pwer generation/CHP test conducted on 22 June 2010 which was selected as a good example of the 50kW biomass boiler-driven micro-CHP tests. The largest lubricating turbine (16AM-FRV-2) was applied on the system to drive the 140A Bosch alternator. The best power output result achieved with the test was 748.6W (11.0V, 68.07A). During the writing up period of this PhD thesis, the micro-CHP system has been further tested by other members of the research team and achieved the maximum power output of about 950W.

The ORC efficiency for the 25kW biomass boiler-driven micro-CHP system was found to be in the range of 2.20% – 2.85%, which is lower than that of the 50kW biomass boiler-driven micro-CHP system (3.48% – 3.89%). Although different types of micro-turbines had been used with the two micro-CHP systems, the turbine efficiency for the non-lubricated turbine which was used with the 25kW biomass-driven micro-CHP system was found to be only marginally higher than that of the lubricated micro-turbine (16AM-FRV-2) which was used with the 50kW biomass boiler-driven micro-CHP system (48.59% – 52.68% vs. 52.88% - 55.45%). The same 140A Bosch alternator was used for the both micro-CHP systems with its efficiency being in the order of 50%. The main reason for the difference in ORC efficiency between two systems is due to the maximum temperature of the hot water: the maximum hot water temperature for the 25kW biomass boiler was 120 ^{0}C whereas for the 50 kW biomass boiler it was 130 ^{0}C. The thermodynamic modelling described in Chapter 3 confirmed that the ORC efficiency increases with the maximum temperature of the ORC cycle. Therefore, the experimental values of the ORC efficiency qualitatively agree with the results of the thermodynamic modelling.

Table 5.6 Results of energy balance analysis of the power generation/CHP test (50kW biomass boiler-driven micro-CHP system, 22 June 2010)

Electric Loads	13bulb (50w each)	14bulb (50w each)	16bulb (50w each)	18bulb (50w each)
Turbine RPM	707	778	789	796
Alternator RPM	1414	1556	1578	1592
Power output(W)	656.8	686.3	715.1	748.6
Turbine efficiency (%)	53.40	52.88	52.94	55.45
Alternator efficiency (%)	50.77	50.64	50.94	49.47
ORC efficiency (%)	2.76	3.37	3.73	3.89
Electrical efficiency (%)	1.30	1.38	1.39	1.43
Thermal efficiency (%)	78.95	78.36	78.37	79.63
CHP efficiency (%)	80.25	79.74	79.78	81.06

However, experimental values of the maximum electricity generation efficiency of the two micro-CHP systems were found to be much smaller than those predicted by the thermodynamic modelling (ca. 1.45% vs. ca. 8% - 10%). Comparing the assumed parameter values shown in Chapter 3(Table 3.3) with the test results shown in Table 5.5 and Table 5.6, it can be found that there are two main factors responsible for the apparent difference in the electrical generation efficiency between the experiments and the thermodynamic modelling:

(1) The electricity generating system were not optimised

As shown in Table 3.3, the model assumed the turbine efficiency of 85%, but the experimental results show that the experimentally determined turbine efficiency was only in the order of 50%. Besides, the thermodynamic modelling also assumed that the alternator efficiency of 90% which was much higher than the experimental values of around 50% with these two micro-CHP systems. This means the combined

efficiency of the micro-turbine and the alternator which are connected by the pulley-belt assembly was only around 25%.

The lack of commercially available micro-turbines is one of the main difficulties facing the developers and researchers of ORC-based micro-CHP systems as already pointed out in Chapter 4. The micro-turbines used in this preject were modified from air motors and are nowhere near ideal. Although they had been proved to be feasible and successful during the tests, their isentropic efficiencies were found to be relatively low. On the other hand, the connection between the turbine and alternator by an assembly of pulley and belt is not ideal, as shown in Figure 4.26.

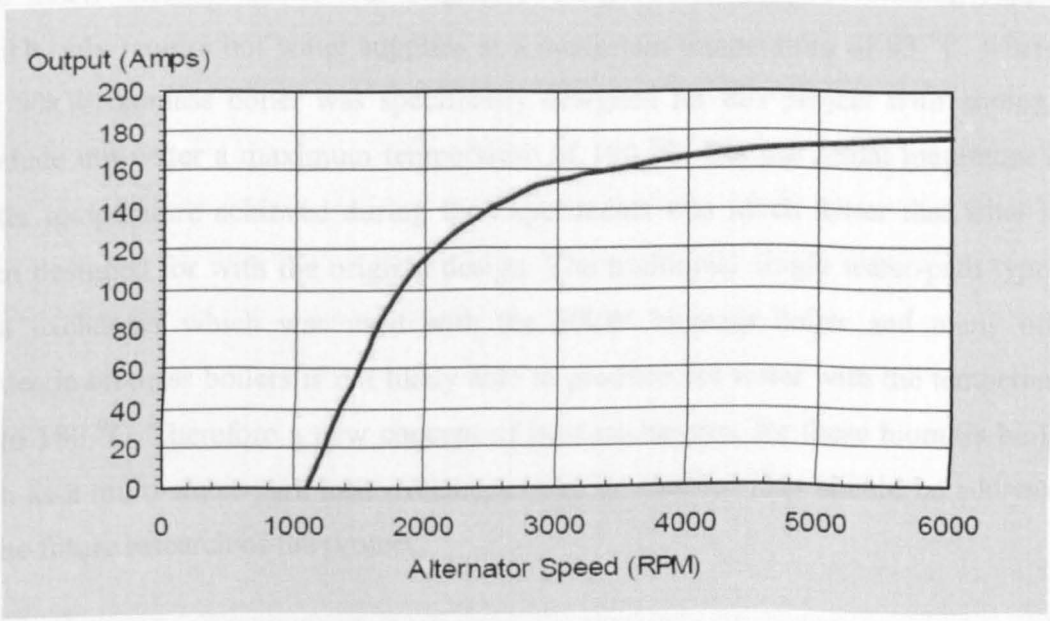

Figure 5.23 Typical performance curve of an alternator

Moreover, the alternators used in this project were those of automobiles and they were designed to run at high RPM. As shown in Figure 5.23, the alternator RPM needs to be over 4000 to be more efficient. But the RPM of the Prestolite alternator (applied on the 50kW boiler drive system) during the tests was only around 1000 - 2000 which was just above the minimum RPM for the alternator to generate any power; and the Bosch alternator (applied on the 25kW boiler drive system) during the tests was also below 4000.

(2) The evaporator temperatures of the experimental systems were low

The current designs, particularly the heat exchanger, of the biomass boilers used in the present experimental study need to be modified in order to improve the ORC efficiency and the electrical efficiency. Thermodynamic modelling of the proposed micro-CHP system in Chapter 3 has shown that the ORC efficiency and the electrical efficiency increase with the evaporator temperature. The maximum hot water temperature achieved with the 25kW biomass boiler was 120^0C and 130^0C with the 50kW biomass boiler with corresponding evaporator temperatures significantly lower than the maximum temperature (160^0C) that was used for thermodynamic modelling. The 25kW biomass boiler was originally designed for domestic heating supplies which only require hot water supplies at a maximum temperature of 95 ^{0}C, whereas the 50kW biomass boiler was specifically designed for this project with aiming to produce hot water a maximum temperature of 180 ^{0}C. But the actual maximum hot water temperature achieved during the experiments was much lower that what had been designed for with the original design. The traditional single water-path type of heat exchanger which was used with the 50kW biomass boiler and many other domestic biomass boilers is not likely able to produce hot water with the temperature up to 180 ^{0}C. Therefore a new concept of heat exchangers for these biomass boilers such as a multi-water-path heat exchanger may be needed. This should be addressed in the future research of the project.

5.5. Biomass Boiler Flue Gas Emissions

As pointed out in the previous Chapters, biomass fuel is a renewable energy and the combustion of biomass produces very little net CO_2. Besides, due to the low sulphur and low nitrogen contents of most biomass materials, substituting biomass for fossil fuels, particularly coal, can reduce SO_x and NO_x emissions. However, biomass combustion does generate pollution, in particular carbon monoxide and NOx.

This section of the chapter presents and discusses the flue gas emissions, particularly carbon monoxide and nitrogen oxides, of the two biomass boilers, which were the key component of the investigated micro-CHP system, under various operating conditions. The biomass boilers used in the present study satisfy the current EU regulation (EN 303-05) on the emissions of domestic biomass boilers. The emissions of the $25kW_{th}$ boiler had been measured not only under normal combustion conditions, but also under 'idle' combustion conditions when the boiler was not in but was ready for full operation, whereas the emissions of the 50kW biomass were only investigated under normal operating conditions.

5.5.1. Flue gas composition and emissions of the 25kW biomass boiler

Any fluctuations in fuel feeding rates or combustion air supplies can cause the composition and emissions of the flue gas to fluctuate. As shown in Figure 4.9 in Chapter 4, the wood pellets of the 25kW biomass boiler were fed into the combustion furnace by the fuel feed screw in a low rotating speed, and the air was supplied by the combustion air fan from the bottom of the boiler. The low rotating speed of the fuel feeding screw can cause some fluctuations of the flue gas composition and emissions. However, even bigger changes in flue gas compositions and emissions were observed as a result of 'stop-restart' cycle, i.e. the occurrence of the 'idle' states according to the boiler control programme, fuel feeding and air supply would be stopped when the hot water temperature of boiler meets its set point, and would restart if the water temperature is 2^0C below the set value. The heat energy released by the boiler was absorbed by the micro-scale combined heat and power (CHP) system that was connected with the boiler. Therefore, the frequencies of the boiler stop/restart cycle

occurring depended on the boiler load and the amount of heat extracted by the CHP system.

During the tests with the 25kW biomass boiler, the heat supplied by the boiler could not exactly match the heat absorbing rate of the HFE7000 loop of the micro-CHP system, and therefore the boiler operated intermittently. The test on 14 Sep. 2009 was once again selected as a typical example of the 25kW biomass boiler-driven micro-CHP tests. Figure 5.24 clearly shows that the flue gas temperature and the boiler output water temperature fluctuated in cycles of 'stop-restart'.

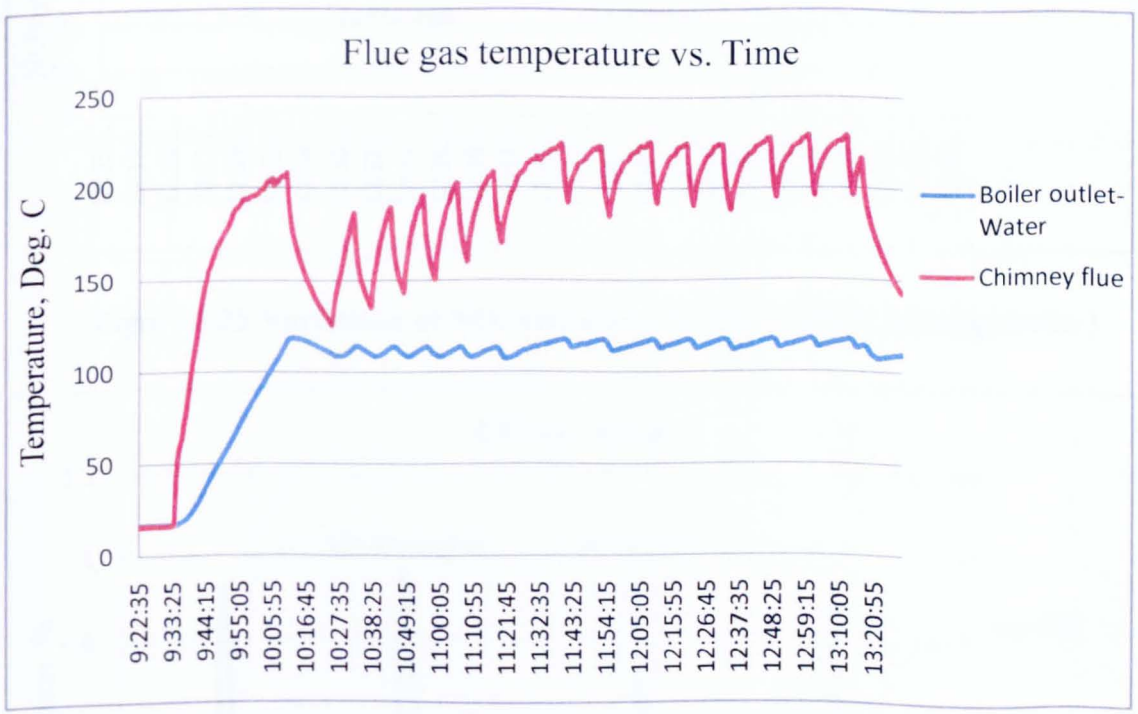

Figure 5.24 Variations of the flue gas temperature and boiler output water temperature (25kW biomass boiler)

In an ideal case, biomass combustion should represent the complete oxidation of the solid organic part of the biomass into the gases of CO_2 and H_2O. However, the actual biomass combustion process is far from ideal and involves the formation of pollutants (CO, NO_x, etc.). Figure 5.25 to Figure 5.27 show the variations of the measured NO_x and CO emissions, and CO_2 and O_2 concentrations in the flue gas. They clearly demonstrate that the flue gas emissions of the domestic 25kW wood

pellet boiler are quite different under two different combustion conditions: normal combustion and idle combustion.

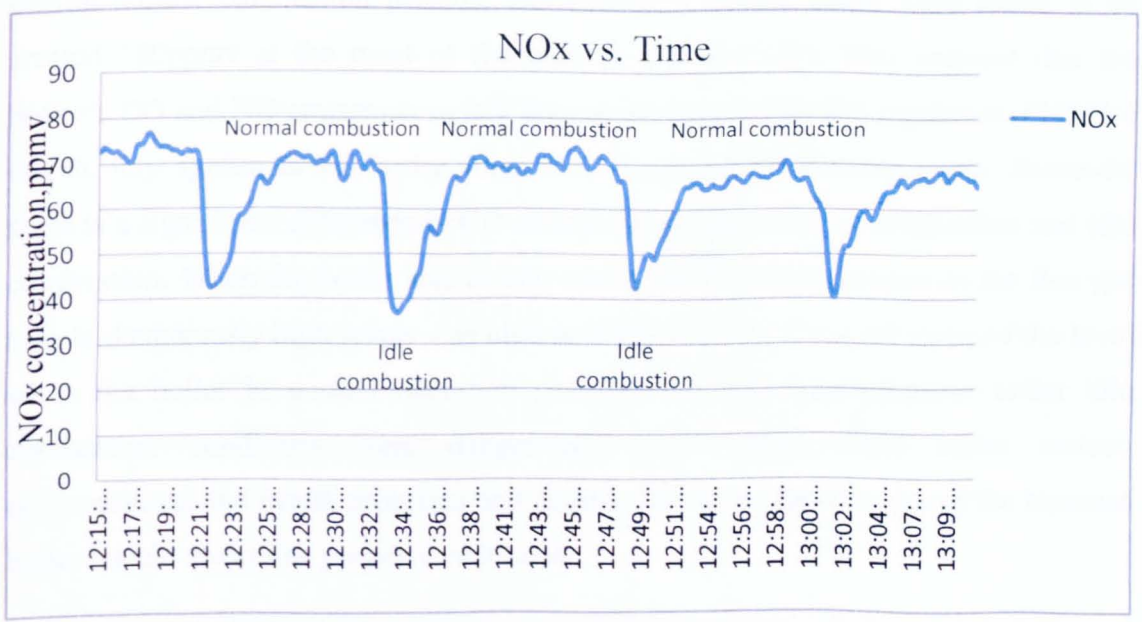

Figure 5.25 Variations of NO_x emissions vs. Time (25kW biomass boiler)

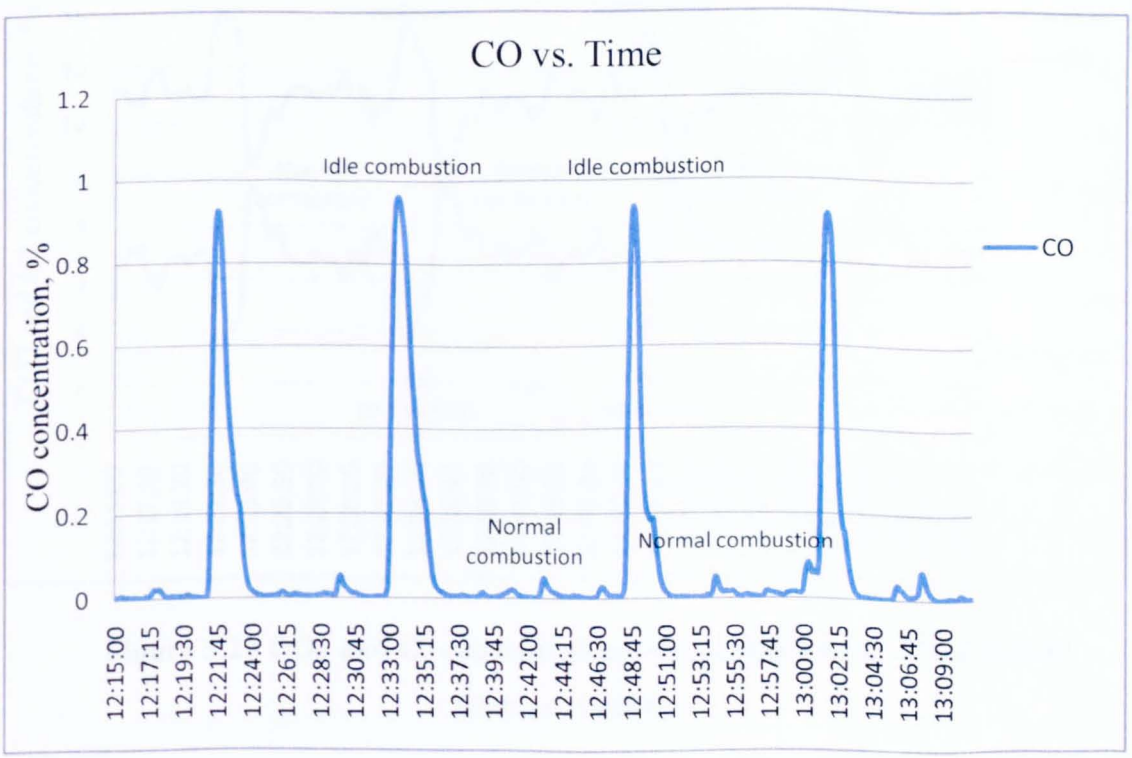

Figure 5.26 Variations of CO emissions vs. Time (25kW biomass boiler)

Figure 5.25 shows the NOx emissions of the boiler were below 80 ppmv during all the operation time, irrespective of normal combustion or idle combustion. In addition, during normal combustion periods, CO emissions of the boiler were found to be around 100ppmv at the most of the periods (Figure 5.26). This indicate that the boiler's CO and NO emissions satisfy the requirement of the EU regulation EN303-5 which only applies to the boiler when it is in normal combustion states. However, there is a significant difference in CO emissions between normal combustion and idle combustion. When the boiler was in idle states, the CO concentration in the flue gas rose to dangerously high levels – as high as 0.9% which is about 90 times of the level when the boiler in normal operation periods. The CO concentrations under idle combustion conditions were dangerously high which could cause serious environmental and health problems and deaths. Therefore, the flue gas of the biomass boiler should always be properly ventilated.

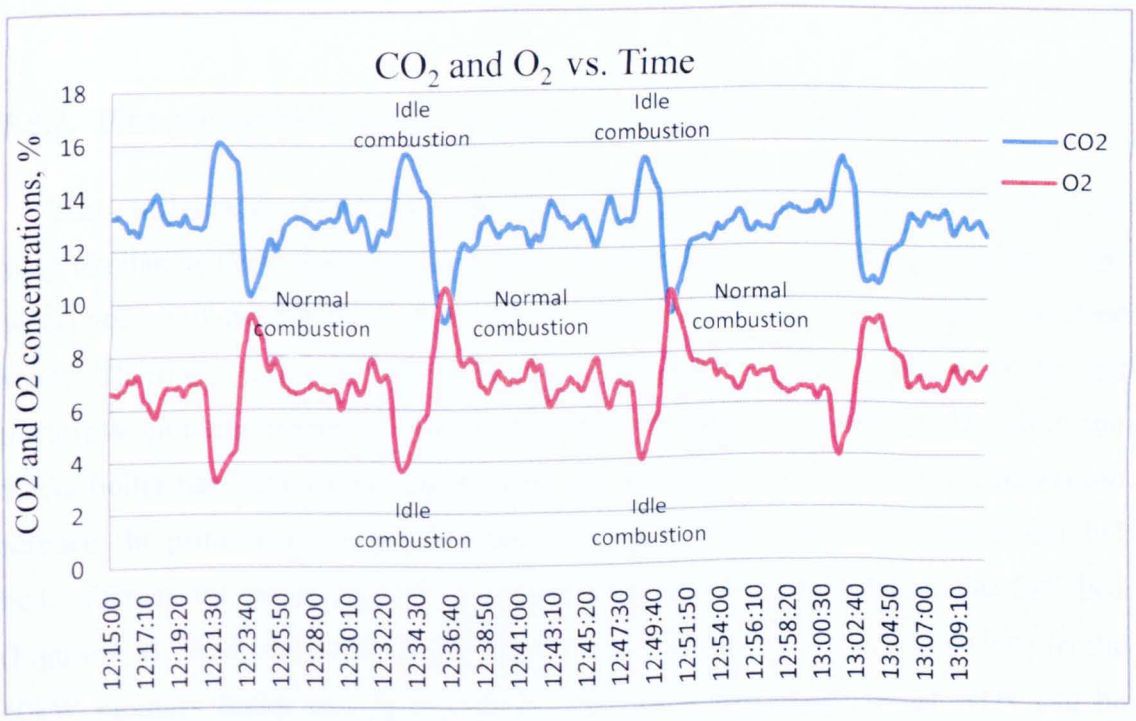

Figure 5.27 CO_2 and O_2 concentrations in the flue gas vs. Time (25kW biomass boiler)

Comparing Figure 5.25 with Figure 5.27, It can be seen that the NO_x emissions follow the similar fluctuation trend of CO_2 concentrations in the flue gas, whereas the concentration of O_2 follows the opposite fluctuation trend of CO_2. It should be noted that the NO_x emissions expressed in ppmv shown in Figure 5.25 were not corrected by the O_2 concentrations in the flue gas. Nitrogen oxides during biomass combustion are mainly due to thermal-NO_x mechanism and fuel-NO_x mechanism(Kenneth W. Ragland *et al.* 2010) and therefore the more biomass fuel is burned, the more nitrogen oxides are to be formed. The fluctuation trend of CO emissions shown in Figure 5.26 appears to follow the opposite trend of O_2 concentration in the flue gas Figure 5.27. If there was insufficient air supply, incomplete combustion and hence high CO emissions would be expected. The peaks of CO shown in Figure 5.26 corresponded to the moment when the boiler started its 'idle' period following a normal combustion period.

5.5.2. Flue gas composition and emissions of the 50kW biomass boiler

The configuration and components of the $25kW_{th}$ and $50kW_{th}$ biomass boiler are very similar as they were designed and manufactured by the same company. The wood pellets of the 50kW biomass boiler were also fed by the low speed fuel feed screw. There is a major difference, however, between the 50kW biomass boiler and the 25kW biomass in terms of the combustion air supply. The combustion air of the 50kW boiler has been split to primary air and secondary supplies to the combustion furnace; the primary air is supplied through the small holes at the bottom of the fuel bed, whereas the secondary air is supplied by the four pipes above the fuel bed (Figure 4.8). With the adopted air staging, the formation of nitrogen oxides in the 50kW biomass boiler can be controlled and hence the emissions of NOx can be reduced (Kenneth W. Ragland *et al.* 2010).

There was a similar control system to feed in fuel and control the air supply automatically to that of the 25kW biomass boiler. However, during the CHP tests of the 50kW biomass boiler, the heat supplied by the boiler was matched by the heat absorbed by the HFE loop of the micro-CHP system. As the temperature of the boiler hot water could not meet its set point, the boiler was operating constantly during the

test periods. Therefore, the 'idle' periods such as those existed for the 25kW biomass boiler during its CHP tests did not occur during the tests with the 50kW biomass boiler-driven micro-CHP system.

The test on 10 June 2010 is again selected as a typical example of the 50kW$_{th}$ biomass boiler emission tests. The flue gas temperature followed the trend of the hot water temperature as shown in Figure 5.28.

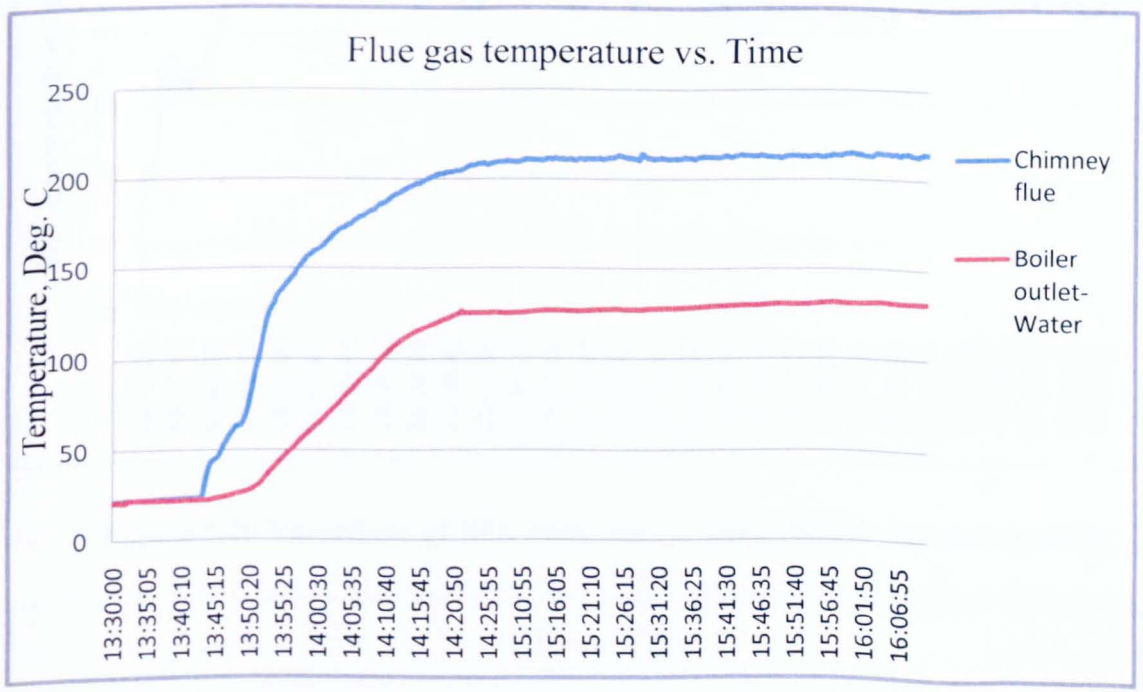

Figure 5.28 Variations of the flue gas and boiler output water temperature (50kW biomass boiler)

Comparing Figure 5.28 with Figure 5.24, the fluctuations with the flue gas temperature curve and the hot water temperature are much smaller for the 50kW biomass boiler as the biomass boiler operated under normal combustion conditions all the time – there was no idle period for this boiler.

Figure 5.29 to Figure 5.31 show the variations of the measured NO_x and CO emissions, and CO_2 and O_2 concentrations in the flue gas of the 50kW biomass boiler.

The NOx emissions of 50kW$_{th}$ boiler were found to be below 50 ppmv during the testing period as shown by Figure 5.29 and much smaller than the NOx emissions of

25kW biomass boiler which were found to be around 70 ppmv under normal combustion conditions (Figure 5.25). This confirms that air staging was proved to be effective for the control of NOx emissions (Kenneth W. Ragland *et al.* 2010).

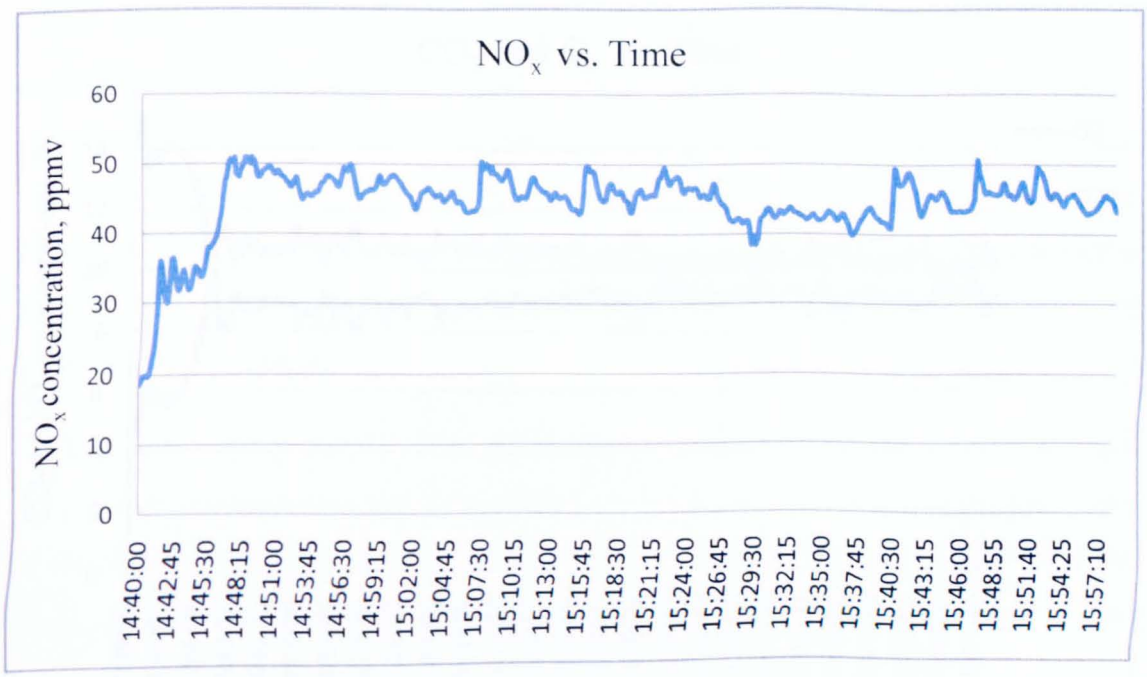

Figure 5.29 Variations of NO_x emission vs. Time (50kW biomass boiler)

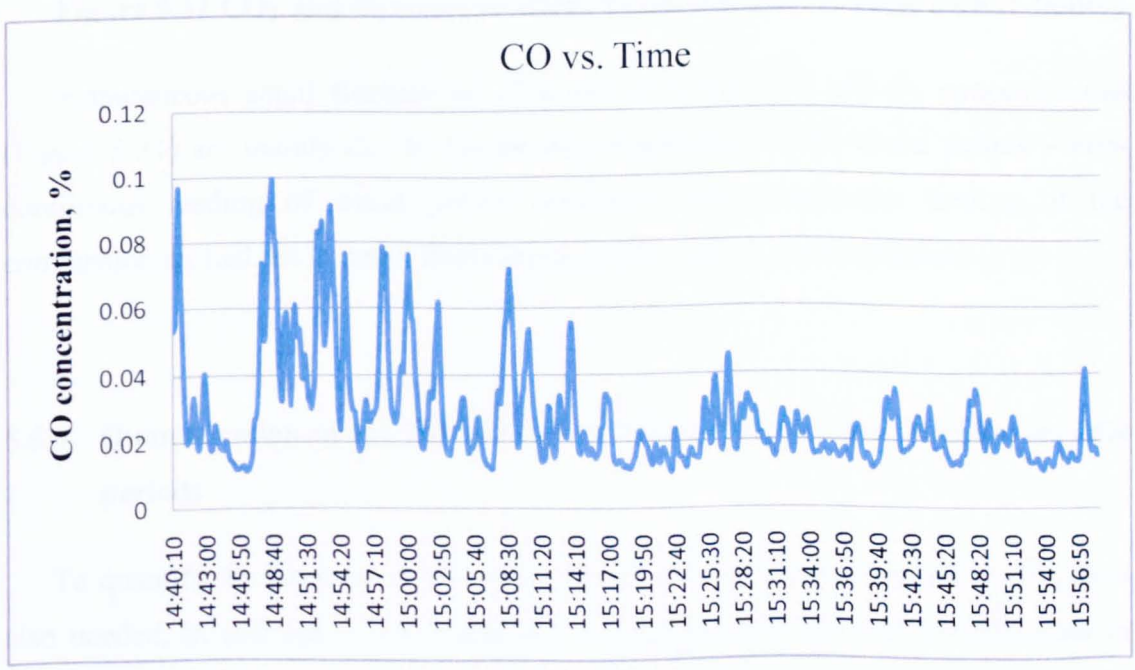

Figure 5.30 Variations of CO emission (%) vs. Time (50kW boiler)

In addition, during normal combustion periods, CO emissions of the 50kW biomass boiler were found to be around 200ppmv at the most of the operation periods (Figure 5.30).

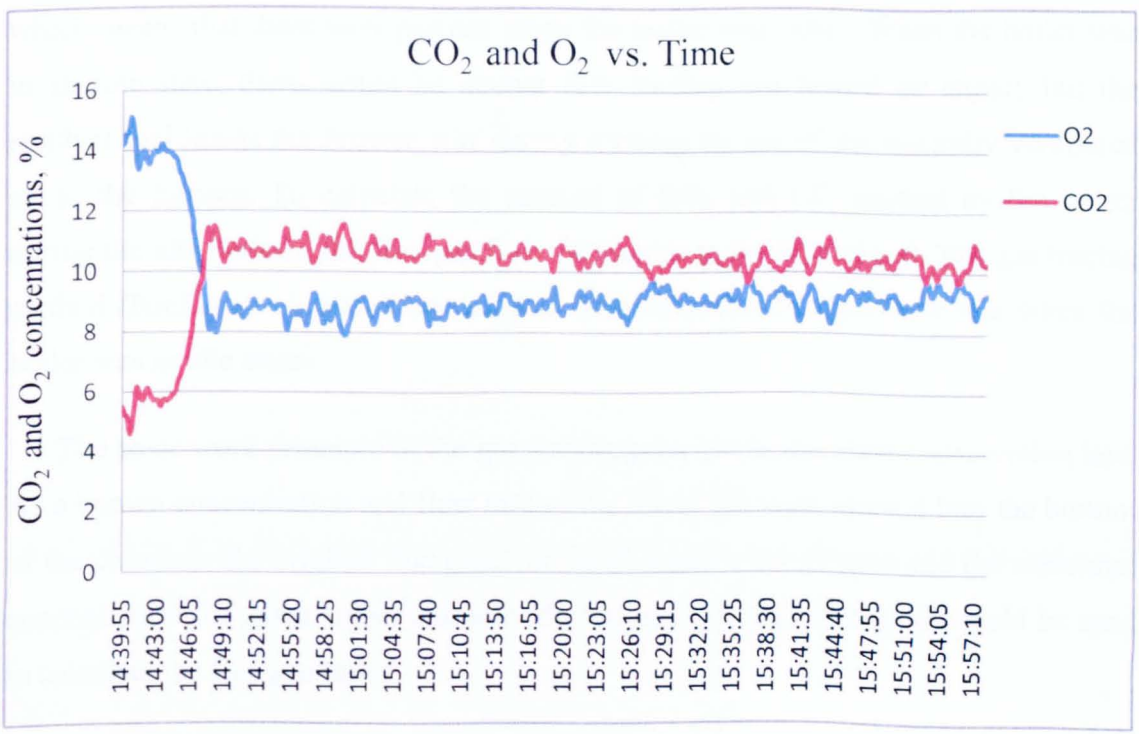

Figure 5.31 CO_2 and O_2 concentrations in the flue gas vs. Time (50kW boiler)

Instantaneous small fluctuations observed with the CO_2 and O_2 concentrations (Figure 5.31) are mainly due to the feeding mechanism of the wood pellets – non-continuous feeding of wood pellets combined with continuous feeding of the combustion air had led to small fluctuations in CO_2 and O_2 concentrations.

5.5.3. Quantification of the 25kW biomass boiler flue gas flow rate during idle periods

To quantify the amounts of CO and NOx emissions, the dry flue gas flow rate is also needed, in addition to the measured emissions which are usually expressed in concentrations. The dry flue gas flow rate of a biomass boiler under normal combustion conditions can be estimated by use of the fuel analysis (Table 4.1), the theory of combustion stoichiometry, the measured O_2 concentration in the flue gas and assuming the fuel is completely burned(Kenneth W. Ragland *et al.* 2010). For the

25kW biomass boiler, the dry flue gas flow rate was estimated to be 550 l/min (15 ^{0}C, 1atm) under normal combustion conditions(Liu *et al.* 2010).

As discussed above, the 25kW biomass boiler was operating in stop/restart cycles, which means that there were periods when the boiler was 'idle'. When the boiler was in an idle state, there would be neither fuel feeding nor forced air supply but the residual fuel inside the furnace was slowly burning by use of the naturally ventilated air to the furnace. To calculate the amount of NO_x and CO emitted by the boiler during the idle periods, the flue gas flow rate needs to be determined. The gas tracing method (Foulart *et al.* 2006) was used to determine the flue gas flow rate when the boiler was in idle states.

The basic work principle of the gas tracing principle is the mass conservation law. As a known concentration and flow rate of the tracer gas was injected into the bottom of the chimney, the original flue gases in the chimney were diluted and the measured concentrations of gases before and after the injection of the tracer gases could be used to calculate the flue gas flow:

$$Q_{flue}\ C_{bef\,0ore,i} + Q_{tracer}\ C_{tracer,i} = (Q_{flue} + Q_{tracer})C_{after,i} \qquad (5.20)$$

Where Q is the flow rate and C is concentration. The calibration gas – 1500 ppmv CO/15 vol% CO_2/N_2 balance was used as the tracer gas. The flow rate of the tracer gas used was 60 litre (15^{0}C & 1atm)/min.

When the boiler was in an idle state, i.e. after the boiler reached the set water temperature but before restarting, the flue gas compositions were measured before and after the injection of 60 litre/min of the tracer gas. Using formula (5.16) and the data shown in Figure 5.32, the flue gas flow rate when the boiler was in a idle state was estimated to be around 93 ± 5 litre(15^{0}C, 1atm)/min, which was about 17% of the flue gas flow when the boiler was in normal operation at its designed load. Figure 5.32 shows that both CO_2 and O_2 are good as the tracer gas components, whereas CO and NOx are less reliable and accurate as the tracer gas components.

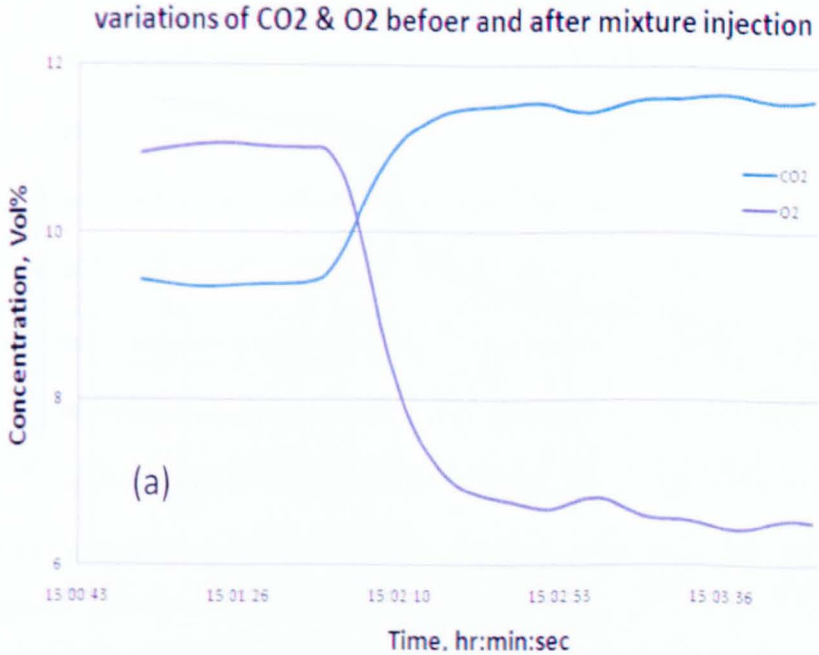

Figure 5.32 Measured concentrations of CO_2 and O_2 in the flue gas before and after the injection of the tracer gas at 60 litres/min

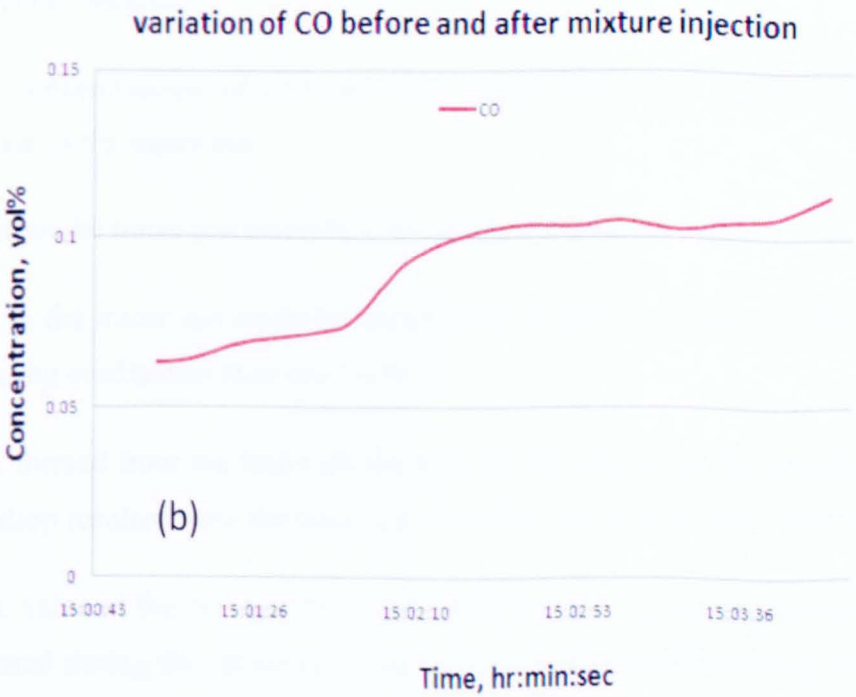

Figure 5.33 Measured concentrations of CO in the flue gas before and after the injection of the tracer gas at 60 litres/min (25kW biomass boiler)

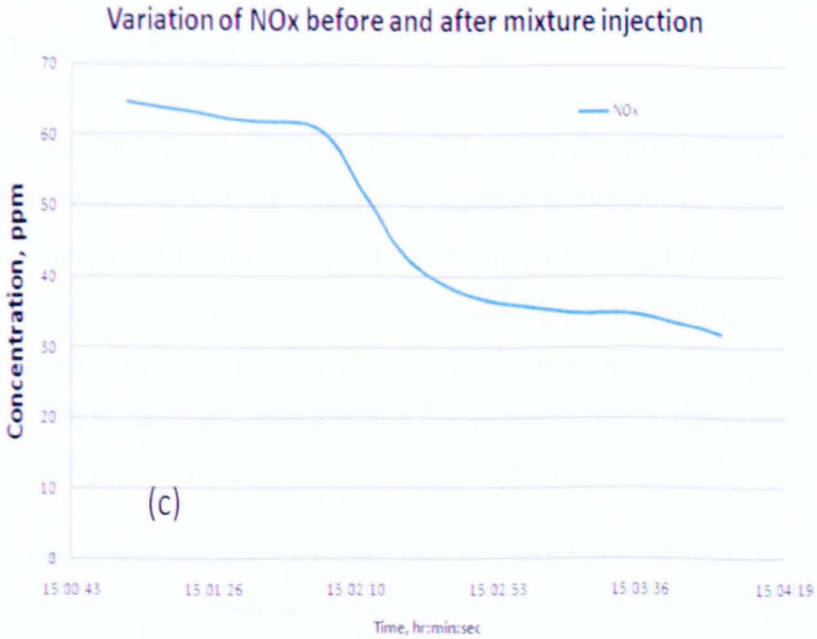

Figure 5.34 Measured concentrations of NOX in the flue gas before and after the injection of the tracer gas at 60 litres/min (25kW biomass boiler)

This is mainly because:

(1) The concentrations of CO and NOx before the tracer gas injection were similar to those of the tracer gas;

(2) CO from the tracer gas could be oxidised in the furnace;

(3) NOx in the tracer gas could be reduced by the fuel-rich flame in the furnace via the reburning mechanism (Liu *et al.* 1997).

(4) NOx formed from the fuel-rich flame in the furnace could be affected by the temperature drop resulted from the tracer gas injection and by CO from the tracer gas.

Using the value of the flue gas flow rate for an idle period and the concentrations of CO measured during the idle period, the amount of CO emitted during the period can be estimated. Using the data shown in Figure 5.26, the amount of CO emitted during a 3 minute idle period was estimated to be as much as twice of that was emitted during a 12 minute normal operation period.

5.6. Potential carbon saving with the micro-CHP system driven by 50kW biomass boiler

A brief description was made in section 2.3 about the great energy and carbon emission savings by using M-CHP system to replace conventional separate heat and power, i.e. a central heat boiler and grid electricity, in typical UK homes. A CHP system fuelled by a renewable energy resource, such as biomass in this test, would deliver even more environmental benefits than a fossil fuel-driven CHP. The potential carbon saving with the 50kW biomass-fired micro-CHP system over a conventional separate heating and electricity system has been estimated and presented in this section.

To estimate the carbon savings, CO_2 emission factors of the UK grid electricity, fossil fuels and biomass pellets are needed. Table 5.7 shows the carbon emission factors of various fuels and electricity recommended by The Carbon Trust (Carbontrust, 2011).

Table 5.7 CO2 emission factors

Energy source	Units	kg CO_{2e} per unit
Grid electricity	kWh	0.54522
Natural gas	kWh	0.18523
LPG	kWh	0.21445
	litres	1.492
Gas oil	kWh	0.27533
	litres	3.0212
Fuel oil	kWh	0.26592
	tonnes	3219.7
Burning oil	kWh	0.24683
	tonnes	3164.9
Diesel	kWh	0.25301
	tonnes	2.672
Petrol	kWh	0.24176
	tonnes	2.322
Industrial coal	kWh	0.32227
	tonnes	2336.5
Wood pellets	kWh	0.03895
	tonnes	183.93

Greenhouse gas conversion factors are used to calculate the amount of greenhouse gas emissions caused by energy use. They are measured in units of kg carbon dioxide equivalent. In order to convert 'energy consumed in kWh' to 'kg of carbon dioxide equivalent', the energy use should be multiplied by the CO_2 emission factor given in Table 5.7.

As a result of its cool maritime climate, the UK has a significant heating season spread over several months, with the demand for space heating ranging up to 4,000 running hours per year (Jeremy Harrison 2010) which has been used to estimate the total CO_2 emissions of the micro-CHP and the separate heat and power systems.

The 50kW biomass boiler-driven micro-CHP system generates electricity of 748.6W and heat of 43.7kW by consuming 52.35kW wood pellets. The CO_2 emission of the 50kW biomass boiler-driven micro-CHP system can be calculated as:

$$M_{CO2-tseted} = Q_{biomass\ input} * wood\ pellets\ emission\ factor * 4000 \quad (5.21)$$

Hence the CO_2 emission of the biomass micro-CHP system can be estimated as 8156kg per year.

The CO_2 emission released by a conventional separate heat and power system, which supplies the same amounts of electricity and heat as those of the biomass micro-CHP, consists of two parts: one due to the heat used for space and water heating inside the building mostly from a nature gas boiler, and the other due to the electricity used within the house supplied by the grid. Assuming the energy conversion efficiency of the natural gas boiler is 80%, the CO_2 emission of the conventional separate heat and power can be calculated as:

$$M_{CO2-conventional} = (I_{ele} * Grid\ electricity\ emission\ factor + Q\_thermal/\eta\_(gas\ boiler) * Natural\ gas\ emission\ factor) * 4000 \quad (5.22)$$

With the CO_2 emission factors given in Table 5.7, the CO_2 emission of the conventional separate heat and power system is found to be 61788kg per year.

The above estimates indicate that the biomass micro-CHP system can save CO_2 emissions of 53632kg per year and the percentage of CO_2 emission saving is 86.8%.

5.7. Conclusions

The micro-scale biomass-fired CHP with ORC has been constructed and tested with a 25kW biomass boiler and a 50kW biomass boiler. The experimental results are presented and discussed in this chapter.

The 25kW biomass boiler-driven micro-CHP system, having an ORC efficiency in the range of 2.20% – 2.85%, can generate electricity of 344.6W and heat of 20.3kW, corresponding to electricity generation efficiency 1.17% and CHP efficiency 86.22%. The $50kW_{th}$ biomass boiler-driven micro-CHP system, having an ORC efficiency of 3.48% - 3.89%, can generate electricity of 748.6W and heat of $43.7kW_{th}$, corresponding to electricity generation efficiency 1.43% and CHP efficiency 81.06%.

Several modified air motors have been experimentally evaluated as the ORC micro-turbines with the present project. The tests have confirmed the feasibility of the modified air motors as ORC micro-turbines. However, the turbine efficiency was found to be relatively low, only in the order of 50% for both of the non-lubricated turbine and the lubricated turbine (16AM-FRV-2).

To convert the mechanical energy of the micro-turbine to electricity, car alternators have been connected to the micro-turbine by the pulley-belt assembly. Under the same conditions, the 140A Bosch Alternator leads to the highest electrical output among the three alternators tested: the 140A Bosch Alternator, the 100A Bosch Alternator and the Prestolite 200A alternator. However, the alternator efficiency is low, only as high as ca. 50%.

The relatively low turbine efficiency (ca. 50%) and low alternator efficiency (ca. 50%) of the current experimental systems and the low evaporation temperatures of the organic working fluid are the main factors responsible for the low electrical efficiency observed with the experiments than that predicted by the thermodynamic modelling.

Monitoring of the flue gas emissions confirms that both of the 50kW biomass boiler and 25kW biomass boiler emit low levels of CO and NOx under normal combustion conditions, which confirms that the boilers satisfy the EU regulations on domestic biomass boiler emissions (EN303-5). In addition, air staging adopted with the 50kW biomass boiler was proved to be effective in controlling NOx emissions.

However, during the idle periods of the 25kW biomass boiler, the CO concentration in the flue gas could be dangerously high – up to 0.9%. The gas tracing method was successfully used to determine the flue gas flow rate when the boiler was in an idle state, which was found to be about 17% of the flue gas flow when the boiler was in normal operation at its design capacity. The amount of CO emitted during a 3 minute idle period was estimated to be as much as twice of that was emitted during a 12 minute normal operation period.

If the 50kW biomass boiler-driven micro-CHP system is used to replace a conventional separate heat and power system of a natural gas boiler and grid electricity, over 80% of the CO_2 emissions of the conventional separate heat and power system could avoided.

Chapter 6. Conclusions and Recommendations for Future Work

The present PhD thesis has reviewed the current development of biomass-fuelled micro-CHP and discussed the potential advantages of micro-CHP system with ORC driven by biomass. Then it has described and discussed the thermodynamic modelling of the proposed micro-scale biomass-fired CHP system with ORC. Finally it has detailed the laboratory testing of the assembled micro-scale biomass-fired CHP system driven by a 25kW biomass boiler and a 50kW biomass boiler, respectively.

The micro-scale biomass-fired CHP system with ORC developed by the research team of University of Nottingham including the author of this PhD thesis mainly consists of a biomass boiler, an ORC fluid evaporator, an ORC turbine, an alternator, a heat recouperator and a condenser. The boiler produces hot water which transfers heat to the organic working fluid via the evaporator. The generated organic fluid vapour drives a turbine to rotate an alternator, producing power. The expanded organic fluid vapour leaving the turbine transfers some of its heat to the recouperator and then is condensed by cooling water which can be heated to around 40 – 50 ^{0}C for domestic washing and under-floor heating purposes.

6.1. Conclusions

The following conclusions can be drawn from the present PhD research:

(1) CHP represents a major alternative to traditional energy systems in terms of significant energy saving and environmental conservation. A CHP system fuelled by a renewable energy resource, such as biomass would deliver even more environmental benefits than a fossil fuel-driven CHP.

(2) Biomass plays an important role to the world primary energy supplies, currently providing approximately 14% of the world's primary energy needs and being the fourth largest contributor following coal, oil and natural gas.

Although many medium- and large-scale biomass-fired CHP plants have been demonstrated and commercialized in many parts of the world, few biomass-fuelled micro-scale CHP (1-10kW$_e$) systems suitable for building applications have been demonstrated or commercialized.

(3) ORC is a suitable thermodynamic cycle that can operate with waste heat and renewable energy resources that are available at relative low temperatures. The biomass-fired micro-scale CHP system with ORC developed at University of Nottingham has potential benefits in terms of safety, stability, high energy efficiency and reducing environmental impacts.

(4) The proposed biomass-fired micro-CHP system with ORC has been thermodynamically modelled with three selected dry organic working fluids, namely HFE7000, HFE7100 and n-pentane with various ORC configurations. The modelling conclusions are listed as following:

a) The modelling results have shown that the electrical efficiency of the micro-CHP system depends on not only the modelling conditions but also the ORC fluid. A comparison of the three fluids shows that n-pentane exhibits the best electrical efficiency and follows the following order: n-pentane > HFE7000 > HFE7100. But as n-pentane is a flammable fluid, the use of n-pentane in a domestic micro-CHP system might not be straightforward. Consequently, HFE7000 is recommended as the preferred working fluid of the proposed micro-CHP system for the experimental testing stage. HFE7100 can yield a better efficiency than HFE7000 at the highest modelled evaporator temperature (433K) and therefore if the biomass boiler can produce a hot water with a minimum temperature of 443K, HFE7100 can be used as the preferred ORC working fluid for the experimental testing.

b) The modelling results also show that using an Internal Heat Exchanger improves the CHP electrical efficiency. An IHE will increase the system electrical efficiency, whilst keeping the overall efficiency nearly the same. Under the system operating conditions assumed in the model, the efficiency curve almost follows a linear pattern; the efficiency increase can be estimated to be 0.4-0.5% for every 10 K of temperature drop in the internal heat

exchanger. The increase rate for n-pentane is slightly lower than those for HFE7000 and HFE7100.

c) The modelling results have shown that both superheating and subcooling have a negative effect on the predicted electrical efficiency. As only dry fluids are to be used with the proposed micro-CHP system, superheating is not required for safety reasons with regard to turbine blades. The additional heat input required for superheating does not increase the pressure difference across the turbine, and therefore the work output will almost the same as that with no superheating and hence leads to a lower electrical efficiency. Subcooling is used to prevent vapour from going into the pump; therefore a low degree of subcooling is acceptable. However, subcooling the working fluid has a negative effect on the system electrical efficiency. For the same work output in the turbine, more heat is needed to bring the fluid to the evaporator temperature.

(5) The micro-scale biomass-fired CHP with ORC has been constructed and tested with a 25kW biomass boiler and a 50kW biomass boiler, respectively.

a) The 25kW biomass boiler-driven micro-CHP system, having an ORC efficiency in the range of 2.20% – 2.85%, can generate electricity of 344.6W and heat of 20.3kW, corresponding to electricity generation efficiency 1.17% and CHP efficiency 86.22%.

b) The $50kW_{th}$ biomass boiler-driven micro-CHP system, having an ORC efficiency of 3.48% - 3.89%, can generate electricity of 748.6W and heat of $43.7kW_{th}$, corresponding to electricity generation efficiency 1.43% and CHP efficiency 81.06%.

c) Several modified air motors have been experimentally evaluated as the ORC micro-turbines with the present project. The tests have confirmed the feasibility of the modified air motors as ORC micro-turbines. However, the turbine efficiency was found to be relatively low, only in the order of 50% for both of the non-lubricated turbine and the lubricated turbine.

d) To convert the mechanical energy of the micro-turbine to electricity, car alternators have been connected to the micro-turbine by the pulley-belt assembly. Under the same conditions, the 140A Bosch Alternator has been found to lead to the highest electrical output among the three alternators

tested: the 140A Bosch Alternator, the 100A Bosch Alternator and the Prestolite 200A alternator. However, the alternator efficiency is low, only as high as ca. 50%.

e) The relatively low turbine efficiency (ca. 50%) and low alternator efficiency (ca. 50%) of the current experimental systems and the low evaporation temperatures of the organic working fluid are the main factors responsible for the low electrical efficiency observed with the experiments than that predicted by the thermodynamic modelling.

f) Monitoring of the flue gas emissions confirms that both of the 50kW biomass boiler and 25kW biomass boiler emit low levels of CO and NOx under normal combustion conditions, which confirms that the boilers satisfy the EU regulations on domestic biomass boiler emissions (EN303-5). In addition, air staging adopted with the 50kW biomass boiler has been proved to be effective in controlling NOx emissions.

However, during the idle periods of the 25kW biomass boiler, the CO concentration in the flue gas could be dangerously high – up to 0.9%. The gas tracing method has been successfully used to determine the flue gas flow rate when the boiler was in an idle state, which was found to be about 17% of the flue gas flow when the boiler was in normal operation at its design capacity. The amount of CO emitted during a 3 minute idle period was estimated to be as much as twice of that was emitted during a 12 minute normal operation period.

6.2. Recommendations for future work

The current biomass-fired CHP system with ORC has proved to be feasible, but with lower power output efficiency than that predicted by the thermodynamic modelling. The relatively low turbine efficiency and low alternator efficiency of the current experimental system are the main factors that need to be improved in the future. Micro-turbines and alternators with better performance in relative low PRM ranges will make visible improvements to the system electrical efficiency. Besides, different connection methods between the micro turbine and alternator such as direct coupling may be considered in the future.

In addition, a new concept of heat exchanger for the biomass boiler such as a multi-water-path heat exchanger may be needed in order to generate hot water with temperature higher than 130 ^{0}C which was achieved with the 50kW biomass boiler. Thermodynamic modelling of the proposed biomass-fired micro-CHP system has shown that the ORC efficiency increases with the evaporator temperature but the 50kW biomass boiler used in the experimental investigation of this project has never achieved its deigned hot water temperature of 180 ^{0}C.

The thermodynamic modelling of the proposed biomass-fired micro-CHP system with ORC could also be extended to other environmentally friendly fluids such as HFE7200. Obviously, the modelling of any new ORC fluids will depend on the availability of thermodynamic properties with the selected modelling software such as EES that has been used in the present research.

References

3M Ltd. from http://solutions.3m.co.uk/wps/portal/3M/en_GB/3M-Technologies/Home/.

A Demirbas (2000). "Recent advances in biomass conversion technologies." Educational Science and Technology.

A.V. Herzog, T.E. Lipman and D.M. Kammen (2002). "Renewable energy sources." Our Fragile World: Challenges and Opportunities for Sustainable Development.

ABB Ltd. from http://www.abb.com/product/us/9AAC100047.aspx?country=00.

ADORATEC. from http://www.adoratec.com/companyprofilnav.html.

AGE Ltd. from www.aeg.co.uk.

Ahrenfeldt, J., U. Henriksen, T. K. Jensen, B. G 鳍 el, L. Wiese, A. Kather and H. Egsgaard (2006). "Validation of a continuous combined heat and power (CHP) operation of a two-stage biomass gasifier." Energy & Fuels **20**(6): 2672-2680.

Albert Faber, Marco Valente, Peter Janssen and K. Frenken (2008). "Domestic micro-cogeneration in the Netherlands: an agent-based demand model for technology diffusion ".

Alfa Laval Ltd. from www.www.alfalaval.co.uk.

Angelino, G. and P. C. di Paliano (2000). Organic Rankine cycles (ORCs) for energy recovery from molten carbonate fuel cells, IEEE.

Ashwell Ltd. from http://www.ashwellengineering.com/.

BACKONE Equations of State. from http://onlinelibrary.wiley.com/doi/10.1002/aic.690420423/pdf.

Badami, M. and M. Mura (2009). "Preliminary design and controlling strategies of a small-scale wood waste Rankine Cycle (RC) with a reciprocating steam engine (SE)." Energy **34**(9): 1315-1324.

Balcas Ltd. from http://www.brites.eu.

Biedermann, F., H. Carlsen, M.Schoch and I.Obernberger (2004). "Operating Experiences with a small-scale CHP pilot plant based on a 35kWe Hermetic four cylinder stirling engine for biomass fuels."

Bilgen, S., K. Kaygusuz and A. Sari (2004). "Renewable energy for a clean and sustainable future." Energy Sources, Part A: Recovery, Utilization, and Environmental Effects **26**(12): 1119-1129.

Biomass Energy Centre. from http://www.biomassenergycentre.org.uk.

BIOS BIOENERGIESYSTEME GmbH. from http://www.bios-bioenergy.at/en/electricity-from-biomass/stirling-engine.html.

Bocsh Ltd. from http://www.bosch.co.uk.

Borsukiewicz-Gozdur, A. and W. Nowak (2007). "Maximising the working fluid flow as a way of increasing power output of geothermal power plant." Applied Thermal Engineering **27**(11-12): 2074-2078.

Brown, J. E., C. N. Hendry and P. Harborne (2007). "An emerging market in fuel cells? Residential combined heat and power in four countries." Energy Policy **35**(4): 2173-2186.

Cengel, Y. A. and M. A. Boles (2006). Thermodynamics: an engineering approach, McGraw-Hill Higher Education New York.

Chen, Y., P. Lundqvist, A. Johansson and P. Platell (2006). "A comparative study of the carbon dioxide transcritical power cycle compared with an organic rankine cycle with R123 as working fluid in waste heat recovery." Applied Thermal Engineering **26**(17-18): 2142-2147.

Committee on Climate Change UK (2008). "Climate Change Act 2008."

Cong, C. E., S. Velautham and A. Darus (2005). "Sustainable power: solar thermal driven organic Rankine cycle." Proceedings of the International Conferences on Recent Advances in Mechanical and Materials Engineering **91**: 424-429.

Daminabo Ferdinand (2009). A novel 2kWe biomass-organic rankine cycle micro cogeneration system / Ferdinand F.O. Daminabo. . Architecture and energy conservation, University of Nottingham.

DataTaker Ltd. from http://www.datataker.com.

Defra UK and U. DTI (2007). "Biomass Strategy UK." London HMSO (Department for Environment Food and Rural Affairs, Department for Transport, Department for Trade and Industry).

Denntice d'Accacia M, S. M., Sibilio S., Vanoli L. (2003). "Micro-combined heat and power in residential and light commercial applications." Applied Thermal Engineering **23**(10): 1247-1259.

Department for Environment and F. a. R. Affairs (2006). "Climate change: The previous term UK next term programme."

Department of Energy & Climate Change (2010). "2050 Pathways Analysis."

Department of Energy & Climate Change (2010). "Annual Energy Statement 2010."

Department of Energy & Climate Change (2010). "Digest of UK Energy Statistics 2010."

Department of Trade and Industry (2006). "Microgeneration strategy."

Dijkstra, S. (2010). "Micro-CHP edging towards the mass market."

Dong, L., H. Liu and S. Riffat (2009). "Development of small-scale and micro-scale biomass-fuelled CHP systems-A literature review." Applied Thermal Engineering **29**(11-12): 2119-2126.

Drescher, U. and D. Brügemann (2007). "Fluid selection for the Organic Rankine Cycle (ORC) in biomass power and heat plants." Applied Thermal Engineering **27**(1): 223-228.

DWFRA UK (2007). "Synthesis of Climate Change Policy Appraisals ".

Elektroteknisk, S. (2003). "Micro-CHP Techology and Economic review."

Energy Nexus Group (2002). "Technology Characterization: Microturbines."

Environmental Analysis, i., ,, I. Eastern Research Group, U. S. E. P. Agency and Energy (2007). Biomass Combined Heat and Power: Catalog of Technologies, US Environmental Protection Agency, Combined Heat and Power Partnership.

EU Cogeneration Directive (2004). "EU Cogeneration Directive 2004/8/EC."

European Commission (1997). "DIRECTORATE GENERAL FOR ENERGY."

European Commission (2010). "Europe 2020 ". from http://ec.europa.eu/europe2020/index_en.htm.

European Parliament (2001). "Renewable energy: the promotion of electricity from renewable energy sources."

European parliament and of the council (2006). "Energy end-use efficiency and energy services and repealing Council Directive ".

European Renewable Energy Conference (2004). "Intelligent Policy Options."

European renewable energy council (2004). Renewable Energy Scenario to 2040.

European Union (2004). "EU-25." from http://www.eu25.org/.

F-Chart Software. "Engineering Equation Solver." from http://www.fchart.com/ees/.

Fernandes, S. D., N. M. Trautmann, D. G. Streets, C. A. Roden and T. C. Bond (2007). "Global biofuel use, 1850-2000." Global Biogeochemical Cycles **21**(2).

Foulart, V., B. Petit and J. P. Schiltz (2006). CO2 Tracing Method for Measuring Raw Exhaust Gas Flow Rate at Exit From an Internal Combusting Engine for a Motor Vehicle and Measuring Equipment for Carrying Out Said Method, Google Patents.

Friedl, G., W. Moser, A. McCarry, K. Berndt and R. Sch 鱔 ke (2009). Micro-CHP 肸 xperiences with thermoelectric generators integrated in a wood pellet combustion unit.

Gast Ltd. from http://www.gastmfg.com/airgearmotors.html.

Grundfos Ltd. from http://www.grundfos.com.

Harmon, M. E., W. K. Ferrell and J. F. Franklin (1990). "Effects on carbon storage of conversion of old-growth forests to young forests." Science(Washington) **247**(4943): 699-699.

Herzog, A. V., T. E. Lipman and D. M. Kammen "Renewable energy sources." Our Fragile World: Challenges and Opportunities for Sustainable Development.

Hill, J., E. Nelson, D. Tilman, S. Polasky and D. Tiffany (2006). "Environmental, economic, and energetic costs and benefits of biodiesel and ethanol biofuels." Proceedings of the National Academy of Sciences **103**(30): 11206.

HORIBA Ltd. from http://www.horiba.com/.

Hung, T., T. Shai and S. Wang (1997). "A review of organic Rankine cycles (ORCs) for the recovery of low-grade waste heat." Energy **22**(7): 661-667.

Hung, T. C. (2001). "Waste heat recovery of organic Rankine cycle using dry fluids." Energy Conversion and Management **42**(5): 539-553.

IEA Bioenergy. from http://www.ieabioenergy.com/.

Intergovernmental Panel on Climate Change (2007). "IPCC Fourth Assessment Report." The Physical Science Basis.

international Energy Agency (2007). "Tracking Industrial Energy Efficiency and CO2 Emissions."

International Energy Agency (2008). "Combined Heat and Power- Evaluating the Benefits of Greater Global Investment."

International Energy Agency (2008). "Key World Energy Statistics."

International Energy Agency (2008). "World Energy Outlook 2008."

International Energy Agency (2009). "CHP/DHC Country Scorecard: Germany."

International Energy Agency (2009). "CHP/DHC Country Scorecard: Japan."

International Energy Agency (2009). "World Energy Outlook 2009."

International Energy Agency (2010). "CO2 Emissions from Fuel Combustion 2010."

International Energy Agency (2010). "Energy Balances of OECD Countries."

Jacobsson, S. and A. Bergek (2004). "Transforming the energy sector: the evolution of technological systems in renewable energy technology." Industrial and corporate change **13**(5): 815.

Jeremy Harrison (2004). "Micro Combined Heat & Power (CHP) for housing."

Jeremy Harrison (2010). Micro Cogeneration in Britain Micro CHP: The Big Picture, Big Picture Publishing: pp 243 - 264.

Kenneth W. Ragland and K. M. Bryden. (2010). Combustion Engineering, CRC Press Inc.

Knoef, H. and J. Ahrenfeldt (2005). Handbook biomass gasification, BTC biomass technology group.

Kralova Iva and S. Johan (2010). "Biofuels-Renewable Energy Sources: A Review." Journal of Dispersion Science and Technology.

Larkin S., R. J. and S. J. (2004). "Bioenergy, in Renewable Energy - Power for a Sustainable Future " Oxford University Press: pp 106 - 146.

Liu, B. T., K. H. Chien and C. C. Wang (2004). "Effect of working fluids on organic Rankine cycle for waste heat recovery." Energy **29**(8): 1207-1217.

Liu, H. and B. M. Gibbs (2002). "Modelling of NO and N2O emissions from biomass-fired circulating fluidized bed combustors." Fuel **81**(3): 271-280.

Liu, H. and B. M. Gibbs (2003). "Modeling NH3 and HCN emissions from biomass circulating fluidized bed gasifiers* 1." Fuel **82**(13): 1591-1604.

Liu, H., E. Hampartsoumian and B. M. Gibbs (1997). "Evaluation of the optimal fuel characteristics for efficient NO reduction by coal reburning." Fuel **76**(11): 985-993.

Liu, H., G. Qiu, Y. Shao and S. B. Riffat (2010). "Experimental investigation on flue gas emissions of a domestic biomass boiler under normal and idle combustion conditions." International Journal of Low-Carbon Technologies **5**(2): 88.

Liu H. (2011). Biomass fuels for small and micro combined heat and power (CHP) systems: resources, conversion and applications. Small and micro combined heat and power (CHP) systems: Advanced design, performance, materials and applications. Beith R., Woodhead Publishing Limited.

Liu H. and N. Y. (2010). Gasification. High temperature processes in chemical engineering. M. Lackner, Verlag ProcessEng Engineering GmbH: pp 361 - 408.

Mago, P. J., L. M. Chamra, K. Srinivasan and C. Somayaji (2008). "An examination of regenerative organic Rankine cycles using dry fluids." Applied Thermal Engineering **28**(8-9): 998-1007.

Marathon ecopower micro-CHP (2007). "Ecopower vs Coal Brochure."

Marciniak, T., J. Krazinski, J. Bratis, H. Bushby and E. Buyco (1981). Comparison of Rankine-cycle power systems: effects of seven working fluids, Argonne National Lab., IL (USA).

Maribu, K. M., , (2004). "Distributed Generation in Liberalized Electricity Markets." A SUMMARY OF PhD PROJECTS 2004.

McMahan, A. C. (2006). "Design & Optimization of Organic Rankine Cycle Solar-Thermal Powerplants." Master's Thesis, University of Wisconsin-Madison.

Minea, V. (2007). Using Geothermal Energy and Industrial Waste Heat for Power Generation, IEEE.

Montreal protocol (2007). "Quickens HCFC phase-out." from http://www.acr-news.com/news/news.asp?id=429&title=Montreal+protocol%27s+%20birthday+deal+quickens+HCFC+phase-out.

Naphtha launch. from http://en.wikipedia.org/wiki/Naphtha_launch.

Nguyen, V., P. Doherty and S. Riffat (2001). "Development of a prototype low-temperature Rankine cycle electricity generation system." Applied Thermal Engineering **21**(2): 169-181.

NIMMO, W. and H. LIU (2010). Developments in NOx Emission Control By Reburning in Pulverised Coal Combustion. Coal Combustion Research. C. T. GRACE, Nova Science Publishers, Inc.: pp. 85 - 170.

Nishio, M., J. Itoh, K. Shiroko and T. Umeda (1980). "A thermodynamic approach to steam-power system design." Industrial & Engineering Chemistry Process Design and Development **19**(2): 306-312.

Office of Gas and Electricity Markets (2011). " Carbon Emissions Reduction Target ".

Oliver, J. R. (2006). A micro-cooling, heating, and power (m-CHP) instructional module, Mississippi State University.

Onovwiona, H. and V. Ugursal (2006). "Residential cogeneration systems: review of the current technology." Renewable and Sustainable Energy Reviews **10**(5): 389-431.

Orlando, J. A. (1996). "Cogeneration design guide."

Photosynthesis. "Photosynthesis." from http://transpacifica.biz/images/photosynthesis.

Prestolite Ltd. from www.prestolite.com.

Quoilin, S., Lemort, V. (2009). "Technological and economical survey of organic Rankine cycle systems."

R. Kannan. and N. Strachan (2009). "Modelling the UK residential energy sector under long-term decarbonisation scenarios: Comparison between energy systems and sectoral modelling approaches." Applied Energy **86**(4): 416-428.

Rankine, W. J. M. from http://en.wikipedia.org/wiki/William_John_Macquorn_Rankine.

Ren, H. and W. Gao (2010). "Economic and environmental evaluation of micro CHP systems with different operating modes for residential buildings in Japan." Energy and Buildings **42**(6): 853-861.

Saleh, B., G. Koglbauer, M. Wendland and J. Fischer (2007). "Working fluids for low-temperature organic Rankine cycles." Energy **32**(7): 1210-1221.

Sawin, J. L., E. Martinot and R. E. P. N. f. t. s. Century (2010). Renewables 2010: Global status report, Renewable Energy Policy Network for the 21st Century.

Schaeffer, M., B. Eickhout, M. Hoogwijk, B. Strengers, D. Van Vuuren, R. Leemans and T. Opsteegh (2006). "CO2 and albedo climate impacts of extratropical carbon and biomass plantations." Global Biogeochemical Cycles **20**(2).

Second World Climate Conference (1992). "Climate Convention." from http://www.un.org/ecosocdev/geninfo/sustdev/climate.htm.

Secretary of State for Energy and Climate Change (2009). UK Renewable Energy Strategy 2009.

Sekiya, A. and S. Misaki (2000). "The potential of hydrofluoroethers to replace CFCs, HCFCs and PFCs." Journal of Fluorine Chemistry **101**(2): 215-221.

Shafiee, S. and E. Topal (2009). "When will fossil fuel reserves be diminished?" Energy Policy **37**(1): 181-189.

Simader, G. R., R. Krawinkler and G. Trnka (2006). "Micro CHP systems: state of the art." Final Report, contracted by European Commission and Austrian Federal Ministry of Economics and Labour.

Strehler, A. (2000). "Technologies of wood combustion* 1." Ecological Engineering **16**: 25-40.

SWEP Ltd. from http://www.swep.net.

The Carbon Trust Ltd. (2011). "Micro-CHP (Combined Heat & Power) Accelerator - Final report ".

The European Association for the Promotion of Cogeneration (2001). A guide to cogeneration, Brussels, Belgium: Author.

Tsai, W. T. (2005). "Environmental risk assessment of hydrofluoroethers (HFEs)." Journal of hazardous materials **119**(1-3): 69-78.

TURBODEN Ltd. from http://www.turboden.eu/en/home/index.php.

Unipoint Ltd. from http://www.unipoint.com.tw.

United Nations Framework Convention on Climate Change (1997). "Kyoto Protocol ". from http://unfccc.int/kyoto_protocol/items/2830.php.

Vamvuka, D. and E. Kakaras (2010). "Ash properties and environmental impact of various biomass and coal fuels and their blends." Fuel Processing Technology.

Van Loo, S. and J. Koppejan (2008). The handbook of biomass combustion and co-firing, Earthscan/James & James.

Wei, D., X. Lu, Z. Lu and J. Gu (2007). "Performance analysis and optimization of organic Rankine cycle (ORC) for waste heat recovery." Energy Conversion and Management **48**(4): 1113-1119.

Wolfe, P. (2008). "The implications of an increasingly decentralised energy system." Energy Policy **36**(12): 4509-4513.

World Energy Council (2004). Renewable Energy Projects Handbook.

Yagoub, W., P. Doherty and S. Riffat (2006). "Solar energy-gas driven micro-CHP system for an office building." Applied Thermal Engineering **26**(14-15): 1604-1610.

Yamamoto, T., T. Furuhata, N. Arai and K. Mori (2001). "Design and testing of the organic Rankine cycle." Energy **26**(3): 239-251.

Appendix

Publications

Liu, H., Y. Shao and J. Li (2011). "A biomass-fired micro-scale CHP system with organic Rankine cycle (ORC)-Thermodynamic modelling studies." Biomass and Bioenergy. doi:10.1016/j.biombioe.2011.06.025

Liu, H., G. Qiu, Y. Shao, F. Daminabo and S. B. Riffat (2010). "Preliminary experimental investigations of a biomass-fired micro-scale CHP with organic Rankine cycle." International Journal of Low-Carbon Technologies **5**(2): 81.

Liu, H., G. Qiu, Y. Shao and S. B. Riffat (2010). "Experimental investigation on flue gas emissions of a domestic biomass boiler under normal and idle combustion conditions." International Journal of Low-Carbon Technologies **5**(2): 88.

Qiu,G., Y.Shao, J.Li, H.Liu and S. B. Riffat. "Experimental investigations of a biomass-fired ORC-based micro-scale CHP for domestic applications", submitted to Fuel, Aug 2011

Qiu, G., H. Liu, F.Daminabo, Y. Shao and S. B. Riffat 2009. Experimental investigation of a biomass-fired micro-scale CHP with organic Rankine cycle, 8th Intl Conference on Sustainable Energy Technologies. Aachen, Germany.

Liu, H., G. Qiu, Y. Shao and S. B. Riffat 2009. Experimental investigation on flue gas emissions of a domestic biomass boiler, 8th Intl Conference on Sustainable Energy Technologies. Aachen, Germany.